Modified tethered bilayer lipid membranes for detection of pathogenic bacterial toxins and characterization of ion channels

Thet Naing Tun

A thesis submitted for the degree of Doctor of Philosophy

Department of Chemistry
University of Bath
October 2010

To my daughter Fiona

"Research is to see what everybody else has seen and to think what nobody else has thought"

Albert von Szent-Györgyi
Hungarian Biochemist
1937 Nobel Prize in Physiology or Medicine
1893-1986

Abstract

Pathogenic bacteria secrete various virulence factors as their biochemical weapons to gain access to and destroy the target cells. They can directly interact with the outer lipid bilayer membrane of eukaryotic cells, inducing the premature cell death by either apoptosis or necrosis. Such virulence factors account for much of the toxic actions associated with bacterial infection; therefore the detection of such proteins could provide a methodology for sensing/detection of pathogenic bacteria in, for example, food or human tissue. Detection and identification of pathogenic bacteria by conventional methods such as plating and counting in laboratory is expensive and time consuming. With growing concerns over emergence and re-emergence of pathogenic bacteria with high resistant to current antibiotics, there is a potential need for effective detection of pathogenic toxins *in-vitro*.

On the other hand, artificially prepared lipid bilayer membrane on planar metallic surfaces provides the cell membrane mimics which are extremely useful in exploring the cellular functions and processes at the molecular level. Therefore in this work, an application of planar tethered bilayer lipid membrane (pTBLM) as a biomimetic sensing platform for the detection of clinically important pathogens, *Staphylococcus aureus* and *Pseudomonas aeruginosa* via their secreted virulence factors was presented. Planar TBLM was modified by incorporation of cholesterol and detection of bacterial toxins at human body temperature was examined by impedance and surface plasmon resonance methods. The results of pathogenic bacterial toxin detection were compared with those of *Escherichia coli* (DH5α), the human gut normal flora with non-pathogenic strain, as a control.

Additionally pTBLM was transferred onto single nanoporous Si_3N_4 membrane to enhance the toxin sensitivity and extend the lifetime for the possible realization of future membrane chips for ion channel characterizations and drug screenings. Then the single ion channel measurement was demonstrated with nanopore-suspended TBLM (Nano-psTBLM) using α-toxin of *S. aureus*. The results presented in this work therefore, may pave the more effective and efficient ways for future pathogenic bacterial detection in which the sensing mechanism was solely based on the nature of interactions as well as modes of action between bacterial toxins and artificial lipid bilayer membranes.

Table of Contents

List of Figures

List of Tables

Abbreviations

α-HL	Alpha Hemolysin
α-PFT	α-Poreforming Toxin
β-PFT	β-Poreforming Toxin
AAO	Anodic Aluminium Oxide
AC	Alternating Current
ADP	Adenosine Diphosphate
AFM	Atomic Force Microscopy
BLM	Black Lipid Membrane
BoNTs	Botulinum Neurotoxins
cAMP	cyclic Adenosine Monophosphate
C_{dl}	Double Layer Capacitance
C_m	Bilayer Membrane Capacitance
Ctx	Cholera enterotoxin
CBTs	Cholesterol binding toxins
CDCs	Cholesterol-dependent Cytolysins
CE	Counter Electrode
CFU	Colony Forming Units
CholPEG	Cholesterol-pentaethyleneglycol
CNFs	Cytotoxic Necrotizing Factors
CNS	Central Nervous System
Dtx	Diphtheria toxin
DC	Direct Current
DLS	Dynamic Light Scattering
DMPC	1,2-dimyristoyl-*sn*-glycero-3-phosphocholine
DNA	Deoxyribonucleic Acid
DPhPC	1,2-dipalmitoyl-*sn*-glycero-3-phosphocholine
DPhyPC	1,2-di-O-phytanoyl-*sn*-glycero-2-phosphocholine
DPhyTL	2,3-di-O-phytanyl-glycerol-l-tetraethylene glycol-D,L-lipoic acid ester lipid
DPPC	1,2-dipalmitoyl-*sn*-glycero-3-phosphocholine
DPPTE	1,2-diphytanoyl-*sn*-glycero-3-phosphothioethanol
DPTTE	2,3-di-O-phytanyl-*sn*-glycerol-l-tetra-ethylene glycol-(3-triethoxysilane) ether lipid
DSC	Differential Scanning Calorimetry
DSPC	Distearoyl Phosphatidylcholine
E	Potential
E. coli	*Escherichia coli*
E. coli DH5α	*Escherichia coli* DH5α
EBL	Electron Beam Lithography
EDTA	ethylene-di-amine-tetra-acetic acid
EFs	Elongation Factors
EIS	Electrochemical Impedance Spectroscopy
ELISA	Enzyme-linked Immunosorbent Assay
FIB	Focus Ion Beam
FRA	Frequency Response Analyzer
FRAP	Fluorescence Recovery After Photobleaching
GNP	Glass Nanopore
GPCRs	G Protein-coupled Receptors
hCG	human Chorionic Gonadotropin

HIV	Human Immunodeficiency Virus
I	Current
IPA	Isopropanol
KOH	Potassium Hydroxide
LB	Langmuir Blodgett
LB	Lauria Broth
LOD	Limit of Detection
LOS	Lipo-oligosaccharides
LPC	Lysophosphatidylcholine
LPCVD	Low Pressure Chemical Vapour Deposition
LPI	Lysophosphatidylinositol
LPS	Lipo-polysaccharides
LUVs	Large Unilamellar Vesicles
Micro-psBLM	Micropore suspended Bilayer Lipid Membrane
MHC	Major Histocompatibility Complex
MPC	Micropipette Patch Clamping
MRSA	Methicillin-resistant *Staphylococcus aureus*
MSSA	Methicillin-suspected *Staphylococcus aureus*
nAChR	nicotinic Acetylene Choline Receptor
Nano-BLM	Nano Black Lipid Membrane
Nano-psBLM	Nanopore suspended Bilayer Lipid Membrane
Nano-psTBLM	Nanopore suspended Tethered Bilayer Lipid Membrane
OD	Optical Density
OmpF	Outer membrane protein F
pTBLM	planar Tethered Bilayer Lipid Membrane
P. aeruginosa	*Pseudomonas aeruginosa*
PBS	Phosphate Buffer Saline
PC	Phosphatidylcholine
PCA	Patch Clamp Amplifier
PCR	Polymerase Chain Reaction
PE	Phosphatidylethanol
PECVD	Plasma Enhanced Chemical Vapour Deposition
PEEK	Polyetheretherketone
PFTs	Poreforming Toxins
PG	Phosphatidylglycerol
PI	Phosphatidylinositol
PLA1	Phospholipase A1
PLA2	Phospholipase A2
PLB	Phospholipase B
PLC	Phospholipase C
PLD	Phospholipase D
PLs	Phospholipases
PMMA	Poly (methyl methacrylate)
PNS	Peripheral Nervous System
POPC	1-palmitoyl-2-oleoyl-*sn*-glycero-3-phosphocholine
PPC	Planar Patch Clamping
PS	Phosphatidylserine
PVL	Panton-Valentine leukocidin
QCM-D	Quartz Crystal Microbalance – Dissipation
R	Resistance
R_e	Electrolyte Resistance
RE	Reference Electrode

RF	Radio Frequency
RI	Refractive Index
RIS	Radioimmunoassay
R_m	Bilayer Membrane Resistance
RME	Receptor-mediated Endocytosis
RMS	Root Mean Square
RNA	Ribonucleic Acid
RT-PCR	Reverse Transcriptase Polymerase Chain Reaction
sn-1	stereospecific numbering-1
sn-2	stereospecific numbering-2
sBLM	supported Bilayer Lipid Membrane
S. aureus	*Staphylococcus aureus*
SAM	Self Assembled Monolayer
SDS	Sodium Dodecyl Sulphate
SEM	Scanning Electron Microscope
SM	Sphingomyelin
SPR	Surface Plasmon Resonance
SPs	Surface Plasmons
STM	Scanning Tunneling Microscope
SUVs	Small Unilamellar Vesicles
TBLM	Tethered Bilayer Lipid Membrane
TCRs	T-cell Receptors
TeNTs	Tetanus Neurotoxins
TIR	Total Internal Reflection
T_m	Phase Transition Temperature
TSG	Template Stripped Gold
TSS	Toxic Shock Syndrome
TSST-1	Toxic Shock Syndrome Toxin-1
UV	Ultraviolet
VAMP	Vesicle-associated Membrane Protein
WE	Working Electrode

Acknowledgements

Throughout my study and research work, I am indebted to many people for their assistance in many ways. Without their supports and contributions, my research work, regardless of much effort will not be accomplished and fruitful. First of all I would like to thank deeply to my supervisor Dr. Toby Jenkins, Department of Chemistry, University of Bath, United Kingdom. His supervision and guidance throughout my research work in University of Bath are really appreciated and carried me through difficult times during the rise and fall of a research student life. Secondly I would like to express my gratitude to former supervisor Prof. Wolfgang Knoll (currently at AIT Austrian Institute of Technology, Vienna, Austria) who gave me an opportunity to start my lipid bilayer research in Max-Planck Institute for Polymer Research (MPIP), Mainz, Germany. Thirdly I am thankful to my former supervisor Dr. Ingo Köper (currently at Flinders University, Adelaide, Australia) for his care during my second year of research in MPIP. Finally it is a kind of blessing for me to work among the friends with great concerns and care to each others. For that I would like to thank deeply to all the members of Dr. Jenkins's physical chemistry research group at the Department of Chemistry, University of Bath and the members of Dr. Köper's former research group in MPIP, Mainz. Finally, my thanks and appreciations go to my wife Kyawt and little girl Fiona for their patience and supports without which this work would not have been borne.

Half of this research work was performed in MPIP and the remaining half was done at the Department of Chemistry, University of Bath with overall financial supports from the following fundings:

1) Marie Curie Fellowship through seventh framework program (FP7)
2) International Max-Planck Research Schools (IMPRS for Polymer Materials Science)
3) EMBEK1-FP7 project number 211436

1 Introduction

It is a well known fact that the cells are fundamental units and the building blocks of all living organisms. Regardless of prokaryotes or eukaryotes, plant, animal or bacterial cells, they all are made of cell membrane which basically divides the interior and the exterior of a cell. Importantly cell membrane, known as plasma membrane not only defines the cell boundary but also protects and encompasses the cytoplasmic organelles to be able to perform their functions in intercellular environment. Indeed, cellular organelles of an animal cell such as lysosomes, endosomes, mitochondria, endoplasmic reticulum and nucleus are all membrane-bound and compartmentalized within the cell by bilayer membranes made of diverse lipids composition. Most biochemical functions of an animal cell including; uptake of nutrients, disposal of intracellular metabolic wastes, transport of ions and molecules, and transduction of electrochemical signals were basically occurred at the cell membrane. Embedded within the plasma membrane is a variety of proteins which serve as channels, pores or pumps to transport ions and molecules in and out of the cell.

As cells are functional basic units of life, cellular malfunction due to internal and external factors mainly contributes to various diseases occurred in human and animals. Internal malfunction of cellular membrane constituents, for example dysfunction of protein ion channels causes diseases in many tissues. The number of human diseases known to be associated with defects in ion channels, called channelopathies has been growing considerably [1]. This demands the growing needs of developing an artificial lipid bilayer system sensitive and stable enough for analysis and screening of ion channels *in-vitro*. On the other hand, external factors such as bacterial cytotoxins, venomous insect stings or toxins of poisonous animals can directly cause cell membrane lyses possibly by necrosis or apoptosis and premature death of cells in host by various means. Pathogenic bacteria produce variety of toxins and enzymes which are capable of damaging the cell membrane by different modes of action. Since cell membranes are primary target of these virulence factors, the understanding of functional interaction between cell membranes and toxins or enzymes *in-vitro* may lead to develop the methods of detection and identification of pathogens in, for example, food, water and human tissues.

In this work, modification of planar tethered bilayer lipid membrane (pTBLM) for the detection and possible identification of common bacterial toxins and the major human pathogens including *Staphylococcus aureus*, *Pseudomonas aeruginosa* and *Escherichia*

coli is presented. Detection and identification are based on the common modes of action of protein and enzymatic toxins against the cell membrane in which the degree and the way the lipids in bilayer are damaged, are measured by electrochemical impedance spectroscopy (EIS) and surface plasmon resonance spectroscopy (SPR). Additionally pTBLM is modified into nanopore suspended TBLM (Nano-psTBLM) by spanning over a single nanoporous Si_3N_4 membrane. By using Nano-psTBLM, it is demonstrated that the single ion channel measurements are possible while sensitivity, mechanical stability and lifetime of Nano-psTBLM are improved. The additional work is aimed to realize a better TBLM sensing platform for analysis and screening of ion channels for new drug developments [251].

1.1 Cell membranes

Cells are surrounded by cell membranes. Basic constituents of a cell membrane are a class of amphiphilic biomolecules called lipids. Being amphiphilic in nature, a lipid molecule is composed of a hydrophilic (water-loving) head group and hydrophobic (lipid-loving) hydrocarbon chains. Due to their nature of solubility in water and oil, they spontaneously form a molecular lipid bilayer in an aqueous solution, making a semi-permeable hydrophobic barrier in the hydrophilic environment. Mitochondria and endoplasmic recticulm, for example, have the typical cell membrane thickness of about 5-6 nm. Embedded in the lipid bilayer of cell membranes are many different types of lipids, proteins, carbohydrates, cholesterols and all of their complexes (figure 1.1). All the membrane constituents are held together by non-covalent, hydrophobic interactions within the cell membrane. Type and composition of lipids, proteins, carbohydrates and cholesterols in cell membranes varies from cell to cell. This depends on the distinctive identity of the individual cells and the specialized functions that they are to perform. In most cell membranes, proteins constitute the largest fraction by weight and the lipid to protein ratio usually is taken as an index of functional activity, comprising the higher the ratio, the lower the activity and vice versa.

Cell membrane is an important medium where the exchange of information and materials take place. Many functional cellular processes such as signal transduction, cell division, metabolic waste disposal, transport of ions and molecules etc., occur at the cell membrane [2]. Moreover cellular organelles such as mitochondria, endoplasmic reticulum and Golgi complex (of the eukaryotic cell) are membrane-bound and all the intracellular communications and the transport of materials within the cell are also

associated with the lipid bilayer membranes. Communication across the cell membrane can be in the form of information, transmitted through conformational changes induced in membrane components or a passage of ions or molecules flowing through the transmembrane channel protein complexes. As cell membranes control all possible means of access into the cell, they become primary targets of the foreign invasions such as bacterial toxins and infections [252]. Despite the fact that the detailed information on membrane-bound processes at the molecular level is crucial to understand the living organisms, the efforts and works are mostly hindered by the complicated nature of cell membranes. Their compositional complexity and different varieties of membrane constituents pose the challenges, making it difficult to study, for example the functions of a typical channel protein naturally incorporated into the cell membrane. This initiated the development of simplified artificial model lipid bilayers composed of one or a few types of lipid molecules. Since model lipid bilayers can mimic the cell membrane in many ways and provide the integration of membrane proteins by creating natural cellular environment, they allow not only the possibility to examine the functional processes of cell membrane constituents but also become a potential future platform for biomolecular applications such as drug delivery [3].

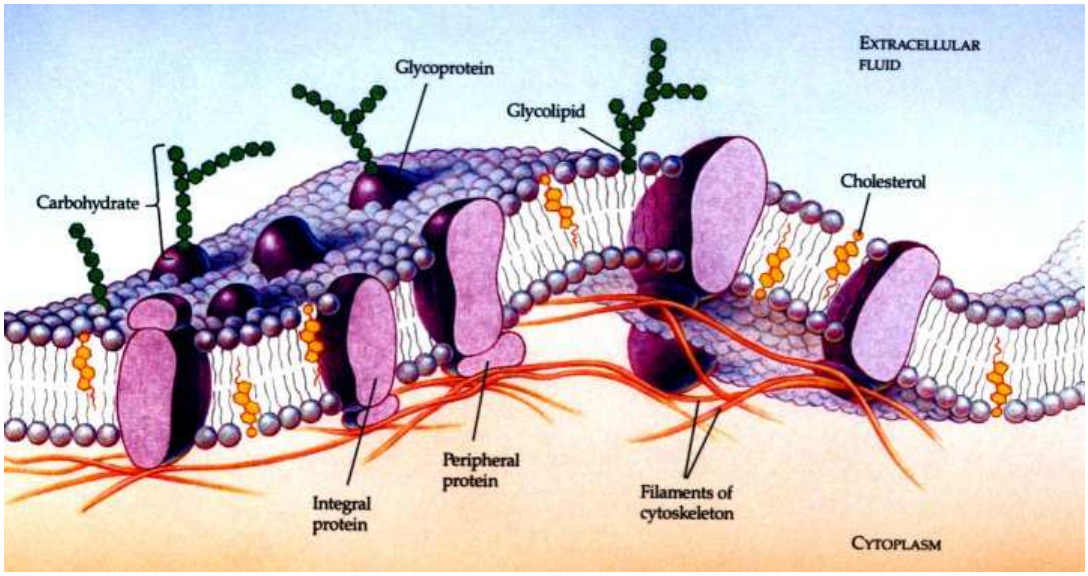

Figure 1.1 Schematic of a eukaryotic cell membrane with typical transmembrane constituents

1.2 Model membranes

Model membranes are simplified mimics of a cell membrane. Instead of using a variety of lipids, one or only a few types of lipids are used to form a model membrane which

allows studying biophysical and thermodynamic properties of a particular lipid in cell membrane. This also gives the possibility to examine the functional interaction between a specific lipid and a particular protein. Development of model membranes broadened the knowledge about the cellular processes down to the molecular level. The first and foremost types of model membrane system is black lipid membrane (BLM) developed in parallel with liposomes and lipid vesicles in the 1960s. Since then different types of artificial model membrane systems have been developed to study cellular processes such as transport of ions and molecules across the cell membrane, structure function relationship between membrane and integrated proteins and to exploit the nature of cellular processes such as cell signalling for biotechnological applications. Here in the following sections, the discussion is mainly focused on the type and development of artificial lipid bilayer membrane systems.

1.2.1 Black Lipid Membrane

Although lipid bilayer concept was dated back to three centuries by the time of R. Hook and I. Newton [4], the experimental realization of lipid bilayer research was only started in 1962 when P. Mueller et al formed a lipid bilayer suspended across an underwater loop (or a frame) with an area of up to 10 mm^2 [5]. In their technique known as Mueller-Rudin method, the lipid molecules were mixed with chloroform and painted over an aperture. A lipid bilayer was formed as the hole was brought inside the aqueous solution. When the solvent was evaporated and the lipid film reached to a minimal thickness of two molecules (figure 1.2), there was no reflected light under microscopic observation and hence it was named the Black Lipid Membrane (BLM) [6]. This type of BLM contained some solvents trapped inside and the effect of residual solvent altered the physical properties of the lipid bilayer [7]. About a decade later, an elegant way of forming a ‘solvent-free’ BLM by Mueller-Montal method was introduced [8]. In their method, lipids were first mixed with a solvent and spread at the air-water interface, allowing the self-organization of lipid monolayer. Usually Langmuir Blodgett (LB) method was used to compress the molecules at the air-water interface to result a suitable monolayer packing density [45]. Then the water surface was raised across a Teflon film containing a macroscopic aperture. This made the “zipping” of two monolayers and a planar lipid bilayer was formed across the aperture. The formation could be done by either rising the water surface carrying the monolayer film or dipping the Teflon partition vertically into the water (figure 1.3). Large planar lipid bilayers were formed

by modified Mueller-Montal method for better stability and the electrical parameters of the BLM were explored [9]. Although the latter method is termed solvent-free, there are still remaining solvent residues in the lipid bilayer. To eliminate the residual solvents, lipid bilayers were formed from glyceryl monoleate [10], phospholipids [11, 12] dispersed in low solubility squalene and monounsaturated monoglycerides and lecithins in n-hexane [13].

Basically, planar lipid bilayers are characterized by optical and electrochemical means. Physical appearance and formation of a lipid bilayer are observed by the reflected light through a microscope when the hole is illuminated. As thinning of lipid-solvent mixture is in progress, the reflected light appears by the light interference reflected from the water-lipid interface and that of phase-shifted from the lipid-water interface. Finally a black spot covers the hole when the complete lipid bilayer is formed. However the optical characterization does not provide the physical information of the bilayer. On the other hand, electrochemical measurement across the lipid bilayer in saline solution can reveal bilayer capacitance, resistance and conductance. Capacitance is related to thickness and quality of coverage of the bilayer while resistance and conductance reveal the electrical sealing quality of the bilayer. The latter is important because the successful voltage/current clamp measurement of a single-channel event through the transmembrane protein inserted into the planar lipid bilayer mainly depends on the quality of electrical seal [14]. Typically solvent containing BLM has a capacitance usually less than 0.6 $\mu F/cm^2$ while that of solvent-free BLM has about 1 $\mu F/cm^2$ which is close to the capacitance of real cell membranes (1.0 – 2.0 $\mu F/cm^2$). A decrease in membrane thickness for the hydrogen carbon region of the solvent-free BLM and exclusion of the hydrocarbon solvent in turn contributes to increase in membrane capacitance [15]. However, the resistance of a BLM in general is 1 $M\Omega\ cm^2$ ~1 $G\Omega\ cm^2$ which is typically higher than that of a cell membrane (< 1 $M\Omega\ cm^2$) probably due to in lack of membrane constituents in BLM [253].

Planar lipid bilayers are only 4 to 5nm in thickness yet they are able to form over the macroscopic holes with a few millimetres in diameter. Not like liposomes, they allow full electrical and chemical access on both sides providing the necessary condition for electrochemical characterization of membrane-bound proteins and lipid bilayer membrane by direct conductance measurement with patch clamping [16]. Since then, the electrophysiological response of lipid bilayer due to reconstitution of hemocyanin [17], alamethicin [18], neuronal acetylcholine receptor (nAChR) [19], *Staphylococcus aureus* α-toxin [20], gramicidin A [21], cyclodextrins [22], phospholipase A2 [23] and

bacterial porin (OmpF) [24] were studied and the voltage-dependent change in electrical conductance of the lipid bilayer by transmembrane constituents was demonstrated. Despite the advantages of planar lipid bilayer membranes, they are systems of local energy minima and tend to collapse in order to reach energy minimum [25] while the bilayer itself is vulnerable to external perturbations. The lifetimes of only a few hours [9] and mechanical fragility became major barriers for BLMs to be used in laboratory setups as a standardized method. In search for the better stability and longer lifetime of BLMs, a lot of efforts have been put into BLM research for many years.

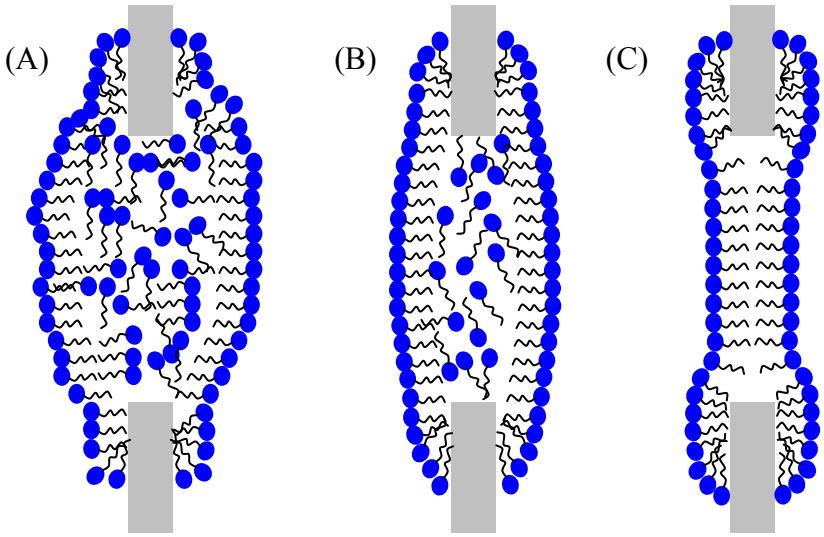

Figure 1.2 Schematic of sequential formations of BLM across an aperture by Mueller-Rudin method, (A) lipid-solvent mixture at the aperture, (B) lipid reorganization as the solvent evaporation continues and (C) final formation of BLM

It was found that the selection of material, thickness and diameter of the aperture played an important role in stability and lifetime as they affected the size and volume of annulus of BLMs [26]. To lower the surface tension and enhance the stability of BLM, crystalline bacterial cell surface (S-layer) protein lattices were used as a support on the microfiltration membrane [27] and a microporous Teflon septum [28]. Alternatively, BLMs encapsulated in hydrogel [29, 30], sandwiched between agarose gel [31] and supported on aerogel/xerogel surfaces [32] were explored. Increase in lifetime up to a few days and enhanced stability of BLM were achieved while possible reconstitution of toxin proteins were demonstrated. Nevertheless BLMs are still difficult to integrated, miniaturized and automated into practical sensing devices. These drawbacks of BLM were to be overcome by transferring them onto the solid supports and the new era of supported lipid bilayers was born [33].

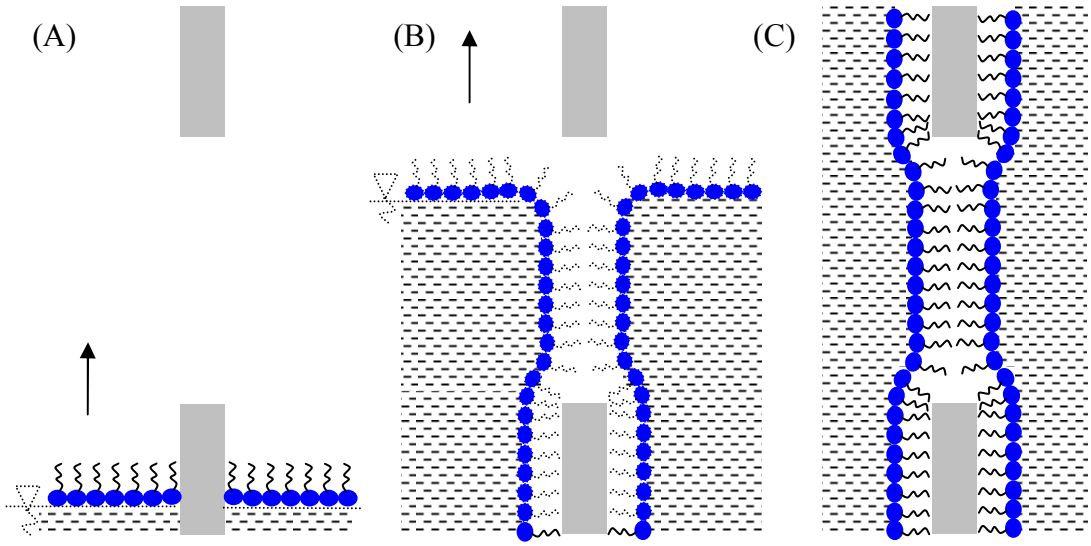

Figure 1.3 Schematic of sequential formations of solvent-free BLM across an aperture by Mueller-Montal method: (A) spreading and formation of lipid monolayer at air-water interface, (B) rise of water surface on both sides of an aperture and (C) final formation of BLM by "zipping" hydrophobic hydrocarbon chains of the monolayer on both sides across an aperture (arrow indicates the direction into which the air-water interface is raised)

1.2.2 Supported Bilayer Lipid Membranes

Lipid bilayer membranes when they are transferred onto a solid surface in an aqueous medium have several advantages over conventional BLM. First, mechanical stability is improved and membrane fluidity in most cases is not restricted. Second, supported bilayer lipid membrane (SBLM) can be characterized and analyzed by surface sensitive analytical tools such as atomic force microscope (AFM) [34, 100], surface plasmon resonance (SPR) [35], quartz crystal microbalance-dissipation (QCM-D) [36, 37] and electrochemical impedance spectroscopy (EIS) [38]. Most importantly, in combination with developed surface modification and advanced micro/nano-fabrication techniques, the study on lipid bilayer membranes opens promising possibilities in the future cell membrane research. Generally, SBLM can be divided into two major groups; directly supported and surface decoupled (tethered) types. The former can be either supported freely or in attachment. In freely-supported type, the lipid bilayer is neither anchored nor attached to but freely spread on the surface (glass, mica, quartz and gold). The lipid bilayer is separated by an ultra thin, 1 ~ 2 nm thick aqueous film from the surface. The aqueous film is balanced by electrostatic charges, van der Waals and hydration forces formed between the lipid polar head groups and the substrate surface [39]. Additionally, it serves as a lubricant and provides sufficient fluidity to the lipid bilayer membrane. In

the attachment-support type, the monolayer is first anchored directly onto the surface, for example, alkanethiol monolayer on the gold surface and the bilayer is completed either by fusion of vesicles or LB transfer of second monolayer [40, 45]. There is no aqueous film between SBLM and substrate surface while the lower leaflet of bilayer is laterally immobilized. This type is hence termed hybrid supported lipid bilayer which can be asymmetric in nature such as the lower leaflet is made of alkyl monolayer while the upper leaflet is composed of phospholipids. In both cases above, sBLM can be formed by both vesicles fusion and Langmuir Blodgett (LB) transfer [45] methods.

Vesicles fusion onto a hydrophilic surface is a common method of formation of SBLM however the mechanism with which the vesicles fuse onto the surface is still not fully understood at the molecular level. An AFM study in aqueous medium proposed the most possible scenario that the vesicles fusion occurred in several distinct steps such as vesicles adsorption, fusion of small ones to the large vesicles, rupture of each large vesicle into a bilayer patch and merging of bilayers patches subsequently on the surface [34]. After fusion of enough vesicles, bilayer sealing over the surface is getting better with time due to self-healing of voids and defects in the lipid bilayer. However some studies revealed that vesicles were not always fused onto the surface and just the formation of vesicles layer was also possible. Exact mechanism behind the vesicle fusion onto hydrophilic surface was not fully explained but it was found out in their study that it also depended on the type of lipid used [41].

How vesicles fuse onto the hydrophobic surfaces (either surface itself is hydrophobic in nature or a surface covered by a monolayer which is hydrophobic) is also not fully understood although there are many hybrid bilayers formed by vesicles fusion onto hydrophobic monolayers, for example, alkanethiol covered gold surface [40]. Among a few works to exploit the vesicles fusion process [42, 43], a proposed mechanism by E. Kalb et al is realistic and resonable [42]. In their proposal, the vesicles approached and adsorbed on the monolayer surface first and then the rupture of vesicles was initiated by hydrophobic interactions between the alkyl chains of monolayer and the outer surface of the lipids of vesicles. As the lateral spreading of monolayer started, disintegration of the vesicle took place due to surface tension within lipid bilayer of the vesicles leading to a complete fusion into a planar lipid bilayer on the surface. The latter is a type in which the lipid bilayer is decoupled from the surface by means of tethering or cushioning part in the monolayer and this type of lipid bilayer will be discussed in the following section.

There are many possibilities in formation of directly supported bilayer membranes depending on the type of substrate surface used, the choice of lipid, the method of

formation of mono/bilayers and the type of characterization techniques employed. Type of substrate surface is closely related to the characterization technique.

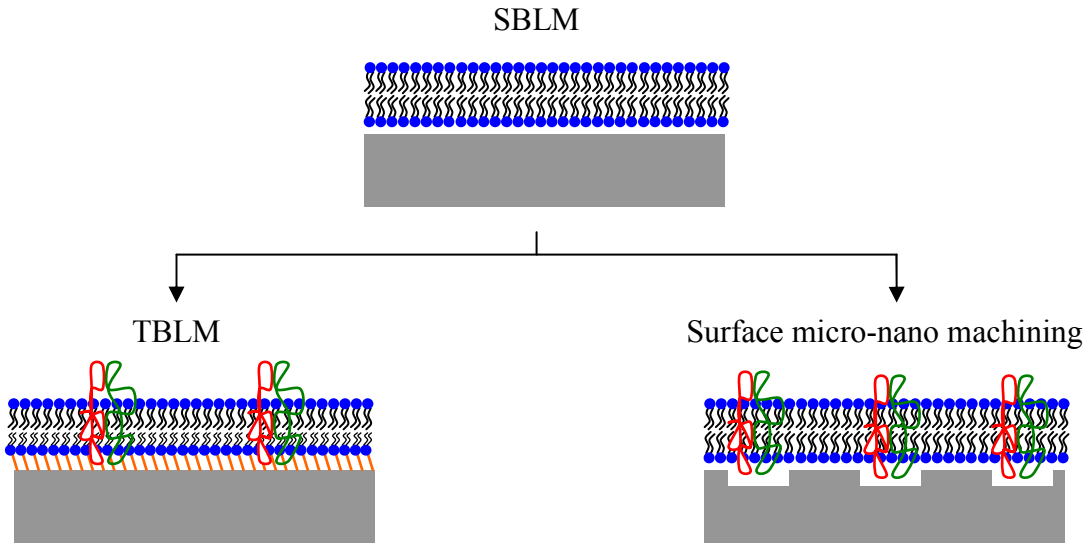

Figure 1.4 Schematic of supported bilayer lipid membranes (SBLM) modification into tethered bilayer lipid membrane (TBLM) and surface micro-nano machining with inserted membrane proteins (represented by red and green ribbons)

For electrochemical impedance measurement and scanning tunnelling microscopy (STM) analysis [44], a conductive surface is essential. But for scanning probe microscopic techniques, it requires the formation of SBLM on flat and smooth substrates such as polished silicon/silicon oxide or mica. In principle, surface flatness and smoothness plays a very important role on the quality of SBLM because the rough surface can distort the lipid bilayer. If the vesicles are fused onto a monolayer anchored on the surface, then surface roughness can result the defects in monolayer and the quality of subsequent bilayer is undermined. For this reason, common substrates used in SBLM formation are polished silicon, template stripped gold (TSG) and mica. Polished silicon, silicon oxide and silicon nitride surfaces have very low surface roughness (RMS<0.3 nm) and they are commonly employed in lipid bilayer research because of their compatibility with standard micro and nano-machining processes. Simplest yet the most common method of formation is either Langmuir Blodgett/Langmuir Schäfer transfer of lipid monolayer at air-water interface onto the surface or direct fusion by lipid vesicles. Formation also depends on the charged, neutral or zwitterionic natures of lipid especially when SBLM is formed by the fusion of vesicles which is induced by van der Waals forces and electrostatic interactions [42].

Both supported and hybrid bilayer lipid membranes are reliable and reproducible. Electrochemical impedance measurements indicate that they, regardless of different

membrane lipid compositions and the formation methods, have membrane resistance and capacitances which are comparable to that of planar lipid bilayer membrane [33, 38, 46]. This makes the supported bilayer lipid membranes useful in study and characterization of transmembrane proteins of cell membranes. However, most works done on SBLMs were on structural investigations, mechanism of formation, different lipids and different surface interactions etc by various characterization methods but practical application of SBLMs for example biosensor use, were limited mostly due to insufficient space between the bilayer and the substrate. This restricts for example, the insertion of membrane proteins which are likely to denature or unfold upon interaction with substrate surface. In case of hybrid supported bilayers, there is not even the space in between to accommodate the aqueous film making impossible for such bilayers to provide the natural environment for the membrane proteins. There were some applications of SBLMs for analysis of ligand-receptor binding and study of interaction forces between the cell and the bilayer membrane [33]. But extended applications of SBLMs are very limited and these situations demand the modification of supported lipid bilayers in two major ways. The first one is to decouple the lipid bilayer to provide the enough space for the lower ionic reservoir and the second one in an innovative way is to create engraved structures on substrate surface for aqueous space onto which the lipid bilayer is to be suspended (figure 1.4). Surface engraved structures are fabricated by standard photolithography and micro/nano-machining techniques.

1.2.3 Tethered bilayer lipid membranes

Early surface-decoupled lipid bilayer is the polymer cushion type in which the lipid bilayer is supported by a polymer network on the surface. An amphiphilic copolymer with hydrophobic lipid-like part, hydrophilic spacer monomers and a disulphide anchor group was synthesized and the copolymer network was covalently anchored onto the gold surface. Then the small unilamellar DMPC vesicles were fused in saline solution and the formation of bilayer was characterized with SPR [47]. Another group studied the lateral mobility of test proteins in polymer cushion lipid bilayers by fluorescence recovery after photobleaching (FRAP). Similarly, polyethyleneglycol lipid polymer with an anchor group designed to covalently attach onto quartz or glass surfaces was synthesized and bilayer formation was done by vesicles fusion [48]. Although lateral diffusion of Cytochrome b5 and annexin V proteins were observed, their mobility was partly hindered by viscous coupling with the polymer cushion network. Alternatively,

mobility of lipid bilayer cushioned by the lipopolymer layer film surface functionalized by photocross-linking with benzophenone silane on the glass substrate was studied by FRAP and the lateral mobility of lipid bilayer was restricted with increase in lipopolymer tethering density [49]. In general, polymer cushion lipid bilayer membranes are promising but there is a trade-off between the stability of the system and the lateral mobility of membrane proteins in the lipid bilayer.

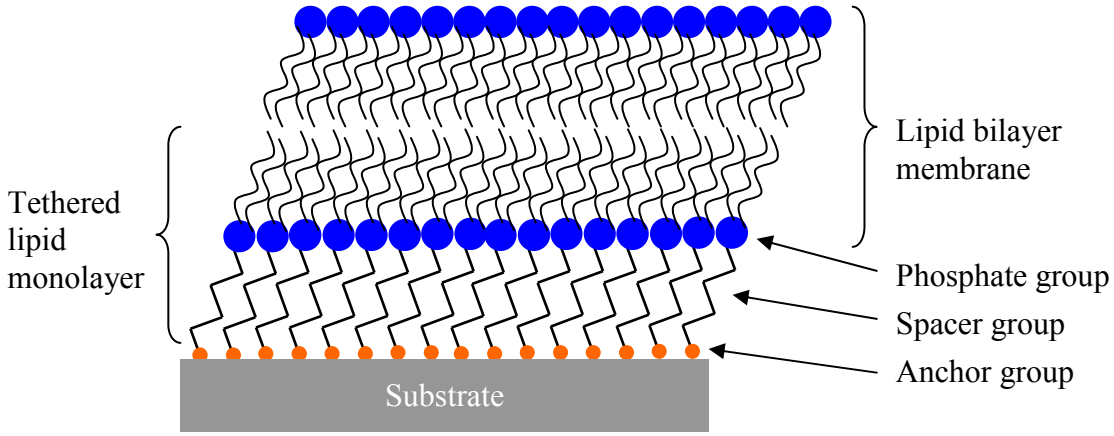

Figure 1.5 Schematic depiction of tethered monolayer lipid molecule after complete formation of tethered bilayer lipid membrane (TBLM)

Tethered bilayer lipid membranes (TBLMs) on the other hand, are a class of surface-decoupled bilayers but their significant difference from polymer cushion type is the hydrophilic spacer part of tethered monolayer which provides the aqueous space as an ionic reservoir in between the lipid bilayer and the substrate surface. Three distinct regions of a tethered monolayer are depicted in figure 1.5. Lower end of the molecule is terminated with an anchor group which can attach onto the surface. The flexibility is the use of disulfide or thiol ends for the attachment onto zero-valent metals such as gold, silver, platinum or copper and the use of silane derivatives for anchorage onto the surfaces terminated with O-H groups such as silicon and silicon oxide. An important part is a spacer region which decouples the lipid bilayer from the surface while providing an ionic reservoir underneath the membrane. It serves also as an elastic cushion to the lipid bilayer. Most importantly, it enables the insertion and the lateral mobility of large integral or peripheral proteins without losing their native conformation which is mostly impossible in SBLMs. Usually the spacer part is linked to the hydrophobic lipid tails via phosphate linker group which essentially separates the hydrophobic and hydrophilic regions in the tethered lipid molecule.

The first known thiolipid was synthesized and the formation of TBLM was studied by H. Lang et al [50]. Thiolipid was composed of two disulfide ends attached to the hydrophilic spacer and the two phospholipid chains coupled to the end of spacer by phosphate linker. Tethered monolayer was transferred onto the gold surface by LB method and the formation of lipid bilayer was completed by vesicle fusion onto the monolayer covered surface in an aqueous medium. SPR and EIS studies revealed the successful fusion of vesicles made of different phospholipids and electrical sealing (10^4~10^5 Ω cm^2) and capacitance (0.5 ~ 0.8 μF/cm^2) of the formed lipid bilayer was in agreement with the values of classical planar lipid bilayer membranes [15]. Most of TBLM were anchored onto the gold surface mainly due to nobility property, ability to support covalent bonds with both disulfide and thiol ends of the monolayer and the usefulness of gold surface as an electrode for the electrochemical modulation of lipid bilayer membranes. But, as an alternative, the formation of TBLM on silicon dioxide surface attached by the synthesized lipid molecules with monochloro- and trichlorosilane anchor groups was also demonstrated [51]. Electrical sealing of TBLM on the silicon oxide surface was comparable to the gold supported TBLM and the oxide film on highly-doped silicon surface was conductive enough to use as an electrode for analysis with EIS. Comparison on electrical sealing and capacitance of TBLM tethered on different surfaces via modified anchor and spacer groups were also reported [59]. It was reported that TBLM based on lipids with thiol-anchor provided a better seal resistance and relatively higher membrane capacitance compared to those of TBLM based on lipids with silane-anchor.

The space available for the ionic reservoir under lipid bilayer depends on the length of the spacer part which in turn affects the overall electrical capacitance of TBLM. This was studied using different model TBLMs formed by varying the spacer length of the tethered monolayer molecules [52]. Ion carrier valinomycins were integrated into TBLM and the carrier mediated ion transport across the lipid bilayer was demonstrated. Since there was almost no restriction to the lateral mobility of membrane-spanning proteins in TBLM, several groups have reported the results of TBLM with incorporated membrane constituents, ion channel Gramicidin A [51, 53], ion carrier valinomycin [51, 52, 54, 55], synthetic ligand-gated ion channel [56] and pore-forming α-toxin [57]. Interestingly, the long-term stability of the TBLM made of several thiolipid monolayer molecules on template stripped gold (TSG) surface up to three months was reported although the fluctuations in electrical impedance of TBLM with the time were observed [58]. In general, TBLM provides the membrane stability and sufficient fluidity which

are very important for insertion, lateral mobility and functional performances of the membrane proteins as they were in cell membranes. High electrical sealing and capacitance of TBLM are essential to be able to measure and record the tiny ionic current (a few pico-amperes) conducted by gatings of voltage-gated ion channels. Moreover, modifications of lipid monolayer molecules in their anchor group, and different types of surfaces that suit the method of characterization of lipid bilayer are possible. Both thiolipid and ethoxysilane based lipid monolayer molecules were employed in this work. Molecular structure in detail, formation and characterization of both thiol and silane based TBLMs were discussed in chapter 3.

1.2.4 Lipid bilayers on porous substrates

It was always desirable to combine the model lipid bilayer membranes with standard electrical, electrochemical, optical and surface analytical characterization techniques in order to realize the fast and accurate sensing at the molecular level for biosensing and biodefence applications. Knowledge of plant and animal cells acquired by basic research and studies for several years helped us to understand the structures and functions of the cells and their constituents to some extent. However, at the cellular level, for example, the knowledge on how membrane-bound proteins involve or link to diseases, how malfunctioning of the channel proteins of the cells initiates etc are still not fully understood [60]. Moreover many, but not all, ion channels are primary drug targets and several drugs developed were designed to treat the diseases by modulating ion channels in target cells. This required preliminary *in-vitro* study of specific ion channels to observe the effect of drug-assisted ion channel modulations and the lipid bilayer membrane based ion channel sensing platforms with high selectivity and sensitivity to specific analyte molecules are in highly demand.

Direct electrophysiological measurement across the cell membrane dates back to early 1980s when Neher and Sakmann used a miniature glass micropipette tip, later it was known as “patch clamp technique”, to clamp the membrane patch of a cell electrically and the single channel current across the cell membrane was recorded [61]. In their pioneer work, the micropipette tip was brought to physical contact with the cell membrane by the control of micro-manipulator. Under microscopic observation, negative suction pressure was applied from the pipette to create the seal which provided an electrical resistance in excess of 10^9 Ohm between the pipette tip and the cell membrane. By varying applied electrical voltage from micropipette containing saline

solution, the ionic current (in the order of 10^{-12}A) through ion channels trapped in the cell membrane patch was recorded. Their pioneer work was won a Nobel Prize in Physiology or Medicine in 1991. Interestingly, a group reported the use of nano-pipette tip (with approximate opening of ~200 nm in diameter) for scanning and simultaneous recording on a relatively small cell such as sperm cells [96]. In their so called 'smart patch-clamp system', the nano-pipette tip connected to three-axis piezo actuator was used to scan over the cell surface. Then the electrical seal was created by applying suction onto the cell membrane at the place of interest and the recording was carried out.

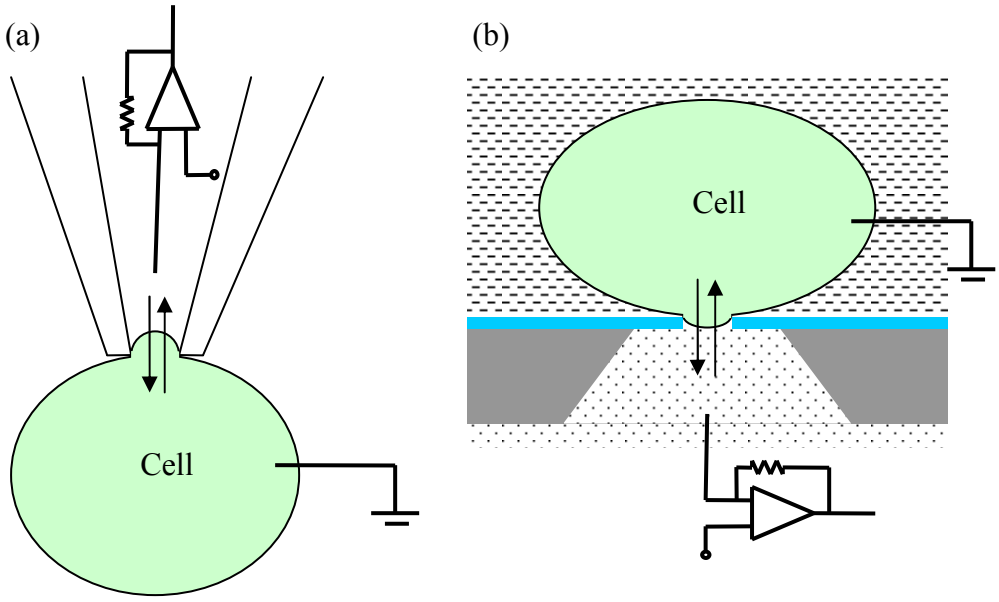

Figure 1.6 Schematic of (A) micropipette patch clamping (MPC) and (B) planar patch clamping (PPC)

Although patch clamping using a micropipette is powerful and single ion channel recordings are demonstrated, there are many disadvantages and restrictions for the realization of the technique as a standard recording method for future use. It requires highly trained personals to conduct the experiment while throughput of the successful experiment is very low. Moreover in pipette-based patch clamping, the cell and its membrane are not easily accessible by other physical means and this is a major drawback especially in combining it with optical, fluorescence and scanning probe microscopy methods. All these factors were driven forces in search for the successor, planar patch clamping (PPC) which provides relatively higher throughput and better compatibility with analytical experimental techniques [63]. Planar support also allows

the possible integration of patch clamping chip with micro-fluidic devices. The schematic mechanisms of both techniques are depicted in figure 1.6.

In PPC, the cumbersome micropipette was replaced by a planar support in which a micro hole is machined for sealing the cell membrane as shown in figure 1.6B. Instead of positioning a pipette on the cell, the cell suspension is placed on the surface with micro aperture. With the aid of a microscope, a single cell is then position on the hole by applying the suction below the surface through the hole and electrophysiological recording usually is done by electrodes connected to the patch clamp amplifier. Type of planar surface can be polyimide film [62], micro-machined glass surface [63], micro-porous silicon nitride membrane and silicon substrates [64, 67, 94], lithographically structured photoresist film [65, 66, 68] and porous alumina substrate [74]. Except the experiments in references [62, 67], the rest were studied using model lipid bilayer membranes because of promising possibilities to chip-based biosensor devices in future [99].

Successful patch clamping experiment solely depends on the seal between the lipid bilayer and the surface because the current leaking through the seal in parallel to the ion channel creates noise in signal recorded [14]. If the noise signal is high enough compared to the measured signal, it is difficult to measure the response of ion channels with low conductance. Sordel et al demonstrated the planar patch clamping using the surface machined silicon micro-pits with real cell lines. It was reported that the sealing of the cell membrane to the surface was improved by coating the surface with plasma deposited silicon dioxide layer [67]. Pantoja et al formed a painted lipid bilayer across 50 ~ 200 μm diameter holes in 200 μm thick silicon substrate with surface silicon oxide layer [69]. Maxi K ion channels were integrated into the lipid bilayer formed across 100 ~ 200 μm diameter holes and ionic current were measured. Capacitance and resistance of the suspended bilayer were 0.4 ~ 1μF/cm^2 and above 5 GΩ respectively. However, the use of silicon as a support imposed some problems: additional capacitance due to the free charge carrier density of silicon introduces electrical noise and several groups explored the glass substrate as an alternative to silicon. An attempt was made to reduce the intrinsic noise associated with the silicon substrate by patterning with SU-8 resist around the micropore [73] and RMS noise level was significantly decreased by a factor of four. On the other hand, the major challenge with glass substrate is its incompatibility with silicon micro-machining techniques. A group explored the method of glass micro-machining by irradiation of a glass substrate (80 μm thick) with a single heavy ion and subsequent wet track etching [70]. The bilayer capacitance was in the order of 0.5 μF

cm^{-2} and bilayer diameters of 1 ~ 5 μm, the capacitance reduced to very low noise level of 5 ~ 100 fF. Lipid bilayer made of DPhPC lipid was formed across the micropore by painting method and the seal resistance of the bilayer on the glass surface was in the range 1 ~ 100 GΩ. However the bilayer only lasted for a few hours. Such a micropore suspended lipid bilayer rupture process was studied by Weiskopf et al [72]. Fluorescently-labelled hybrid lipid bilayer membrane was suspended over fabricated 7×7 μm^2 microholes in the gold coated silicon substrate and the bilayer rupture process was observed by fluorescence microscopy and impedance spectroscopy. It was found out that the thiol or silane functionalization of lipid bilayer on the silicon surface did not influence the rupture process significantly.

When a lipid bilayer is suspended over a microscopic pore, then the stability and lifetime of the pore suspended bilayer mainly depend on the two major factors: how the lipid bilayer is attached onto the surface and what the method of bilayer formation is used. This was explored by Steinem's group from Germany [94]. In their work, two types of micropore suspended lipid bilayers were employed. The first one was an asymmetric hybrid bilayer in which the lower leaflet was chemisorbed on the Au coated surface (analogous to figure 1.7B) and the second one was a symmetric lipid bilayer just simply suspended over the porous surface (analogous to figure 1.7C). In both cases, the substrate was porous silicon substrate with array of 1 ~ 2 μm in diameter pores. It was found that the first type of lipid bilayer lasted for about three days with the seal resistance of above 1 GΩ while there was not enough electrical seal formed over the substrate in the second type, freely suspended lipid bilayer. There was always a thin aqueous layer below the lipid bilayer when the bilayer was directly supported on the hydrophilic surface [39]. In-plane ionic conductivity of such ~1 nm thick water film trapped on the single microporous glass substrate below the POPC lipid bilayer was examined [71]. It was reported that the conductivity of the aqueous layer was nearly independent of the concentration of bulk buffer solution, KCl in this case. In above studies, the lipid bilayers are suspended over the microholes ranging from a few microns to 500 μm in diameter, but in general, only a few nanometres thick lipid bilayer suspended over such microholes is vulnerable and sensitive to perturbations such as mechanical vibrations, electrical disturbances. Therefore the lipid bilayer is very fragile and only survives for a few minutes to hours after formation. Moreover, electrical capacitance of the lipid bilayer is increased with the size of the pore over which it is suspended. It is desirable to keep the bilayer capacitance low enough to minimize the capacitive associate noise for better resolution in ion channel recordings. This requires

decreasing aperture size to submicrometer to improve mechanical and electrical stability to increase the lifetime of the pore-suspended lipid bilayer membranes.

1.2.5 Nanopore suspended bilayer lipid membranes

With the progress and development of nanofabrication methodologies such as focus ion beam (FIB), electron beam lithography (EBL) etc, the miniaturization of surface patterns down to submicrometer scale is easily achievable. This is very advantageous to combine the nano-structured surfaces for example, nanopores, with the lipid bilayer membrane systems and it becomes significantly important for the advances in current and future lipid bilayer research [99]. With enormous efforts to put the lipid bilayer devices for automation and practical applications, portable nanoporous chips carrying the lipid bilayers for fast and efficient sensing is very promising. Nanopore suspended lipid bilayer membranes can enhance stability and lifetime and this exciting research has been pursuing by different groups. The choice of substrate to host the nanoporous surface depends on the type of nanofabrication and the selection of lipid bilayer anchorage on the surface. Silicon nitride films [75, 76, 77] were commonly used in their ease in nano-machining but the use of anodic porous alumina (AAO templates) [78, 79] and glass chip [80] were also used alternatively. All the substrate surfaces have pros and cons. Silicon nitride has high capacitance (and noise) inherited by the semiconductive nature but chemical inertness and low aspect ratio (thickness to size) of Si_3N_4 films are excellent. With today's powerful FIB or EBL methods, nano pores with a diameter of less than 10 nm are possible to produce [81, 82]. More importantly there is an absolute control over pore size and periodicity at the nanometre scale. On the other hand, anodic alumina and glass substrates have comparatively lower capacitance and noise [70] however the reduction in pore size below 50 nm is almost impossible.

First report believed to be the study of isolated cell membrane patches over nano holes (50 ~ 500 nm in diameter) fabricated in free standing Si_3N_4 membrane [75]. The cell membrane was marked with fluorescent marker bisoxanol and characterized with confocal laser scanning fluorescence microscopy. Another group also reported the study of cell membrane patches positioned over the 50 ~ 600 nm diameter nanopores in Si_3N_4 membrane [76]. The planar cell membrane sheets of living cells were press-adhered and transferred onto the nanoporous surface in Si_3N_4 membrane. Again accessibility to both sides of the membrane patches was visualized by fluorescent markers but no electrochemical characterizations were reported. An interesting study was finally

reported on the study of model lipid bilayer membrane suspended over the nanopores in Si_3N_4 membrane [77]. Array of 300 nm diameter nanopores were milled in a thin freestanding Si_3N_4 membrane and the chip was silanized to promote the spontaneous formation of lipid bilayers within the nanopores. DPhPC and POPC lipid bilayers were formed across the nanopores by painting method and the formation was characterized by electrochemical impedance spectroscopy. Both lipid bilayers yield the mean resistance above 10 GΩ and capacitance of about 1 $\mu F/cm^2$ as of formation. The existence and functionality of the lipid bilayers were proved by incorporation of ion carrier Valinomycin. Impedance measurement indicated that the lipid bilayer (without Valinomycin incorporation) resistance decreased with time and it reached to about 100 MΩ after about 160 hours in the case of DPhPC lipid bilayer. This type of lipid bilayer can be considered as nano-black lipid membrane because the lower leaflet of the bilayer interacts with silanized surface within the nanopore while the upper leaflet interacts with the silanized surface above the nanopore. There was annulus region depicted with lipid aggregates at the edge of the nanopore [77].

Steinem's group from Germany continuously worked with the anodic nanoporous alumina substrate. In their study [79], a porous alumina substrate with pore diameters ranging from 55 ~ 280 nm was first selectively coated with a thin gold layer (7 mm^2 area) and the hydrophobic monolayer DPPTE was chemisorbed, to form the lower leaflet of lipid bilayer. Then the lipid DPhPC in n-decane was painted over the DPPTE monolayer in aqueous medium and the hybrid asymmetric lipid bilayer was formed. Although the term nano-BLM was used, the bilayer was suspended over the entire surface over the nanopores. It was understood that the symmetric DPhPC bilayer was formed over the nanopore while asymmetric DPhPC+DPPTE bilayer was on the Au support. The suspended bilayer was characterized by impedance measurement. Initial membrane resistance and capacitance went up to 7 GΩ and 11.7 nF respectively but the resistance went down to ~ 1 MΩ after 120 hours as the suspended lipid bilayer degenerated slowly with time until the final rupture. However before the entire rupture of suspended lipid bilayer membrane, incorporation and ionic conductance gatings of ion channel gramicidin and alamethicin were demonstrated.

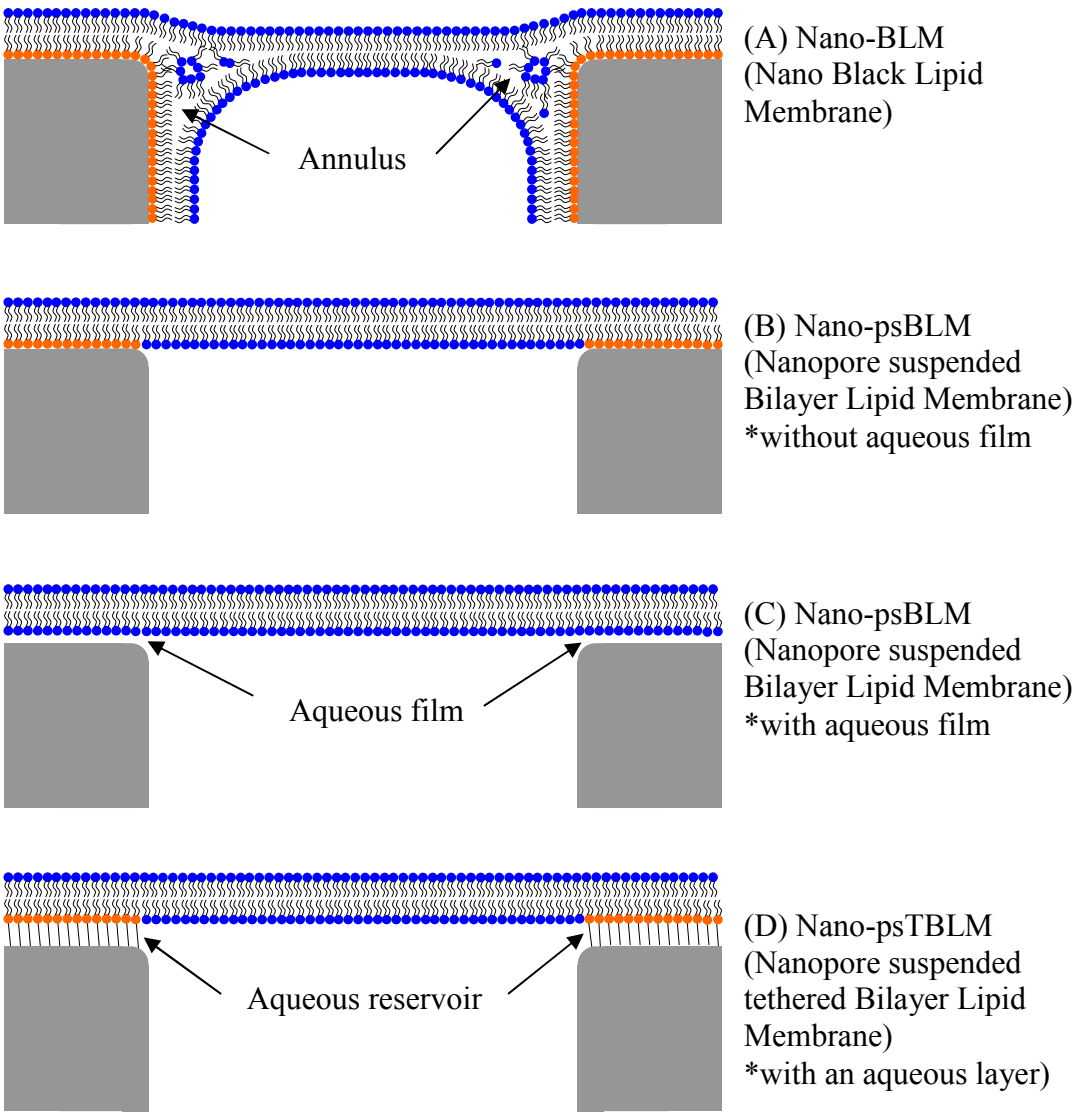

Figure 1.7 Different nanopore suspended bilayer lipid membranes (A) Nano-BLM (black lipid membrane formed by Mueller-Rudin method across a nanopore pre-functionalized with hydrophobic monolayer: note that there is a solvent-filled annulus encircled the bilayer and suspended BLM is symmetric), (B) Nano-psBLM (bilayer lipid membrane suspended over the nanopore with the surface pre-functionalized by hydrophobic monolayer: note that there is no aqueous film between the surface and the bilayer, suspended bilayer is usually symmetric and bilayer formation can be done by both vesicles fusion and LB transfer), (C) Nano-psBLM (bilayer lipid membrane suspended over the nanopore by LB or vesicles fusion: entire bilayer is symmetric and there is an aqueous film between the surface and bilayer membrane) and (D) Nano-psTBLM (tethered lipid bilayer suspended over the nanopore: suspended bilayer is symmetric and the spacer region is wide enough to support the membrane fluidity and lateral mobility of the inserted proteins)

The same group reported the use of porous alumina substrate again but with the smaller pore diameter (60 nm) with the same type of suspended DPPTE+DPhPC bilayer [78]. The outer membrane protein OmpF of *E. coli* pores were incorporated into the lipid

bilayer and single channel recording was monitored by impedance analysis. Additionally, the blockade of flow of ion passage upon interaction of the antibiotic ampicillin with OmpF was verified. Regardless of more uniform and smaller pore sizes, the lifetime of the suspended lipid bilayer was within a day. The resistance of the lipid bilayer was above 1 GΩ for up to 8 hours and the mean specific capacitance measured was 0.4 ± 0.1 $\mu F/cm^2$. So far the lifetime and stability of the nanopore suspended lipid bilayer was satisfactorily achieved by a group using so called glass nanopore membrane (GNP) [80]. A conical shaped single nanopore with the pore diameter ranging from 200 ~ 800 nm was fabricated in 50 μm thick glass sheet at the end of the glass capillary. The glass nanopore was then chemically modified with a 3-cyanopropyldimethylchlorosilane monolayer to produce the hydrophobic glass surface. DPhPC or POPC lipids mixed in decane was painted over the nanopore and the free standing planar lipid bilayer was formed across the nanopore. This was Mueller-Rudin method and hence the lipid bilayer contains solvent especially at the annulus region. Due to an excellent sealing of lipid acyl chains against the glass surface, membrane seal resistance as high as 70 GΩ with the breakdown voltage of ~0.8 V was achieved. Bilayer formation was tested with the subsequent insertion of wild type α-Hemolysin ion channels and stochastic detection of a small molecule, heptakis (6-O-sulfo)-ß-cyclodextrin. Additionally, insertion and removal of single α-HL channels induced by hydrostatic pressure difference across the lipid bilayer was successfully demonstrated. Importantly, the lifetime of such planar lipid bilayer was tested by monitoring the seal resistance and it was claimed that the bilayer was stable up to two weeks.

Apart from electrochemical impedance characterizations, lipid bilayers supported on mica and porous silicon substrates [100], nanoporous Si_3N_4 membranes [97] were topographically examined by AFM. Force spectroscopy measurements on DMPC and DPPC lipid bilayers directly supported on mica and porous silicon substrates revealed the effects of the underlying substrate and of the lipid phase transition [100]. An interesting work on examination of the stability of nanopore spanning lipid bilayers probed by AFM tip with local indentations was done very recently [95]. Two types, solvent-containing Nano-BLM (analogous to figure 1.7A) on hydrophobic porous silicon substrate and solvent-free directly supported Nano-psBLM (analogous to figure 1.7C) on nanoporous silicon substrates were employed. It was observed in their study that the Nano-BLM was higher in membrane spring constant due to possible pre-stress and they were ruptured easily upon indentation with AFM tip. On the other hand, pre-stress in Nano-psBLM was significantly less and as a consequence lateral tension and

bending dominated the mechanical response upon indentation. No ruptures of Nano-psBLM by AFM tip indentation in their experiments were observed. There is no doubt about that the formation, stability and lifetime of the nanopore suspended lipid bilayers strongly depend on the type and surface chemistry of substrate. It is also closely related to the number and the size of the nanopores. There are two types of lipid bilayer when it formed across/over the nanopores; with and without the existence of annulus region.

Hence the correct termed for the one with the annulus should be the nano black lipid membrane (Nano-BLM) [77, 80]. Second type is just simply suspended over the nanopore without the existence of the annulus and it should be the termed nanopore suspended bilayer lipid membrane (Nano-psBLM) [78, 79] (see figure 1.7 for schematic comparison of different nanopore suspended bilayer lipid membranes). Major advantage of the glass surface is its ability to provide an excellent seal with the lipid bilayer if the lipid tails were oriented towards the glass, for example Nano-BLM in reference [80]. When Nano-psBLM was formed over the glass surface by direct fusion of vesicles, the lifetime was not reported but it was doubt that it would be last as long as the one in reference [80]. Although lifetime and stability of Nano-BLM was improved, nano-structuring of glass membrane was still difficult and most importantly such a glass capillary was not easily integrated to or compatible with the current platform of sensing and automation techniques. On the other hand, the main drawback of the porous alumina was possible parallel leakage of the current across the pores which were uncovered by the lipid bilayer or the bilayer ruptured pores. This is due to the lack of control over the formation of number of pores in the alumina substrate. Moreover control insertion of channel proteins was difficult because of relatively large area occupied by the lipid bilayer over the pores. If the asymmetric bilayer was formed by monolayer directly anchored on the alumina surface, the lateral mobility of the proteins was hindered over the alumina surface and possible denature or unfolding of inserted proteins upon contact with alumina substrate was possible. This might be the reason for the use of relatively small channel proteins such as gramicidin [79] and OmpF [78] in experiments with Nano-psBLM. Such systems are not suitable to work with channel proteins with large external membranous domains such as α-Hemolysin toxin channels [83].

In contrast to glass and alumina substrates, Si_3N_4 has many advantages. Single or multi nanopores with the pore diameter down to sub 100nm can be easily achieved in Si_3N_4 membrane with either EBL or FIB. Sub 100 nm diameter pores can also be produced in porous alumina but control over number of pore and pore size uniformity is not

possible. Glass substrates traditionally encounter difficulty in forming a relatively thin free-standing film compared to a Si_3N_4 membrane (thickness <50 nm). Therefore, it is almost impossible to mill a nanopore through a few microns thick glass substrate with standard FIB or subsequent micromachining with EBL. It always requires cumbersome, irregular methods even to create the submicron holes in glass substrate/membrane [70]. Aspect ratio (i.e. the ratio of pore height/depth to diameter) can be as small as 1 or even less in Si_3N_4 membranes but aspect ratio of porous alumina is as high as 40 [84] and so is the glass membrane. Small aspect ratio nanopores provide better access to both sides of the suspended lipid bilayer. Finally, in term of surface roughness, polished Si_3N_4 membrane surface is much superior to that of the glass and porous alumina. Minimum surface roughness is mostly desirable because of its influence on the formation of a quality, high packing density monolayer if the lipid bilayer is either hybrid tethered or asymmetric type. The only possible drawback of the Si_3N_4 membrane is its high membrane capacitance and associated noise accompanied by its semiconductive nature of silicon. But some prior works have already successfully demonstrated that the high capacitance and noise can be reduced to a minimum level at which it has no interference with the measured signal [67, 85].

1.3 Bacteria

Bacteria are unicellular microorganisms, most abundantly found everywhere on earth. They live in and on other living systems, and form a variety of biological associations with other bacteria as well as other kinds of living things. Bacteria are prokaryotes and unlike eukaryotes and animal cells, they lack nucleus and other membrane-bound intercellular organelles such as mitochondria and endoplasmic reticulum. A bacterial cell generally has only three types of intracellular components – nucleoid, ribosomes and plasmids. Genetic material is a single circular chromosome stored in nucleoid. It contains the chromosome with associated proteins and DNA. Ribosomes are sites of proteins synthesis while plasmids are double stranded circular molecules, separated from nucleoid, carrying additional DNA for bacterial cell divisions and reproduction [101]. The cell membrane of bacteria is usually covered by a thick cell wall which protects the bacteria against immune system and antibiotic agents. Bacteria are collectively maligned as the cause of various diseases to human and animals. The fact is that many, but not all, bacteria are harmless while some are even beneficial to living organisms. Only a few bacterial species are pathogenic i.e. responsible for a range of

diseases - from simple infections like strep throat to life threatening diseases such as pneumonia to humans [102].

1.3.1 Classification of bacteria

Most clinically prominent and microbiologically important bacteria are collected, identified and grouped based on their size and shape, requirement of oxygen for respiration, role of temperature for their growth, intake of nutrients for their survival and by Gram staining of bacterial cell wall. Correct identification is important for precise diagnosis and effective treatment in case of diseases due to the bacterial infection.

1.3.1.1 Cellular morphology

Bacteria display different sizes and shapes. In general their size ranges from 0.5 to 5 μm, about ten times smaller than the size of a typical eukaryotic cell. The small size allows some of them to be able to live inside the host cells of plants and animals. In case of pathogenic bacteria i.e. the bacteria responsible for causing several diseases, this can be beneficial as they can access plenty of host nutrients and get protection against the defence mechanisms of the host. Then they are termed – intracellular pathogens (e.g. *Chlamydia* and *Rickettsia*). On the other hand, extracellular pathogens living outside the host cell have many opportunities for growth, reproduction and dissemination. Bacteria generally form into three basic shapes when they are observed under a microscope i.e. coccus, bacillus and spirillum. Coccus (plural: cocci) is spherical or nearly spherical in shape, bacillus (plural: bacilli) is in the form of a cylindrical rod and spirillum (plural: spirilla) is in tightly-coiled spiral-shaped configuration [102].

Such varieties of shapes are controlled by the cell wall and the cytoskeleton. The shape of bacteria plays an important role in their attachment to surfaces, formation of biofilm, acquiring nutrients and movement of bacteria. Aggregation of bacterial cells naturally occurs on the surfaces and this gives another classification and identification that provide the particular information on the type of bacteria. When cocci grow two-dimensionally along one axis in a chain configuration, they are called Streptococci and if they grow all dimensionally in a group and form a cluster then they are named Staphylococci. The clinically important *Staphylococcus aureus* forms grapelike clusters and hence they belong to the group of staphylococci. Cellular morphologies of common bacterial cells and their forms of aggregation are schematically represented in figure 1.8.

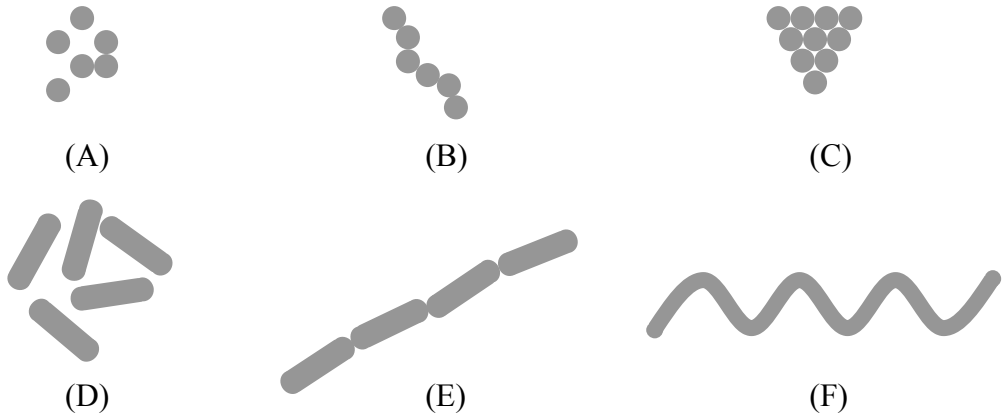

Figure 1.8 General morphologies of bacteria (A) cocci, (B) Streptocci, (C) Staphylococci, (D) bacilli, (E) Streptobacilli and (F) spirillum (Note: minority bacteria with other morphologies are not depicted)

1.3.1.2 Effect of oxygen

Presence or lack of oxygen plays an important role in growth and survival of bacteria. Therefore bacteria show the varying tolerance to oxygen i.e. air. Some bacteria are *aerobic* as they need the presence of oxygen for their existence while some are *anaerobic* i.e. they do not require oxygen for their survival at all. Anaerobic bacteria, in principle cannot exist in oxygen containing environment but there is no precise line to which the presence or absence of oxygen can matter the survival of bacteria. This is because a few bacteria can tolerate a tiny amount of oxygen although they are anaerobic, so they are classified as *aerotolerant.* Some bacteria thrive in the environment regardless of present or absence of oxygen and they grow very well in either environment. They are regarded as *facultative*. Even in the group of aerobic bacteria, some requires only a minute amount of oxygen in their surroundings to grow. They are known as *microaerophilic*. Apart from oxygen, many bacteria prefer carbon dioxide as their primary respiratory gas and many pathogenic bacteria grow better in an environment containing 4 % to 9 % of carbon dioxide. Classification of bacteria related to oxygen is usually tested by test tube method [103].

1.3.1.3 Role of temperature

For the optimum growth and reproduction, bacteria basically depend on the temperature of environment where they present. In general bacteria are tolerable to a fairly broad range of temperature. Pathogenic bacteria exhibit a relatively narrower range of temperature for their growth and survival compared to non-pathogenic species. As the

bacteria are microorganisms, lower temperature extends and higher temperature shortens their lifespan and they are even killed at extreme temperature. However requirement of temperature vary from bacteria to bacteria depending on their environmental conditions, for example, human intestinal bacteria grow very well at the body temperature (i.e. 37 ºC). In microbiology, the growth and survival of most bacteria depend on three temperatures namely minimum, optimum and maximum temperatures. Minimum temperature is the lowest temperature at which the bacterial growth can occur and this can be varied for species of bacteria. Optimum temperature is the temperature at which a particular bacterium can grow well and reproduce optimally. Most human pathogens such as *S. aureus*, *Pseudomonas aeruginosa* and *Escherichia coli* grow the best at 37 ºC which is their optimum growth temperature. Maximum temperature is defined as the highest temperature at which the bacteria can survive. Most bacteria cannot survive above the maximum temperature as the extreme heat eliminates all the microbes with the exception of some microorganisms including bacteria which can thrive at extreme temperature and pH environments (e.g. in hot springs). These minorities are classified as *extremophiles* in general. All these temperatures depend again on different bacteria species [103]. This knowledge has been utilized for a long time in hospitals such as sterilization of surgical instruments for operation. In laboratory the microbes including bacteria are killed by exposing them to a high pressure steam in a process called autoclaving.

1.3.1.4 Intake of nutrients

In term of nutrients, bacteria cannot be collectively regarded as parasites because some types of bacteria can produce their own foods themselves. They are self-sufficient and known as *autotrophs* which can covert carbon dioxide and water into organic molecules (nutrients) they require. But most of pathogenic bacteria are considered as parasites because they exploit and utilise the nutrients from the host cells they invade and hence they are identified as *heterotrophs*. All heterotrophs are medically important as most of them are responsible for causing diseases.

1.3.1.5 Gram staining

Bacteria can be classified depending on structure and composition of the plasma membrane i.e. the outer layer of the bacterial cell wall. Gram staining method, developed by a Danish Physician, Dr. H.C.J. Gram in 1884, divides the bacteria into

two distinct groups: Gram-positive and Gram-negative bacteria. Cell wall of bacteria is mostly composed of peptidoglycan which is either thick and continuous or thin and discontinuous. During the staining process, bacterial cells take up Crystal Violet and iodine which form a complex inside the cell wall. Gram-positive bacteria have a thick mesh-like cell wall with 50 – 90 % of peptidoglycan composition which can retain and trap the complex dye inside the cell wall. This is revealed in purple colour after decolourization and counter staining. On the other hand, thin and discontinuous peptidoglycan layer of Gram-negative bacteria does not impede solvent extraction of the dye complex and exhibits pink colour. Therefore Gram-staining distinguishes the two basic structures of bacterial cell wall, which is closely related to toxigenesis of Gram negative pathogenic bacteria species. However, this technique is unable to differentiate some bacteria which are insensitive to Gram staining and they belong to either Gram-variable or Gram indeterminant groups. Nevertheless, Gram staining played an important role in quick and efficient determination of bacteria until the modern microbiology developed more specific and information-rich methods of bacteria classification such as genetic sequencing and other molecular techniques.

1.3.2 Growth and reproduction

Bacterial reproduction is the multiplication of bacterial cells by a process of binary fission. For growth and reproduction of a bacterium, the nutrient and the temperature play an important role. In an environment with sufficient nutrients and optimum temperature, bacteria grow and reproduce very well. In laboratories, bulk bacterial cell culture is usually taken place in the stirred liquid or solid nutrient medium in an incubator at 37 ºC. As the bacteria divide themselves, the resulting cells are genetically identical to their mother cells if no mutation occurs during their growth. When bacteria are grown in a controlled environment, they exhibit four different phases differentiated by the number of bacteria in bulk medium. The growth of bacteria is described as different phases in bacterial growth curve. In the beginning, bacteria do not grow and reproduce as they start adapting to the new environment. This is known as the lag phase (see figure 1.9). In exponential phase, bacterial population doubles with time as they reproduce quickly on expense of the available nutrients. As the new cells proliferate and the rate of cell division is much higher than the rate of cell death, cell growth produces a straight line with positive slope in growth curve (figure 1.9). The slope, essentially the

bacterial growth rate, represents the number of division per cell per unit time and it varies according to each growth conditions and species of bacteria.

In culture with constant capacity of nutrient medium, the exponential growth stops at a certain time as the limited nutrients are depleted and the metabolic wastes (mostly toxins and byproducts of metabolism) are accumulated. This causes the growth to enter into stationary phase where the rates of growth and death of bacteria are equal. Finally the death phase occurs and the population of living bacteria decline quickly as a result of short of nutrients. During death phase bacteria die and the medium with death bacteria contains most of bacterial toxins and metabolic wastes. Figure 1.9 depicted the growth curve of a bulk bacterial culture indicating distinct transitions between phases. The four phases in real bulk bacterial culture are sometime not well defined and the growth curve exhibit non-ideal configuration. However, the real growth curves of bacteria follow the general shape of schematic growth curve in figure 1.9.

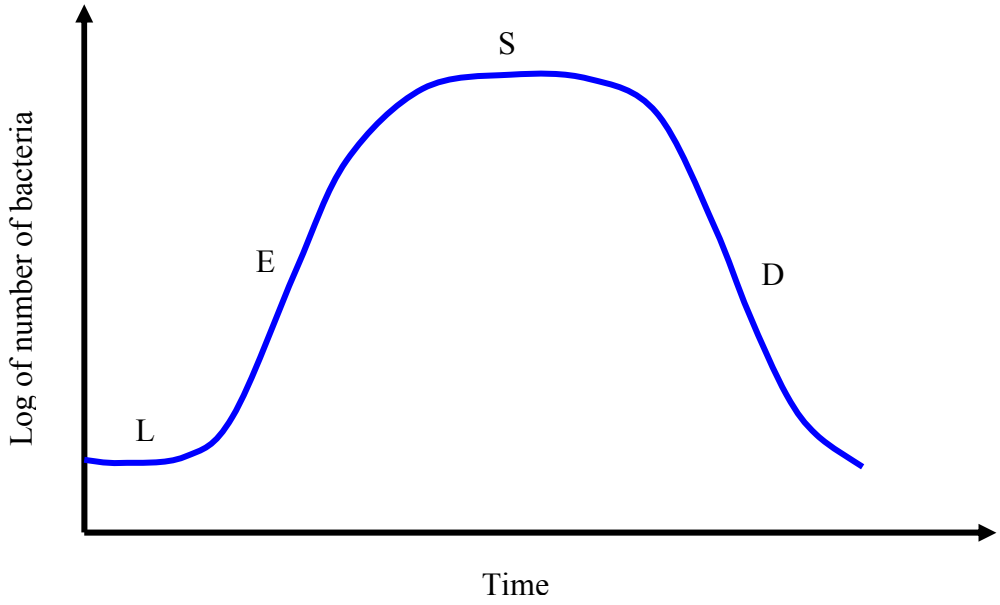

Figure 1.9 A typical bacterial growth curve with different phases: L – lag phase where bacteria adapt to the environment without growth, E – exponential phase where the bacterial cells grow logarithmically, S – stationary phase where the rate of growth and death are equal and D – death phase as the bacterial population declines due to shortage of nutrients

1.3.3 Commensal bacteria

Commensal bacteria are parts of normal flora which harbours on and inside the bodies of human and animals. In human, they commonly reside in saliva, oral mucosa, in the gastrointestinal tracts, on and under the surface of the skin. Some of them are involved

in metabolic processes which are beneficial to the host but, under normal circumstances the majority of commensal bacteria are not known to be beneficial or harmful [101]. However some bacterial flora with mutated strains can be harmful to the host. Among bacterial flora, *E. coli* is known to be commensal bacteria mostly resides in colon but under certain condition, *E. coli* with mutated strains, for example, *E. coli* O157:H7 can change to human pathogen and cause diseases [104].

1.3.4 Pathogenic Bacteria

Most of microorganisms are harmless while some commensal bacteria are even beneficial to human and animals but with the exception of a few which are defined as pathogens because they can cause a variety of infectious diseases to the host. Pathogens in general can be classified as viral, bacterial, prionic, fungal and other parasites depending on their structural characteristics and specific effects on the host of infection [103]. Special attention is made to the pathogenic bacteria here as they are the cause of a wide range of diseases to human with rising number of causalities. Pathogenic bacteria usually cannot infect the human host especially when the natural barrier (e.g. skin) and the resistant mechanisms of the body protect the host and function properly. Opportunity for human pathogens to enter the body occurs when the barrier is broken (e.g. skin bruises, burns and wounds etc) or resistant mechanism is prevented from functioning (e.g. during surgery). Then they can establish within the host, grow with the expense of host and thus adversely affect the metabolism of human body. Immune system of human body is capable of controlling this primary establishment of pathogens if the infected host is still in healthy condition. The infection is contained within a small area and the pathogenic bacteria are isolated and even killed by a part of the immune system (e.g. phagocytes). However the body immune system is suppressive or limited in functioning due to various factors such as age, illness, alcoholism, hereditary disorder etc. This can weaken the normal resistance of human body to the infection and as a result, pathogens gain opportunity to further invade the host and cause infectious diseases [103].

1.3.4.1 Bacterial Toxins

Bacterial toxins are regarded as the infectious agents that can adversely attack the host and stimulate the various responses of the host, leading to the cause of various

infections and diseases [105]. They release potent toxins (toxic proteins or enzymes) that can kill host cells and destroy connective tissues of the skin and mucous membranes [101, 102, 106]. Therefore, they are regarded as biological weapons of pathogenic bacteria. Bacterial toxins can be generally classified as: endotoxins, exotoxins and extracellular enzymes [107, 108].

1.3.4.1.1 Endotoxins

Endotoxins are lipo-polysaccharides (LPS) or lipo-oligosaccharides (LOS) which are usually cell-associated substances and structural components of Gram-negative bacteria [110]. They can be released from the bacterial surfaces upon lysis of bacteria or by vesicles blebbing from the outer membrane. Therefore they usually act in the vicinity of the sites of bacterial growth. LPS consists of polysaccharides (sugar) chain and lipid A which is responsible for causing toxic effect on the host [109]. Typical molecular weight of LPS is around 10 kDa but they can form into aggregates of up to 1000 kDa. LPS is known to be potent stimulant of the human immune system and even at the presence of low concentration of LPS can cause extreme immune response by the host [111]. Such an excessive immune reaction during the infection of Gram-negative bacteria may lead to toxic shock and even death of the host can occur at high LPS concentration [112, 113].

1.3.4.1.2 Exotoxins

In contrast to endotoxins, exotoxins are extracellular diffusible proteins and/or polypeptides secreted by living pathogenic bacteria. They are released in soluble monomeric forms and can act away from the site of bacterial growth with more virulence effects compared to endotoxins. Exotoxins can act enzymatically or through direct action with host cells and stimulate various host responses. Exotoxins vary in their molecular structure, biological function, mechanism of secretion and immunological properties. Their actions against the host however, are differed among individual exotoxins. Some facilitate the adhesion to the host while others act as invasions because they locally act to promote bacterial invasion. Many exotoxins are known to cause physiological and pathological damages to the host cells. Physiological damage is to impair the particular functions of the host without killing the cell e.g. cholera enterotoxin (Ctx) of *Vibrio cholera* promote water and electrolyte secretion from enterocytes, leading to diarrhea [114]. On the other hand, some exotoxins cause

pathological damage to the host such as diphtheria toxins (Dtx) from *Corynebacterium diphtheria* [115, 116] and exotoxin A from *Pseudomonas aeruginosa* [117, 118] bring about the death of target cells by inhibiting protein synthesis. As they are variety of proteins, some exotoxins have very specific cytotoxic activities i.e. they only attack specific types of cells. Common toxins such as tetanus toxin of *Clostridium tetani* and botulinum toxin of *Clostridium botulinum* are in this type as they only target neurons [119]. However, other exotoxins secreted by clinically important pathogens such as *S. aureus* exhibit rather broad cytotoxic effects [120]. These toxins have capacity to damage the cells or tissues non-specifically and result in necrosis (or apoptosis) i.e. premature death of cells.

Table 1.1 Some PFTs secreted by human pathogenic bacteria

Name of PFTs	**Source of bacterium**	**Target substrate**
Alpha toxin	*Staphylococcus aureus*	Cell membrane
Leukocidin	*Staphylococcus aureus*	Phagocyte membrane
Hemolysin	*Escherichia coli*	Cell membrane
Anthrax EF	*Bacillus anthracis*	Cell membrane
Pneumolysin	*Streptococcus pneumoniae*	Cholesterol
Streptolysin O	*Streptococcus pyogenes*	Cholesterol
Listeriolysin	*Listeria monocytogenes*	Cholesterol
Perfringiolysin O	*Clostridium perfringens*	Cholesterol

1.3.4.1.3 Pore-forming toxins (PFTs)

Pore-forming toxins represent a large family of protein exotoxins secreted by pathogenic bacteria. As suggested by the name, many PFTs are able to form pores in different sizes across the plasma membrane of host cells. Toxins are secreted as subunits in their soluble monomeric forms and transmembrane pores are formed by self-assembly of toxin monomers within the membrane [121]. Cell membrane, as a two dimensional molecular layer is a complex mixture of lipids, cholesterol and various proteins. At the molecular level, protein toxins of bacteria must have an affinity to bind to membrane protein, cholesterol or lipids in order to insert and form the pore to complete their particular tasks. Some toxins require the presence of cholesterol to be able to form a pore and they are grouped as cholesterol binding toxins (CBTs). Among more than twenty CBTs identified [122], common pore-forming CBTs are streptolysin of *Streptococcus pyogenes*, pneumolysin of *Streptococcus pneumoniae*, perfringolysin O of *Clostridium perfringens* and listeriolysin of *Listeria monocytogenes* (Table 1.1).

Secreted CBTs compose of three to four domains in their monomeric state and one of the domains is responsible for binding to cholesterol. Therefore cholesterol-rich regions of cell membrane such as lipid rafts are the insertion/binding sites of CBTs and the resulting oligomeric transmembrane pores are very large (24 to 48 nm in diameter) [123]. Some bacterial PFTs are secreted as the soluble monomers and do not require the specific binding sites in the cell membrane. Monomers insertion followed by the subsequent conformational changes result the oligomeric pores. They are considered as bacterial PFTs in general and classified into two groups i.e. α-PFTs and β-PFTs based on membrane interaction mechanism through either α helices or β sheet structures of the pores [121]. α-PFTs form the pores using helices while β-PFTs insert β-sheet domains into the membrane to form the β-barrel pores. Some PFTs belong to β-PFTs are aerolysin of *Aeromonas hydrophila*, α-toxin of *Clostridium septicum*, α-hemolysin of *S. aureus* and cytotoxin of *P. aeruginosa* [121].

Functions of PFTs are specific and depend on the primary targets of each types of PFTs. Targets may be either cytoplasmic organelles or extracellular surface receptors of the attacked cells. Directly formed heptameric pores can disrupt the electrochemical potential and permeation barrier of the cell by allowing the flow of ions and small charged molecules in and out of the cell [124]. Such an uncontrolled permeability of pores may be used by pathogenic bacteria as the pathways to access the intracellular nutrients of the host cells. Adversely the target cells may lyse and die by necrosis. This group of direct PFTs includes streptolysin O of *S. pyogenes* and α-hemolysin from *S. aureus*. An important aspect of some PFTs is their ability to retain their structure and functions *in-vitro* [92]. For example, the molecular structure of alpha toxin secreted by *S. aureus* was determined [90] and the toxin in its purified form was demonstrated to reconstitute and function into artificial lipid bilayer membranes [86]. Detail structure and function of alpha toxin *in-vitro* are discussed in section 4.1.

1.3.4.1.4 PFTs with enzymatic activities

Most of protein exotoxins resemble enzymes in many ways and they exhibit some enzymatic activities. These exotoxins may act catalytically at the tissue sites. Like enzymes, they are denatured by heat and inherently unstable as they tend to lose their toxic properties with time. Some exotoxins require activating inside the cytoplasm and need to be transported into the cell. These types of PFTs with intracellular targets consist of at least two components and they are termed binary or multi-component

toxins [126]. First subunit is responsible for the enzymatic activity of the toxin and transported by second subunit which binds to the specific receptors of the cell membrane. Translocation of enzymatic subunit across the membrane may be either through the pore formed by binding of second subunit onto the receptors or by encapsulating inside the endosomes [121]. Well studied diphtheria toxins of *C. diphtheriae* and exotoxin A of *P. aeruginosa* belong to this group of PFTs.

1.3.4.1.5 Extracellular enzymes

Many bacterial pathogens secrete a wide range of extracellular enzymes that are involved in the process of invasion. Each enzyme targets either the tissue matrices (and fibrins) of the host or the specific lipids of cell membranes. Degradation of tissue matrices in the host subsequently allows the spread of bacteria and hence they are regarded as invasions. These include collagenase [147, 148], hyaluronidase [149] and streptokinase [150]. Collagenase for example can break peptide bonds in collagen, the major component of the extracellular matrix of eukaryotic cells [101]. Hyaluronidase, on the other hand, degrades the hyaluronic acid which is the anionic glycosaminoglycan widely found in connective, epithelial and neural tissues [127]. Other enzymes such as phospholipases and lecithinases attack and degrade the different types of phospholipids by hydrolysis [128, 129]. Different phospholipases recognize the particular sites of cleavage in different phospholipids (see figure 1.10).

1.3.4.1.6 Bacterial toxin superantigens

Several bacterial toxins have ability to stimulate the immune system of host and various diseases in human are adversely related to impairment of the immunologic functions of the infected host cells [132]. They are highly lethal as the toxin concentration as low as 0.1 picogram/ml is sufficient enough to stimulate the T-cell lymphocytes uncontrollably [111, 112]. This immunostimulation is potent and triggered by extracellular binding of superantigens onto the specific receptors of T-cells and major histocompatibility complex (MHC) of the antigen-presenting cells of immune system [113]. In normal condition, only 0.001 % - 0.0001 % of T-cells are activated when antigens presented by MHC bind onto T-cell receptors (TCRs). But in case of superantigen bindings, 5 % - 20 % of T-cells are proliferated and triggered the massive release of both monocyte and lymphocyte-derived cytokines [130]. Cytokines are small protein molecules transferring signals and communicating among the cells; and the massive proliferation of cytokines

can cause acute responses such as toxic-shock syndrome (TSS), food poisoning and chronic autoimmune-related responses e.g. coeliac disease [131].

The number of known and identified bacterial toxin superantigens has been increasing and the majority among them belongs to the group of pyrogenic exotoxins secreted by staphylococcal and streptococcal bacteria [111, 133]. Pyrogenic exotoxins are secreted with molecular weights ranging from 21 kDa to 29 kDa and involve in a number of diseases including food poisoning, fever and toxic shocks [112, 134].

1.3.4.2 Mode of action of bacterial toxins

Biological warfare of pathogenic bacteria against the host depends on the types of toxin, their specific targets and their particular functions for causing damage at the target sites. The main barrier for the toxins to go through or interact with during invasion is the plasma membrane which is the primary defence of eukaryotic cells to the extracellular space. Some toxins are designed to attack the intracellular targets and hence they need to go through the cell membrane to function their tasks [135]. On the other hand, other extracellular toxins are activated by binding onto the receptor targets, for example guanylate cyclase receptors for binding of heat-labile enterotoxins (ST) of *E. coli*, pre-existing at the outer membrane of the cells [105]. In both cases, toxins are essentially required to interact with the cell membrane. Common modes of action of toxins against the host cells in general, include damaging cell membranes, inhibiting protein synthesis, activating second messenger pathways, inhibiting the release of neurotransmitters or activating the immune response of the host [105].

1.3.4.2.1 Lipid damaging

There are approximately 300 bacterial protein toxins responsible for the various diseases in human and about one third are known to damage the cell membranes [107]. Damage can be either by lipid-degradable extracellular enzymes or by endotoxin LPS [128, 129]. Phospholipases (PLs) are common extracellular enzymes secreted by many human pathogenic bacteria [110]. They are very site specific and the target lipids of PLs include phosphatidylcholine (PC), phosphatidylinositol (PI), phosphatidylethanol (PE), phosphatidylserine (PS), phosphatidylglycerol (PG), lysophosphatidylcholine (LPC), lysophosphatidylinositol (LPI) and sphingomyelin (SM). The degree and type of damage to phospholipids depends on the individual PLs and the species of target substrates i.e. lipids. Since phospholipids constitute more than 75 % of lipids (% mol) in

animal cells [2], damage caused by various PLs onto cell membranes is quite considerable and linked to many diseases. PLs are classified into five different types depending on the sites of phospholipid at which particular PLs hydrolyze enzymatically (figure 1.10). They are PLA1, PLA2, PLB, PLC and PLD.

PLA1 and PLA2 recognize *sn*-1 and *sn*-2 acyl bonds of phospholipids respectively and catalyze the release of fatty acid by hydrolysis [136, 145] while PLB is an enzyme with the combined activities of both PLA1 and PLA2 [151]. Phospholipids hydrolyzed by PLA1 or PLA2 reduce to lysophospholipids and release fatty acids [144]. PLC and PLD on the other hand, catalyze the bonds before and after the phosphate group of phospholipid respectively [137]. Lipid hydrolyzed by PLC release the phosphate-containing head group while PLD breaks the lipid down and releases the phosphatidic acid and alcohol [146]. Overall damage to cell membrane carried out by PLs is the gradual loss of lipids which degrade integrity of the membrane and the host cell may finally encounter the lysis by necrosis (or apoptosis).

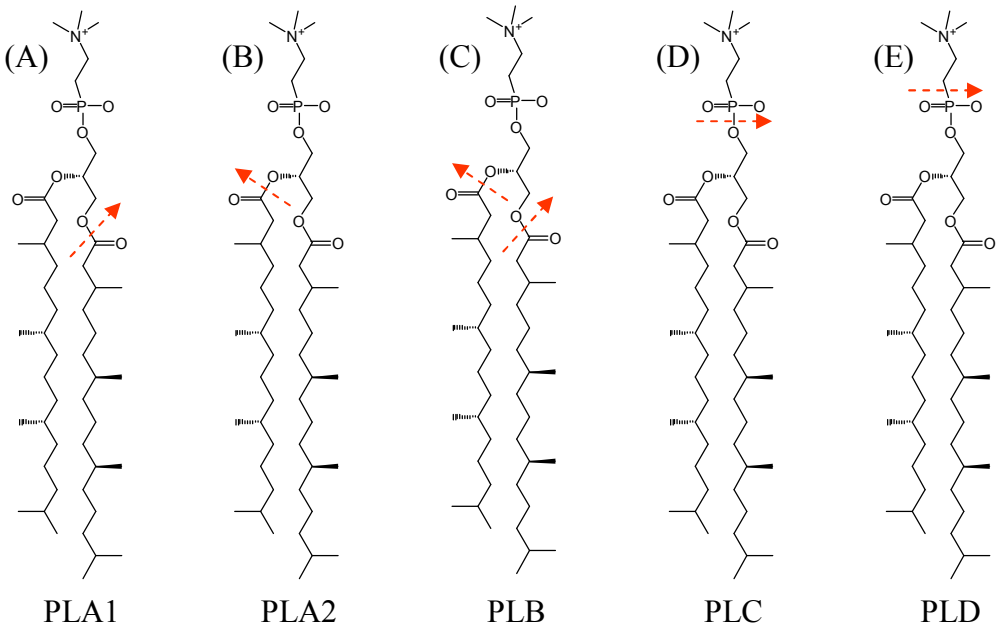

Figure 1.10 Cleavage sites of bacterial phospholipases (indicated by dashed red arrows): (A) PLA1 by *sn*-1 acyl bond below the glycerol group (B) PLA2 by *sn*-2 acyl bond below the glycerol group (C) PLB by both *sn*-1 and *sn*-2 bonds below the glycerol group (D) PLC before phosphate head group and (E) PLD after phosphate head group

1.3.4.2.2 Pore formation

All PFTs are able to form the transmembraneous pores across the cell membrane however their modes of action after the pore formation are different. Some toxins require no surface affinity or receptor binding for the pore formation. But some require

the presence of receptor on the cell surface and binding to specific receptors induced the pore formation. The former toxins known as direct PFTs are well known and their main task carried out against the target cell is to disrupt the influx and efflux of ion and molecules across the plasma membrane [122, 123]. Among them, alpha toxin of *S. aureus* is considered as a model PFT [138]. Alpha toxins in their monomeric form can bind to the plasma membrane of the target cells and laterally diffuse within the membrane [124]. A water-filled transmembrane ion channel is formed upon oligomerization of seven monomers. Diameter of the pore formed by alpha toxins is 1 – 2 nm in diameter and molecules up to 2 kDa can easily pass through the pore [90] (figure 4.1). These α-HL channels have no control on transport of solutes, molecules etc. and hence uncontrolled permeation of water, ions, and small organic molecules through the channel can cause death to the target cell by irreversible osmotic swelling causing the rupture of the cell wall [91]. On the other hand, CBTs require the presence of cholesterol and pore formation is triggered by binding to cholesterol [139]. Pores formed by CBTs have exceptionally large pore sizes up to 25 nm in diameter. These CBTs which are also known as cholesterol-dependent cytolysins (CDCs), are secreted by common pathogens with genera including *Streptococcus*, *Listeria*, *Clostridium*, *Bacillus* and *Arcanobacterium* [122]. Both direct PFTs and CDCs (also known as CBTs) are able to disrupt the cell membrane permeability by allowing the flow of ions and charged molecules [152]. Some pores formed by the toxins are not for the transport of ions but for the translocation of enzymatic domain of toxin inside the cell to reach the intracellular targets [140]. These pore formers are discussed detailed in following sections.

1.3.4.2.3 Other modes of action

Inhibition of protein synthesis

Some protein toxins in nature are designed to disrupt the cellular functions of the host cells by targeting the cytoplasmic organelles. Diphtheria toxin of *Corynebacterium diphtheriae* [115, 118], shiga toxin of *Shigella dysenteriae* [141] and exotoxin A of *P. aeruginosa* [117] belong to this group of toxins and they can particularly inhibit the synthesis of proteins by the host cells. They are intracellular acting protein toxins with the targets including elongation factors (EFs) and ribosomal RNA. These toxins are usually binary toxins as they consist of A-B subunits in general: subunit A is responsible for the enzymatic activity while subunit B is designed to bind the specific

receptor on the host cell and translocate the enzyme across the membrane to reach the intracellular targets [126]. Enzymatic subunit A enters the cell either by pore-forming or receptor-mediated endocytosis (RME). In first mode of entry, subunit B binds to the specific receptor on the target cell and induces the formation of a pore through which the subunit A is translocated [142]. Alternatively in second mode, binding of toxin into target cell receptor triggered the formation of endosome which is an enclosed vesicle budding inward by the cell membrane. Endosome carries the entire toxin and the change in intracellular pH separates the subunits. Separated subunit A then reaches and inactivates the functions of internal targets [105].

Shiga toxin, for example, inactivates ribosomal RNA in such a way that the EF becomes non-interactive with the affected ribosome. The end result is death of target cells due to its inability to synthesize the proteins [141]. Exotoxin A of *P. aeruginosa* and diphtheria toxins, on the other hand are known to use both entry mechanisms into the cell and final task is to inactivate the function of EF leading to inhibit the synthesis of proteins by target cells [115, 117].

Activating the secondary messenger pathways

Some bacterial toxins have the ability to kill the target cells indirectly by altering the functions of intracellular proteins. These toxins can activate or modify the secondary messengers and result the change in signal transduction pathways which are vital in maintaining the many cellular functions [153]. Heat-labile, heat-stable toxins and cytotoxic necrotizing factors (CNFs) of *E. coli* [114], cholera toxin of *Vibrio cholerae* and pertussis toxin of *Bordetella pertussis* belong to the toxins affecting the secondary messenger pathways and their targets include guanine nucleotide-binding proteins (G-proteins) and Rho G-proteins [143]. Similar to toxins inhibiting the protein synthesis, both cholera and pertussis toxins utilize RME modes of translocation to enter the target cells but the tasks that they carry out inside the cells are different. Enzymatic domain of cholera toxin ribosylates the Gs alpha subunit of G protein and results the production of cyclic adenosine monophosphate (cAMP) which promote secretion of fluid and electrolytes in intestinal epithelium leading to diarrhea. Pertussis toxin, on the other hand catalyzes the adenosine diphosphate ribosylation (ADP-ribosylation) of the alpha subunits of G-proteins and this in turn partly hinders the interaction of some subunits of G-protein with G protein-coupled receptors (GPCRs). G-protein subunits in their

inactive state are unable to inhibit the activity of adenylate cyclase and increases levels of cAMP which affect hormone activities such as increasing release of insulin.

Inhibition of the release of neurotransmitters

Bacterial toxins affecting the nerve cells of peripheral nervous system (PNS) and central nervous system (CNS) are classified as neurotoxins and their modes of action against the target cells include the interfering with the ion transport function of many voltage-gated ion channels and inhibiting the release of neurotransmitters of the nerve cells. Although the source of neurotoxins may be venomous insects and vertebrates, some are secreted as inactive protein toxins from the bacterial sources [248]. Many bacterial species of *Clostridium* with various strains secrete seven different types of Botulinum neurotoxins (BoNTs) (A to G) and all of them are able to inhibit the release of acetylcholine [119]. Their targets are receptors on the presynaptic membrane of motor nerve cells of PNS. Degradation of the target proteins in affected neurons inhibits the release of acetylcholine and the toxin interferes with the nerve impulses which results the flaccid paralysis of muscles in the host. On the other hand, tetanus neurotoxins (TeNTs) of *Clostridium tatani* have same mechanism as BoNTs but affecting only the neurons belong to CNS. Upon binding to receptors on presynaptic membrane, TeNTs are transported to the spinal cord by vesicular mean and reach the inhibitory interneurons. Toxins then cleave the vesicle-associated membrane protein (VAMP) and synaptobrevin of interneurons and disrupt the release of glycine and gamma-amino-butyric acid which causes the spastic paralysis in the host [248].

Activation of host immune responses

Toxins that stimulate the host immune responses were previously discussed in section 1.3.4.1.6.

1.4 Current methods of bacterial detection

Detection and quantification of pathogenic bacteria and their toxins are primary importance to prevention and identification of problems related to health and safety. Immediate and long-term requirements for the bacterial detection play an important role generally in three main sectors: (i) food industry, (ii) health and clinical sectors and (iii) water and environmental safety. First and foremost detection of foodborne pathogens is

always essential in food industry to ensure safety and quality of the foods as well as to prevent the massive outbreak of food-related, lethal diseases such as food poisoning [154]. It is also vital requirement for rapid detection and accurate identification of human pathogenic bacteria which are clinically significant and important in healthcare and clinical sectors such as in hospitals [221]. Last but not least, firsthand detection of waterborne bacteria and their toxins in water resources and supplies is necessary to prevent the outbreak of diseases linked to contaminated water such as diarrhoea and to maintain the standard of safe drinking water [222, 223]. Bacterial detections are different in term of method, type and nature of signal extracted from the measurement and application where the detection is employed. But the primary requirements for a pathogen sensor for the bacterial (and toxin) detections are sensitivity, selectivity, throughput, and ease and rapidity in detection.

1.4.1 Conventional method of culture and counting colonies

The method of growing (culturing) bacteria on the agar petri dish under controlled environment and counting the growing colonies of bacteria is probably the oldest method of bacterial detection and identification. In this gold standard method, typically unknown amount of bacteria from a suspected area of infection is inoculated in the growth medium and serial dilution is carried out several times. A certain amount of finally diluted bacterial medium is then plated on the agar petri dish thoroughly until the medium is dried and incubated at 37 ºC for a proper period of time [155]. After incubation, bacterial colonies grow on agar surface and each colony mostly represents an individual bacterial cell. Quantity of estimated bacteria, in colony forming units per millilitre (CFU/ml) is derived from the number of colonies and the dilution factor while the morphologies of colonies observed under the light microscope reveals the possible information about the type of pathogen involved in the infection.

This method of culture and plating has many advantages. It is simple in methodology and the result is not affected by the presence of contamination and other irrelevant materials such as proteins and enzymes. Only the bacterial cells in the test sample show up as the growing colonies. On the other hand the method reveals the viable cell count only and the major disadvantage is the slow throughput (due to lengthy process and long time consuming) which is not tolerable with the demanding requirements of rapid and accurate detection nowadays.

1.4.2 Enzyme-linked immunosorbent assays (ELISA)

ELISA, also known as enzyme immunoassay (EIA) is a fundamental immunological and biochemical technique based on the process of antibody-antigen recognition [156]. Depending on lock and key mechanism, unknown antigen in a given sample for example human serum is quantified by binding to the known respective antibody attached to the substrate [157]. Developed in early 1970s as an alternative to avoid the use of radioactive-labelled signal in radioimmunoassay (RIA) [157, 210], ELISA employed the appropriate enzymes to attach to antibodies for signal amplification and detection [158]. The process involves at least one antibody which is specific to the antigen to be detected and identified. Typical sensor surface is made of polystyrene (i.e. microtitre well plate) onto which the unknown antigen is either adsorbed non-specifically or attached specifically to the pre-treated antibody as in case of sandwiched-ELISA [157]. Then the antibody is added onto surface antigens forming antibody-antigen complexes. For the indirect signal detection, the second antibody which is covalently linked to the enzyme is added. The sensor surface is then washed thoroughly in mild detergent so that the non-specifically bound proteins or antibodies are removed, leaving only relevant antibodies bound to the right antigens on the surface. Finally the substrate for the enzyme used is added which change the colour of enzyme, for example alkaline phosphatase purified from calf intestinal mucosa, and the fluorescent signal extracted from the enzyme-link surface antibody-antigen complexes is detected. The signal then represents the quantity of unknown antigens on the surface. Depending on the way the signal is read, many modifications to conventional ELISA have been reported including the utilization of signal-conveyers as fluorogenic and electrochemiluminescent [156, 157]. But the rest of modified ELISA techniques are not discussed in this literature review.

Since the invention of ELISA, this technique has been extensively used as a diagnostic tool in the field of medicine and screening tool for the certain class of drugs in toxicology. Broad applications of ELISA includes from the screening of human chorionic gonadotropin (hCG) in home pregnancy test kits to the detection of Human Immunodeficiency Virus (HIV) antibody in human serum [156]. Despite usefulness and relevance of the technique in biosensing, not many application of ELISA for the direct detection of pathogenic bacterial toxins *in-vitro* has been reported [159]. It was reported to be able to detect 10^5 CFU/ml of *C. perfringens* and the respective α-toxin as low as 60 ng/ml in birds by using ELISA [160]. It was also performed the ELISA tested with

purified α-toxin of *C. perfringens* and the minimum detection limit of 19 ng/ml was reported [161]. Detection limit of less than 2 ng/ml BoNT B neurotoxin of *C. botulinum* proved good *in-vitro* sensitivity to toxins by ELISA method [162]. Other than *Clostridium* genus, *Vibrio harveyi* detection in penaeid shrimp and water was also reported [163]. For the food safety in milk, *Staphylococcus* species and *S. aureus* responsible for causing mastitis in dairy cows were reportedly detected to the sensitivity of 10^4 – 10^5 CFU/ml by immunomagnetic separation-ELISA and ELISA based on monodisperse magnetic particles within the measuring time less than 3 hours [164, 165]. Although ELISA in bacteria detection is high in reproducibility and throughput with possible automation, its application is only limited to antigen detections while the validation of data is difficult and complicated. Above all the assay development time is long, up to days and this makes the technique less efficient in applications where quick and sensitive detections are required.

1.4.3 Polymerase chain reaction (PCR) – gene assay

Polymerase chain reaction (PCR) is considered more useful and efficient than the contemporary ELISA method for pathogen detection. ELISA targets the antigen/antibody while PCR aims to genetic materials of the bacterium in the sample for the multiple duplications. This method imitates the natural function of the enzymes known as polymerases which are present in all living cells with their primary task including the copying, proofreading and correcting the genetic materials if necessary. Therefore PCR is accurately able to characterize, analyze and synthesize by copying any specific piece of the target DNA and RNA molecules [166]. PCR simply requires three things to get started: a template molecule, DNA or RNA to be copied and two primer molecules which are required to initiate and carry on the DNA copying. Primers terms as nucleotides or bases, are short single-stranded chains of four basic chemical components of genetic materials.

First in PCR process, the target DNA is denatured and the strands of double helix are unwound by heating above 90 ºC. This makes target DNA into single strands. Second step is the DNA hybridization where the primers bind to the complementary bases on single strand DNAs. Starting from the primer in third step, new DNA is synthesized by a polymerase which reads the template strand and matches it with complementary nucleotides quickly. End result is two new identical double helix DNAs which are used again as the target DNAs for the second duplication process. In this way with the cycle

of rapid heating and cooling, the exponential amplification of DNAs is repeatedly taken place until the minimum amount of amplified DNAs is reached for the signal detection and interpretation. Each cycle takes approximately between 1 and 3 minutes and within a few hours, PCR generates millions of copies of the target DNA. As PCR target the genetic materials while the technique itself is less time-consuming, it quickly becomes the method of choice for bacterial detection in field of different applications [166]. Different PCR methods developed for the pathogen detections are real-time PCR [167], multiplex PCR [168] and reverse transcriptase PCR (RT-PCR) [166].

In conventional PCR, the amplified DNAs are detected and interpreted by gel electrophoresis. In real-time PCR method, post-amplification process of gel electrophoresis is avoided and the results are generated in real-time by the fluorescence emission of the specific dye as it attaches to amplified DNAs [169]. Multiplex PCR on the other hand, allows the simultaneous detection of various cells by using different nucleotides to amplify regional DNA coding for specific genes of each targeted bacterial strains [170]. Since DNA exists regardless of the living cells are alive or dead, the major limitation of the conventional PCR is its inability to discriminate between viable and non-viable bacterial cells. This leads to the modification of PCR into RT-PCR which is able to detect the viable bacterial cells only [166]. Using oligonucleotide microarray and real-time PCR, pathogens including *S. aureus*, *E. coli* and *P. aeruginosa* in waste water were quantified but only *E. coli* DNA was detected in municipal sewage [171, 167]. PCR experiments in which the detection of *S. aureus* and its toxin supernatant were carried out for the food safety and the results were examined for the associated role in food poisoning [172, 173]. About 35 % of *S. aureus* tested were identified as enterotoxigenic strains [172], and the thermonuclease and enterotoxins of *S. aureus* were detected [173]. Clinically important strains of *S. aureus* were mostly studied by PCR and enterotoxins and toxic shock syndrome toxin-1 (TSST-1) [174], exfoliative toxin A [175] and *S. aureus* itself from blood plasma culture specimens [169] were broadly detected. Moreover *E. coli* virulence factor genes [176] and human pathogen *V. cholerae* [170] were quantified by multiplex real-time PCR assay. Interestingly the three waterborne bacteria: *S. aureus*, *P. aeruginosa* and *E. coli* DH5α with pathogenic strains were detected and identified with real-time PCR-based microfluidic array chip recently [167]. In their work, it was reported that the *S. aureus* and *E. coli* DNA copies as low as 1600 and 1000 copies respectively were able to provide the detectable signal in term of fluorescence intensity.

Despite improved and faster throughput of PCR compared to ELISA, overall time-consumption in PCR is still relatively long during pre-DNA purification and post amplification processes. Another issue with current PCR technique is the contamination of sample with other genetic materials which results the copies of irrelevant DNAs and complications arise when it comes to interpret the PCR result. It requires initial identifying of the individual PCR protocol to detect and discriminate the target pathogens, and hence the prior DNA information must be known. Finally the selectivity of PCR technique is a challenge especially when pathogenic bacteria with the modified genes which sequence the strains with more and more resistance to current antibiotics in treating infectious diseases.

1.4.4 Other methods of bacterial detection

1.4.4.1 Optical density (OD)

Optical density (OD) measurement utilizes the principle of light scattering. When the laser light is shined on the suspension containing bacteria, some of incident light beams are scattered while some are transmitted through the suspension. The intensity of incident light beam is related to that of transmitted light beam in term of OD as follows:

$$OD_{\lambda} = \log_{10} O = -\log_{10} T = -\log_{10}\left(\frac{I}{I_o}\right) \qquad (1.1)$$

Where λ is the wavelength of light

I is the intensity of transmitted light beam

I_o is the intensity of incident light beam

Therefore OD is a measure of fluid turbidity which represents the amount of biomass i.e. bacteria in the suspension. OD is typically measured with the laser light with wavelength between 550 – 600 nm and it is equivalent to the number of bacteria in CFU/ml. In measurement, the blank OD of the suspension (culture medium) without containing the bacteria is measured first. Then the bacteria in same suspension are diluted (typically 10 times) and the measured OD of bacterial suspension is correlated to CFU/ml. OD method has advantages of simple in methodology while the measurement is non-destructive and rapid. However there are a few limitations associated with OD technique. It measured all the particles in suspension including fragments and debris of the cell and hence only the viable cell count is not possible. It can only measure

between 10^5 – 10^8 CFU/ml and the calibration is still required by conventional plating method. Above all it has no selectivity on bacterial species.

1.4.4.2 Surface plasmon resonance (SPR)

SPR is a highly surface sensitive optical sensing method which can reveal the real-time binding kinetics of biomolecules onto the receptor attached onto gold surfaces. The sensing mechanism relies on the quantum electro-optical phenomenon occurred at the interface where the light interact with the metal surface. SPR biosensors based on change in local refractive index of the surface due to binding of biomolecules in term of the minimum resonance angle shift accurately. Theory and instrumentation about SPR is described in next sections but only the experimental applications using SPR for the detection of bacteria is briefly discussed here. A major advantage of SPR as a biosensor is its nature of label-free detection which reveals the amount of bound analytes, its affinity for the receptor and the association and dissociation kinetics of the interaction between analytes and receptors [177]. Detection is usually based on the surface either treated in monolayer [178, 181], lipid vesicles [179, 189], bilayer [89] or monolayer with surface immobilized receptor molecules [181] targeting the bacterial toxins in purified form [179] as well as the bacteria [180]. Detection targets the bacterial binding onto the monoclonal antibodies attached to the protein G and SAM on Au surface and selective detection of *E. coli* O157:H7, *Salmonella typhimurium*, *Legionella pneumophila* and *Yersinia enterocolitica* was demonstrated. It was claimed that the protein chip based on SPR was able to detect the bacteria concentration about 10^5 CFU/ml selectively [180]. For the human pathogen *E. coli* O157:H7, effects of bacterial preparation on the limit of detection by SPR was explored [181]. Bacterial detection using SPR is promising in term of sensitivity and quantification but the reliability of the technique is still questionable and much related works has yet to be done in order to improve the selectivity and qualification of the technique.

1.4.4.3 Electrochemical methods

These methods in general, examine the change in electrochemical properties at metal-electrolyte (containing analytes) interface in terms of current (amperometric), potential (potentiometric) and impedance (impedimetric). Among these methods, the use of electrochemical impedance spectroscopy (EIS) as an analytical tool for the detection of bacteria, bacterial toxins and the biofilm formation on the planar metallic electrode with

or without surface modifications has been mostly demonstrated. Theory and experimental instrumentation of EIS is discussed in detail in next sections while the discussions here is only confined into the EIS methodologies and results relevant to bacterial detection. Impedance in other words, resistance and capacitance of the metal electrode surface is very sensitive to the surface interactions. Under applied potential, the current signal driven by the flow of ions to and from the electrode surface gives rise to the useful data of surface interaction. Attachment of bacteria or binding of bacterial toxin if the surface is covered with receptor molecules induces localized change in capacitance which is detected as a useful signal for the analysis.

Many works have been done especially in attachment and biofilm formation of *P. aeruginosa* and *E. coli* on conductive surfaces using impedimetric assays [182, 183, 184]. Metallic surfaces were not modified for bacterial attachment and biofilm formation was studied [185]. Commonly employed electrode surface is Au which is used to support the formation of self-assembled monolayer (SAM) for the subsequent attachment of surface receptors. The immobilization of albumin on the activated Au surface was studied by monitoring capacitive measurement and the obtained detection limit was achieved as low as 15 nM [186]. As the electrode surface is modified with monomolecular layer (and subsequent bilayer), the ionic current is electrically impeded. Then the change in resistance provides the useful information of attachment of toxins and proteins which in turn alter the surface impedance. The use of attached lipid bilayer membranes onto the Au surface and studied the binding of purified toxins α-hemolysin [86, 89], ion transporter valinomycin [187, 192] and bacterial polypeptide gramicidin [188, 195, 220]. In above studies, binding of toxins and proteins affected the lipid bilayer ion permeability by allowing the flow of ions through the pores and channels. Then the change in resistance and capacitance of the lipid bilayer membrane was detected and correlated to the quantity of toxins or proteins bound onto the surface. Unfortunately the limitation of this technique lies in interpretation of impedance results into reliable data as the data presentation presents complex functions and requires fitting with correct equivalent circuit which represents the combined medium of study between the working electrode and reference, and counter electrodes.

1.4.4.4 Sensing of bacterial toxins using lipid bilayer membranes

As a matter of the fact that the cell membrane is the primary target of various bacterial toxins, detection and identification of toxins (and pathogenic bacteria) based on

artificial lipid bilayer membranes is possible and promising because it mimics the nature in which the toxins interact with the cell membrane. Lipid bilayer systems combined with advanced surface analytical tools are therefore useful to explore the interactions of bacterial toxins with cell membrane at the molecular level. Events of toxin-lipid bilayer interactions such as binding, enzyme translocation, pore-formation and lipid damaging etc. convey the surface sensitive signals in term of optical, electrical and electrochemical means. These signals are useful in understanding the specific toxin-lipid bilayer interaction and the nature of toxins involved. Some purified forms of toxins are known to retain their structure and functions *in-vitro* and hence various works have been performed on the interaction of toxins with the lipid bilayer membrane. These include pore-formation of α-toxin of *S. aureus* with lipid bilayer [124] and exotoxin A of *P. aeruginosa* with lipid vesicles [179]. Moreover, binding of clinically important toxins such cholera, tetanus and pertussis toxins into lipid bilayer has been studied using fluorescence microscopy [198], fluorescence immunoassay [201], quartz crystal microbalance [199], scanning probe microscopy [200] and bindings of toxins onto lipid bilayer membrane were demonstrated. However, the bacterial toxins studied in above-mentioned works were specific and in their purified form. Therefore the broad and combined effect of various toxins produced by pathogens *in-vivo* with cell membrane has been largely neglected. Despite the fact that these purified bacterial toxins are only a fraction of the toxins produced by different strains of clinically significant bacteria such as *S. aureus* and *P. aeruginosa*, the effect of other major toxins produced by these pathogens causing several diseases are still not well understood. The potentially synergistic, multiple interaction of pathogenic bacterial toxins with lipid bilayer membrane *in-vitro* has been little explored.

1.5 Motivations of this work

This work presented here is divided into two parts. The first part of the work is motivated by the nature of interaction of major bacterial toxins with the cell membrane *in-vivo* and *in-vitro*. It is about the work with the detection and identification of pathogenic bacteria based on their toxins by biomimetic planar tethered bilayer lipid membranes (pTBLM). The second part is the extended work in which the planar substrate is replaced with the single nanoporous Si_3N_4 surface and the nanopore suspended TBLM (Nano-psTBLM) is explored. This second work is aimed to improve the signal detection and enhance the lifetime of Nano-psTBLM for ion channel analysis.

1.5.1 Detection and identification of pathogenic bacterial toxins

Rapid detection and identification of human pathogenic bacteria is vitally important and primary requirement in control and prevention of serious, sometimes lethal infections. Early detection of the presence of pathogens in patients with wounds (e.g. burns) is necessary prior to receive any treatments with relevant antibiotics. This requires rapid, sensitive and selective means of detection before the spread of pathogens reaches beyond the curable scope of infection in wounds. Since more and more pathogens with high resistant-to-antibiotics strains are persistently growing and spreading in hospitals and community places, firsthand detection and identification play a very important role in battles against pathogenic bacteria. For the development of a reliable pathogen sensor, the nature in which the way pathogens invade and infect the host is to be mimicked. Much similar to the warfare of humans, biological warfare of pathogens against the host (cells) involves various toxins as pathogenic weapons which adversely interact with the cell membranes and destructively invade the cell at the molecular level. Since the cells are primary targets of pathogenic infection, the cell membrane becomes frontline defence against bacterial toxins and their invasions. To date, there are approximately 300 bacterial protein toxins responsible for various diseases in human and about one third are known to damage the cell membrane [107]. Many of these are PFTs secreted mostly by Gram-positive bacteria [121] and the enzymes such as phospholipases produced commonly by Gram-negative pathogens [128].

Although all human pathogens secrete the broad range of toxins, each of them has different mode of action against the cell membrane and not all of them are valid to function *in-vitro* with the artificial lipid bilayer [190, 191]. But the nature creates the toxins with the similar modes of action in which neither the particular binding sites nor the molecular affinity to bind the cell membranes are specifically required. These include direct PFTs and lipid damaging enzymes such as phospholipases commonly secreted by clinically important human pathogens such as *S. aureus*, *P. aeruginosa* and *E. coli*. Direct PFTs form the pores across the cell membrane while the phospholipases hydrolyze and damage the phospholipids in both *in-vivo* and *in-vitro* [128, 144]. However at the molecular level, the way these two types of toxins interact with the lipid bilayer is different. PFTs simply interact with the lipid bilayer and induce the formation of transmembrane pores which certainly disrupt the ion permeability of the cell across the membrane but there is no lipid loss involved by pore formation. On the other hand, phospholipases hydrolyze and release the lipid tails out of the membrane and this causes

the certain time dependent lipid loss. Although both toxins clearly degrade the bilayer and cause the permeation of ions partly across the lipid bilayer, the electrochemical signals derived from the transport of ions across the damaged lipid bilayer are different, as presumably depicted in figure 1.11. These prominent phenomenons of lipid damaging at the molecular level are explored by EIS as well as the surface sensitive SPR, and detection and possible discrimination of bacterial toxins by PFTs and phospholipases are evaluated.

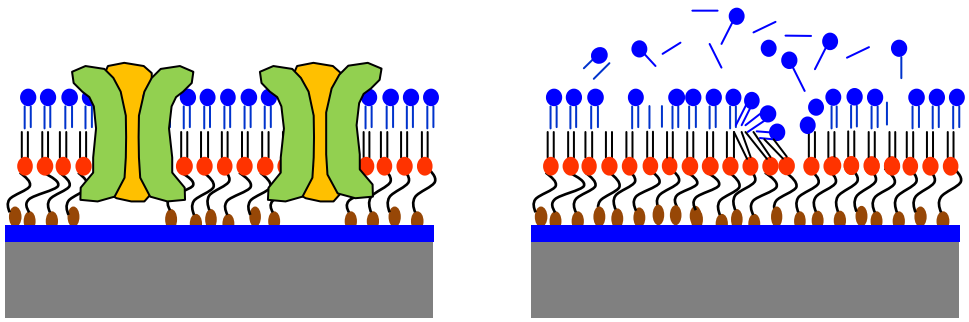

Figure 1.11 Schematic depictions of the modes of action of (A) PFTs and (B) phospholipases on artificial pTBLM. PFTs form the hydrophilic pores which allow the flow of ions across the lipid bilayer membrane driven by the electrical potential difference as depicted in figure A. There is no lipids loss involved and the impedance signal therefore is directly changed with the number of pores i.e. concentration of PFTs in the medium. On the other hand, phospholipases hydrolyze, cleave and release the lipids from upper half of bilayer as depicted in figure B. But the lipids in nature are highly mobile and the surrounding lipids quickly heal and cover the damage sites to minimize the energy loss. Hence the immediate change in impedance of lipid bilayer is not expected until the neighbouring lipids are unable to cope with the coverage over the damaged sites due to continuous lipid loss. Then the immediate change in impedance comes after a certain delayed time.

1.5.2 Nanopore suspended TBLM for single ion channel analysis

It was the fact that since inception, BLM opened the promising opportunity for future use in ion channel screenings, characterization and new drug discoveries [193, 194]. Conventional BLM was transferred onto the planar porous support and the planar BLM paved the way to today's many commercially available BLM systems for ion channel analysis and screenings [196, 197]. Ultimate merit of BLM is its exceptionally high in electrical sealing which allows the detection of tiny current in a few picoamperes by voltage-gated ion channels *in-vivo* and *in-vitro*. However, the major shortcoming associated with BLM is its inherited instability and shorter lifetime which hinder the

system to be integrated with surface analytical techniques. Regardless of several attempts to extend the life and improve mechanical stability of BLM by various means [29, 30, 31, 32], the improvements in BLM was still unsatisfactory and further to be progressed.

On the other hand as it was discussed previously, TBLM model membrane systems as compared to SBLM are promising as it creates aqueous space in tethered part while maintaining the native environment of cell membranes. It also provides the wide selection of materials for tethered part of lipid monolayer with various anchor groups for different supports [53] and TBLM is useful for studying the cell membrane-protein interactions at the molecular level [231]. Thiolipid based monolayer anchored on Au surface as well as (ethoxy)silane based monolayers on dielectric surfaces have been used for the successful formation of TBLM, and allowed the electrochemical and optical means of characterization with the incorporation of transmembrane proteins [51, 54, 55]. Importantly, the structural stability and lifetime of TBLM based on thiolipid monolayers were tested [58], and insertion and transport of bacterium toxin α-HL ion channels were analysed with TBLMs formed on TSG substrate [57, 86]. The only possible limitation in TBLMs is the restricted accessibility from the tethered side. The lower ionic reservoir formed in the linkage part of tethered monolayer is limited in capacity. It is inaccessible chemically or compositionally anymore once the monolayer is hydrated and subsequent TBLM is formed after vesicles fusion.

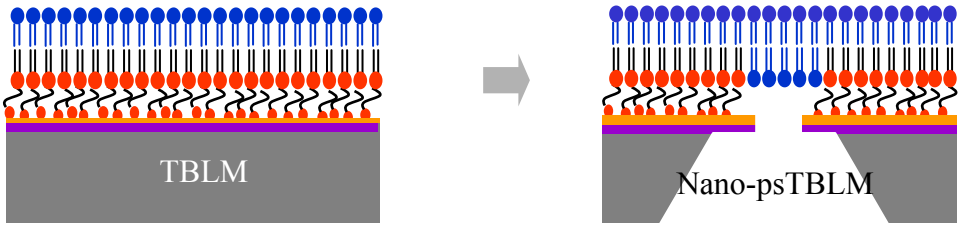

Figure 1.12 Schematics depictions of comparison between (A) Conventional pTBLM on Au surface and (B) Nanopore suspended TBLM (Nano-psTBLM) over a single nanopore

A promising alternative could be to create a bilayer platform by combining the merits of existing BLM and TBLM systems. The proposed idea is to replace the solid support for TBLMs with a single nanoporous Si_3N_4 membrane as depicted in figure 1.12. In this work, nanoporous Si_3N_4 membrane chips were designed and fabricated. Then these nanoporous membrane chips were fully passivated electrically by thermal oxidation with SiO_2. Both thiol and triethoxysilane based TBLMs were formed across each single

nanopore and electrical properties of Nano-psTBLMs were characterized with EIS and PPC. Single channel recording was demonstrated by integration of bacterial toxin alpha hemolysin into Nano-psTBLM. Objectives of the work include (i) the surface design, assembly and characterizations of single nanopore suspended TBLMs for stable and reliable biosensing platform, and (ii) the subsequent integration of transmembrane proteins for single/multiple ion channels analysis for possible biosensing in future bio-medical, environmental and bio-defence applications.

2 Experimental and instrumentation

Experimental and analytical tools employed mainly in this work are electrochemical impedance spectroscopy (EIS), surface plasmon resonance (SPR) and planar patch clamping (PPC).

2.1 Electrochemical Impedance Spectroscopy (EIS)

2.1.1 Theory

Electrochemical impedance spectroscopy (EIS) is a powerful analytical technique to study the dielectric properties of a medium in electrolytic environment. It is employed routinely as a major analytical tool in the fields of corrosion, battery and fuel cell research but recently the application of EIS has extended into the biochemical and biotechnological research. Impedance, analogous to electrical resistance, is a property to resist the flow of alternating current (AC) in complex systems. Resistance (R), on the other hand is defined as the ratio between electrical voltage (E) and current (I) as described in well known Ohm's Law:

$$R = \frac{E}{I} \qquad (2.1)$$

Unfortunately, many simplifying assumptions for the resistor are considered in Ohm's law. In an ideal resistor, it is assumed that the AC current and the voltage signals are in phase at all times. The resistance of an ideal resistor is frequency independent and it obeys Ohm's law at all levels of current and voltage. However in practical situations, real electrical circuits such as biological cell membranes exhibit more complex behaviours of energy storage and dissipations. Therefore simplified Ohm's law is not sufficient to study the complex systems and the impedance, a generalized form of resistance, is introduced. Impedance defined as Z, also relates the electrical voltage with the current as in Ohm's law but frequency dependent and phase difference properties of excitation potential and output current are taken into consideration.

Electrochemical cells are not linear in nature as changing electrical potential cannot produce proportional output current linearly. However, when voltage against current graph is divided into small portions, each confined segment is almost linear. In order to confine the electrochemical cell into so called pseudo-linear range, only a small excitation signal (AC electrical voltage in the order of a few mV) in different frequencies is applied across the system under study and the resulting output signal (AC

electrical current) is measured. In a linear system when a sinusoidal excitation signal is applied at a certain frequency, then the output current signal is also sinusoid at the same frequency but with the different phase (figure 2.1).

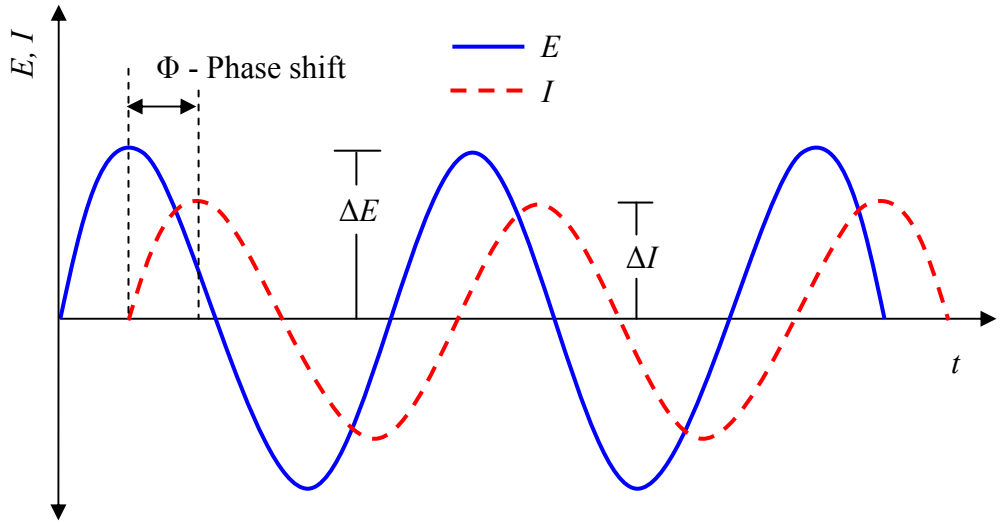

Figure 2.1 Sinusoidal excitation voltage and output current as a function of time in linear systems

The applied excitation AC potential as a function of time t is

$$E_t = \Delta E \sin(\omega t) \tag{2.2}$$

where ΔE is the amplitude of voltage and ω is the radial frequency which is related to the linear frequency f as:

$$\omega = 2\pi f \tag{2.3}$$

Then the output AC current as a function of time which is phase-shifted by Φ is

$$I_t = \Delta I \sin(\omega t - \Phi) \tag{2.4}$$

Then the impedance of the system becomes

$$Z = \frac{E_t}{I_t}$$

$$= \frac{\Delta E \sin(\omega t)}{\Delta I \sin(\omega t - \Phi)}$$

$$= \Delta Z \frac{\sin(\omega t)}{\sin(\omega t - \Phi)} \tag{2.5}$$

Therefore in impedance measurements, ΔI and Φ are measured as a function of radial frequency ω. Alternatively the impedance can be described as a complex function in complex plane (figure 2.2).

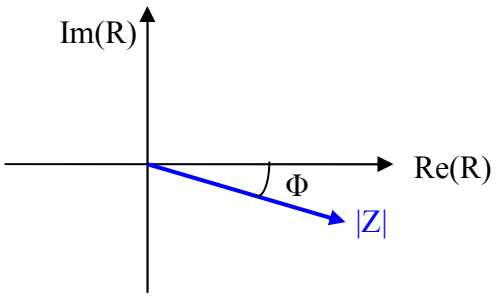

Figure 2.2 Impedance |Z| as a vector quantity described in a complex plane

With the complex function, excitation AC potential is described as:

$$E_t = \Delta E \exp(j\omega t) \tag{2.6}$$

And the respective AC current response is

$$I_t = \Delta I \exp(j\omega t - j\Phi) \tag{2.7}$$

Therefore the impedance as the complex number is represented as:

$$\begin{aligned} Z_t &= \frac{E_t}{I_t} \\ &= \Delta Z \exp(j\Phi) \\ &= \Delta Z \cos\Phi + \Delta Z j \sin\Phi \end{aligned} \tag{2.8}$$

where $\Delta Z \cos\Phi$ and $\Delta Z j \sin\Phi$ are real and imaginary parts of the impedance Z respectively.

2.1.2 Experimental

2.1.2.1 Setup

For the impedance measurement, microAutolab/FRA2 impedance spectrometer (Metrohm, Switzerland) was used to apply the AC excitation potential and measure the AC current response through three electrodes attached to the electrochemical cell. The potentiostat is a feedback amplifier which controls the applied potential at working electrode (WE). Potential at working electrode is measured with respect to reference electrode (RE). The current response is measured between working electrode and counter electrode (CE). Template stripped gold (TSG) was employed as WE and at the same time it was used as a substrate for thiol based monolayer assembly. RE was Ag/AgCl (DRIREF-2 from World Precision Instruments Inc, FL, USA) and CE was a high purity platinum wire with 1 mm in diameter. Electrochemical cell was made of Teflon with a cylindrical enclosure with a capacity of 1 ml.

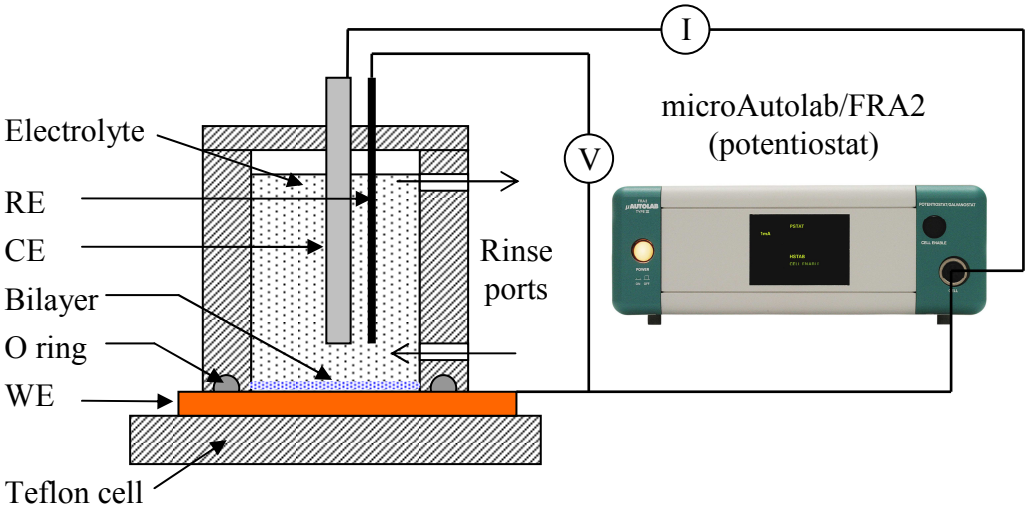

Figure 2.3 Schematic of electrochemical cell and the impedance measurement setup

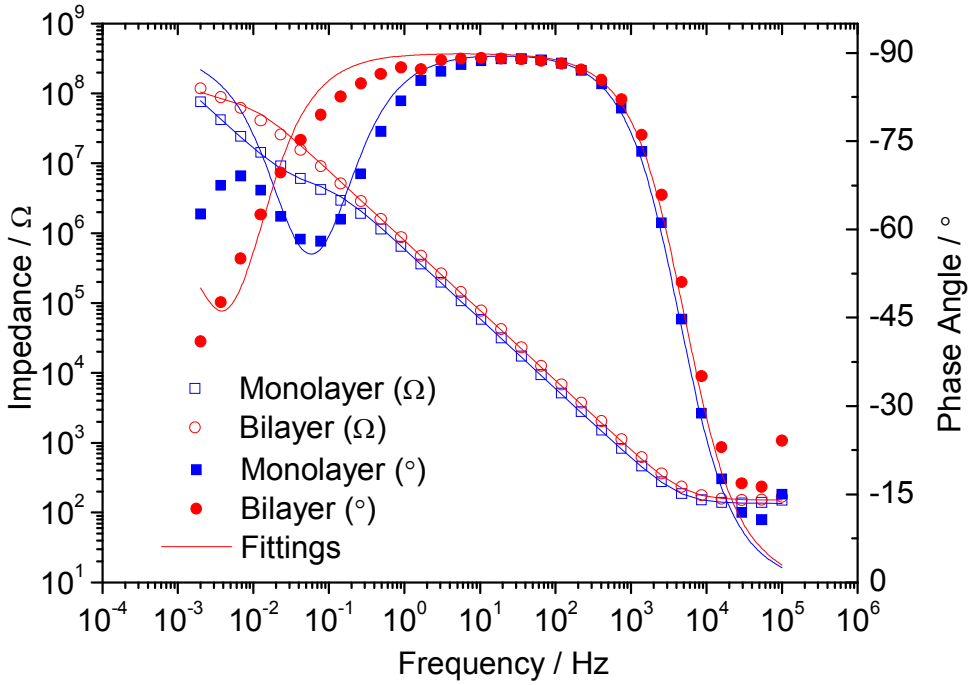

Figure 2.4 Bode plot of impedance of a monolayer and the subsequently formed tethered bilayer lipid membrane after vesicles fusion

Measurement area exposed to saline solution was a circular spot with a surface area of 0.28 cm^2. The electrochemical cell was designed with the fitted ports on the side for easy exchange and rinse of buffer solution. During the impedance measurement, the cell was put inside a Faradic box made of aluminium in order to shield the electromagnetic noises from the surrounding. Impedance spectra were recorded for frequences between 2 mHz and 100 kHz at 0 V bias potential with an AC modulation amplitude of 10 mV. The results were directly plotted in Bode and Admittance plots using the computer

controlled FRA software, and the measured data were analyzed with ZView analysis software (Scribner Associates, NC, USA). Schematic of the electrochemical cell and the measurement setup is shown in figure 2.3. Only the above mentioned parameters were used throughout all the impedance measurement of pTBLM in this work.

2.1.2.2 Measurement

TSG slide self-assembled with the monolayer on its surface was fixed between the base plate and the cylindrical cell with an O ring. 100 millimolar (mM) NaCl buffer was filled into the cell and the monolayer on TSG surface was first hydrolyzed. The Teflon lid carrying RE and WE was covered on top of the cell and the measurement was carried out as schematic shown in figure 2.3. After first impedance measurement, 20 µl of small unilamellar vesicles (SUVs) prepared in Milli-Q water were injected from top of the monolayer onto TSG surface. Then the bilayer formation by fusion of SUVs was monitored by repeated impedance measurements for a few hours. Vesicles fusion and bilayer formation were completed when the bilayer gave steady and constant impedance with time. Then the electrochemical cell was rinsed with 100 mM NaCl electrolyte before the injection of toxins or proteins for the further analysis. Bode and admittance plots of monolayer and subsequent TBLM formed on TSG surface are shown in figure 2.4 and 2.5 respectively.

2.1.3 Data presentation

2.1.3.1 Equivalent circuit elements and models

In electrochemical cells, the medium under study is treated as the combination of electrical circuit elements and fitted with an appropriate equivalent circuit model in order to interpret the experimental results. Common circuit elements are resistors, capacitors and inductors and they are assembled together in series and/or in parallel networks to fit the measured data. The circuit elements need to represent the basic physical and electrical properties of the system, for example a lipid bilayer membrane is modelled as a resistor and a capacitor in parallel (an RC element). The capacitor and resistor represents the energy storage and dissipation respectively as the lipid bilayer exhibits both storage and dissipation of energy. In the following section, useful information and impedance of all the circuit elements and models employed in this work are explained.

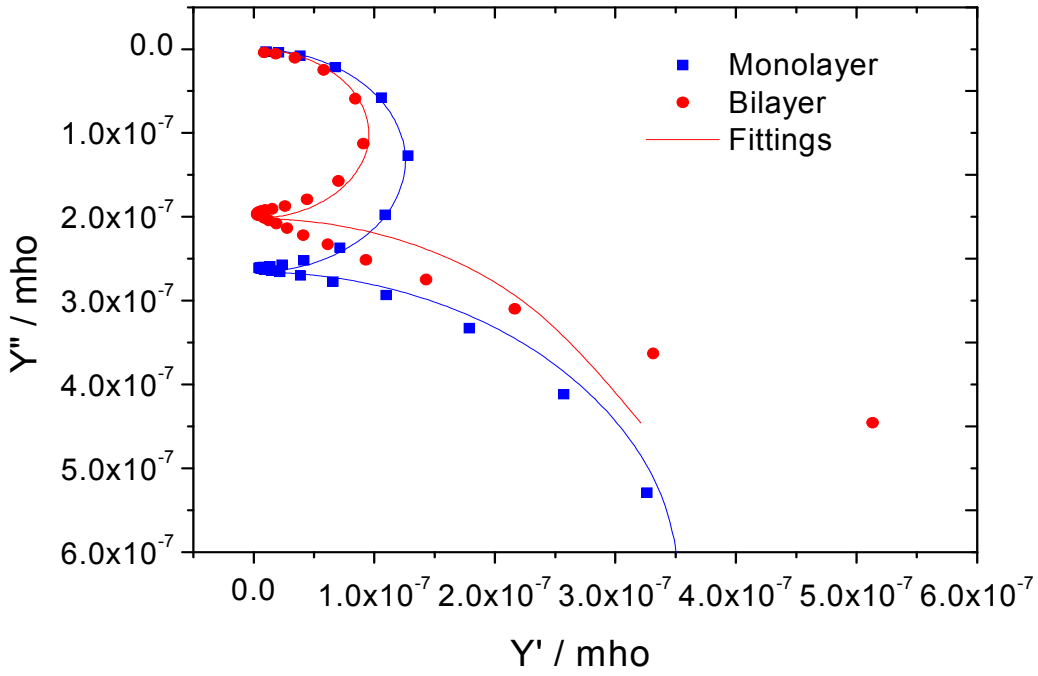

Figure 2.5 Admittance plots of a monolayer and the subsequently formed tethered bilayer lipid membrane after vesicles fusion (admittance plot is frequency independent as the real (Y' on x-axis) and imaginary (Y" on y-axis) parts of the admittance are frequency normalized, and unit of admittance is siemens or mho)

Impedance of a resistor - R

Impedance of a resistor has only the real component as it is the frequency independent and the current flowing through the resistor is in phase with the applied voltage. Therefore the impedance of a resistor is equal to the resistance i.e., $Z = R$ (where $\Phi = 0$) with the current-voltage relationship follows the Ohm's Law of $E = IR$ (figure 2.6A).

Impedance of a capacitor - C

Impedance of a capacitor is frequency dependent and it increases at the lower frequencies. Capacitance is

$$Q = CV \qquad \text{or} \qquad I_t = C\frac{dE_t}{dt} \tag{2.9}$$

In complex function, excitation AC potential is

$$E_t = \Delta E \exp(j\omega t)$$

$$\frac{dE_t}{dt} = \Delta E j\omega \exp(j\omega t) \tag{2.10}$$

Substituting equation (2.10) into equation (2.9)

$$I_t = CEj\omega \exp(j\omega t) \tag{2.11}$$

As the impedance of a capacitor is

$$Z_c = \frac{E}{I} = \frac{\Delta E \exp(j\omega t)}{C\Delta Ej\omega \exp(j\omega t)} = \frac{1}{j\omega C} = -\frac{j}{\omega C} \tag{2.12}$$

where Φ = - 90º

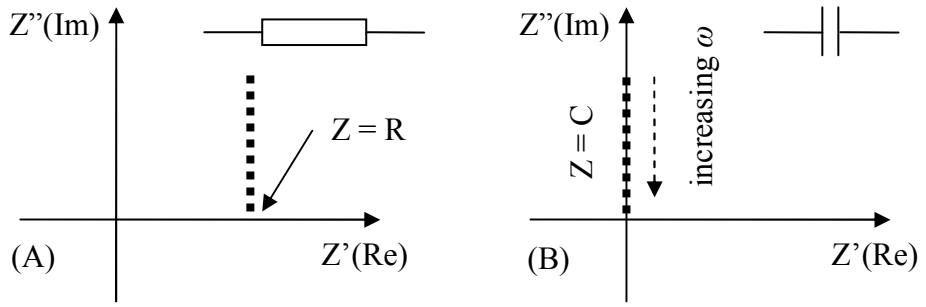

Figure 2.6 Complex planes (Nyquist plots) representing the impedances of (A) a resistor and (B) a capacitor

Therefore capacitor has only imaginary component of impedance and the current through a capacitor is –90 degrees out of phase with the applied voltage i.e., $Z_c = -\frac{j}{\omega C}$ with the current-voltage relationship of $I = C\frac{dE}{dt}$ (figure 2.6B).

Common plots used in impedance data representation are Nyquist (complex plane), Bode and Admittance plots. Real part of impedance (Z') is presented against the imaginary part of impedance (Z") in Nyquist plot. The major shortcoming of this plot is high and low frequency data are compressed and the frequency dependent information of impedance is not presented. This shortcoming is overcome in Bode plot which provide the impedance data vs. frequency. Bode plot represents the absolute impedance (|Z|) and the phase angle (Φ) with the frequency in logarithmic scale. Therefore Bode plot directly gives the approximate resistance information in different frequency regimes but there is no explicit information about the capacitance which is only given in admittance plot. Admittance (Y), in unit of siemens or mho, is related to the impedance (Z) as a function of frequency (ω) as:

$$Y(\omega) = \frac{1}{Z(\omega)} \tag{2.13}$$

Impedance of a resistor in series with a capacitor - RC

When a resistor and a capacitor are connected in series, resultant impedance is the sum of impedances of the resistor and the capacitor (figure 2.7).

$$Z = Z_R + Z_C$$

$$= R - \frac{j}{\omega C}$$

As impedance of a capacitor is function of inverse frequency and therefore,

at high frequencies, $-\frac{j}{\omega C} \approx 0$ and Z becomes $Z \approx Z_R$ (2.14)

at low frequencies, $-\frac{j}{\omega C} \neq 0$ and Z becomes $Z = Z_R + Z_C$ (2.15)

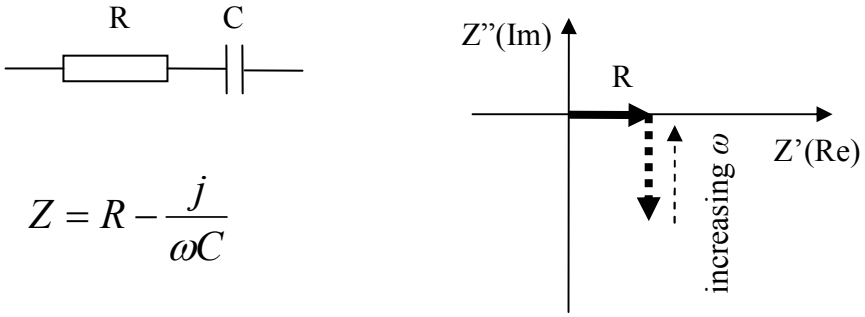

Figure 2.7 Complex plane (Nyquist plot) representing the impedance of a resistor and a capacitor in series

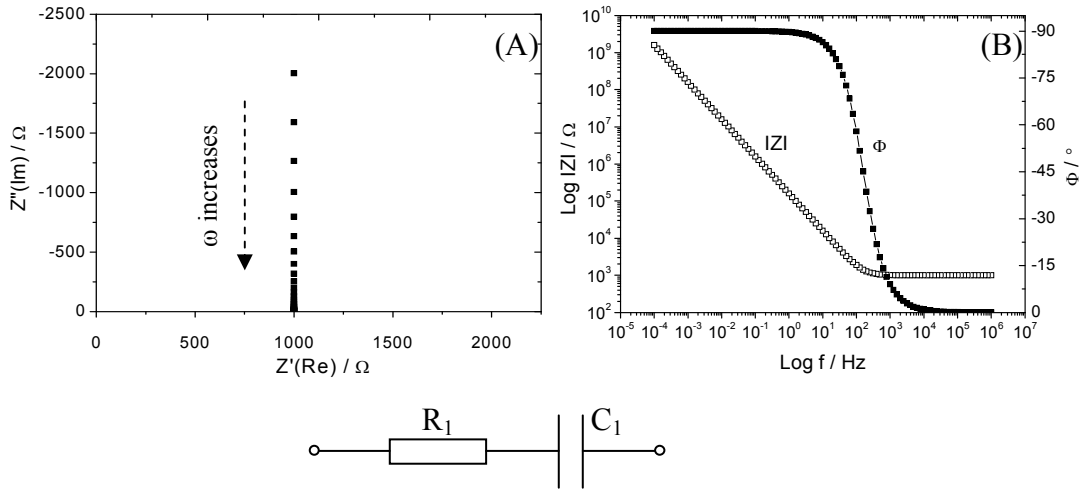

Figure 2.8 (A) Nyquist and (B) Bode plots of an equivalent circuit with a resistor and a capacitor connected in series (inset is a circuit model R_1C_1)

Bode plot and Nyquist plot of a circuit with a resistor and a capacitor connected in series is shown in figure 2.8. For the better representation, the circuit is modelled with 1

kΩ resistor (R_1) in series with 1 μF capacitor (C_1). At higher frequencies above 100 Hz, impedance is dominated by resistor (R_1) (equation 2.14) and both plots in figure 2.8 indicate impedance in high frequency region. In Nyquist plot (figure 2.8A), impedance measured at each frequencies is not informed as the frequency data is compressed. However in Bode plot (figure 2.8B) the frequency dependent impedance is explicitly shown. In lower frequency regime below 100 Hz, impedance is dominated by both resistor (R_1) and capacitor (C_1) with phase shift of -90 degree (equation 2.15).

Impedance of a resistor in series with a resistor and a capacitor in parallel – R(RC)

In this circuit model, a 100 Ω resistor (R_1) is connected in series with a 2 kΩ resistor (R_2) and a 1 μF capacitor (C_2) in parallel as shown in figure 2.9. When R_2 and C_2 are connected in parallel, impedance becomes:

$$\frac{1}{Z_{RC}} = \frac{1}{Z_{R2}} + \frac{1}{Z_{C2}} \qquad (2.16)$$

$$= \frac{1}{R_2} + \frac{1}{1/j\omega C_2}$$

$$= \frac{1}{R_2} + j\omega C_2$$

$$Z_{RC} = \frac{R_2}{(1 + j\omega R_2 C_2)} \qquad (2.17)$$

Therefore for (R_2C_2) element,

at low frequencies, $j\omega R_2 C_2 \approx 0$ and Z_{RC} becomes $Z_{RC} = R_2$ (2.18)

at high frequencies, $j\omega R_2 C_2 \neq 0$ and Z_{RC} becomes $Z_{RC} = \frac{R_2}{(1 + j\omega R_2 C_2)}$

Then resultant impedance of the circuit model is

$$Z = Z_{R1} + Z_{RC}$$

$$= R_1 + \frac{R_2}{(1 + j\omega R_2 C_2)} \qquad (2.19)$$

At high frequency regions, current bypasses R_2 and flow through R_1 and C_2. Above the frequency of 10^4 Hz, impedance is purely resistive and it has only the real part as there is almost no phase difference. This estimates the impedance of 100 Ω in both plots of figure 2.9. In frequency range between 1 to 10^4 Hz, a phase different exists and impedance displays both real and imaginary values. This is indicated by a semicircle in Nyquist plot (figure 2.9A) where each RC element corresponds to a semicircle and

frequency is equal to the inverse of R_2C_2 - time constant at the apex of semicircle. At frequencies below 1 Hz, impedance is again dominated by resistors (equation 2.18 and 2.19) and current flows through resistors. An approximate impedance of about 2.1 kΩ is shown in plots of figure 2.9. It is important to note here that defining relevant circuit elements and correct combination of them to form a model circuit play an important role in representing useful data out of impedance measurements. Depending on the system under study, several circuit elements can be involved. For the work with lipid bilayer membranes, a few circuit elements involved are discussed below.

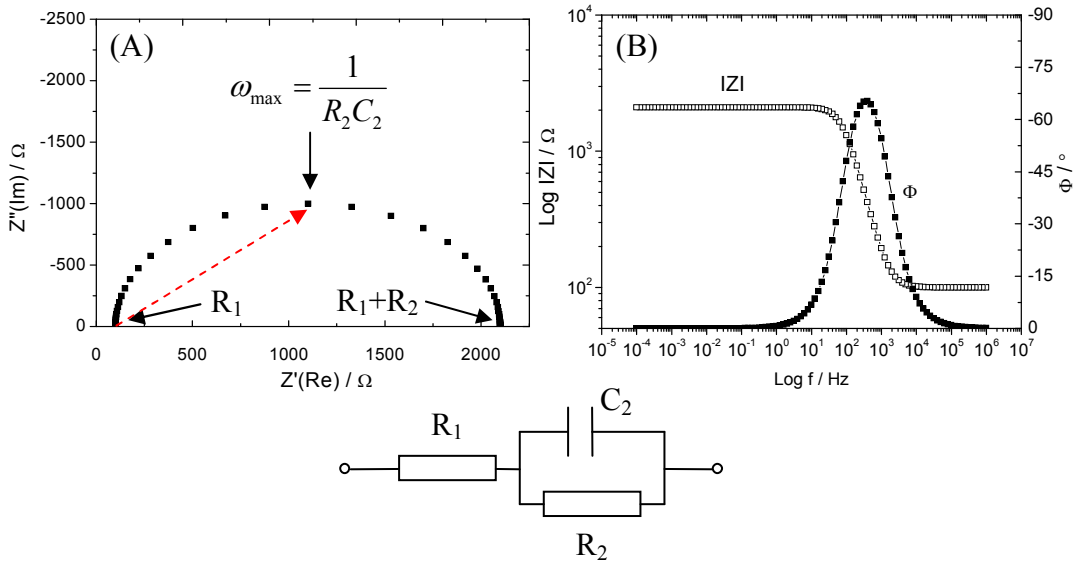

Figure 2.9 (A) Nyquist and (B) Bode plots of an equivalent circuit with R_1 in series with C_2 and R_2 in parallel [inset is the equivalent circuit model $R_1(R_2C_2)$]

Resistance and capacitance of monolayer (R_m and C_m) and bilayer (R_b and C_b)

Lipid bilayer membrane is considered as a two dimensional dielectric layer suspended between an aqueous medium of electrolyte with infinite length (figure 2.10). It is also an effective hydrophobic medium in a hydrophilic environment and therefore when an electrical potential is applied across the lipid bilayer, it exhibits both energy storage and dissipation mechanisms which are modelled with a capacitor and a resistor in parallel (an RC element) respectively. Biological lipid bilayer membranes in eukaryotic cells have a membrane capacitance of about 1 μF/cm^2 but membrane resistance can be varied from a few hundred kΩ cm^2 to tens of MΩ cm^2, depending on ion permeability of specific membranes.

Electrolyte resistance (R_e)

100 mM NaCl buffer has fairly ionic conductiion in general but there exists an electrolyte resistance (R_e) between reference and working electrodes. R_e of an electrolyte depends on type and concentration of ions, temperature of the electrolyte and the geometry of electrode area in contact with the electrolyte. R_e is defined as:

$$R_e = \rho \frac{l}{A} \tag{2.20}$$

where ρ = solution resistivity

A = surface area of electrode in contact with electrolyte

l = length of electrolyte carrying the uniform current

Solution resistivity varies for different types of electrolytes. Electrochemical cells generally do not generate the uniform distribution of current and therefore calculation of R_e using the equation (2.20) is inaccurate. Instead R_e of a particular electrochemical cell is usually obtained by fitting the model to the measured data.

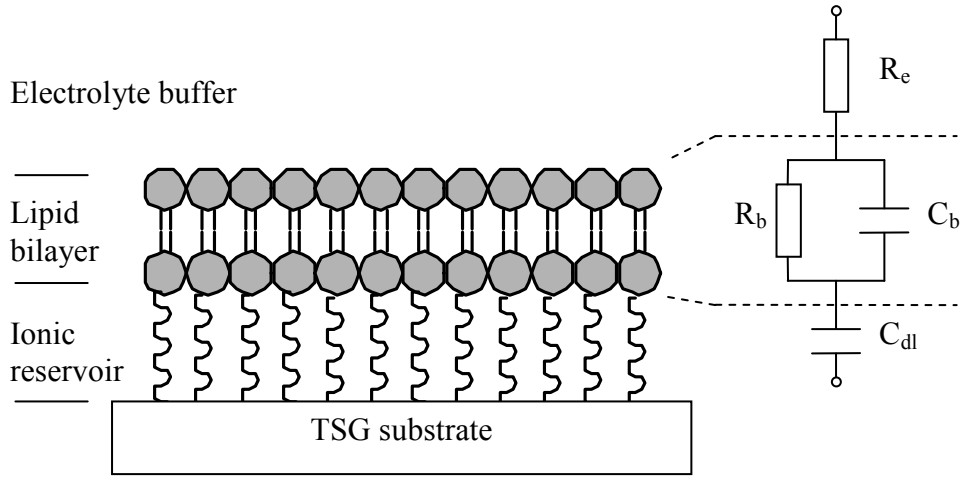

Figure 2.10 Schematic of tethered bilayer lipid membrane (TBLM) on TSG substrate with an equivalent circuit model used to fit the measured data (R_e is electrolyte resistance, C_{dl} is double layer capacitance, R_b and C_b are resistance and capacitance of lipid bilayer respectively)

Double layer capacitance (C_{dl})

When a metal is placed in an electrolyte, there always an electrical double exists at the metal-electrolyte interface. This in electrochemical cells is due to ions in electrolyte which come, contact and shield the electrode surface. Resulting charge separation by a layer of ions is very small, within a distance of a few angstroms from electrode surface, and forms a double layer capacitance which is represented as:

$$C_{dl} = \frac{\varepsilon_r \varepsilon_o A}{d} \tag{2.21}$$

where A = surface area of electrode in contact with electrolyte

d = thickness of electrical double layer

ε_r = relative electrical permittivity

ε_o = electrical permittivity of electrolyte

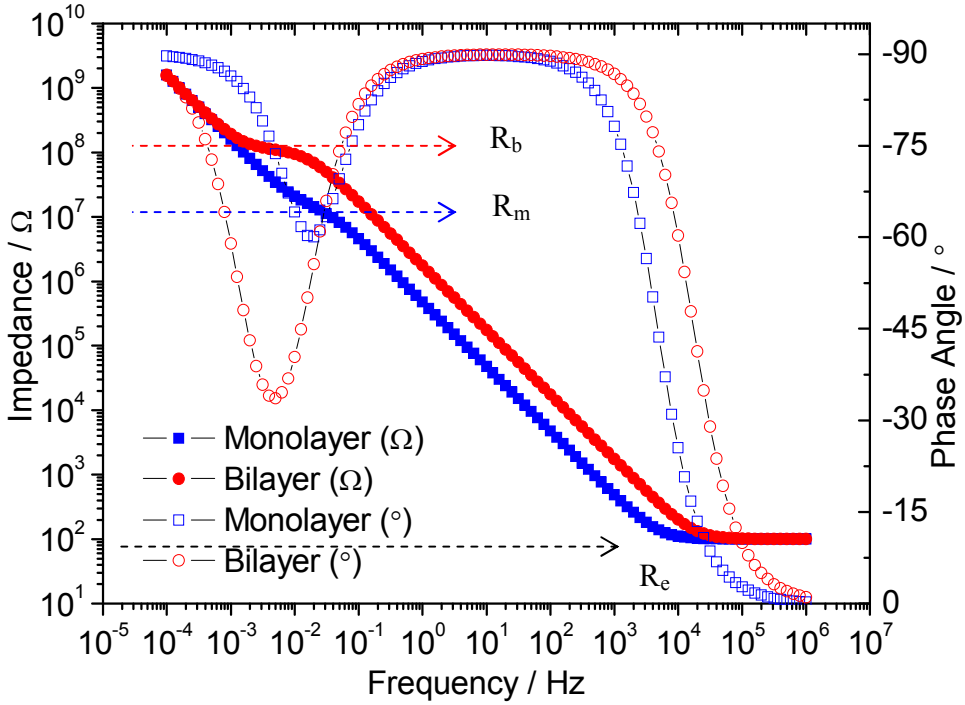

Figure 2.11 Bode plot of the impedance of a monolayer and the subsequently formed pTBLM on TSG surface (this plot is modelled and fitted with the equivalent circuit depicted in figure 2.10, with the circuit elements of R_e (100 Ω), R_m (10 MΩ), R_b (100 MΩ), C_{dl} (1 µF), C_m (0.35 µF) and C_b (0.1 µF) for demonstration purpose)

C_{dl} also depending on many parameters including surface roughness of electrode and electrode potential, type and concentration of ions, temperature, adsorption of impurities and formation of oxide layers. But C_{dl} of bare gold (Au) surface in an electrolyte can be estimated to ~30 µF/cm^2 [202]. Hence RC element of a lipid bilayer is connected in series with R_e and C_{dl}. A schematic of pTBLM on TSG substrate and an equivalent circuit model used in fitting of measured impedance data are depicted in figure 2.10.

2.1.3.2 Data fitting and representation

All impedance data presented in this work are fitted with the model circuits and experimental data were interpreted using Bode and admittance plots. Nyquist plot on the

other hand, is not presented here as it was not useful to represent the data. Model circuit used to fit measured data of monolayer and lipid bilayer membranes is depicted in figure 2.10. An advantage of bode plot is impedance and phase data which are plotted in overlapped fashion and this informs the immediate relationship between impedance and phase in different frequencies throughout the measurement. In figure 2.11, filled and unfilled data points represent impedance and phase respectively. Impedance graph of the monolayer can be separated into two distinct parts: two flat regions with negative slopes and two flat plateaus which are accompanied by low phase angles in higher and lower frequency regions. Impedance in regions of these flat plateau are dominated by resistors and data on left axis indicates two resistances of about 100 Ω (at above 10 kHz) and 10 MΩ (in around 10 mHz) (figure 2.11). This gives approximate resistances: 100 Ω is the electrolyte resistance (Re) and 10 MΩ is the resistance of monolayer (R_m). On the other hand, two flat regions with negative slopes are accompanied by a phase shift of -90 degree and impedances in these regions are dominated by capacitors.

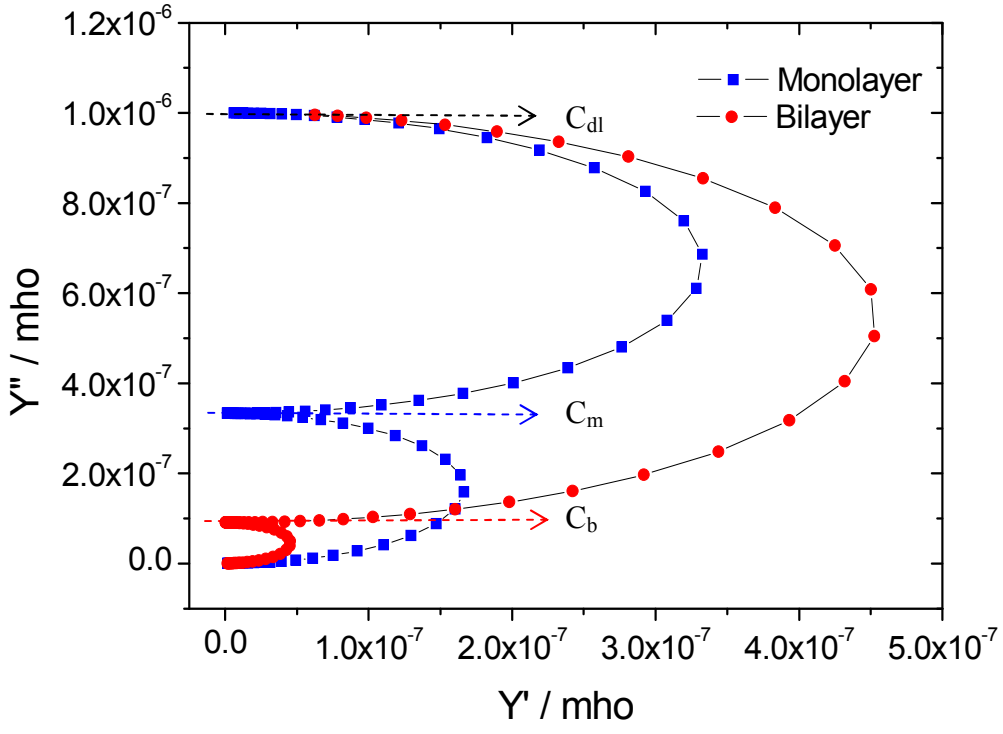

Figure 2.12 Admittance plot of a monolayer and the subsequently formed pTBLM on TSG surface (circuit elements are same as described in figure 2.11 and admittance plot provides the capacitances of monolayer (C_m) and bilayer (C_b) as well as the double layer capacitance (C_{dl}) with the fitting)

When bilayer membrane is formed on top of monolayer, R_e remains the same but resistance of bilayer increases one order magnitude higher than that of monolayer i.e.

100 MΩ (R_b). As the lipid bilayer is an effective barrier to ion permeation in electrolyte, increase in resistance after formation of bilayer is expected and this is estimated by extrapolation of the flat plateau of bilayer impedance graph in lower frequency region (figure 2.11). Therefore Bode plot gives direct approximation of monolayer and bilayer resistances (R_m and R_b) before fitting but it does not provide respective capacitances in approximation. In admittance plot, real and imaginary parts of admittance are frequency-normalized and hence the plot is frequency independent (figure 2.12). The plot presents impedance data in two semicircles that represent two capacitors. C_{dl} due to electrolyte in contact with gold electrode surface is not essentially changed in admittance plots of monolayer and bilayer, but capacitance is changed as the bilayer is formed. Monolayer capacitance (C_m) is estimated about 0.35 μF when the first semicircle of admittance plot intersects Y axis (figure 2.12). As the bilayer is formed, the size of first semicircle decreases and the intersection on Y axis gives an estimated bilayer capacitance (C_b) of around 0.1 μF.

2.2 Surface Plasmon Resonance (SPR)

2.2.1 Theory

Surface plasmons (SPs) are propagation of electromagnetic waves due to oscillation of surface electrons at metal-dielectric interface. The wave propagates on metallic surface in the direction parallel to interface. As oscillations occur on the surface, it is very sensitive to surface changes at the interface in molecular level, for example, adsorption of molecules on metallic surface. Natural propagation of SPs carries lower energy which can then be enhanced by coupling with either electron or photon energy excitations. Out of two coupling methods, photon coupling is widely used. When a light beam hits the interface of two transparent media with different refractive indices (for example from higher refractive index glass prism to lower refractive index air), light is partly reflected and refracted at glass-air interface. This is described by Snell's law:

$$\frac{\sin\theta_p}{\sin\theta_a} = \frac{n_a}{n_p} \qquad (2.22)$$

Where θ_p is the angle of incidence and reflection

θ_a is the angle of refraction and

n_p and n_a are refractive indices of glass and air respectively

As the angle of incidence θ_p increases above the critical angle θ_c, there is no refracted light across the interface and total internal reflection (TIR) is occurred. Electromagnetic component of the incident light penetrates a short distance (a few nanometers) in the medium with lower refractive index (air in this case), and creates the evanescent field which exponentially decays with time normal to the surface. However if the air is replaced with a thin layer of metal (e.g. gold), then the resonance energy transfer can be taken place between evanescent field and SPs at metal surface. An important requirement for the surface plasmon coupling with photons is that the light used for excitation must be monochromatic, p-polarized light which has photon wave vector matched with that of SPs. This is usually done by prism coupling which has two common configurations namely Kretschmann and Otto configurations as shown in figure 2.14.

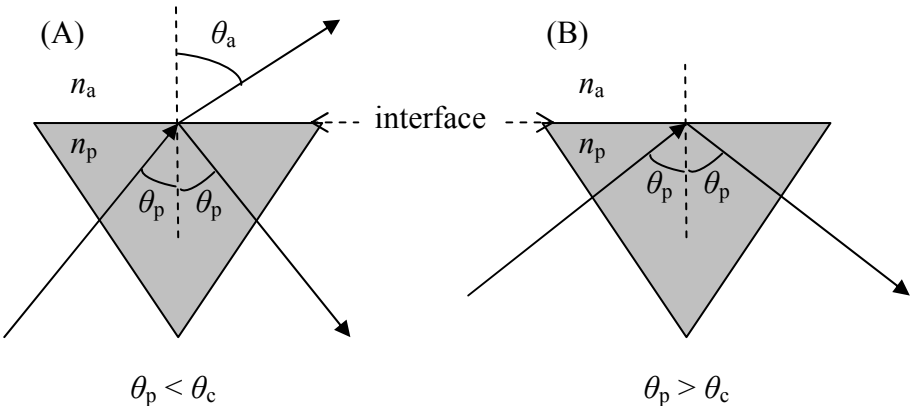

Figure 2.13 Law of reflection (A) incident light is partly reflected and partly refracted as the angle of incident is less than the critical angle and (B) total internal reflection occurs when the angle of incident is greater than the critical angle

In Kretschmann configuration, a thin gold film is coated on a glass prism and the evanescent field generated at the interface penetrates the gold film when light is illuminated from the glass prism. SPs are then excited at the outer surface of gold film (figure 2.14A). This configuration is mostly used in practical SPR setups and applications. On the other hand in Otto configuration, gold film is brought proximity to the glass prism where the light beam is entered. The generated evanescent field crosses the dielectric medium (air for example) and excites SPs at gold surface (figure 2.14B). As the energy transfer is taken place between evanescent field and SPs, the intensity of reflected light is reduced at a specific incident angle (figure 2.15). This surface plasmon resonance condition is strongly influenced by the materials adsorbed on metal surface. Therefore a fairly linear relationship exists between the resonance energy and the

concentration of analyte molecules such as proteins and DNA at metal surface. Binding of analyte molecules on a surface changes the refractive index locally and this can be detected by shift in minimum angle where maximum coupling of surface plasmons is occurred.

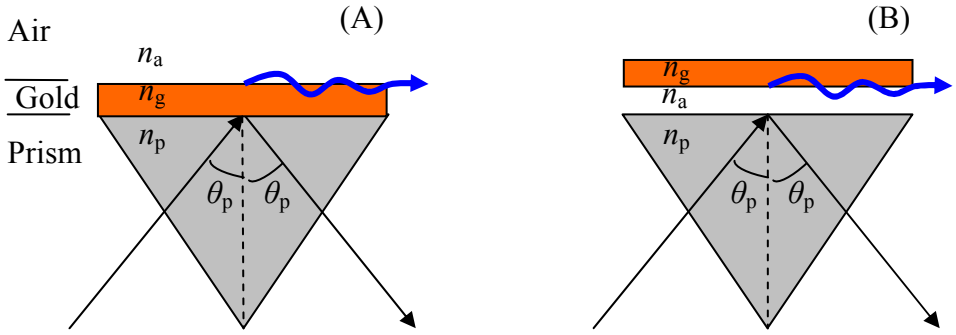

Figure 2.14 (A) Prism coupling by Kretschmann configuration where the surface plasmons (SPs) are excited by the evanescent field generated at the interface where photons of incident light transfer energy to free electrons at the Au surface (note that SPs occurred at the free Au surface and SPs are very sensitive to localized surface conditions, and (B) prism coupling by Otto configuration

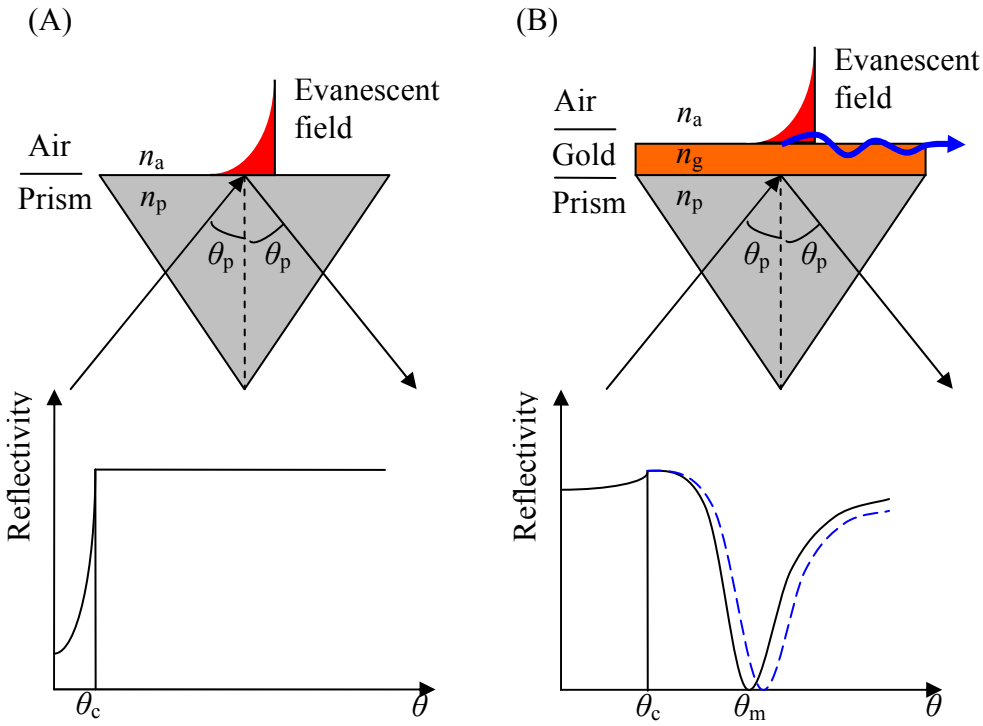

Figure 2.15 (A) Total internal reflection occurs at the prism-air interface where the generated evanescent field decays exponentially as there is no coupling by the metal film (note the reflective intensity remains unchanged as in respective resonance curve below figure A). (B) In attenuated total internal reflection beyond the critical angle, the intensity of reflected light reaches lowest at the minimum angle where the maximum coupling of SPs occurred by the evanescent field (dashed line in resonance curve (below figure B) shifts to the higher angles as in case of the thickness of the adsorbed film increases due to binding of, for example biomolecules)

SPR has been extensively employed as biosensors particularly in binding of biomolecules onto the receptors which are attached onto metallic surfaces. This technique reveals the molecular adsorptions as well as the kinetics of association and dissociation of analytes in real-time scale. The advantage of SPR technique is non-destructive while providing the real-time binding and interaction of molecules onto the surfaces sensitively.

2.2.2 Experimental

2.2.2.1 Setup

The SPR setup employed in this work is the Autolab ESPRIT (Metrohm, The Netherland). It has two separate channels in parallel and the measurement is taken place in cuvette with a sample volume of 20 – 50 µl each. Ports of buffer inlet and outlet are connected to each channel, and exchange and rinse of buffer solution is operated by peristaltic pumps with the computer controlled variable flow rates ranging from 30 µl/sec to 130 µl/sec. A laser light with a fixed wavelength of 670 nm is used through a hemi-cylindrical glass prism for coupling of SPs at the interface of gold and the buffer solution. Measurable angular dynamic range is up to 4000 m° (milli-degree) with the angle resolution less than 0.02 m°.

The substrate is a gold coated circular BK7 glass disk provided from Autolab, Metrohm. Using an appropriate type of immersion oil, refractive index of the glass disk is matched with that of the hemi-cylindrical glass prism. Excitation of SPs is at the gold surface expose to buffer solution in cuvette and the coupling is done with Krestschmann configuration (section 2.3.1). SPR measurement was controlled by computerized data acquisition software (version 4.3.1, Eco Chemie B.V, The Netherland) and SPR data are measured and plotted real-time in two modes. The first is the scope mode which is plotted the minimum resonance angle against the reflectivity in percentage. The second mode is the binding curve plot which displays the absolute minimum of resonance angle (in mº) on y-axis with the measurement time (in seconds) along x-axis. Data are measured and recorded in every 0.5 second. Schematic of the cuvette assembled with a glass disk and hemi-cylindrical prism is depicted in figure 2.16. Temperature of the buffer inside the cuvette is precisely controlled by an external temperature controller. Analog control thermal bath with a circulator (HAAKE, Thermo Electron Cooperation, UK) is used to heat up the distilled water which is then circulated around the cuvette in a close-circuit flow. In this way, the temperature of buffer in cuvette is maintained at

37°C with fluctuations less than ±0.1 °C. As SPR measurement involves bacterial protein toxins and enzymes, the cuvettes and all the tubing for buffer circulation are filled with 60 % ethanol (pure ethanol is diluted with MilliQ water in volume) for the prevention of bacterial growth and contamination when SPR setup is not in used.

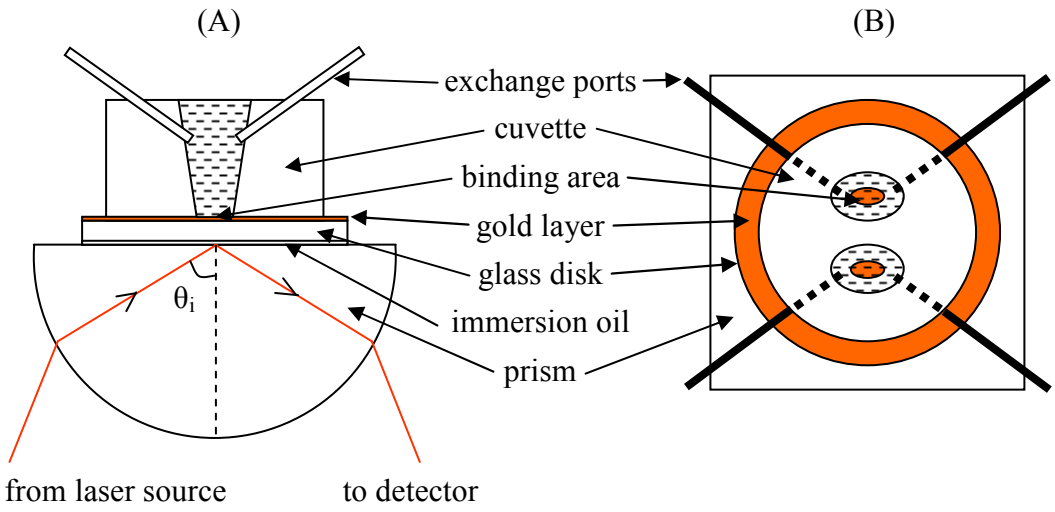

Figure 2.16 Schematic of SPR measurement cell setup (A) side view and (B) top view

2.2.2.2 Measurement

Formation of TBLM

In initial cleaning, the hemi-cylindrical glass prism was ultrasonicated in 2 % (SDS) containing plastic container. Then it was rinsed with Milli-Q water, cleaned in ethanol subsequently and blown dry with nitrogen gas. A gold coated BK7 glass disk carrying DPhyTL monolayer on gold surface was fixed on the planar surface of glass prism with a thin film of immersion oil (with the refractive index of 1.51) in between. The glass prism was then mounted on the holder with the cuvette on top as depicted in figure 2.16. First the cuvette was filled with the electrolyte (100 mM NaCl + 10 mM $CaCl_2$) and the measurement in scope mode which measured the minimum resonance angle against the reflectivity in percentage in both channels was carried out. The 'dip' of the minimum angle should be laid below 10 % of reflectivity, representing the maximum coupling of surface plasmons on gold surface.

By slowly adjusting the micrometer spindle below the optical path cover, the dip of resonance angle minimum was repositioned on to the left around -1500 m°. SPR binding measurement was kept running at this baseline angle for a few minutes. In this case, baseline angle of channel 1 and 2 were not necessarily to be the same. Upon achieving a steady baseline for a few minutes, minimum angle was recorded in scope mode and 20

µl each of 50 nm diameter SUVs prepared in Milli-Q water were injected into both channels from top opening. Fusion of SUVs and formation of lipid bilayer membrane increased the local mass concentration of lipids on gold surface and as a result, resonance angle minimum of monolayer (θ_m) was shifted to the right to that of bilayer (θ_b) (figure 2.17B). Time dependent SPR measurement of bilayer formation was observed in binding curve plot of figure 3.12A where the angle was shifted upward instantaneously upon addition of SUVs. θ_b typically reached to a steady state less than in 3 hours and decreased a little when the channels were rinsed with buffer solution (figure 2.17A).

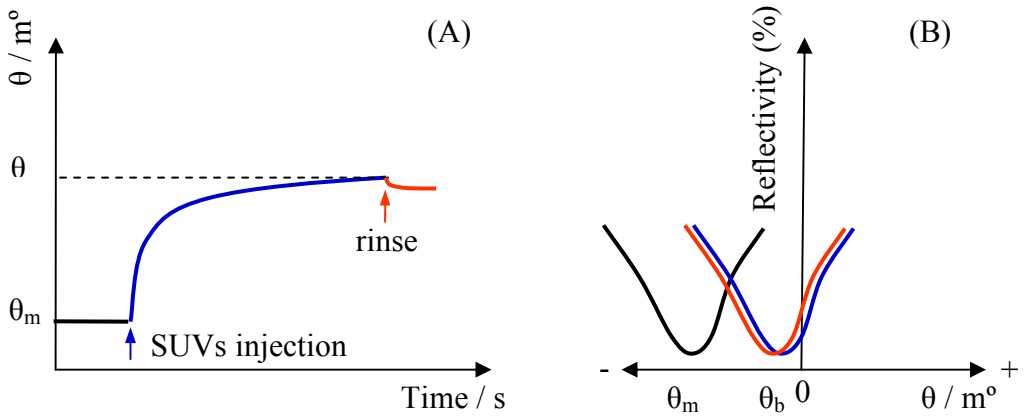

Figure 2.17 SPR data presented in (A) the binding curve plot and (B) the scope mode

Binding of purified bacterial toxin

Commercially available bacterial purified alpha toxin (α-HL) (from Sigma Aldrich, UK) was prepared in concentration of 0.5 mg/ml in PBS solution. Each α-HL ion channel upon oligomerization has a molecular weight of 232.4 kDa and the channels are stable in their heptameric form [90]. Therefore binding of alpha toxins to lipid bilayer membrane in term of change in resonance angle is significant and stable. Typically 0.5 µg/ml of α-HL binding can induce the change in resonance angle minimum of about 800 mº (figure 2.18B for depiction and figure 4.3 for measured SPR data).

2.2.3 Data presentation

2.2.3.1 Resonance angle minimum shift

Formation of lipid bilayer membrane occurs on monolayer by vesicles fusion. As the monolayer is anchored on the gold surface, fusion of vesicles increases the population of lipid molecules in vicinity of the surface and as a result, local mass concentration on

the surface is increased. This in turn changes the refractive index of medium close to the surface. As SPs are very sensitive to change in refractive index, SPR minimum angle θ is shifted to higher value, in order to keep the maximum coupling of SPs for increase in local refractive index. Similar angular shift is also occurred when PFT α-HL binds to lipid bilayer membrane. On the other hand, if the molecules previously bind onto the surface are removed, then the local refractive index of surface is decreased and hence the minimum angle is shifted to lower value for the same reason. Therefore, a general rule of thumb is addition of mass (binding or association of molecules) on the surface shift the angle to positive axis in scope mode. On the other hand, extraction of mass (unbinding or dissociation of molecules) out of the surface shifts the angle to negative axis.

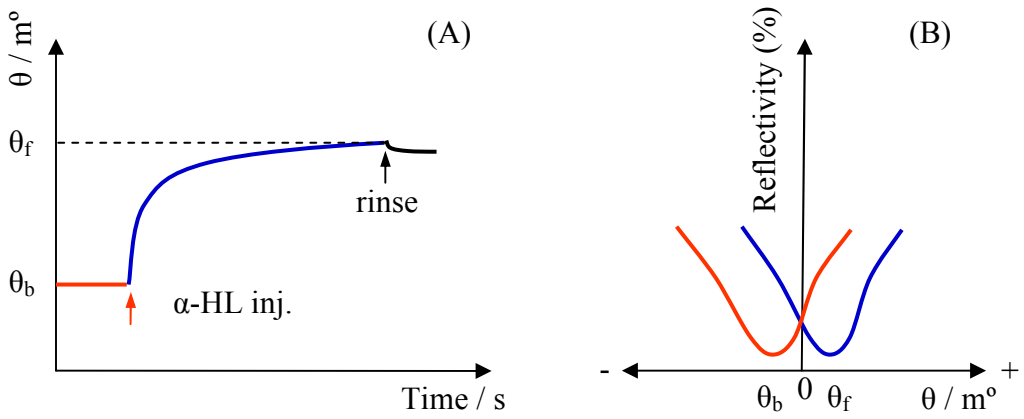

Figure 2.18 Binding of α-HL onto pTBLM where (A) change in reflective angle due to real-time binding of α-HL is measured as the function of time and (B) resonance curve showing the resonance angle minimum shifts (to positive side) due to binding of toxin

2.2.3.2 Real-time kinetic measurement

Binding curve plot is generally useful when the real-time binding of molecules onto lipid bilayer membrane is measured. Not like in scope mode, the signal can be resolved to a slight instantaneous change in minimum angle due to binding of a few toxins. Time dependent measurement also allows the possible measurement of slow binding processes with the minimal concentration of analyte molecules.

2.3 Patch Clamping

Patch clamping, as the name implies, is an electrophysiological technique where a membrane patch of the cell is electrically isolated and clamped with a desired voltage (or current) to study the electrochemical response of ions transport in channel proteins

which are held in the cell membrane patch. This powerful technique, discovered by Neher and Sakmann in early 1980s, is able to resolve and record the ionic current (in the order of 10^{-12}A) as a result of gating by a single voltage-gated ion channel in cell membranes [61]. Single channel recording by patch clamping gives the conductance information and the gating behaviour of ion channels, and leads the discovery of new important ion channels in electrophysiological cell biology [63, 64, 65].

2.3.1 Theory

Depending on clamping modes of the cell membrane, patch clamping is divided into two methodologies namely: micropipette-patch clamping (MPC) and planar patch clamping (PPC).

2.3.1.1 Micropipette-patch clamping

Invented by Neher and Sakmann in 1976, this classical and original patch clamping employed the tip of a very finely polished micro pipette which was brought to the physical contact with a cell membrane suspended in saline solution. Positioning of the micro pipette tip on cell membrane was done by the combined-control of a micro-manipulator and a microscope. Then a negative suction pressure was applied from the micro pipette to create a seal between the pipette tip and the cell membrane which provided an electrical resistance in excess of 10^9 Ohm. By varying applied electrical voltage from micropipette containing saline solution, ionic current in pA gated through ion channels held in the cell membrane patch was recorded. Schematic of pipette patch clamping in cell attached mode is depicted in figure 2.19A. This mode deals with a major shortcoming: ionic species and concentration of cytoplasm of the cell under recording is unknown. When the membrane patch covered by micropipette tip is destroyed by an excessive suction, then the patch clamp accessed to the whole-cell mode where cytoplasmic contents of the cell are replaced by known saline solution (figure 2.19C).

However, whole-cell mode records the resultant current collectively gated by all ion channels of the entire cell membrane. Single or a few channel recording is possible when the tip in cell attached mode is pulled away from the cell while suction pressure was maintained inside the micropipette. This breaks the membrane patch from the cell and inside-out recording is achieved as depicted in figure 2.19B. Inside-out mode has an advantage of working with desired saline solution on both sides of the patch. On the

other hand, outside-out mode is achieved while the micropipette tip is pulled away from the cell in whole-cell mode. As the cell is detached from micropipette, a broken membrane patch re-seals the tip and the outside-out mode is created as shown in figure 2.19D.

Although the patch clamping using a micropipette is powerful and single ion channel recordings have been demonstrated, there are many disadvantages and restrictions for realization of this technique as a standard recording method for use in ion channel research. It requires highly trained physiologists to conduct the experiment while throughput of a successful experiment is very low, from several minutes to a few hours. Moreover in MPC, the cell and its membrane are not easily accessible by other analytical means and this is a major drawback of MPC especially in combining with optical, fluorescence and scanning probe microscopy methods. All these factors become a main thrust in search for the successor, planar patch clamping which provides higher throughput and better compatibility with analytical experimental techniques [98].

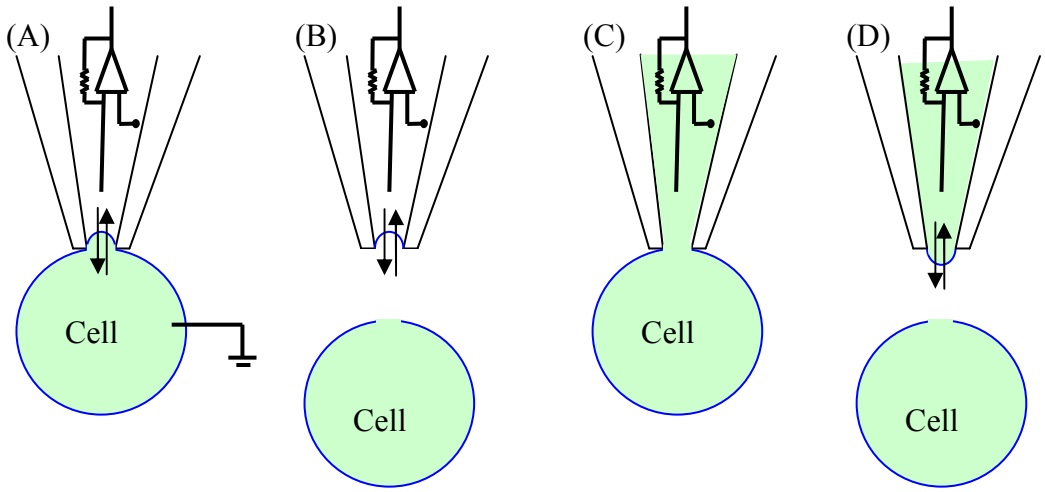

Figure 2.19 Schematic of modes of micropipette patch clamping: (A) cell attached (B) inside-out (C) whole-cell and (D) outside-out

2.3.1.2 Planar patch clamping

In planar patch clamping, the cumbersome micropipette was replaced by a planar support in which a micro hole is machined for sealing the cell membrane as depicted in figure 2.20A. Instead of positioning a pipette on the cell, a cell in suspension is placed on the surface with a micro aperture. With the aid of a microscope and mechanical manipulation, a single cell is then positioned on the hole. By applying suction on the cell through the hole, electrophysiological recording is done by electrodes connected to

the patch clamp amplifier. Type of planar surface can be polyimide film [62], micro-machined glass surface [63], micro-porous Si_3N_4 membrane and silicon substrates [64, 67, 94], lithographically structured photoresist film [65, 66, 68] and porous alumina substrate [74]. Except the experiments in references [62, 67], the rest were studied using the model lipid bilayer membranes motivated by the realization of possible chip-based biosensor devices in future [99].

Successful patch clamping experiment solely depends on electrical sealing between the lipid bilayer and the surface because the current leaking through the seal in parallel to ion channels creates noise in signals recorded [14]. If the noise signal is high enough compared to the measured signal, it is difficult to discriminate the response of ion channels with low conductance. PPC was demonstrated using the surface machined silicon micro-pits with real cell lines and reported that the sealing of cell membrane to the surface was improved by coating the surface with plasma deposited silicon dioxide layer [67]. Planar support also allows the possible integration of patch clamping chip with micro-fluidic devices. Not necessarily limited to living cells, PPC can be applied to measure across the artificial lipid bilayer suspended across the micro/nanopores. This is the major advantage of PPC over its rival and conventional MPC technique.

2.3.1.3 Methods of patch clamping

In general, information desired to measure across the cell membrane decides the methods of patch clamping. This can be either current clamp where voltage signal is measured or the voltage clamp where the current signal is measured.

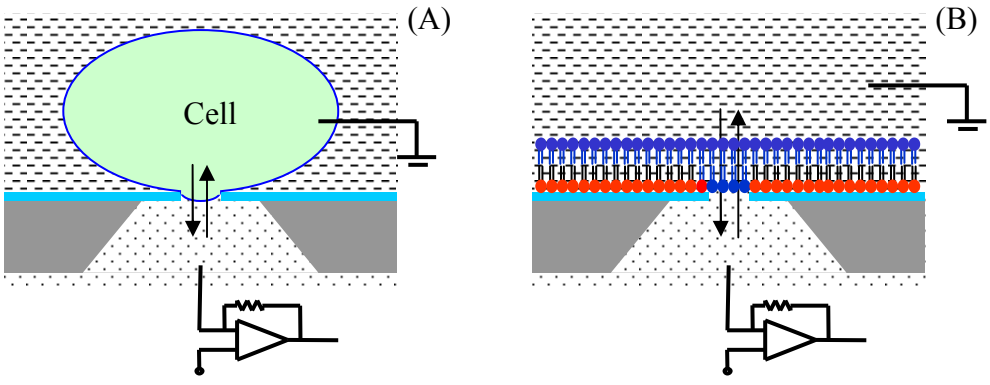

Figure 2.20 Schematic of a planar patch clamping with (A) a cell in suspension and (B) artificial lipid bilayer membrane over a micro/nanopore

2.3.1.3.1 Current clamp

Current clamp method measures and records the transmembrane potential of the cell while the current generated by electrodes is injected across the cell membrane. When the current flows through ion channels held in a membrane patch, the response of membrane potential with time is recorded by the patch clamp amplifier. This membrane potential is functions of the number and the type of ion channels, their nature of gating and the quality of seal formed between the membrane and the surface. This current clamp technique is useful for looking into the response of cell when it is subjected to an electrical current.

2.3.1.3.2 Voltage clamp

Voltage clamp method is the complement of current clamp and it is more commonly used method of choice for ion channel characterization. In this method, a desired cell membrane potential is applied across an electrically isolated patch of the cell membrane with ion channels and the current response is recorded. If the patch contains only a few ion channels, then the single channel recording is possible to be observed by voltage clamping. Most of ion channels are voltage-gated and they have their specific potential range where the gating triggers the ion transport. By tuning the clamping voltage, it is then possible to measure and identify the ion channels by their ionic current and gating behaviours. This can be observed as the fluctuations in ionic current at the holding membrane potential in voltage clamp measurements. In single channel recording, gating of each ion channel exhibits in a few pA discrete steps of ionic current.

2.3.2 Experimental

In this work, PPC was used only in the measurements of ion transport behaviour of α-HL toxin channels inserted in nanopore suspended TBLM (Nano-psTBLM). This method was employed as an alternative to EIS which is only able to measure the change in overall impedance of the membrane due to collective gating of ion channels. PPC, on the other hand provides single channel gating events by ion channels in Nano-psTBLM and this is required for the characterization of ion channels.

2.3.2.1 Setup and measurements

Axopatch 200B low-noise patch clamp amplifier (Axon Instruments/ Molecular Devices, CA, USA) was used to measure current, conductance and capacitance of the Nano-psTBLM. The signal was recorded and analyzed with Digidata 1322A interface using pClamp 9.2 acquisition software (Molecular Devices, CA, USA) by forming data histogram, especially for the measured conductance. For the electrical characterization of Nano-psTBLM, ±15 mV AC triangular voltage with the ramp of 1 V per second (with 60 milliseconds duration each from peak to peak) was continuously applied by two Ag/AgCl electrodes (World Precision Instruments Inc, FL, USA), and then the ionic current flowing through the nanopore was measured. Calibration of the number of nanopores against the respective ionic conductance was also examined. Conductance of the nanopore was directly measured by applied DC potential (from ±10 mV to ±35 mV with ±5 mV increment in each sweep) as shown in figure 6.14.

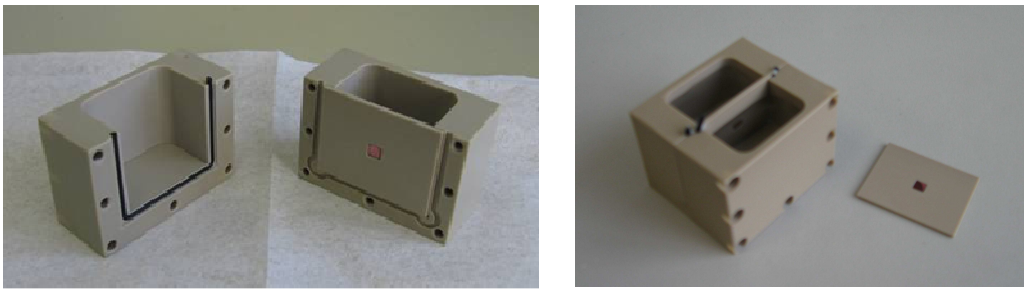

Figure 2.21 Photograph of PPC measurement cell made of organic polymer thermoplastic, polyether ether ketone (PEEK)

When α-HL ion channels were inserted into Nano-psTBLM, single ion channel transport was measured with various DC holding potentials ranging from ±25 mV to ±200 mV (figure 6.23). Ion channel gating was observed as the steps of quantized jump in ionic current while the holding potential was maintained during the measurement. In voltage clamp experiment, -75 mV holding potential was used although α-HL ion channels could response to various holding potentials up to ±200 mV. During all the measurements, the electrochemical cell carrying a Si_3N_4 membrane chip was kept in a black Faraday cage and the whole setup was mounted on an air-table to isolate the setup from mechanical vibration of the surroundings.

The ionic current response of Nano-psBLM is first measured by applying the triangular voltage in 1 M KCl electrolyte. The sole reason for applying the triangular voltage is to

make the differential of electrical potential over time constant (i.e. dV/dt = constant). Bilayer current and capacitance of the Nano-psTBLM is then calculated by analysis of the current response curve. Based on current-voltage relationship, resistance of Nano-psTBLM was first calculated and then it is transformed into conductance which is simply the reciprocal of resistance. Current response of Nano-psTBLM due to triangular voltage composes of two parts (figure 2.22). The first instantaneous increase in current (almost vertically) within a very short time is due to charging of underlying Si_3N_4 membrane. Then the second increase in current with a slope is accompanied by the relatively longer time and this part of current represents the current response of the Nano-psTBLM. The slope of this current i.e. $\Delta I/\Delta t$ is useful for calculation of capacitance.

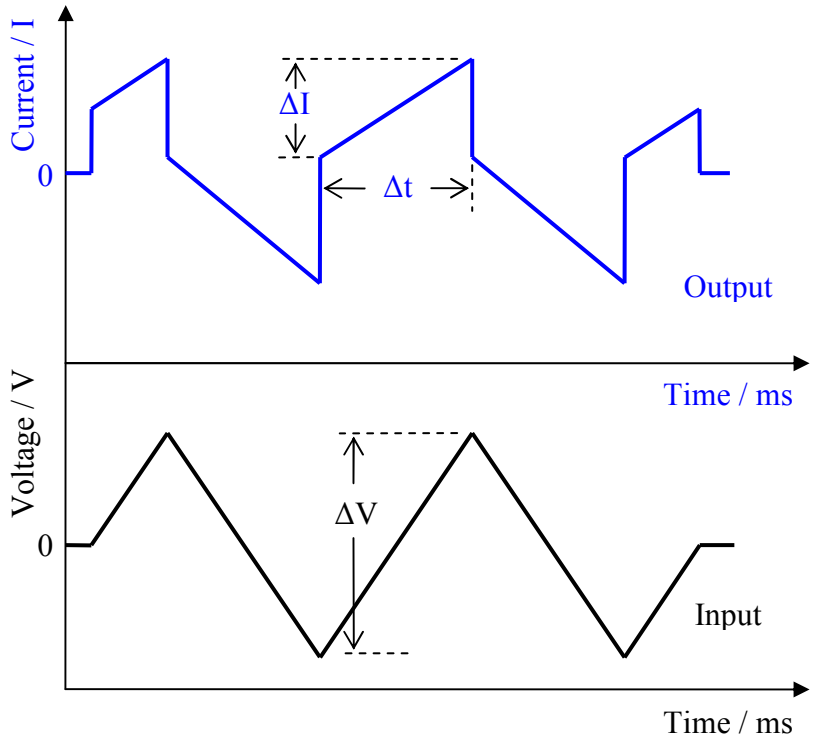

Figure 2.22 Schematic of output current response of the Nano-psTBLM measured by the triangular input voltage

2.3.2.2 Current histogram

When a single or a few ion channels are gating, discrete change in ionic current is only in the order of a few pA. Therefore it is required to construct the current histogram in order to differentiate each step of increase (or decrease) in current by gating of ion channels. Current histogram gives information on number of current levels (also called the states) of a particular ion channel in voltage clamping. To eliminate the capacitive

current, applied DC holding potential is applied instead of AC or triangular potential where the voltage is time dependent. A typical current histogram of α-HL ion channel with two current states (opening and closing) is seen in figure 6.27.

3 Tethered bilayer lipid membrane (TBLM)

TBLM employed in this work is a hybrid, tethered lipid bilayer composed of two types of lipids in forming a bilayer membrane on a planar substrate. Therefore it was termed planar TBLM (pTBLM). The lower half of pTBLM is the synthetic lipid molecules anchored onto the planar surface via the spacer chain terminating with thiol or silane groups. The upper half is made of lipids which are similar in structure of the lipids in lower half. Therefore, lipid bilayer membrane is attached to the surface by gold-sulphur bonds (or hydrogen bonds of silane-hydroxyl group) but decoupled from the surface by the spacer linkage. Schematic of pTBLM used in this work is depicted in figure 3.1. With this configuration, the monolayer is immobilised on the surface but without affecting their molecular fluidity and flexibility. Lipids in upper half are free to diffuse and exchange the position laterally.

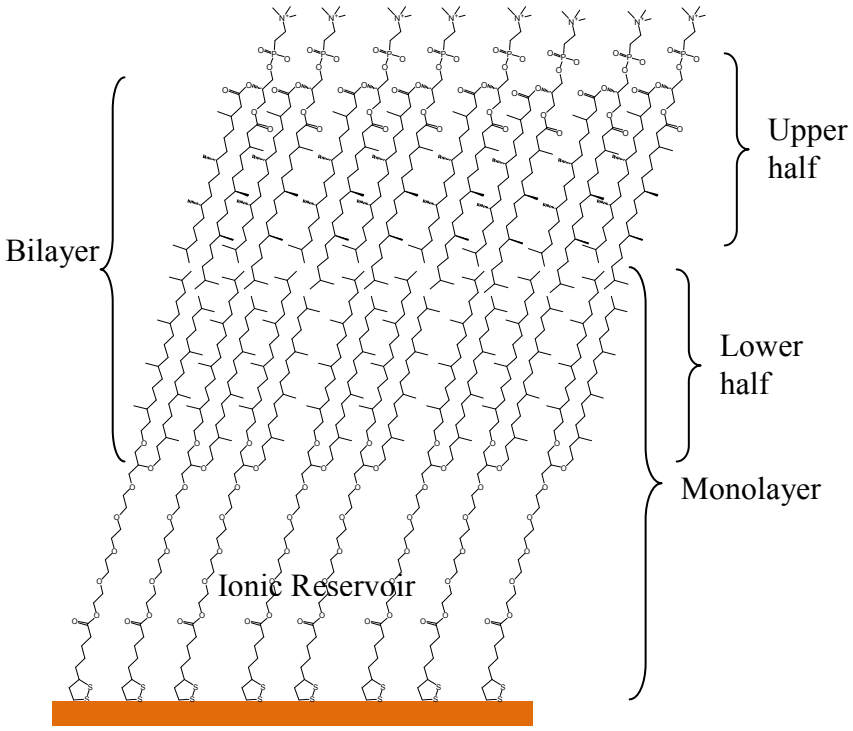

Figure 3.1 Schematic of normal pTBLM (without incorporation of cholesterol) on template stripped gold surface (lipid bilayer membrane is attached to but decoupled from the surface by gold-sulphur bonds)

An important aspect of the monolayer is its spacer region which offers the accommodation for electrolytes and serves as an ionic reservoir. This allows the use of electrochemical measurements such as EIS to characterize across the bilayer membrane

electrically. In applications, some globular and peripherial proteins have extra-membranous domains which may come in contact with the surface if there is no ionic space below the bilayer and the proteins might be denatured. This is not the case in pTBLM here as the bilayer is decoupled from the surface and provides the native environment to the proteins without affecting their structure and functions [232].

3.1 Monolayer

Monolayer is typically assembled on the surface either by self-assembly [241] or Langmuir Blodgett (LB) transfer methods [45]. There are two main types of self-assembled monolayers (SAM) based on terminating end for surface anchorage such as thiols and silanes. Thiol based monolayer such as alkanethiol can spontaneously assemble onto noble metal surfaces such as gold [241] while silane based monolayer, for example ethoxysilanes, needs active OH groups on the surface to be anchored [230]. Regardless of thiol or silane based molecules, the primary requirement to achieve a good monolayer with highest possible packing density is a flat and smooth surface with a minimum surface roughness. In principle, the roughness of a surface for a good monolayer assembly should be as low as 0.3 nm [55], such as that of the polished silicon wafer surface (figure 3.2A).

3.1.1 Materials

3.1.1.1 Au and Si_3N_4 substrates for pTBLM

Template stripped gold (TSG)

For thiol based monolayer surface assembly, creating gold surface which is as smooth and flat as a polished silicon wafer surface is a challenge. An elegant way of fabricating a gold surface is copying the surface finish of polished silicon wafer called the template stripped gold (TSG) [55]. Metallic Au is either evaporated or sputtered onto a clean polished silicon wafer. Another substrate, mostly a microscopic glass slide, is glued onto Au covered silicon slab using epoxy paste and the assembly is thermally cured at an elevated temperature. When the silicon chip is stripped, the glass substrate results with an Au film which is as smooth and flat as polished silicon surface [229].

In this work, 4 inches diameter one-sided polished silicon wafers (CrysTec GmbH, Germany) were diced into 2 cm × 4 cm chips. These diced chips were heated in the solution mixture of H_2O, H_2O_2 and NH_4OH (with the ratio of 5: 1: 1 in volume) at 70 ºC

for an hour. Then the chips are thoroughly rinsed with Milli-Q water and blown dry with nitrogen. Finally 50 nm thick Au was evaporated onto the pre-clean chips by thermal evaporation (Balzers PLS 500 thermal evaporation system, MPIP, Mainz). Microscopic glass slides were cut into 2 cm × 5 cm chips and agitated in detergent solution for 15 minutes before they were rinsed in Mill-Q water, and stored in ethanol. Substrate bonding was between the silicon chip carrying Au film and the clean glass slide with the Epoxy glue (Epoxy resin and hardener from EpoTek, USA) in between, and the bonding was taken place between the mechanical clamps with hand pressure. Bonded chips were then thermally cured in an induction oven at 150 ºC for an hour before they were cooled down and stored in the desiccator. The surface roughness of TSG by AFM measurement gives around 0.3 nm (figure 3.2B) comparable to that of the polished silicon wafer surface (figure 3.2A). In this work, TSG is mainly used as the substrates to support the pTBLM experiments.

Evaporated Au surfaces on polished silicon substrate

Transferring TSG onto silicon chip carrying a Si_3N_4 membrane is not possible for two reasons. Firstly, Si_3N_4 membrane with thickness of less than 150 nm is extremely fragile and this cannot withstand the bonding pressure with epoxy glue, and subsequent thermal curing at high temperature. Secondly, milling of sub 100 nm nanopores through the membrane by FIB is practically impossible even if the Si_3N_4 membrane is intact after TSG transfer because the thickness of epoxy film is more than a few microns. Therefore alternative methods have been explored. The first method is the evaporation of Au at cryogenic temperature. 25 nm thick Au was evaporated onto a clean silicon chip (covered with an LPCVD Si_3N_4 film) held at –160 °C, with a slow evaporation rate of 0.4 Å/sec. The surface roughness of cryogenically evaporated Au measured by AFM is less than 0.6 nm (figure 3.2C). It was also observed that the sizes of Au grains were relatively smaller due to the effect of very low temperature of the substrate during cryogenic evaporation. The smaller the grain sizes, the smaller the peak to peak difference among the grains and as a result, the surface roughness was minimized. Despite reduction in surface roughness, this cryogenic evaporation requires a special vacuum chamber equipped with the flow of liquid nitrogen to the substrate holder. This type of evaporation facility is not easily accessible. The second method is just a normal thermal evaporation of Au onto the polished silicon chips covered with Si_3N_4 film at

room temperature. Non-contact mode AFM scan of normal Au surface reveals relatively large Au grains with higher surface roughness of about 0.9 nm (figure 3.2C).

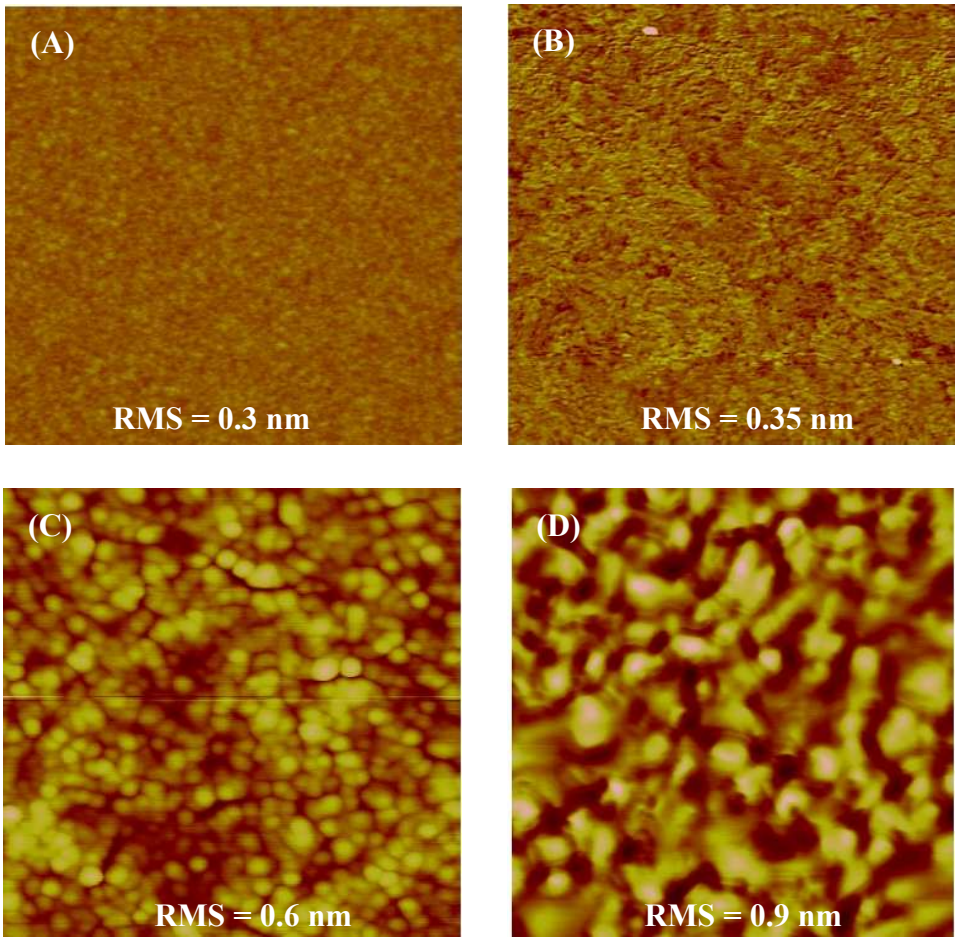

Figure 3.2 Contact mode AFM images of the surface of (A) polished silicon wafer (B) TSG (C) cryogenically and (D) normally evaporated Au on polished silicon wafer (all the surface scanned by AFM were done in 1 μm^2 area)

3.1.1.2 DPhyTL

Thiolipid molecule used as the monolayer by surface assembly is 2,3-di-O-phytanyl-glycerol-1-tetraethylene glycol-D,L-lipoic acid ester lipid (DPhyTL). DPhyTL was first synthesised by Schiller et al. in 2003 [10]. The lipid has four distinct regions namely; anchor, spacer, linkage and lipid tails (figure 3.3). Anchor unit is made of cyclic disulfide which provides the immobilisation of the lipid molecules by anchoring onto Au surface. The anchorage is achieved by lipoic acid moiety that can form two covalent bonds with the Au surface. The spacer unit consists of four oligoethylene oxide moieties and surface-decouples the lipid bilayer from the substrate. Furthermore, it provides the aqueous space for ionic reservoir and contributes to retain the required density and fluidity of the membrane. The linkage is at the end of spacer moiety where two

hydrophobic phytanyl lipid tails are branched. Phytanyl chains serve as the lower leaflet of pTBLM after vesicle fusion. The use of phytanyl lipids for hydrophobic part instead of fatty acids is to enhance the stability of the lipid against oxidation. Theoretical length of DPhyTL in its fully stretched orientation is about 5 nm. The chemical structure of DPhyTL is represented in figure 3.3.

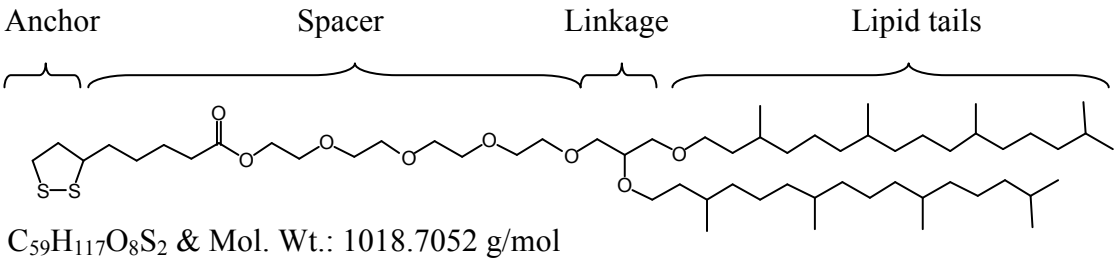

$C_{59}H_{117}O_8S_2$ & Mol. Wt.: 1018.7052 g/mol

Figure 3.3 Molecular structure of thiolipid DPhyTL

3.1.1.3 DPTTE

The silane based molecule used for monolayer assembly on Si_3N_4 surface is 2,3-di-O-phytanyl-*sn*-glycerol-1-tetra-ethylene glycol-(3-tryethoxysilane) ether lipid (DPTTE). It was previously synthesised by Petia Atanasova and Catherine Breffa in Max Planck Institute for Polymer Research, Mainz, Germany [59]. Similar to DPhyTL, this triethoxysilane lipid has four distinct regions namely; anchor, spacer, linkage and lipid tails and each part has their own functional role in forming the monolayer. Silane derivatives anchor group is used to immobilize the molecule on silicon surface terminating with OH-groups. Spacer part is made of oligo(ethylene glycol) chains which create hydrophilic region between anchor and linkage. It is required the spacer chains to be physically inert to prevent adsorption onto surface. They are also required to be chemically inert to prevent interaction with either membrane lipids or incorporated proteins. Linkage is synthesized with ether bridges which are known to be more stable against the hydrolytic cleavage. Lipid tails are also similar to DPhyTL and they are composed of phytanyl chains to support the vesicle fusion for complete pTBLM formation. Theoretical length of DPTTE in its fully stretched orientation is around 4.6 nm and the chemical structure is depicted in figure 3.4.

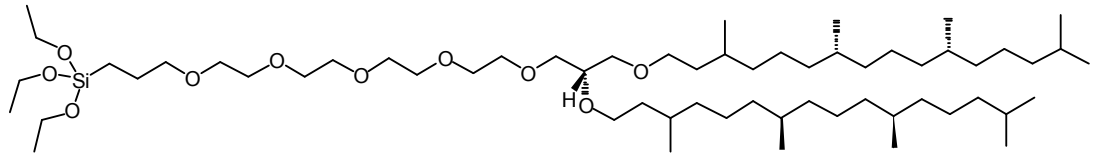

$C_{60}H_{124}O_{10}Si$ & Mol. Wt.: 1033.71 g/mol

Figure 3.4 Molecular structure of triethoxysilane lipid DPTTE

3.1.1.4 CholPEG

Cholesterol is abundantly found in eukaryotic cell membranes naturally. This molecule is classified as a lipid as it has hydrophobic steroid rigid rings with a short hydrocarbon tail linked to a small hydrophilic OH head group. When naturally comprised in cell membrane, rigid rings of cholesterol hinder the close interaction among surrounding lipid molecules and enhance the overall fluidity of the cell membrane indicated by broadening the range of phase transition temperature of the lipids [234]. Therefore cholesterol is known improve thermal stability of the cell membrane at elevated temperatures [236]. Imitating from nature of cholesterol in cell membranes, cholesterol-pentaethyleneglycol (CholPEG) lipid was synthesized previously [237]. This molecule has basically the similar structures in spacer and anchor parts as in DPhyTL but the linkage and lipid tails are different from DPhyTL. Lipid tail of two hydrophobic phytanyl units in DPhyTL is replaced with a cholesterol unit in CholPEG (figure 3.5). Since the cholesterol is a relatively small molecule, the theoretical length of CholPEG in its fully stretched orientation is 4.8 nm, slightly shorter than that of DPhyTL.

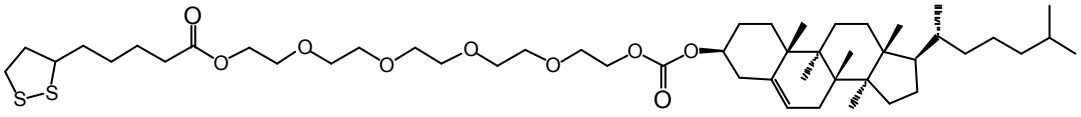

$C_{46}H_{78}O_9S_2$

Figure 3.5 Molecular structure of cholesterol-pentaethyleneglycol (CholPEG)

3.1.1.5 Self-assembly of monolayer

DPhyTL by self-assembly

DPhyTL molecules were dissolved in ethanol to a concentration of 0.2 mg/ml. A TSG slide was placed in DPhyTL solution and the monolayer self-assembly was carried out for 24 hours. Then the chip was thoroughly rinsed in fresh ethanol and blown dry with

nitrogen. If it was not in immediate use, the chip was stored in a tube filled with nitrogen. The assembly process is time dependent. A study of monolayer formation on gold surface in ethanol containing molecules by self-assembly with different assembly time from a few minutes up to 48 hours was done [58] Packing density and quality of monolayer examined by contact angle measurement revealed that the optimal self-assembly time was around 24 hours [58]. Longer assembly time for more than 24 hours was not recommended as this could lead to the formation of undetermined multilayer structures. According to the study, assembly of lipids occurred quickly in the beginning and then the process was getting slower when the assembly time was longer. EIS measurement results on surface assembly of DPhyTL on TSG surface indicated high surface coverage occurred quickly in the beginning and then followed by molecular rearrangements and settlements such as filling up the uncovered spaces etc., until the final coverage was achieved [58]. When the surface has full coverage by DPhyTL monolayer, it becomes relatively hydrophobic due to phytanyl lipid tails facing up on the surface. The major requirement of a good monolayer is to achieve high monolayer packing density for maximum electrical sealing on the surface. However it is also difficult to induce the vesicle fusion to form the complete bilayer if the monolayer is too hydrophobic due to highest packing density. Therefore it is important to have an optimum surface hydrophobicity to help induce the vesicle fusion on the monolayer.

DPTTE by self-assembly

DPTTE molecules were dissolved in ethanol at 0.2 mg/ml concentration. A silicon chip with LPCVD (low pressure chemical vapour deposition) Si_3N_4 film was agitated first in IPA and ethanol for 5 minutes each. Then the chip was thoroughly rinsed in running MilliQ water and blown dry with nitrogen. After cleaning in solvent, silicon chips were additionally clean in ultraviolet (UV) ozone cleaner for twice in each 10 minutes, followed by thorough rinse in running MilliQ water. This step made sure to remove the possible organic contaminants from the Si_3N_4 surface [233]. Self-assembly of monolayer was carried out in ethanol containing DPTTE for 24 hours. After self-assembly process, the chip was rinsed in ethanol and blown dry with nitrogen. Monolayer quality is characterized by static contact angle measurement (drop shape analysis system DSA10, Krüss GmbH, Hamburg, Germany) directly after self-assembly.

3.1.1.6 Langmuir Blodgett transfer of monolayer

DPhyTL by Langmuir Blodgett

A planar layer of amphiphilic molecules can be transferred from air water interface onto a desired surface by Langmuir Blodgett film transfer technique [45]. The major advantage of this technique compared to self-assembly method is that it can precisely control the desired packing density of monolayer to be transferred. Moreover, one can form a hybrid monolayer with amphiphilic molecules in different compositional ratio [45]. In an LB transfer process, amphiphilic molecules mixed in solvent such as hexadecane or chloroform are spread onto the clean deionised water surface. When the solvent evaporates, the molecules spread on water surface with weak surface interaction among each other as the surface area available for the molecules is large relatively. At this point, surface pressure of molecules is rather low and has little effect on water surface pressure. When these molecules are brought together by surface compression with adjustable Teflon barriers from sides, the molecules exert each other repulsively and the surface pressure of molecules grows higher. This surface pressure is directly measured by Wilhelmy Plate Method which measures the weight of the liquid drawn by a plate (made of either platinum foil or paper) when it is lifted from air-water interface. The weight of the liquid is proportional to the surface pressure of the liquid which is monitored by a highly sensitive balance measuring the force exerted on the plate. The balance is controlled by the tensiometer and with known dimensions of the balance; the force exerted by surface molecules is converted into surface pressure in mN/m. The resultant surface pressure can be defined as follows:

$$\pi = \gamma_o - \gamma \tag{3.1}$$

where γ_o is the surface pressure of pure water

γ is the surface pressure of water covered by molecules

Water surface area available for each molecule can be calculated by the equation,

$$A = \frac{A_f \times M_w}{C \times N_A \times V} \tag{3.2}$$

where A_f is the water surface area between barriers (m^2)

M_w is the molecular weight of monolayer molecules (g/mol)

C is the concentration of molecules (g/l)

N_A is Avogadro's number (6.022×10^{23} /mol)

V is the volume of molecular solution (solvent) (l)

When the molecules at water surface are compressed by barriers, the force exerting on the balance is increased as the mean molecular area decreases. Then the graph of surface pressure (π) against the mean molecular area (A) on the water surface, called surface pressure isotherm, is plotted to determine the highest pressure that the molecular layer can maintain before it collapses. A typical surface pressure isotherm for DPhyTL molecules can be seen in figure 3.6.

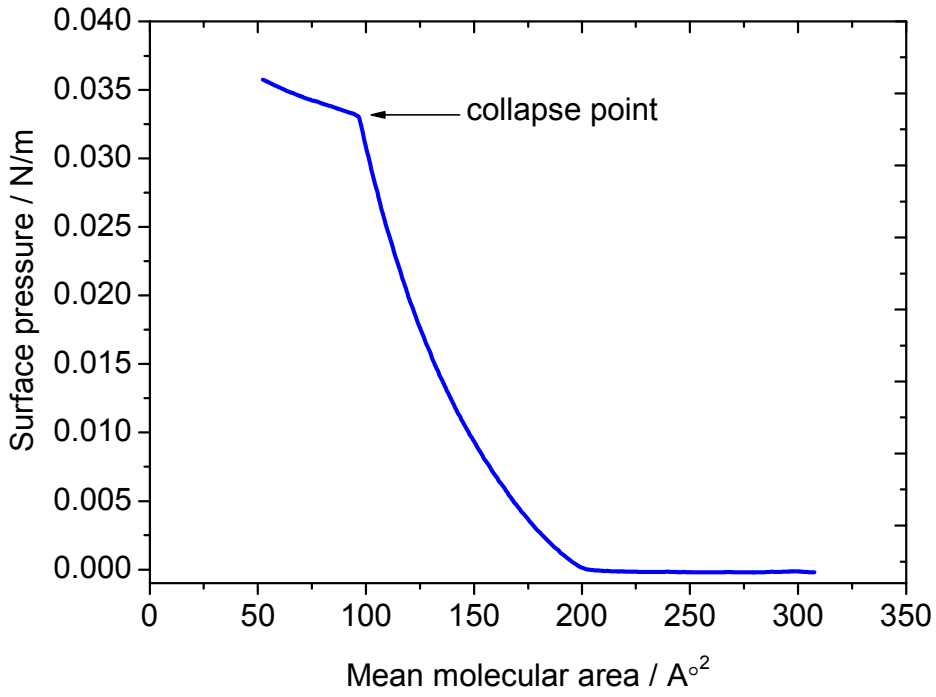

Figure 3.6 Surface pressure isotherm of a DPhyTL monolayer

In experiment, the surface pressure of a paper balance which was partially immersed in deionised water was set to 73 mN/m. Then the barriers were compressed at a rate of 5 mm/min while observing the balance reading. If the water surface is clean, the surface pressure of balance is not shifted noticeably. The next step was dipping of membrane chip which was clamped at the edge with a metal clamp linking to a transducer unit that controlled up and down motion of the clamp. Then 40 µl (1 mg/ml in concentration) of DPhyTL in chloroform was spread onto the water surface. After waiting for 20 minutes to let the chloroform evaporated, the surface compression of molecules with barriers was started at a speed of 1 mm/min and the surface pressure isotherm was recorded.

This step is to measure the surface pressure at which the DPhyTL monolayer collapses. As shown in figure 3.6, the graph changed abruptly around 33.1 mN/m while mean molecular area was about 96 $Å^2$. Actual monolayer transfer took place at 32 mN/m and this was to make sure that the highest possible packing of monolayer (before the collapse point) was achieved. The chip was pulled upward at the rate of 1 mm/min during monolayer transfer. After monolayer transfer, the chip was stored in a desiccator overnight before performing the static contact angle measurement to determine quality of the monolayer.

DPTTE by Langmuir Blodgett

A surface pressure isotherm of DPTTE molecule was first measured. The molar concentration of DPTTE in chloroform was 3.5 mg/ml and the amount spread onto the water surface was 10 µl. After allowing the evaporation of chloroform for 20 minutes, compression with barriers was started from both sides with the speed of 10 mm/min and the recorded surface pressure isotherm was as shown in figure 3.7. DPTTE monolayer collapsed at 31 mN/m while mean molecular area was 109 $Å^2$. The actual monolayer transfer took place at 30 mN/. Monolayer was transferred at a pulling rate of 1 mm/min. An additional step for LB transfer of DPTTE was thermal treatment of the chip in oven at 70 °C for an hour. If not for immediate use, the chip carrying monolayer can be stored in a desiccator with the control of relative humidity and temperature.

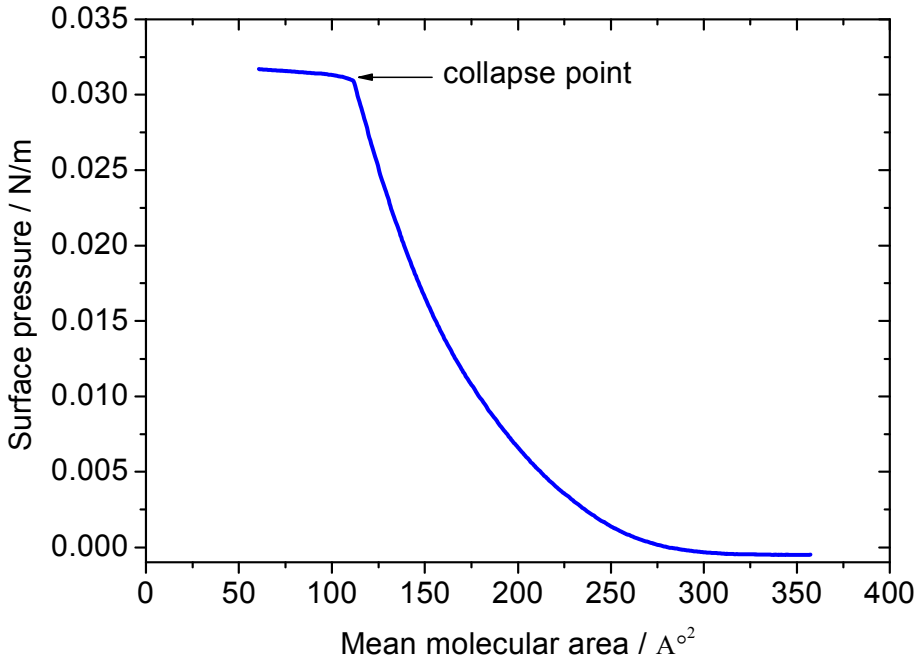

Figure 3.7 Surface pressure isotherm of a DPTTE monolayer

There are significant steps of silane based monolayer formation on Si_3N_4 surface [230]. When DPTTE molecules are spread over the water surface, triethoxysilane anchor groups are hydrolysed. During transfer of the film, triethoxysilane anchors are bound to hydroxyl-group on Si_3N_4 surface by hydrogen bonding. At this point there are water molecules being trapped between anchor and surface hydroxyl groups. After elimination of residual water by heating at 70 °C for an hour, the condensation reaction takes place and each lipid linked onto surface as well as the neighbouring lipids to form a monolayer network. The monolayer quality is measured by static contact angle measurement. For all the monolayer transfer by LB, KSV Mini-Trough (MPIP, Mainz, Germany) was used.

3.1.2 Characterization of monolayer

3.1.2.1 Contact angle measurement

The quality of a monolayer transferred by both self-assembly and LB depends on the monolayer packing density. Better monolayer packing density results in higher surface hydrophobicity which can be determined by measuring the surface contact angle (CA) of the monolayer. CA on the other hand is also partially dominated by the surface roughness at the nano/micrometer scale. A clean Si_3N_4 surface is quite hydrophilic and it has CA not more than 25° (figure 3.8A) while a freshly cleaved TSG surface exhibits a slight higher CA of about 32° (figure 3.8B). Above all, a normally evaporated Au surface on silicon chip gives relatively higher CA of about 62° (figure 3.8C) which is twice as high as that of TSG surface. On the other hand, Au film on Si_3N_4 surface by cryogenic evaporation exhibits the intermediate CA of about 47º (figure 3.8I). This ascending surface hydrophobicity of bare Si_3N_4 and Au surfaces by different evaporation conditions is due to the differences in surface grain sizes of Si_3N_4 and Au (figure 3.2).

Surface wetting behaviour of Si_3N_4 and Au surfaces is drastically changed when the monolayer is transferred. CA of DPhyTL monolayer (about 96° in figure 3.8E) by LB process shows less hydrophobicity (in other word, lower monolayer packing density) compared to the one by self-assembly method (around 105° in figure 3.8D). This indicates that self assembly is better choice if the higher monolayer packing density is preferred. At the same time, both DPhyTL monolayer by self-assembly on TSG and normal Au surfaces shows similar CAs (figure 3.8D and 3.8H) regardless of the roughness of Au surfaces (figure 3.8B and 3.8C). This clearly indicates that the surface

hydrophobicity of Au is governed by the monolayer after self-assembly. On the other hand, CA of DPTTE monolayer by LB (around 90° in figure 3.8F) is observed higher than the one transferred by self-assembly (around 73° in figure 3.8G). Monolayer packing density by LB method is better in DPTTE and it might be due to the fact that the film transfer occurs at water sub-phase which supports hydrolysis of anchor lipid onto surface. In contrast to LB, self-assembly of DPTTE takes place in solvent ethanol despite the longer assembly time and hence packing density might not be as good as the one transferred by LB. All contact angles were measured in static mode with drop shape analysis system DSA10 (Krüss GmbH, Hamburg, Germany).

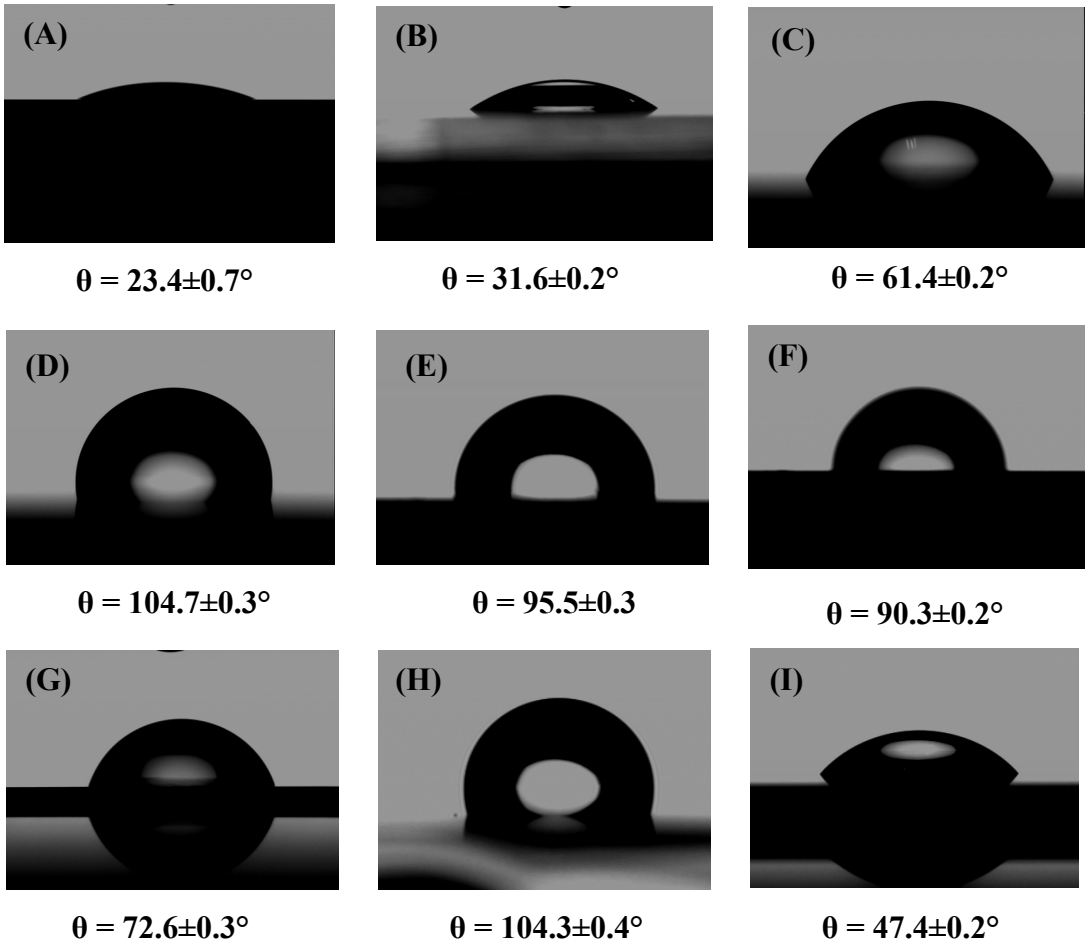

Figure 3.8 Surface contact angles of (A) Si_3N_4 surface (B) TSG (C) normal Au surface (D) DPhyTL self-assembly on normal Au surface (E) DPhyTL on normal Au surface by LB (F) DPTTE on Si_3N_4 surface by LB (G) DPTTE on Si_3N_4 surface by self-assembly (H) DPhyTL self-assembly on TSG and (I) normal Au surface on Si_3N_4 surface by cryogenic evaporation (CAs are measured 5 times for each surface and averaged for analysis)

3.1.2.2 EIS measurement

Characterization of the quality of monolayer using EIS is only available for DPhyTL as this technique requires an underlying Au surface as the working electrode for impedance measurement. Impedance spectra were recorded for frequences between 2 mHz and 100 kHz at 0 V bias potential with an AC modulation amplitude of 10 mV. Bode plots of the impedance measured on bare TSG and DPhyTL monolayer self-assembly on TSG surface are shown in figure 3.9. The equivalent circuit model used to fit the data is $R_e(R_mC_m)C_{dl}$ and measurement is taken place in electrolyte of 100 mM NaCl. Electrolyte resistance (R_e) before and after formation of DPhyTL monolayer is around 100 Ω and it remains unchanged. Measured capacitance of bare TSG surface is around 38 μF/cm^2, which is equivalent to ~11 μF. This is in reasonable agreement with the capacitance of pure gold, in the range of 10-50 μF/cm^2 [202]. Capacitance of Au surface is significantly decreased by ~30 times (from 38 to 1.2 μF/cm^2) after DPhyTL monolayer is formed. A slight change is observed in surface resistance of Au before and after DPhyTL monolayer surface-assembly i.e. from ~1 to 1.1 MΩ cm^2.

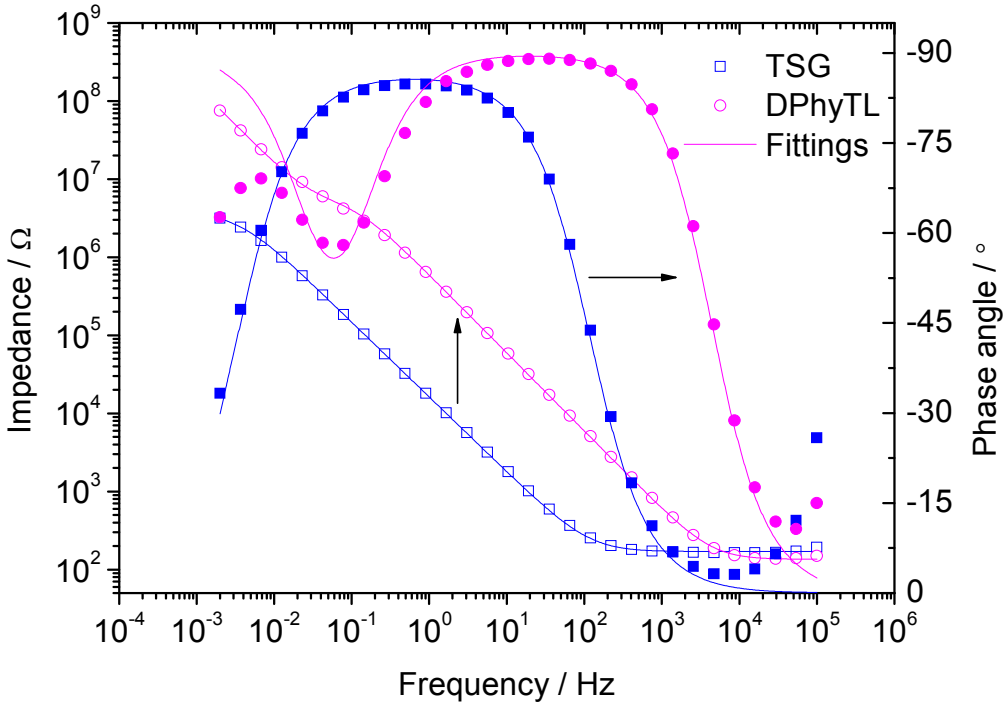

Figure 3.9 Bode plot of the impedances of TSG surface before and after self-assembly of DPhyTL monolayer (unfilled squares represent impedance and filled squares represent phase angle, and the equivalent circuit model to fit the data is depicted in figure 2.10)

3.2 Bilayer formation

Final pTBLM formation is done by fusion of small unilamellar vesicles (SUVs) directly onto the surface-assembled monolayer hydrated in 100 mM NaCl electrolyte solution.

3.2.1 Materials

3.2.1.1 DPhyPC

The upper half of pTBLM was composed of 1,2-di-O-phytanoyl-*sn*-glycero-3-phosphocholine (DPhyPC) (figure 4.1). DPhyPC was purchased directly from Avantis Polar Lipids, Inc and used mainly due to its hydrophobic chains which were structurally similar to the phytanyl chains of thiolipid (DPhyTL) and triethoxysilane (DPTTE). The molecular structure of lipid DPhyPC is depicted in figure 3.10.

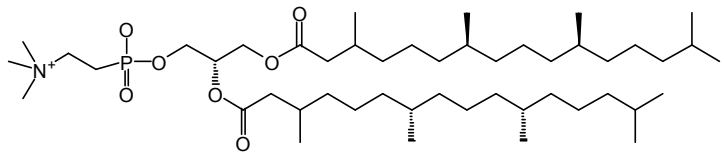

1,2-di-O-phytanoyl-*sn*-glycero-2-phosphocholine (DPhyPC)

Figure 3.10 Molecular structure of DPhyPC lipid

3.2.1.2 Cholesterol

Cholesterol (Sigma Grade, ≥99%) is purchased from Sigma Aldrich in the crystalline powder form and used directly without further treatment or purification. It was used to incorporate into the upper half of pTBLM (figure 3.13) and this was for two reasons. Firstly incorporation of cholesterol into lipid bilayer membrane makes the bilayer membrane biomimetic as the natural eukaryotic cell membranes are composed of cholesterol with varying percentage composition, from traceable amount to 40% in dry weight [2, 235]. Additionally, cholesterol has effects on the activity of bacterial toxins in direct or indirect ways as it controls fluidity, tension and stabilization of lipid rafts in cytoplasmic membrane of the cells [203]. The presence of cholesterol in pTBLM as a bacterial toxin sensor is necessary especially in the case of systems designed to detect the cholesterol binding toxins (CBTs) [122, 139]. Secondly the presence of cholesterol in pTBLM improves the stability of pTBLM at 37ºC as it assists maintaining the liquid crystalline phase of lipid bilayer membrane [236].

3.2.1.3 Preparation of small unilamellar vesicles

DPhyPC lipids were used to produce the small unilamellar vesicles (SUVs) which were prepared manually by simple extrusion through a nanoporous filter with a pair of syringes. First the lipids were dissolved in deionised water at a concentration of 2.0 mg/ml. As the lipids were not easily dissolved in water, harsh vortexing was required for a few minutes to mix the lipids with water. The resulting lipid solution was turbid and translucent at room temperature. Then this lipid solution was heated at 65 °C for an hour and vortexed again before it was extruded up to 21 times through a polycarbonate membrane with 50 nm diameter pores (Avestin Europe GmbH, Mannheim, Germany).

3.2.2 Characterization of bilayer

3.2.2.1 EIS measurement

In EIS measurement, pTBLM formation was characterized by driving the ions across pTBLM and the bilayer impedance as a function of applied voltage with varying frequency was measured electrochemically. After an Au substrate carrying DPhyTL monolayer was fixed to the Teflon cell, it was filled with 1 ml of 100 mM NaCl electrolyte which hydrated the monolayer on the Au surface. Impedance and capacitance of DPhyTL monolayer was first measured and the immediate impedance data in Bode plot were recorded. Then 25 µl of previously prepared DPhyPC vesicles in Milli-Q water was added on top of the monolayer in NaCl electrolyte. The impedance of bilayer as the fusion of vesicles was recorded hourly up to 14 hours. As the vesicles were fused and the bilayer was formed, resistance and capacitance of pTBLM were increased and decreased respectively with time. A Bode plot of pTBLM formation on TSG surface can be seen in figure 3.11. In this measurement, impedance and capacitance of monolayer were 0.11 MΩ cm^2 and 1.5 µF/cm^2 while that of pTBLM after 14 hours of vesicles fusion were 13.94 MΩ cm^2 and 0.80 µF/cm^2 respectively.

When the bilayer was formed, charged ions were naturally unable to flow through the hydrophobic core of lipid bilayer and as a result the ion permeation across the bilayer was largely restricted. This was seen as an increase in resistance more than 100 times as the pTBLM was formed. Bilayer, on the other hand was considered as a parallel plate capacitor because an ultra thin electrically insulating bilayer was sandwiched between two conductive media of electrolytes. Capacitance of a parallel plate capacitor was inversely proportional to the thickness of the insulating film. The thickness of monolayer was increased when the bilayer was formed and its capacitance was halved

as it was seen in figure 3.11. As an alternative verification of lipid bilayer formation, ion channel forming proteins, such as α-HL, were incorporated and the change in impedance of the lipid bilayer with time was monitored. As such proteins were only able to span across the lipid bilayer, the impedance was usually changed if the bilayer was formed on the surface. Typical membrane proteins used for pTBLM validation in this work were valinomycin and α-HL. If no membrane proteins were added and pTBLM was kept hydrated in buffer solution, it was proved to last for several months without significant change in membrane impedance and capacitance [58]. However, formation of pTBLM on planar Si_3N_4 surface with DPTTE monolayer could not be characterized by EIS simply because of lack of metallic surface as working electrode for electrochemical measurement. But one possible way to make the Si_3N_4 surface electrically conductive is doping (or ion implantation). Such an implantation of charged ions makes the semiconductor surfaces conductive and EIS measurement could be possible with DPTTE monolayer based pTBLM on doped Si_3N_4 surfaces. However due to limitations to access the ions implantation facility and complications involved in the process, this work was not explored.

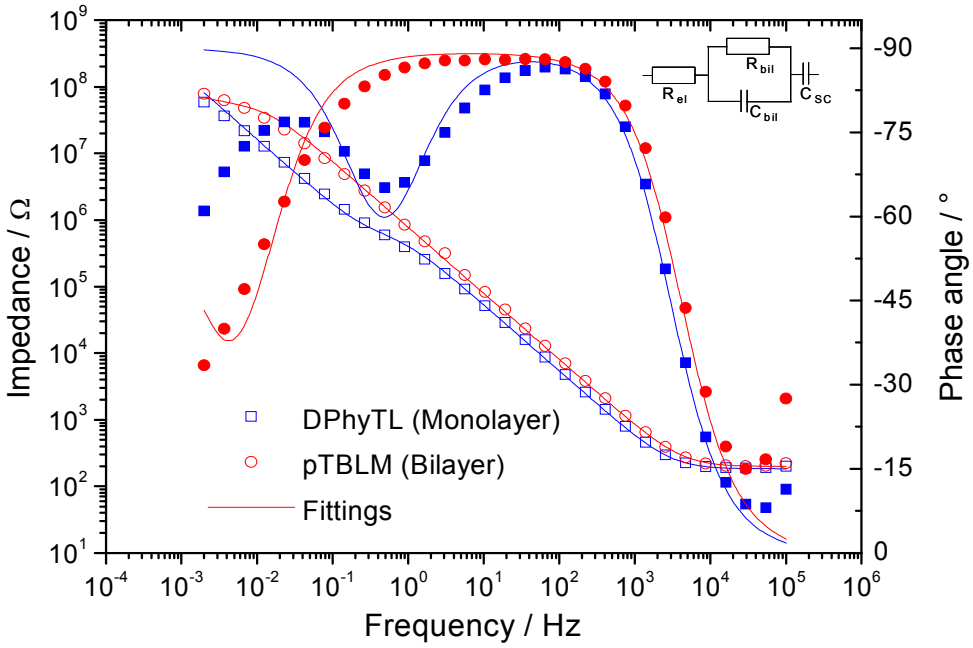

Figure 3.11 Bode plot of the impedance of DPhyTL monolayer and the subsequently formed pTBLM 14 hours after fusion of DPhyPC vesicles (inset is an equivalent circuit used for the simulation of experimental data)

3.2.2.2 SPR measurement

In characterization of pTBLM formation with SPR, binding and fusion of SUVs on the DPhyTL monolayer was measured as the minimum resonance angle shift with time. First DPhyTL monolayer was self-assembled on Au surface coated on BK7 glass disc for 24 hours. Then the glass disc was fixed to SPR cuvette and the monolayer was hydrated in 100 mM NaCl electrolyte. SPR of the monolayer as a steady reflective angle was measured for a few minutes and recorded. This was used as a baseline angle before the formation of pTBLM. 20 µl of freshly extruded DPhyPC SUVs (50 nm in diameter) was then added on to the monolayer while SPR data was recording on binding curve plot. Binding and fusion of SUVs was indicated as an upward shift of minimum reflective angle due to change in local refractive index close to the surface as an additional lipid layer was formed on top of the monolayer. The binding curve was exponential and the upward shift of resonance angle minimum was instantaneous during the first few seconds after adding of SUVs (figure 3.12A). Then this angle shift was slow down with time and binding curve signal was almost steady after 2 hours (figure 3.12B).

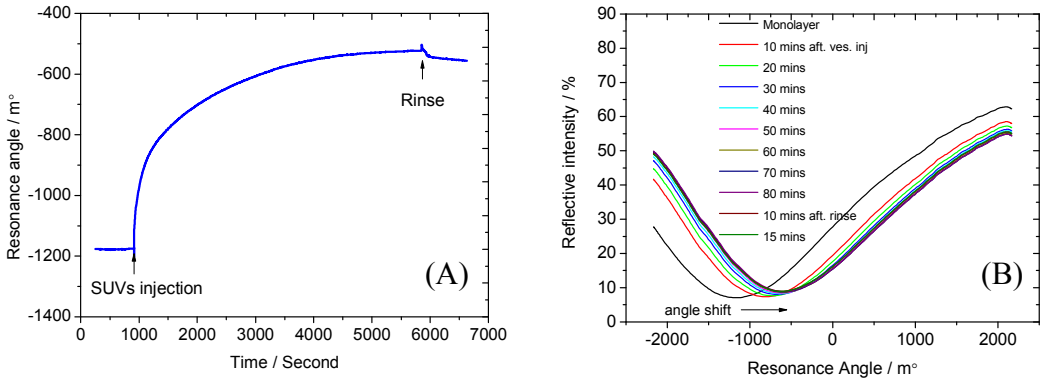

Figure 3.12 SPR measurement of pTBLM; (A) a binding curve plot indicating the change in reflective angle with time and (B) a scan mode plot with the minimum reflective angle shift with time as the TBLM formation is in progress

Time course for formation of pTBLM studied by SPR and EIS are different. In SPR, fusion of vesicles was completed after approximately 2 hours as there was no significant resonance angle shift beyond that period (figure 3.12). After complete fusion of vesicles, lipids in bilayer may carry on with structural rearrangement and orgainzation without a net gain of lipids into bilayer, which keeps the SPR signal in steady condition. In EIS, the saturation of impedance of pTBLM takes longer than 2 hours because the impedance depends on the electrical sealing of the bilayer which in turn influenced by

the time-dependent structural rearrangement of lipids. Therefore, the fusion of vesicles as seen by EIS takes longer than that of SPR. A total of about 600 mº shift in minimum reflective angle was observed after the cuvette was rinsed with NaCl buffer (figure 3.12B).

3.3 Effect of temperature on pTBLM

Lipids in bilayer membrane exhibit different phase behaviour in response to the surrounding temperature. At a given temperature, lipids exist either in solid (gel) or in liquid phases which are governed by change in environmental temperature. Lipids exert strong attractive forces onto each other in gel phase at low temperature and their lateral mobility is greatly restricted. As a result lipids are almost locked in fixed positions in bilayer membrane with minimum lateral mobility. However lipids in liquid crystalline phase have relatively less attractive forces on each other and they are able to diffuse laterally and freely at relatively higher temperature. This provides a lipid bilayer with sufficient fluidity in liquid crystalline phase. The temperature at which a particular lipid changes from gel to liquid crystalline phase is therefore known as the phase transition temperature (T_m). T_m of a lipid is governed by the length of lipid tail (hydrophobic chain length) and the degree of unsaturation of the lipids. Lipids with longer tail length (more carbon atoms in hydrophobic chains) have stronger interaction and attraction to each other, and as a result their T_m is higher than those of the lipids with relatively shorter tails. On the other hand, lipids with unsaturated double bonds create kinks in hydrocarbon chain. This hinders the close interactions among lipid tails and T_m of lipids is lower than those of the lipids without double bonds. Degree of unsaturation has more influence on T_m than length of the hydrophobic chains as it can be seen in table 3.1. A common lipid distearoyl phosphatidylcholine (DSPC) has 18 carbon atoms in its lipid tail and T_m of DSPC with a double bond has 54 ºC lower than the same DSPC with no double bonds (table 3.1).

Lipids employed in this work i.e. DPhyTL, DPTTE and DPhyPC have 16 carbon atoms in each hydrophobic chain (figures 3.3, 3.4 and 3.10). Imitating the lipids of archaea, phytanyl chains were used in hydrocarbon tails, instead of using conventional acyl chains in order to enhance the resistance of lipids to harsh environments such as high salt concentration, temperature and extreme pH [2, 204]. Lipids with 16 carbon atoms in hydrocarbon chains have T_m of around 41 ºC and therefore pTBLM made of DPhyTL and DPhyPC should be in gel phase at room temperature. But this is not the case for

pTBLMs used in this work, which are in liquid crystalline phase at room temperature because of the isoprenoic side groups in phytanyl chains (figure 3.3, 3.4 and 3.10). Isoprenoic side groups are incorporated to improve the stability of lipid against oxidation but the close interactions among hydrophobic chains of lipids in pTBLM are consequently hindered. Then T_m of pTBLM is decreased below room temperature and therefore it maintains sufficient lipid fluidity which is required for proper insertion and precise functioning of membrane proteins [204].

Table 3.1 T_m of lipids as a function of tail length and number of double bonds [2]

Number of Carbon atoms in lipid tail	Number of double bonds	Phase transition temperature (T_m in ºC)
12	0	-1
14	0	23
16	0	41
18	0	55
18	1	1
18	2	-53
20	0	66
22	0	75

3.3.1 Unmodified pTBLM

The lipid bilayer membrane depicted in figure 3.13 is DPhyTL based DPhyPC and cholesterol pTBLM. DPhyTL monolayer was self-assembled on TSG substrate for 24 hours. DPhyPC and cholesterol, with 67 % and 33 % in mole respectively, were mixed in Milli-Q water to a concentration of 2 mg/ml. Lipid solution was mixed thoroughly by vortexing and heated at 60 ºC for 30 minutes. SUVs were extruded through a polycarbonate nanoporous filter with 50 nm pore diameter for 21 times and added to fuse on top of DPhyTL monolayer. Incorporation of cholesterol in upper half of bilayer is to improve the thermal stability of pTBLM at 37 ºC which is the optimum body temperature where most of pathogens and their toxins are designed to function and infect the host cells. In this work, it is utmost important to be able to detect and identify the toxins in term of useful signal without the influential effects of the elevated temperature. This required testing the stability of pTBLM at 37 ºC for thermal evaluation. During experiment with EIS, entire faraday cage with the Teflon cell enclosing pTBLM was put inside a mini-incubator and heated at 37 ºC. The incubator has better thermal uniformity with temperature variation of ±0.5 ºC. Then change in impedance of pTBLM with time at 37 ºC was measured for every 30 minutes.

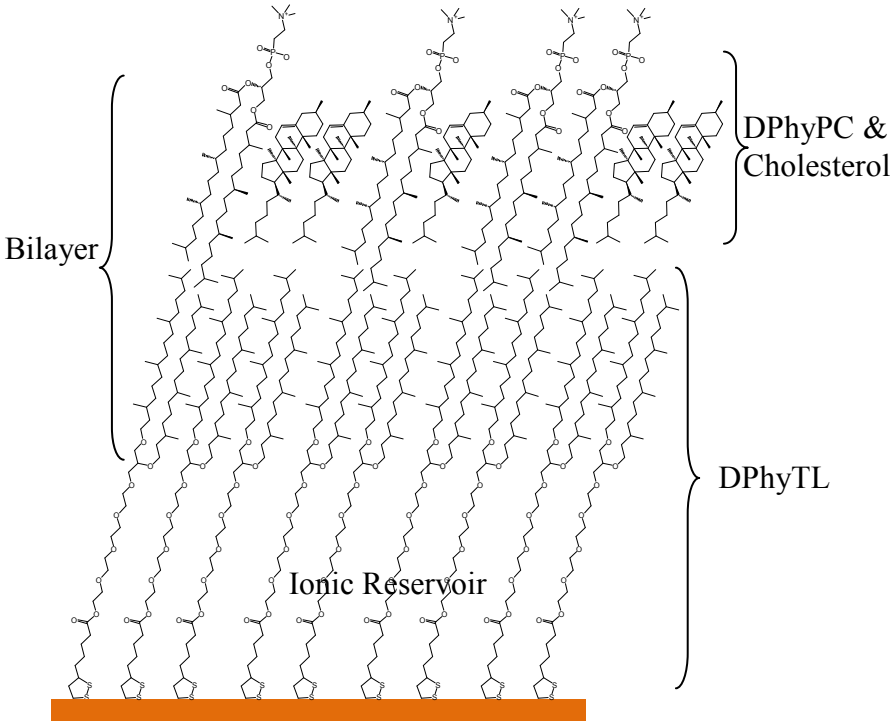

Figure 3.13 Schematic of an unmodified pTBLM made of DPhyTL in monolayer with fusion of vesicles made of DPhyPC and cholesterol (67% and 33% in mole respectively)

3.3.1.1 Results and discussion

Figure 3.14 showed the impedance data (plot of R_m and C_m vs. time) of unmodified pTBLM at 37 ºC for 18 hours. Impedance of pTBLM (recorded for frequences between 2 mHz and 100 kHz at 0 V bias potential with an AC modulation amplitude of 10 mV) was stable with time at 24 ºC. However it was observed that the impedance is strongly influenced by change in temperature of buffer solution. About 90% of initial resistance was exponentially decreased within 15 hours of measurement at 37 ºC. Resistance here is a measure of capability of pTBLM to prevent the flow of ions across it. Therefore it is believed that the decrease in resistance of pTBLM is mainly contributed by rapid increase in lipid fluidity at 37 ºC. Localized leakage of ions across pTBLM is possible when the lipids vibrate deliberately and diffuse rapidly by thermal energy gain. This could happen especially if pTBLM has local sites of defect where lipids might not be able to seal and heal naturally. However resistance alone is not enough to judge the physical condition of pTBLM as the capacitance data also provides the useful information about the lipid bilayer. Capacitance decreased slightly when pTBLM was initially subjected to 37 ºC (figure 3.14). Then it increased gradually with time but overall change in capacitance (about 0.15 $\mu F/cm^2$) was not as pronounced as the overall change in resistance. Capacitance informed that the unmodified pTBLM was still

physically intact and it remained as a bilayer although its permeability to ions under applied electrical potential was gradually deteriorating. This was verified by incorporation of α-HL PFTs and the change in impedance was monitored as shown in figure 3.15.

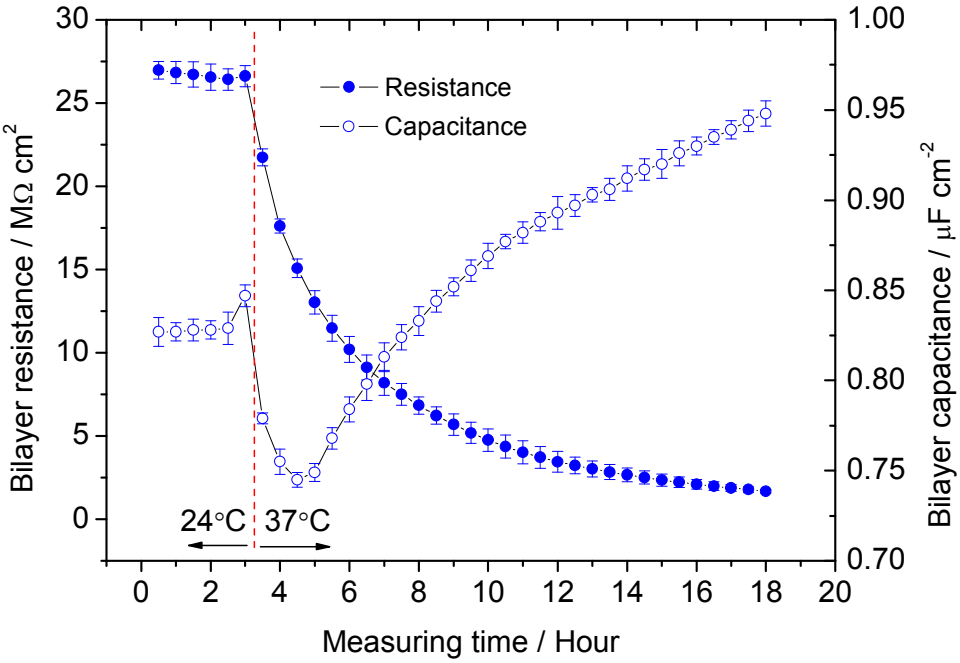

Figure 3.14 Effect of temperature on lipid bilayer resistance and capacitance of DPhyTL based unmodified pTBLM at 37 ºC (each data point represents one complete cycle of impedance measurement from 100 kHz to 2 mHz at 0 V bias potential with an AC modulation amplitude of 10 mV – error bars indicate the error estimation of measured data points)

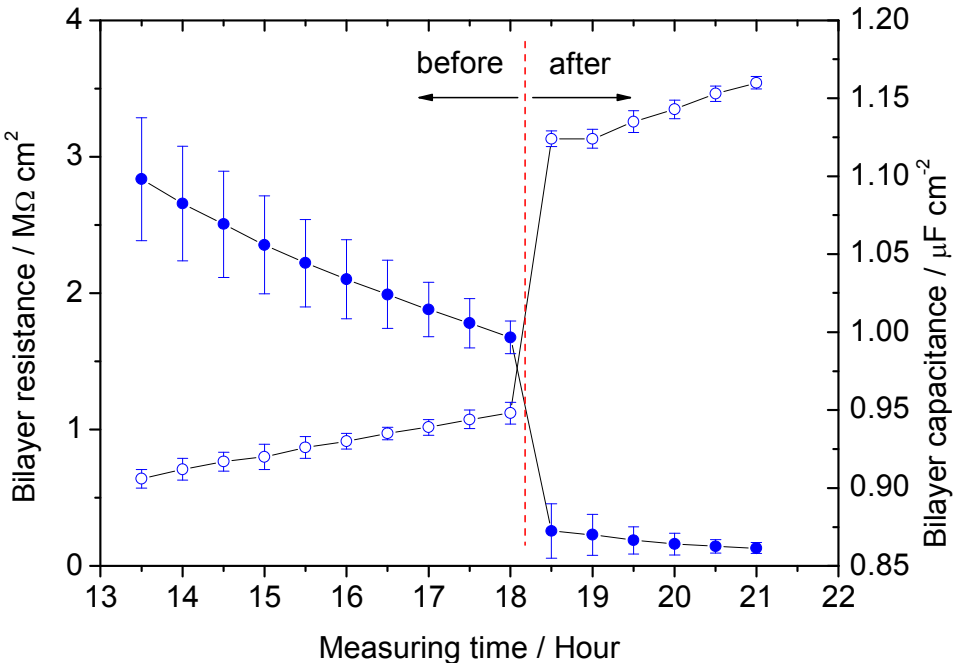

Figure 3.15 Lipid bilayer resistance and capacitance of DPhyTL based unmodified pTBLM with time in NaCl electrolyte at 37 ºC with 150 nM α-HL PFTs

Impedance of unmodified pTBLM changed significantly upon addition of α-HL at 37ºC. As the α-HL channels were formed, resistance was decreased immediately as a result of transport of ions. At the same time, capacitance was increased and this was accompanied by influencing effect of capacitance of TSG surface. This clearly indicated that the unmodified pTBLM was still intact as a lipid bilayer even after 15 hours of exposure at 37 ºC (figure 3.15). However pTBLM with thermally stable and relatively higher resistance 37 ºC is desirable as the toxins secreted by real pathogenic bacteria, in term of composition and virulence factors are certainly different from commercially available purified toxins such as α-HL used for the pTBLM thermal evaluation here.

3.3.2 Cholesterol and CholPEG modified pTBLM

In results discussed in previous section, thermal stability of unmodified pTBLM was not improved regardless of the incorporation of cholesterol (33 % in mole) in upper half of lipid bilayer. In order to comprise cholesterol in both halves of pTBLM, DPhyTL monolayer on TSG was modified by mixing with different percentage composition of CholPEG by self-assembly. Composition of upper half of pTBLM (i.e. DPhyPC and cholesterol) remained unchanged and then the effect of different percentage composition of CholPEG on thermal stability of pTBLM is explored by EIS measurement. Schematic depiction of CholPEG and cholesterol modified pTBLM is shown in figure 3.16 and the respective impedance results were plotted in figure 3.17 and 3.19.

3.3.2.1 Results and discussion

EIS measurement

Impedance of modified pTBLM with different CholPEG compositions in monolayer was measured at 37 ºC in 100 mM NaCl buffer (figure 3.17). It was noted that in general, the more CholPEG in monolayer, the lower the initial resistance of modified pTBLM at room temperature. All modified pTBLMs exhibited decrease in resistance at 37 ºC but to the extent that the resistance decreased after a few hours was different. Modified pTBLM with 25 % CholPEG decreased overall resistance of about 5 MΩ cm^2 while that of 75 % CholPEG decreased overall resistance of 21 MΩ cm^2 after 15 hours at 37 °C (figure 3.18A). Thermal stability in term of bilayer resistance was greatly

improved in modified pTBLM as there were almost no change in resistance at 37 ºC in case of 75 % and 100 % CholPEG in monolayer.

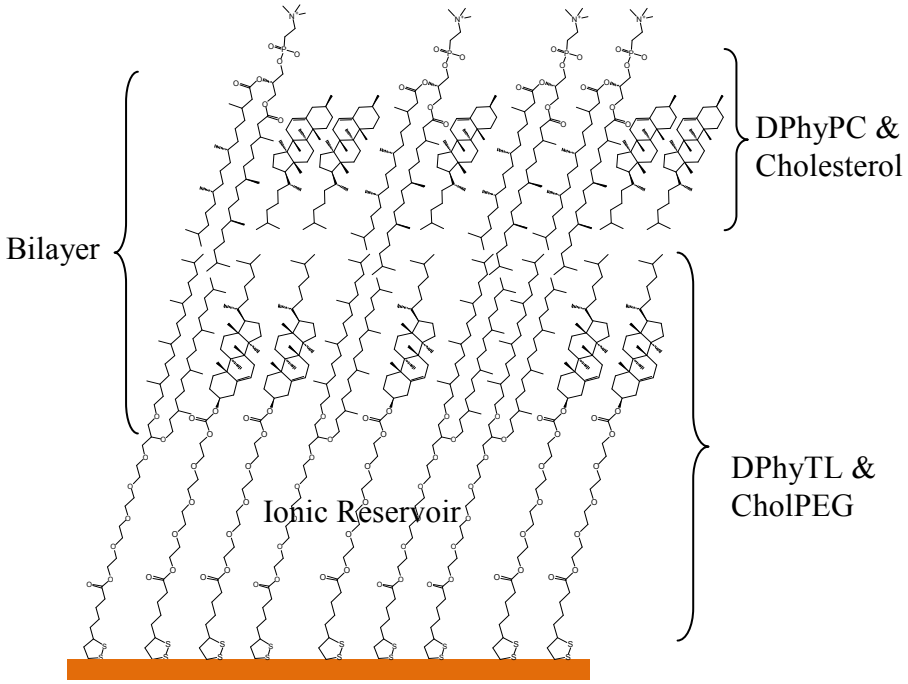

Figure 3.16 Schematic of a modified pTBLM for thermal stability at 37 °C (DPhyTL in monolayer is mixed with CholPEG in different percentage composition while DPhyPC and cholesterol in upper half of pTBLM is same as in unmodified pTBLM)

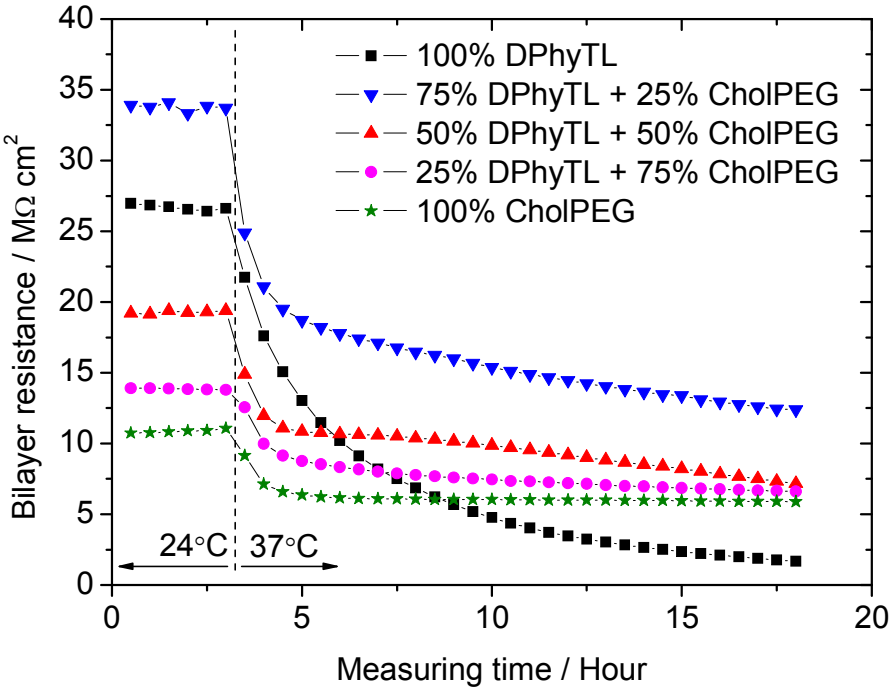

Figure 3.17 Effect of percentage CholPEG composition on thermal stability of modified pTBLM (bilayer resistance of pTBLM was measured with time at 37 ºC)

This enhanced thermal stability is explained by comprising cholesterol units in both halves of modified pTBLMs. When cholesterol is mixed with a lipid, initial T_m of pure lipid (as indicated by a sharp peak by differential scanning calorimetry (DSC)) is widened as there is no sharp phase of transition exhibited [234]. This broadened range of T_m is accompanied by decrease in bilayer fluidity due to cholesterol which slightly immobilises the neighbouring lipids at higher temperature. This in turn improved the resistance of pTBLM with cholesterol composition. On the other hand, all modified pTBLM exhibited decrease in capacitance when the bilayer was subjected to 37 °C. But thermal stability in term of bilayer capacitance indicated that the modified bilayer maintained lipid bilayer structure at high temperature (figure 3.19).

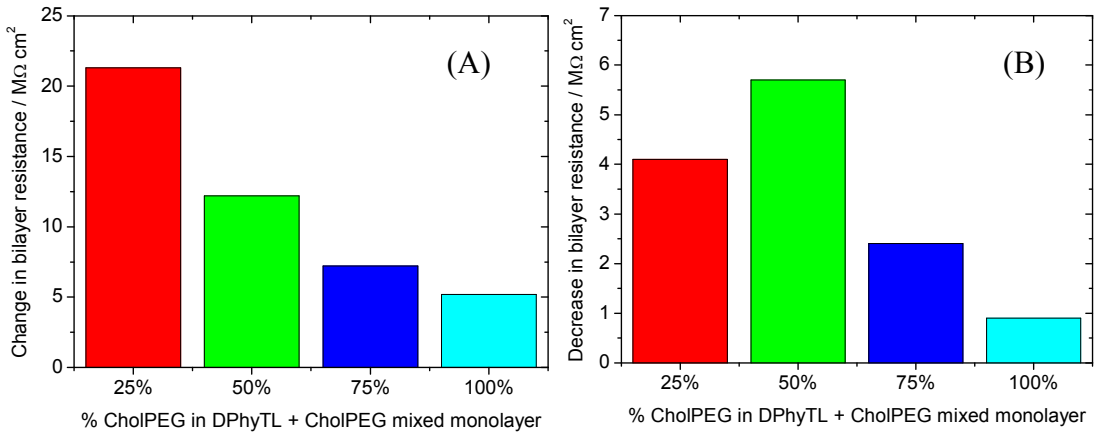

Figure 3.18 Effect of percentage CholPEG composition on decrease in resistance of modified pTBLM (overall decrease in resistance (A) after 15 hours at 37 ºC, and (B) 3 hours after addition of 150 nM α-HL PFTs at 37 ºC)

Unfortunately, an improved thermal stability of modified pTBLM with CholPEG was accompanied by the relatively poor sensitivity of purified PFTs. In figure 3.18B, percentage composition of CholPEG was plotted against decrease in resistance of modified pTBLM upon addition of 150 nM α-HL. It was observed that the more CholPEG composition, the less sensitivity to α-HL. One possible explanation to this observation is the lipid fluidity affected by the presence of cholesterol. It is the fact that the lipid bilayer membranes in nature provide sufficient membrane fluidity for ease of insertion and functioning of transmembrane proteins [205]. A study revealed that when the cholesterol is added into the phospholipid *in-vitro*, it appeared the condensed complexes of cholesterol and phospholipids [239]. Since these complexes were local domains with limited fluidity, the presence of more and more such domains reduced the possibility of insertion of α-HL PFTs. With the increase amount of cholesterol in modified pTBLM, the patches of pure lipids with sufficient fluidity was decreased and

as a result α-HL monomer insertion and channel formation was seem to be slightly restricted. This probably makes the relatively poor sensitivity of modified pTBLM to α-HL at 37 °C.

In practical sensing of bacterial toxins at an elevated temperature, thermal stability and sensitivity to toxins are equally important. However the experimental results indicate that there needs to do a trade off between above two primary requirements of pTBLM for optimum sensing of toxins. Hence 50 % DPhyTL in combine with 50 % CholPEG is nominated as an optimum combination of monolayer because it provides better thermal stability at 37 ºC while it is still sensitive enough to detect the α-HL (figure 3.18).

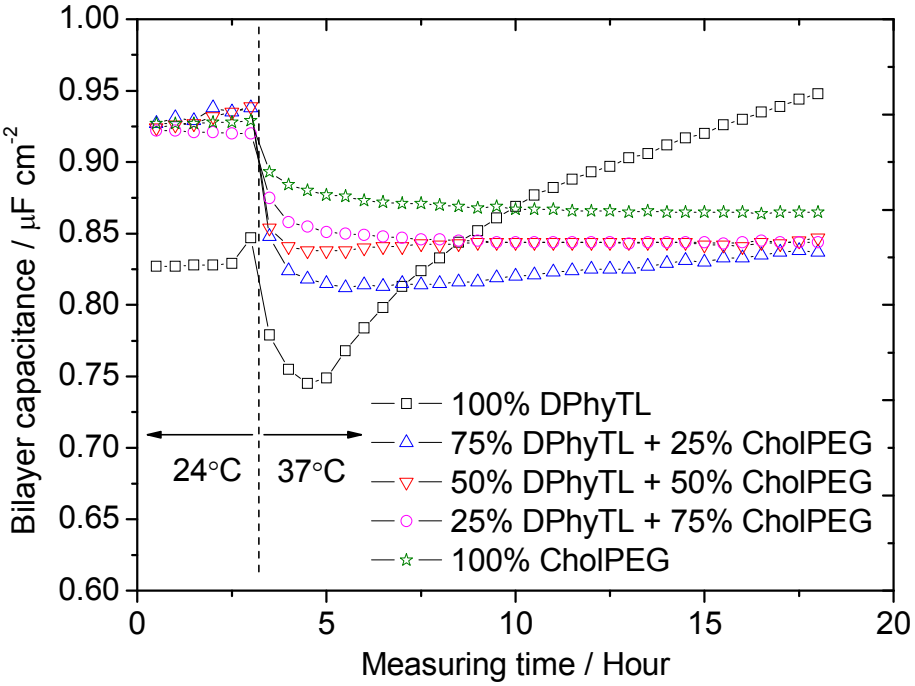

Figure 3.19 Effect of percentage CholPEG composition on thermal stability of modified pTBLM (bilayer capacitance of pTBLM was measured with time at 37 ºC)

SPR measurement

SPR measurement was carried out using 50 % DPhyTL + 50 % CholPEG (in volume) mixed monolayer with 67 % DPhyPC and 33 % cholesterol (in mole) modified pTBLM in an electrolyte of 100 mM NaCl + 10 mM $CaCl_2$ at 37 ºC. From this point onwards, the word "modified pTBLM" represents the bilayer with above mentioned monolayer and bilayer modifications. SPR data of an unmodified pTBLM was shown in figure 3.12A and 3.12B. When the buffer solution in SPR channels were heated and maintained at 37 ºC, it was noticed that the SPR angle was shifted about 350 mº (figure 3.20A). This downward shift was exponential and accompanied by the immediate

temperature rise. Except the increase in lipid fluidity, the bilayer structure of modified pTBLM was not expected to change due to temperature. However this SPR angle shift at 37 ºC was believed to be change in refractive index (RI) of buffer. RI of a liquid changes thermally and it is inversed function of temperature i.e. RI decreases if the temperature is raised. But their relationship is reversible as it can be seen in figure 3.20B. When the buffer temperature was brought back to room temperature, an upward shift of SPR angle was observed. This indicated that the modified pTBLM was intact and maintained its lipid bilayer structure at 37 ºC while the change in SPR angle was because of affected RI of the buffer by change in temperature.

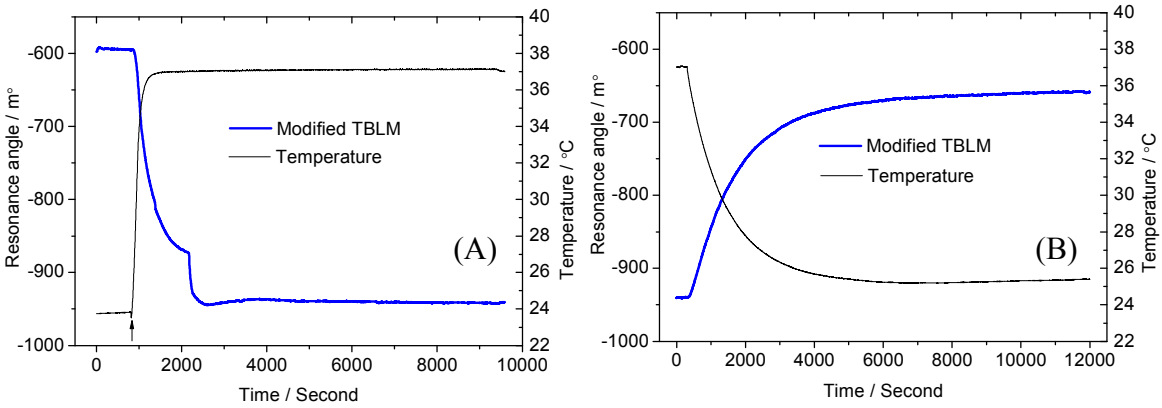

Figure 3.20 (A) Thermally induced resonance angle shift of modified pTBLM in NaCl + $CaCl_2$ electrolyte at 37 °C and (B) thermal restoration of SPR signal when the buffer was brought to room temperature

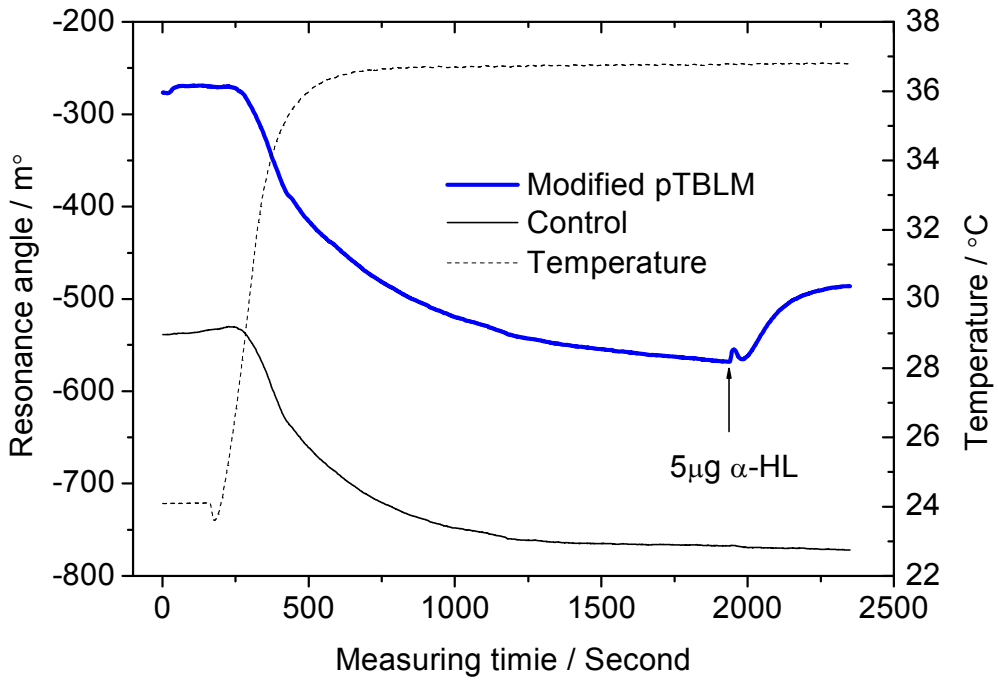

Figure 3.21 Temperature response of modified pTBLM in term of resonance angle shift at 37 °C

An SPR experiment was conducted to see the formation and the functionality of α-HL toxins in modified pTBLM at 37 ºC. This was already experimented with modified pTBLM by EIS measurement previously (section 3.3.1.1 and figure 3.15). Here in this experiment, modified pTBLM was initially formed in both SPR channels at room temperature in NaCl + $CaCl_2$ electrolyte. Then pTBLM was subjected to and maintained at 37 ºC and it was waited until the SPR angles in both channels reached the steady trends. Then 0.5 µg/ml of α-HL in PBS buffer was added onto pTBLM in one channel while another one was maintained as a control, and SPR was continuously measured. Upon addition, binding of α-HL toxins were observed as the upward shift in SPR angle with time. This was in a good agreement with the data measured by EIS in which toxin binding and channel formation was indicated by change in impedance of pTBLM (figure 3.15).

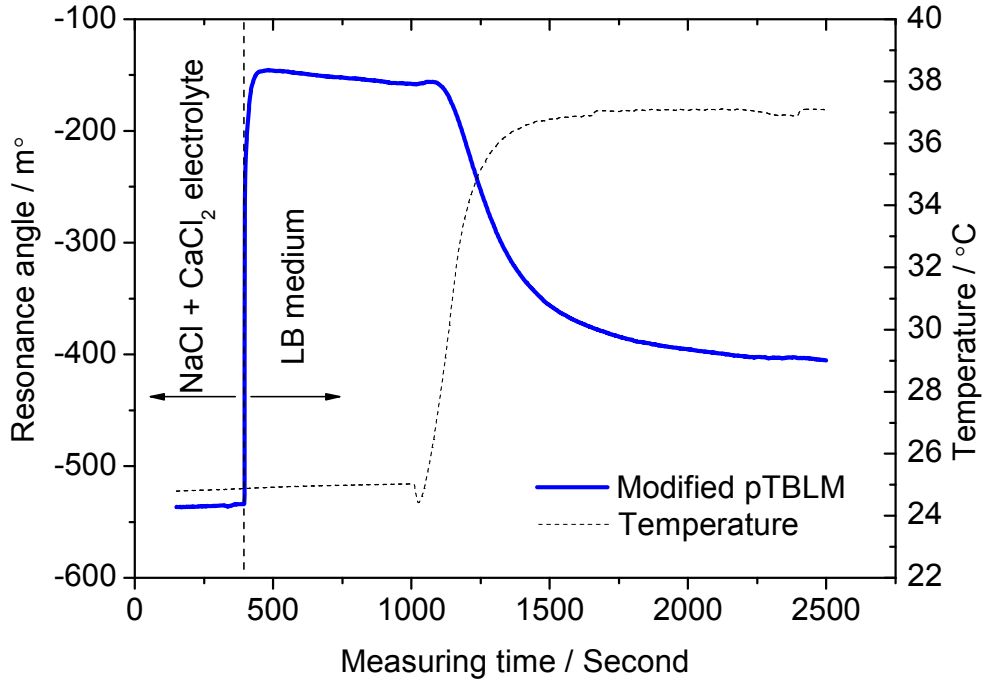

Figure 3.22 Effect of Lauria Broth (liquid nutrient medium for bacterial growth) on SPR angle of modified pTBLM at room temperature and 37 °C

As it was required, the bacterial growth medium Lauria Broth (LB) from Invitrogen was also used as an alternative to NaCl + $CaCl_2$ electrolyte in both EIS and SPR experiments. LB was prepared with a mixture of 10 g of peptone 140, 5 g of yeast extract and 10 g of NaCl in 1 litre of distilled water. Effect of LB medium on EIS and SPR data was not negligible as it affected the measured data. This can be seen in SPR measurement with modified pTBLM in LB medium at both room temperature and 37 ºC

(figure 3.22). At room temperature it caused about 400 mº upward shift of SPR angle upon immediate exchange of saline buffer with LB medium. This change in SPR signal was accompanied by the increase in RI and not likely to be due to binding of ingredient molecules of LB onto pTBLM. When the temperature of LB medium was raised and maintained at 37 ºC later, SPR angle shifted downward about 250 mº due to effect of temperature.

4 Modified pTBLM with purified bacterial toxins

4.1 Alpha hemolysin (α-HL)

Alpha hemolysin is the soluble exotoxin monomers secreted by human pathogen *S. aureus* [90]. These 33.2 kDa exotoxins can bind to the plasma membrane of target cells in their monomeric form. They can laterally diffuse and then oligomerize to form a water-filled transmembrane channel which is 232.4 kDa and made of seven monomers. The channel is composed of a mushroom shaped homo-oligomeric heptamer and a protruded stem. A solvent-filled channel with an approximate length of 10 nm and a diameter of 2.6 nm runs through the stem and a cap heptamer along sevenfold axis of anti-parallel β barrel strands. The stem with an approximate length of 5.2 nm has slight overlapping with about 7 nm long cap heptamer together with a rim. Outer diameter of the cap heptamer is approximately 10 nm and schematic of the structure of α-HL channel is shown in figure 4.1. When the channel is formed, only the approximate 5 nm length of the stem inserts into the lipid bilayer while the cap heptamer of about 5 nm in thickness stays above the membrane on the side where it is inserted. These α-HL channels have no control on transport of solutes, molecules etc. and hence uncontrolled permeation of water, ions, and small organic molecules through the channels can cause death to target cells by irreversible osmotic swelling causing rupture of the cell wall [91].

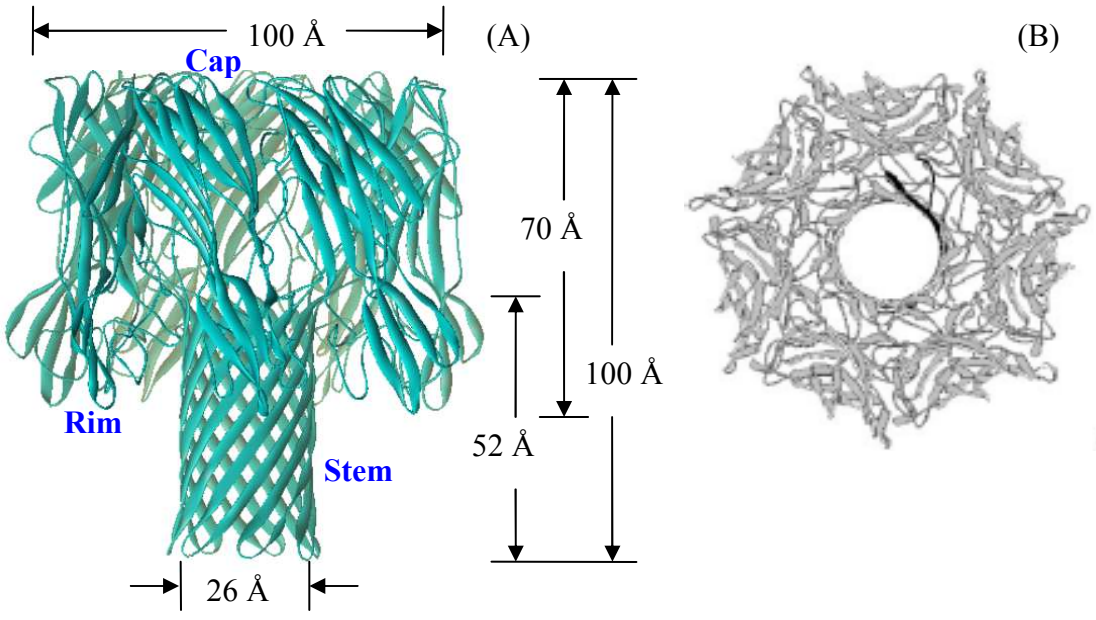

Figure 4.1 Ribbon structures of α-HL ion channel (A) side view and (B) top view, according to [90]

Importantly, this toxin is one of the well studied toxins with bacterial origin and the structure of toxin was already determined to the resolution of 1.9 Å [90]. There are several reasons for making use of α-HL in biotechnological applications such as systems for controlled delivery of small solutes and molecules across lipid bilayer membrane, stochastic sensing of molecules [93], controlled stochastic sensing with molecular adaptor [227] and orientation discrimination of DNA strands etc [228]. α-HL monomers can easily bind to either natural or synthetic lipid bilayer membranes and upon assembly α-HL channels are stable over a wide range of ionic concentration and temperature [91, 92]. Due to its relatively large diameter of the pore, molecules as large as 2 kDa can be able to pass through α-HL channels [93]. Here α-HL was used as the transmembrane channels for two main reasons. Firstly it was used to study as a model ion channel because it could easily bind to pTBLM and channels were spontaneously formed [57, 86]. Secondly it was used to verify the formation of Nano-psTBLM. If there were no Nano-psTBLM formed, then the transport of ions through the ion channels measured by PPC could not be observed. Since α-HL is an unregulated channel, the activities such as transport of ions in response to applied electric potential can be observed. α-HL used in this experiment were in the form of lyophilized powder extracted from *S. aureus* and directly purchased from Sigma Aldrich, UK. Toxins were prepared in aqueous phosphate buffer saline (PBS) at the concentration of 0.5 mg/ml and stored in freezer below –8 °C.

4.2 Phospholipase A2

PLA2 employed in this work was purchased from Sigma Aldrich and is extracted from honey bee venom as the lyophilized powder of 600-2400 units/mg protein. Targets of PLA2 include different phospholipids including PC, PE, PI and PS and it hydrolyses by cleaving the *sn*-2 acyl bond of lipids releasing fatty acids and lysophospholipids [128, 144, 145] (figure 1.12). Repeated hydrolysis of lipids by PLA2 results the rupture of the cell membrane in target cells. In this experiment, PLA2 was mixed with PBS buffer to the concentration of 1 mg/ml and freeze below –8 °C before usage.

4.3 Results and discussion

4.3.1 EIS

Modified pTBLM was prepared in an electrolyte of 100 mM NaCl + 10 mM $CaCl_2$ as the procedure described in section 3.3.2. After pTBLM was formed, it was placed inside the incubator and heated at 37 ºC while the impedance data was measured and recorded for every 30 minutes. When the resistance and the capacitance of pTBLM reach the steady state, 150 nM of α-HL was added onto the bilayer in electrolyte. The impedance of pTBLM was spontaneously changed upon addition of toxins as shown in figure 4.2. Insertion of toxin monomers and subsequent formation of α-HL channels were instantaneous but the effect of ion channels on pTBLM impedance was time dependent exponentially. Decrease in resistance was associated with increase in capacitance. It was observed that after 3 hours; about 1.5 MΩ cm^2 decreases in resistance and about 0.35 μF/cm^2 increases in capacitance was resulted by α-HL channels (figure 4.2). This clearly indicated that the modified pTBLM was able to support the insertion and formation of toxin channels even at 37 ºC. Similar results were observed when the same type of modified pTBLM was added with 150 nM PLA2 in PBS solution. PLA2 induced an immediate change in bilayer impedance by damaging the lipids in upper half of the modified pTBLM.

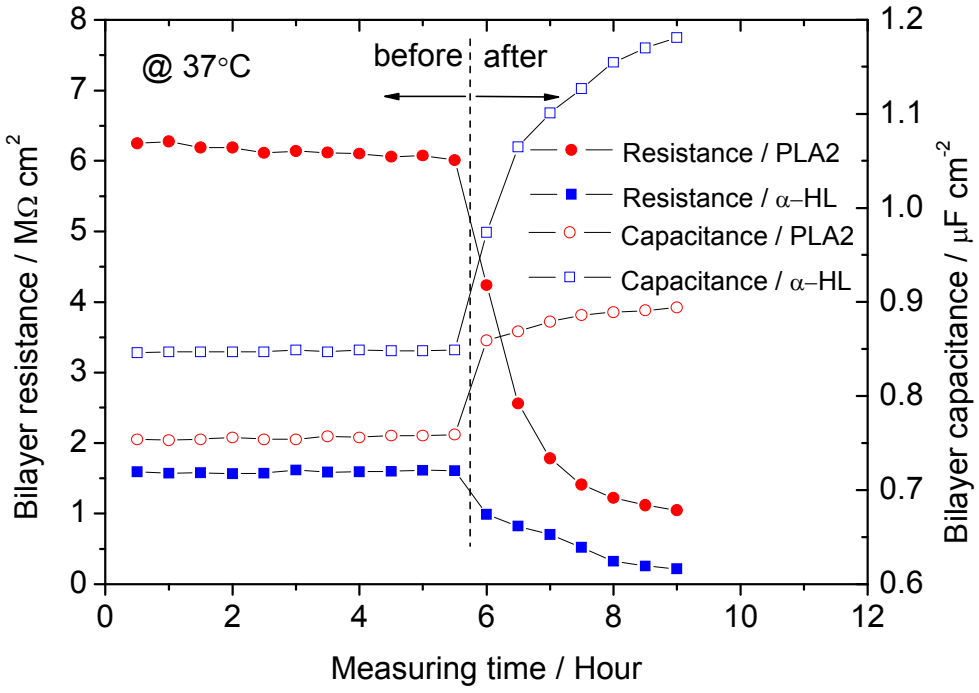

Figure 4.2 Resistance and capacitance responses of a modified pTBLM upon addition of α-HL and PLA2 at 37 ºC in 100 mM NaCl electrolyte

4.3.2 SPR

For the SPR measurement, the same type of modified pTBLM used in EIS experiment (section 4.3.1) was prepared on gold coated BK7 glass substrate. SPR setup and experimental procedure were previously discussed in section 2.2.2. After modified pTBLM was formed on gold surface, the cuvettes were rinsed with an electrolyte of 100 mM NaCl + 10 mM $CaCl_2$. SPR channel 1 was used as the control while channel 2 was used to study the binding of toxins. When the reflective angles on both channels reached a steady trend, α-HL toxins in PBS buffer were injected into SPR channel 2 to comprise the toxin concentration of 0.5 µg/ml. Immediate binding and formation of α-HL channels were observed by upward shift of resonance angle minimum as shown in figure 4.3. Binding was exponential and reached to a steady trend about 15 minutes after addition of toxins. Control SPR signal in channel 1 remained unchanged. However the binding curve was reversed in case of PLA2 binding onto modified pTBLM in a separate measurement as shown in figure 4.3. PLA2 was prepared in PBS buffer at the initial concentration of 1 mg/ml and it was injected into SPR channel 2 to end up the final concentration of 0.5 µg/ml. It was clearly seen that the binding of PLA2 onto modified pTBLM shifted the reflective angle downward.

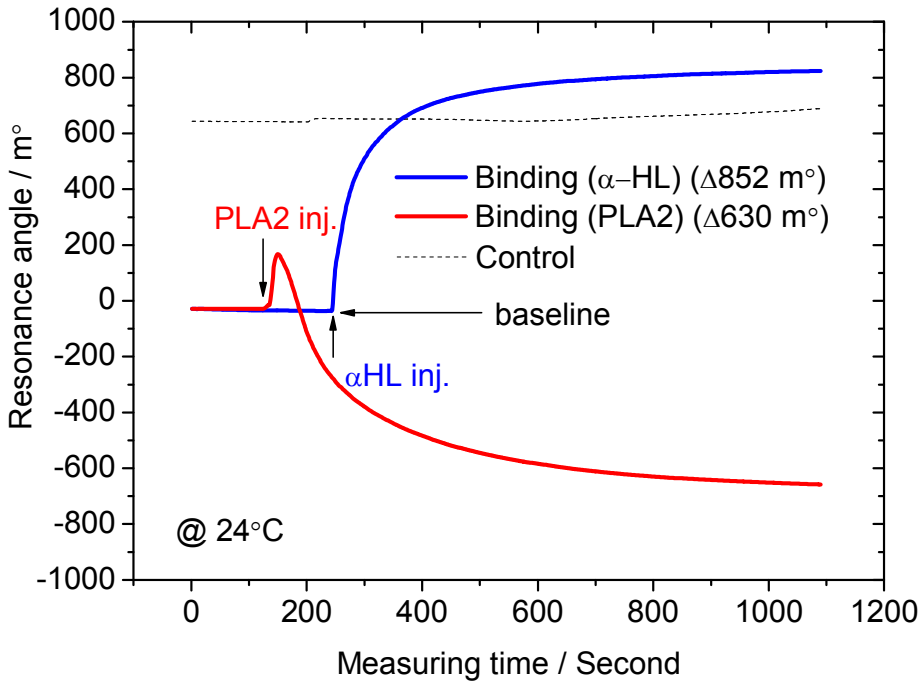

Figure 4.3 Resonance angle shifts with the measuring time due to binding (association) of α-HL toxins (blue) and unbinding (dissociation) of modified pTBLM by PLA2 (red) at room temperature while SPR signal of control remains unchanged (black dashed line)

SPR is basically very sensitive to binding (association) and unbinding (dissociation) of molecules at the gold surface. In this experiment, baseline SPR signal before the injection of toxins was simply based on modified pTBLM attached to gold surface (figure 4.3). Neither binding nor unbinding of molecules occurred onto or out of pTBLM in the state while baseline SPR signal was measured. Binding of α-HL onto pTBLM was simply incorporation of toxin monomers and formation of mushroom shaped ion channels. This association of toxin molecules was not damaged onto pTBLM but caused the SPR resonance angle upward shift. About 850 mº of resonance angle shift was observed upon binding of α-HL. On the other hand, a short upward angle shift followed by the long downward shift of resonance angle was observed when PLA2 was added (figure 4.3). This significant action of dissociation was due to lipid loss from upper half of pTBLM. PLA2 hydrolysed the *sn*-2 phytanyl chain of DPhyPC lipids and released the lipids out of pTBLM. As a result, dissociation of lipids induced the significant SPR angle downward shift with time (figure 4.3). Action of PLA2 on modified pTBLM changed the SPR angle shift of about 630 mº in 15 minutes. These results above were important as it was possible to distinguish or discriminate the different bacterial toxins on their modes of action against lipid bilayer membranes in term of SPR signal shift.

4.4 Sensitivity of pTBLM to α-HL

4.4.1 α-HL sensitivity of unmodified pTBLM

Sensitivities of α-HL toxins to mammalian cells *in-vivo* are different. It was previously reported that α-HL toxin above 1 μM was enough to lyse the human erythrocytes while α-HL toxin as low as 1 nM was able to lyse the human platlets and rabbit erythrocytes [90]. However *in-vitro* sensitivity of α-HL toxins onto lipid bilayer membrane is not reported. It has been proved that the quantitative presence of α-HL toxins in planar lipid bilayer membranes can directly alter the membrane impedance by ion channel formation. In review to previous works related to α-HL toxins, most experiments were done by simple incorporation of a relatively large quantity of α-HL into bilayer membrane to amplify the current signal (in term of change in bilayer impedance) as a proof of channel formation in model membranes [57, 86]. Unfortunately the quantitative relationship between α-HL and bilayer impedance was yet to be known. More importantly the minimum amount of α-HL toxins that can form the ion channel and alter

the bilayer impedance was still to be explored. Theoretically α-HL monomers can insert and freely diffuse laterally in the synthetic lipid bilayer membrane and an ion channel is formed when seven of α-HL monomers are collectively assembled by conformational changes [91]. Without a doubt the probability of ion channel formation increases with the more population of α-HL monomers in both buffer and lipid bilayer membrane. Moreover, diffusion of α-HL in lipid bilayer membrane also plays an important role in ion transport of α-HL channels. It was previously reported that the diffusion coefficient of *E. coli* α-HL in gels was about 2.4×10^{-7} cm^2/sec [98] which was about one order magnitude higher than that of lipids in bilayer membrane [125]. On the other hand, α-HL monomers are directly secreted by *S. aureus* bacteria as alpha toxins. Therefore, it is required to evaluate the sensitivity and limit of detection (LOD) of proposed modified pTBLM to α-HL toxins *in-vitro*. This information is necessary to know prior to attempt the sensing of real bacterial toxins of bacteria.

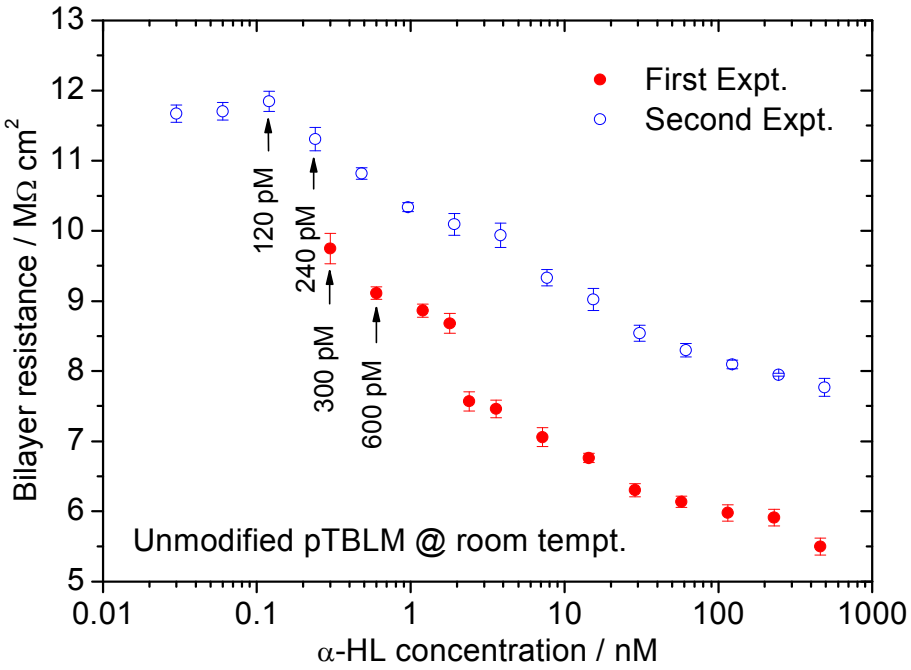

Figure 4.4 Sensitivity (slope) and limit of detection (LOD) of unmodified pTBLM to α-HL toxins at room temperature in NaCl electrolyte (in first experiment, LOD in term of decrease in pTBLM resistance occurs at 300 pM and in second experiment, LOD of pTBLM to α-HL lies between 120 pM and 240 pM – see data in table 4.2)

The EIS experiment was started with an unmodified pTBLM on TSG substrate in an electrolyte of 100 mM NaCl. First DPhyTL monolayer was self-assembled on TSG substrate for 24 hours. Then the bilayer was formed by fusion of DPhyPC SUVs onto monolayer in buffer. After formation of pTBLM and thorough rinse, 500 µl of buffer

solution in the measurement cell was removed and the flow outlet of the Teflon cell was sealed. Injection of α-HL toxins prepared in same buffer was in the order of ascending i.e., from pico-molar (pM) to nano-molar (nM) concentration. Since the minimum concentration of α-HL at which the pTBLM responded was not known, first experiment was started with 300 pM α-HL. First the injection was started with 1 µl of 15 nM α-HL solution into 500 µl of buffer comprising 300 pM concentration in the cell. Then the toxin concentration in Teflon cell was doubled by calculated amount of different molar concentration of α-HL up to 0.5 µM. After each injection, 6 measurements were continuously run for 2 hours before the subsequent injection was started. It is believed that the duration of 2 hours between subsequent injections of α-HL is enough as the diffusion of α-HL is expected to comparable to lipids in bilayer membrane [98, 125].

The measured resistance of unmodified pTBLM in response to different molar concentration of α-HL in first experiment is shown in table 4.1. Change in resistance of unmodified pTBLM vs α-HL concentration was plotted for analysis as shown in figure 4.4. According to table 4.1, decrease in resistance was observed even at 300 pM indicating that 300 pM concentration was still not the lower limit that could give the decrease in distinguishable impedance signal. The trend and slope (sensitivity) of decrease in resistance with increase in toxin concentration was quite linear (filled circles in figure 4.4) except there was a drop in resistance between 1.8 nM and 2.4 nM due to leaving the experiment overnight (filled circles in figure 4.4). This was an indication of time-dependent insertion and formation of α-HL ion channels.

Table 4.1 Resistance of unmodified pTBLM response against α-HL concentration (First experiment)

α-HL (nM)	**none**	**0.3**	**0.6**	**1.2**	**1.8**	**2.4**	**3.6**
R (MΩ cm^2)	10.1	9.75	9.11	8.86	8.68	7.57	7.46
α-HL (nM)	**7.2**	**14.4**	**28.8**	**57.6**	**115.2**	**230.4**	**460.8**
R (MΩ cm^2)	7.06	6.76	6.30	6.14	5.98	5.91	5.50

Table 4.2 Resistance of unmodified pTBLM response against α-HL concentration (Second experiment)

α-HL (nM)	**None**	**0.03**	**0.06**	**0.12**	**0.24**	**0.48**	**0.96**	**1.92**
R (MΩ cm^2)	11.6	11.7	11.7	11.8	11.3	10.8	10.3	10.1
α-HL (nM)	**3.84**	**7.68**	**15.4**	**30.7**	**61.4**	**123**	**246**	**492**
R (MΩ cm^2)	9.90	9.30	9.00	8.50	8.30	8.10	8.00	7.80

This required to conduct a second experiment in which the starting concentration was one order magnitude lower in concentration i.e. 30 pM. The results were tabulated in table 4.2. The graph with resistance vs toxin concentration was plotted in figure 4.4 (unfilled circles). According to the results, distinguishable change in resistance of unmodified pTBLM lies between minimum molar concentrations of 120 pM and 240 pM (table 4.2).

4.4.2 α-HL sensitivity of modified pTBLM

Bacterial toxins are best design to interact and infect the host cells at body temperature and hence sensitivity and LOD of pTBLM to α-HL at 37 °C is also necessary to know prior to experiments with real bacterial toxins. As the conventional pTBLM was modified by incorporation of cholesterol and CholPEG to withstand the effect of temperature, sensitivity test was also conducted using modified pTBLM. First the mixed monolayer with 50 % DPhyTL and 50 % CholPEG (in volume) was self-assembled on TSG. Then the bilayer was formed by fusion of SUVs made of 67 % DPhyPC and 33 % cholesterol in mole. Thermal stability of modified pTBLM was previously discussed in section 3.3.2. The experimental procedure was same as that of unmodified pTBLM in section 4.4.1 except the temperature. Experiment with modified pTBLM was conducted at 37 °C in incubator. The results were plotted as shown in figure 4.5 alongside with the results of second experiment of unmodified pTBLM.

Surprisingly, the minimum LOD of modified pTBLM to α-HL was decreased. It was observed that the noticeable change in resistance only occurred at about 3 nM concentration of α-HL (figure 4.5), compared to around 240 pM in case of unmodified pTBLM. However it was also noticed that the sensitivity (the slope of the graph) of modified pTBLM was better than that of unmodified one. The linearity in sensitivity of unmodified pTBLM on the other hand, was better than that of modified one (figure 4.5). Therefore, this experiment verified that incorporation of cholesterol into pTBLM reduced the sensitivity of lipid bilayer to α-HL. This result agreed well with the results of sensitivity experiment at 37 °C using CholPEG-modified pTBLM (section 3.3.2.1 and figure 3.18B).

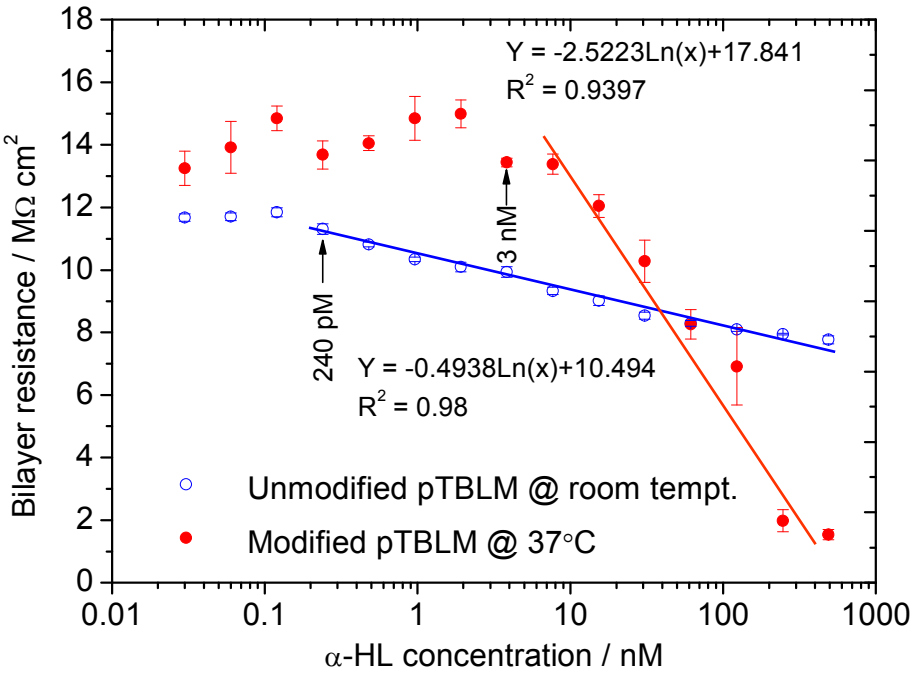

Figure 4.5 Sensitivity of unmodified and cholesterol-modified pTBLM to α-HL toxins (it is tested at 37 °C in incubator for modified pTBLM and its toxin sensitivity in term of slope of the graph was better than that of unmodified one)

4.4.3 Discussion

Limit of detection (LOD)

Unmodified pTBLM exhibited lower LOD to α-HL around 240 pM. Unmodified pTBLM was composed of DPhyTL and DPhyPC and it was known to maintain the liquid-crystalline state at room temperature with sufficient fluidity (figure 3.1). Therefore there should not have any restriction for the insertion of toxin monomers and subsequent ion channel formation at relatively low concentration of α-HL. On the other hand, modified pTBLM comprised cholesterol in both halves of bilayer (figure 3.16). Despite the improved thermal stability of cholesterol modified pTBLM at 37 °C, relatively higher LOD was probably attributed by the cholesterol. Firstly the presence of cholesterol on the outer half of pTBLM affects the lateral fluidity of lipids [125]. Cholesterol was known to form the condensed clusters when it mixed with phospholipids [239]. In the presence of such condensed clusters, toxins monomers might not be favourable to insert and form the successful channels. Consequently same amount of toxin in bilayer may not be able to contribute to channel formation and hence this might probably make LOD relatively high compared to that of unmodified pTBLM.

Sensitivity

Sensitivity is measured as the slope of graph which is change in resistance per unit toxin concentration. It was observed that the sensitivity of unmodified pTBLM to α-HL was not as good as that of modified pTBLM (figure 4.5). As it was proved by the experiment in section 4.3.1 (figure 4.2), α-HL insertion and formation of channels were time-dependent, at least to an extent over time. It was the fact that the bacterial protein toxins secreted by bacterial pathogens, were designed and optimized naturally to function at body temperature although several experiments have proved that they maintained their functionality at room temperature but not optimally. Therefore it is believed that probably α-HL monomers if not for immediate insertion to pTBLM, might not fully function after remaining in buffer for two hours. On the other hand, experiment with modified pTBLM provides the body temperature to toxins and it is believed that α-HL toxins retain their functionality with better sensitivity as the concentration is higher with time (figure 4.5).

5 Modified pTBLM with pathogens and supernatant toxins

5.1 Pathogens studied in this work

Among many human pathogenic bacteria, three different types of clinically important bacteria studied in this works are specific strains of pathogens originally belong to *S. aureus*, *P. aeruginosa* and *E. coli*. *S. aureus* is the gram-positive, facultative bacteria commonly found on skin and nose of humans. They are conditional pathogens and a part of human normal flora in normal conditions but responsible for causing a wide range of infectious diseases from simple skin infection to life threatening diseases such as pneumonia and toxic shock syndrome (TSS) to human. *S. aureus* is known to secrete variety of toxins including pore-forming exotoxins of alpha [83, 207], beta [206], gamma [207] and delta-toxins [208, 209], superantigens [133, 134], exfoliative toxins [120] and Panton-Valentine leukocidin (PVL) bicomponent toxins [211]. *P. aeruginosa*, on the other hand is the bacillus, gram-negative and aerobic bacteria normally harbour in skin flora of humans and animals. *P. aeruginosa* is the opportunistic pathogen with the ability to infect and damage the tissue sites of hosts with reduced or suppressed immunity [117, 212]. It usually involved in gastrointestinal and urinary tract infections as well as the skin and tissue infections in patients with burns or wound in hospitals. Pneumonia in patients suffering from cystic-fibrosis and septic shock in neutropenic patients are also widely infected by *P. aeruginosa*. Toxins associated with *P. aeruginosa* include many pigments, exotoxin A and PLC [190, 213, 137].

E. coli, similar to *P. aeruginosa* is the bacillus, gram-negative but facultative bacteria commonly found in gastrointestinal tract of humans as a part of normal flora. Compared to above two human pathogens, *E. coli* with most of the strains is less harmful but even beneficial to the host such as producing vitamin k_2 and preventing the establishment of other pathogenic bacteria in intestine. But *E. coli* with pathogenic strains is an exception, for example, *E. coli* O157:H7 is commonly known as human pathogen and responsible for causing serious food poisoning in humans [141, 181]. As of being a conditional pathogen, *E. coli* under certain conditions involves in gastrointestinal and urinary infections in human by secretion of various toxins including heat-labile and heat-stable enterotoxins. These three conditional human pathogens are mainly involved in hospital-acquired infections and responsible for causing various life-threatening diseases. The expenses to control, contain and prevention of such hospital-acquired infections by these pathogens have been ever increasing in hospitals nowadays [224,

225, 226]. Despite the enormous efforts to tackle the problems associated with these pathogens, emergence and re-emergence of pathogens with their alarming resistance to current antibiotics have been major challenge and concern in recent years [214, 215].

5.1.1 Methicillin-suspected *Staphylococcus aureus* (MSSA476)

S. aureus was an important human pathogen commonly acquired in communities and hospitals. *S. aureus* infections were originally treated with penicillin in 1940s. But a few years later *S. aureus* acquired resistance to penicillin as it secreted β-lactamase enzymes that hydrolyzed penicillin [216]. Since then many new β-lactamase-resistant penicillins including methicillin, oxacillin, cloxacillin and flucloxacillin have been used as the first line treatment to treat the penicillin-resistant *S. aureus* infections. However for many years *S. aureus* has been undergoing changes in genetic complement successively and that have been resulted the emergence of more and more antibiotic-resistant strains. Nowadays in hospitals and public community places, *S. aureus* resistant to methicillin (MRSA) and other antibiotics are common and responsible for causing various *S. aureus* related diseases. *S. aureus* suspected of resistance to methicillin (MSSA) on the other hand, is the community-acquired pathogen that causes severe invasive diseases in immuno-competent children in community. MSSA476 used in this work was isolated from a patient with the primary upper tibial osteomyelitis and the bacteraemia in 1998 [217] (figure 5.1). This pathogen was resistant to penicillin and fusidic acid but suspect to commonly used antibiotics including methicillin, ciprofloxacin, rifampicin, tetracycline, trimethoprim, erythromycin, gentamycin and amikacin. Since MSSA476 is the gram-positive pathogen, major types of toxins associated with its strains are expected to be proteins and minimally polypeptide exotoxins.

5.1.2 *Pseudomonas aeruginosa* (PAO1)

P. aeruginosa is a well-studied opportunistic pathogen and known for causing serious infections in patients with cystic fibrosis and immuno-suppression. This pathogen successively acquired the strains with resistance to commonly used antibiotics today. The genome for both MSSA476 and PAO1 were sequenced, and their genomic virulence factors reveal that they encode toxins and membrane-damaging agents which are known to interact with cell membranes *in-vivo* and *in-vitro* [217, 218]. *P.*

aeruginosa is the gram-negative bacterium and toxins secreted by this bacterium are expected to be more lipid damaging enzymes and endotoxins.

(A) 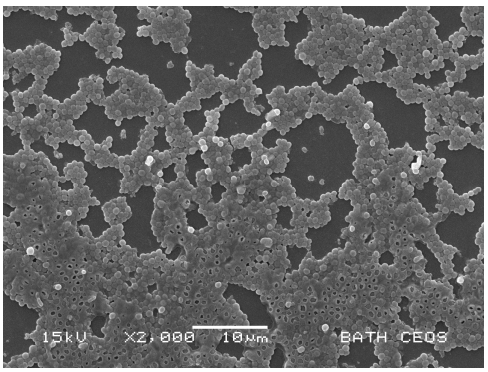

(B) 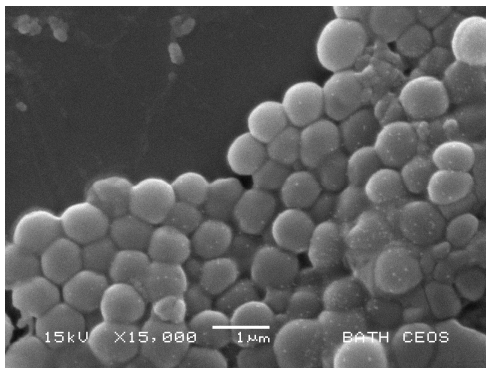

Figure 5.1 SEM images of the clusters of MSSA476 *Staphylococcus aureus* bacteria on TSG surface at (A) lower and (B) higher magnifications

5.1.3 *Escherichia coli* (DH5α)

E. coli usually colonizes and harbours in human gut and most of its strains are harmless as a part of normal gut flora. But certain strains of *E. coli* are highly pathogenic for example *E. coli* O157:H7. Here in this work, genetically modified bacterium, *E. coli* DH5α is used as a reference bacterium. Lab strains of pathogenic *E. coli* with most virulent factors were removed in *E. coli* DH5α. This particular bacterium was used as a reference pathogen as it was not associated with the strains of secreting toxins, to compare the pathogenic strains of MSSA476 and PAO1 in EIS and SPR experiments with modified pTBLM [167].

5.1.4 *In-vitro* haemolysis of selected bacterial pathogens

In order to observe the cell lysis abilities of selected pathogens in this work, *in-vitro* haemolysis test was conducted using MSSA476, PAO1 and *E. coli* DH5α. Blood agar plate containing red blood cells is used to grow three pathogens at 37 ºC in incubator for overnight. Then the growing bacterial colonies on blood agar plate were analyzed. The result was shown in figure 5.2. Both MSSA476 and PAO1 caused extensive lysis of blood cells on agar plate and this was clearly noticed as the change in physical appearance surrounding the growing bacterial colonies (figure 5.2A and 5.2B). In contrast to MSSA476 and PAO1, growing colonies of *E. coli* DH5α with strains of no virulent factors showed no haemolysis to blood cells (figure 5.2C). This haemolysis experiment confirmed that both MSSA476 and PAO1 in their growth secreted lipid

damaging toxins and enzymes while *E. coli* DH5α was almost not associated with such toxins.

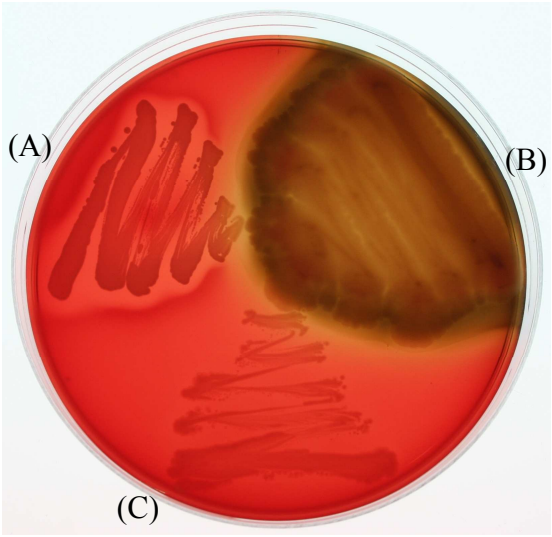

Figure 5.2 Photographic image showing haemolytic behaviour of three pathogenic bacteria with different microbial strains: (A) MSSA476, (B) PAO1 and (C) *E. coli* DH5α (Image credit goes to Dr. Geraldine Mulley from Department of Biology and Biochemistry, University of Bath, UK)

5.2 Modified pTBLM with pathogens

5.2.1 Effect of nutrient and temperature on bacterial growth

It is generally accepted that the optimum secretion of toxins by human pathogenic bacteria is associated with their growth and reproduction. Bacterial growth and reproduction (culture) on the other hand, is functions of the type of nutrient available and the temperature and pH of growth medium [244, 245]. Therefore these bacterial culture parameters have definitely contributed to the secretion of toxins. However which parameters have detrimental effects on the toxin secretion is still uncertain and controversial. To have insight into these important relationships between growth parameters and secretion of toxins, modified pTBLM with MSSA476 was tested as the functions of temperature and nutrient of the medium. First MSSA476 was tested with modified pTBLM in NaCl buffer at room temperature. In this experiment, MSSA476 was cultured overnight in LB medium first and OD of cultured medium was measured. Then LB containing bacteria was centrifuged at 12000 rpm for 3 minutes to separate the bacteria from supernatant LB. After replacing the supernatant with an electrolyte of 100 mM NaCl, the bacteria in the tube were re-mixed in NaCl electrolyte by vortexing thoroughly and again OD of this bacterial solution was recorded. This NaCl solution

containing MSSA476 was then directly injected onto the modified pTBLM held at room temperature while the impedance of pTBLM was being measured and recorded. The result shown in figure 5.3 revealed that there were no significant changes in bilayer impedance with time. Impedance was changed slightly after a day but the change was minimal and might not be due to the effect of pathogenic toxins. Importantly OD of bacterial solution in NaCl electrolyte was not changed after a day. This simply implied that the bacteria remained unchanged without growing, probably due to lack of nutrient and optimum temperature. As a result there were no toxins available to damage the lipids and the impedance of pTBLM was clearly unaffected.

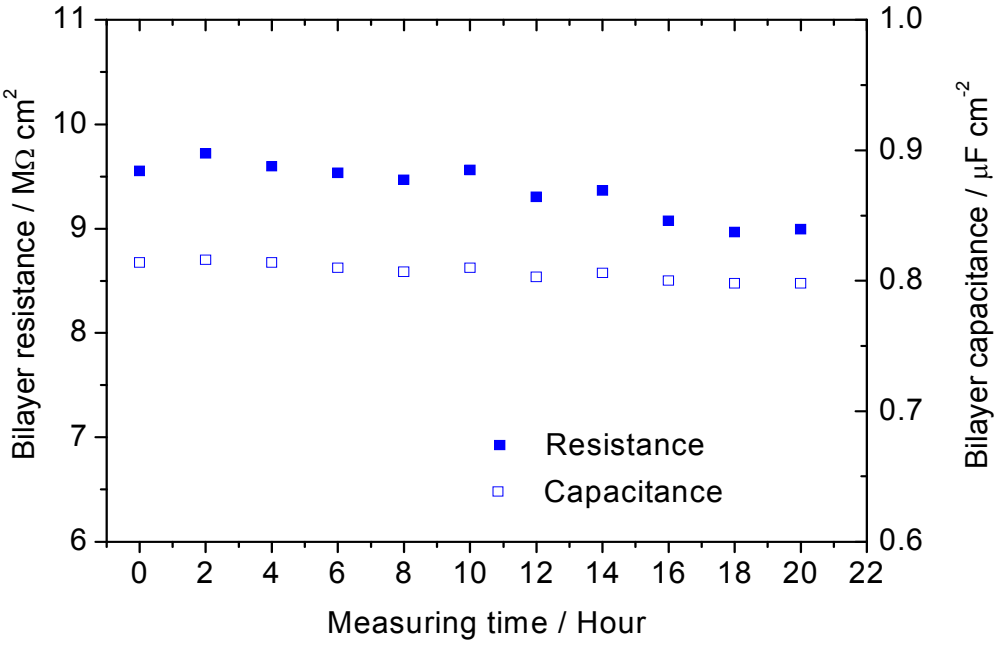

Figure 5.3 Impedance of a modified pTBLM tested in an electrolyte of 100 mM NaCl containing MSSA476 at room temperature (impedance remained unchanged as the bacterial growth was hindered by the lack of nutrient and optimum temperature)

5.2.2 Experiments with pathogenic bacteria

5.2.2.1 EIS with pathogenic MSSA476 and PAO1

Secondly effect of temperature on the secretion of bacterial toxins was explored. The experimental procedure and the bacteria involved were the same as in first impedance measurement except NaCl electrolyte was subjected to 37 ºC. The result was shown in figure 5.4 where the impedance of modified pTBLM was steady and not changed significantly throughout the measuring time. OD of MSSA476 medium in NaCl after the experiment was also not changed noticeably. Therefore the optimum temperature at 37 ºC was not contributed to the growth of bacteria especially in the medium lack of

nutrient and subsequently hinders the secretion of toxins. This result suggested that the effect of nutrient played an important role in bacterial growth as well as the toxins secretion.

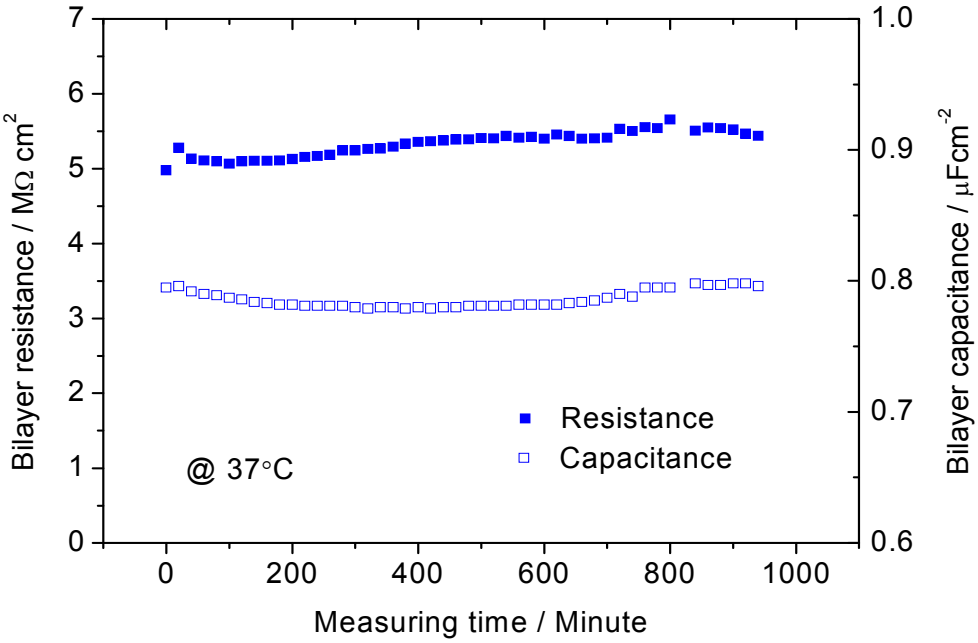

Figure 5.4 Resistance and capacitance of a modified pTBLM tested in 100 mM NaCl electrolyte containing MSSA476 at 37 ºC (impedance of pTBLM remained unchanged as the bacterial growth was hindered by the lack of nutrient despite the temperature was optimum for the bacterial growth)

Finally the impedance of modified pTBLM was measured with the bacterial pathogens as they grew in the electrochemical cell filled with nutrient LB medium and set at the growth temperature. For the experiment, MSSA476, PAO1 and *E. coli* DH5α were cultured as usual in LB medium at 37 ºC for overnight. The cultured medium rich in bacteria was diluted 10 times into freshly filtered LB medium. Then OD of diluted medium containing bacteria was recorded and the medium was subjected at 37 ºC in incubator for half an hour prior to impedance measurements. As the bacteria are diluted into fresh LB medium, the secretion of bacterial toxins by the effect of temperature and nutrient in terms of impedance can be observed and identified. The first experiment started with MSSA476. Modified pTBLM was first prepared in NaCl buffer and subsequently changed into filtered LB medium at 37 ºC. When the impedance was steady, diluted MSSA476 in LB was exchanged into the Teflon cell and measurement was carried out as the bacteria grew overnight. Same experiment with PAO1 was also conducted.

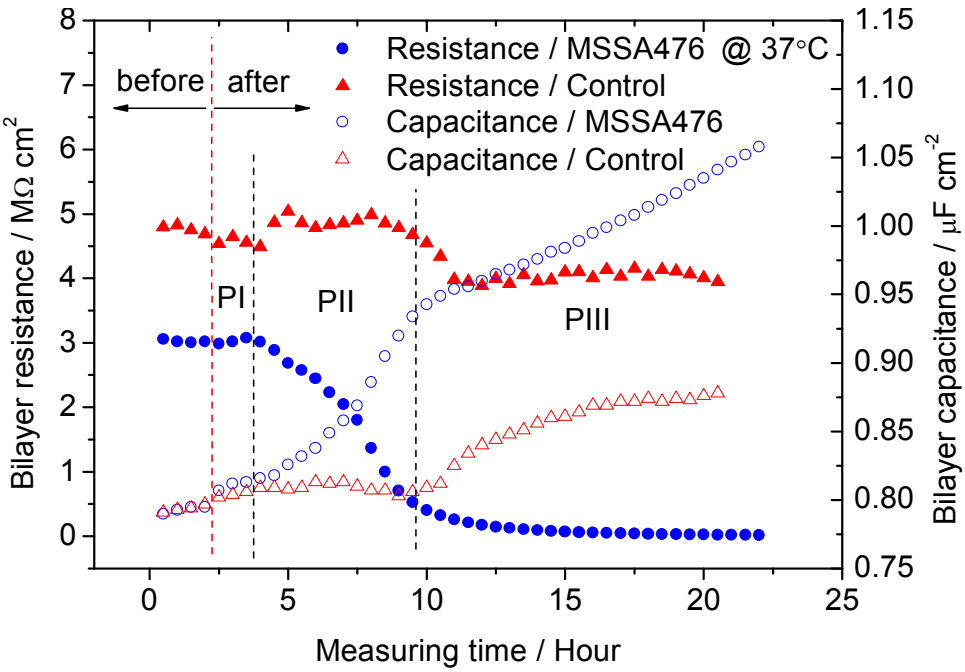

Figure 5.5 Change in bilayer resistance and capacitance of a modified pTBLM with initially 10 times diluted MSSA476 in LB medium at 37 ºC (the red vertical dashed-line indicates before and after the exchange of diluted LB medium with MSSA476; for analysis, the graph is divided into three phases (PI, PII and PIII) according to significant changes in curves of bilayer resistance and capacitance)

The results of MSSA476 and PAO1 were divided into three phases for analysis as shown in figure 5.5 and 5.6 respectively. In both cases in phase I, the impedance was not changed immediately before and after the injection of LB with diluted bacteria. This might probably be due to very low concentration of initial toxins in diluted LB. It was also possible to consider that the bacteria diluted in fresh LB medium, entered into the initial phase (lag phase) of growth. Therefore there were no toxins available to damage the lipids in pTBLM initially and as a result impedance was not changed noticeably in phase I (figure 5.5 and 5.6). When bacteria adapted to the new medium then the growth initiated and entered the log phase where bacterial grew exponentially. This was denoted as the phase II in figures 5.5 and 5.6 where the bilayer resistances decreased immediately within a short period of time while the bilayer capacitance in both experiments steadily increased. In phase II, change in impedance was possibly induced by the secreted toxins of bacteria as their growth multiplied exponentially. It was noted that there was almost no change in impedance of control pTBLM (triangles in figure 5.5). Finally in phase III, the change in resistance was saturated while the capacitance still increased gradually with the change in slope of capacitance curve (figure 5.5 and 5.6). As the bacterial growth reached stationary and death phases, the nutrients in media

were depleted and the bacterial population was declined while the medium was polluted with bulk of secreted toxins and metabolic wastes.

However, it was observed that there was a slight change in resistance and capacitance of control pTBLM in phase III although the change was not significant compared to the impedance of pTBLM with MSSA476 and PAO1 (figure 5.5). It was believed that the LB medium containing control pTBLM might be contaminated with air-borne or harmless bacteria during the measurement. LB medium is rich in nutrients which may attract the bacteria from the surroundings. For that reason, LB medium was sterilized (autoclaved) and always handled inside the cabinet with controlled air flow. Unfortunately impedance measurement was to be done on lab bench to keep away from vibrations and for signal stability. Although the Teflon cell was covered by a lid, air-born bacteria from the surroundings may access into the cell via the ports of electrode connections and grow in LB medium, especially after lengthly impedance measurement above 10 hours. Despite the fact that the air-born, harmless bacteria were not associated with pathogenic strains, their growth and initiation of attachment to lipid bilayer on surface may alter the impedance of control pTBLM in this experiment.

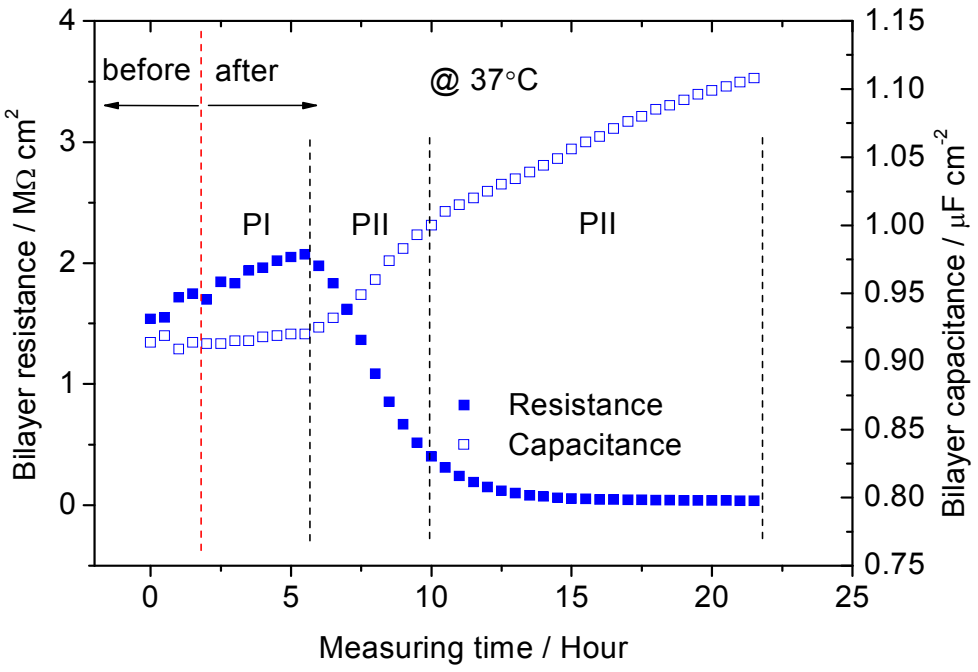

Figure 5.6 Change in impedance of a modified pTBLM with initially 10 times diluted PAO1 in LB medium at 37 ºC with the red vertical dashed-line indicates before and after exchange of diluted LB medium with bacteria (phase I is relatively longer with rather stable impedance followed by a rapid change in impedance in phase II – while the change in impedance was gradual at phase III) Control impedance (not shown here) was relatively stable in LB medium without bacteria

The effect of toxins over modified pTBLM was prolonged and existed with time and hence the capacitances in both experiments were gradually increased until the experiments were stopped. These results were compared and studied with a typical bacterial growth curve as basically the bacterial were grown in Teflon cell while the impedance of pTBLM was measured continuously in these experiments. OD of bacterial solution in Teflon cell before and after the impedance measurement within approximately 20 hours was doubled and this confirmed the growth of bacteria during the measurement. Rapid change in impedance due to possible damage to lipid bilayer occurred in phase II which was related and associated to the exponential phase of growth curve. Therefore in general it can be concluded that the bacterial toxin secretion was optimum and proliferated as the rapid growth of bacteria during exponential phase.

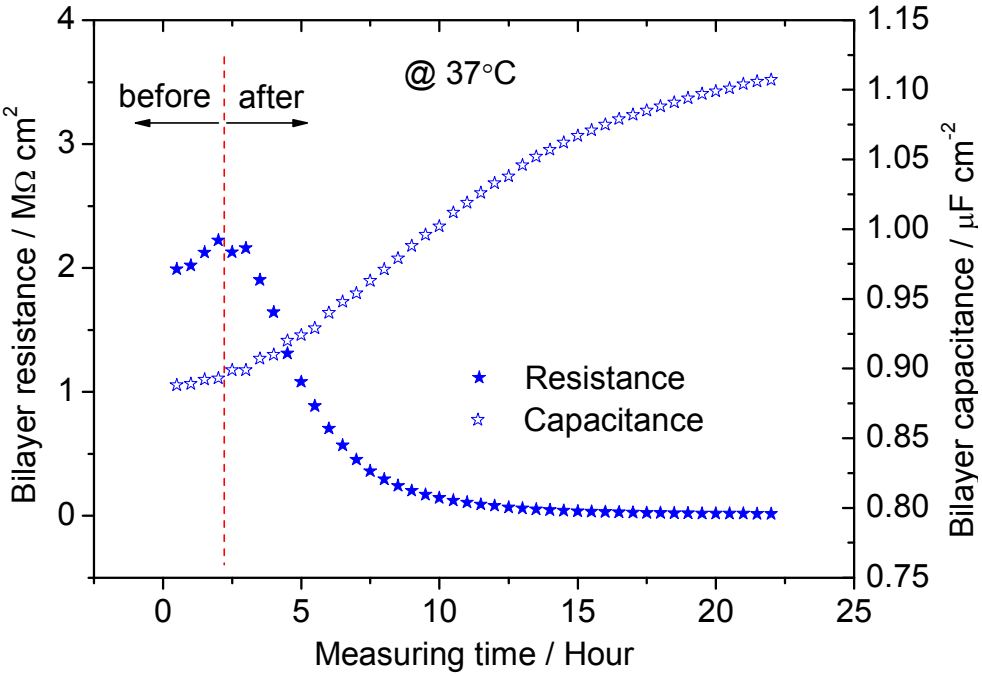

Figure 5.7 Impedance response of a modified pTBLM with initially 10 times diluted *E. coli* DH5α in LB medium at 37 ºC (the red vertical dashed-line indicates before and after exchange of diluted LB medium with bacteria)

However it is required to look into the detail profile of impedance graphs between MSSA476 and PAO1. It was observed that the duration of phase I in case of PAO1 (about 4 hours in figure 5.6) was longer than that of MSSA476 (about 1.5 hour in figure 5.5). At the same time in phase I, particular observations went to the capacitance of bilayer with PAO1 which remained almost constant around 0.92 μF/cm^2 (figure 5.6) while that of bilayer with MSSA476 changed slight increasingly in phase I (figure 5.5). This probably was explained by types and modes of action of major toxins involved by

two pathogens. Both MSSA476 and PAO1 used in both experiments were prepared in LB medium with same dilution (i.e. same initial OD of bacteria) and grown in identical culture conditions, and therefore their growth curves are expected to be similar especially in both initial and exponential phases. However the durations of phase I (equivalent to initial growth phase) for both pathogens were different. According to phase I of MSSA476 (figure 5.5), initial phase of bacterial growth lasted about 1.5 hour before the proliferation of bacteria initiated. It should also be more or less the same for PAO1 but in reality it lasted for about 4 hours for the impedance to change in case of PAO1. This implies that PAO1 must be proliferated and secretes the toxins after about 1.5 hour but the change in impedance was only induced after 4 hours.

PAO1 naturally secretes more endotoxins and enzymes with the ability to damage the lipids. In response to attack by toxins of PAO1, the bilayer is healed itself to minimize the energy loss and there is no significant change in impedance occurred until the lipid damaging was not incurred by self-healing (at the end of phase I after 4 hours). On the other hand, the impact of more protein exotoxins secreted by MSSA476 on the impedance of the lipid bilayer was immediately occurred after the end of initial phase of bacterial growth (after about 1.5 hour in figure 5.5). Therefore it is concluded, by analyzing the trend of the impedance response curve of the lipid bilayer membrane that the majority of types of toxin involved and the modes of action of the particular pathogenic bacteria *in-vitro* can be possible to predict by EIS measurement.

5.2.2.2 EIS with *E. coli* DH5α

For the experiment with *E. coli* DH5α, all experimental procedures were the same as previous ones with MSSA476 and PAO1. As most of pathogenic strains were removed from *E. coli* DH5α, it was expected to see the results of *E. coli* DH5α different from those of pathogenic ones. Impedance result of *E. coli* DH5α was plotted in figure 5.7. Surprisingly the impedance of pTBLM was changed upon addition of diluted LB medium with bacteria. There seemed a very short phase I (lag phase) which is less than an hour and the resistance changed drastically within five hours. Moreover change in resistance was accompanied by steady increase in capacitance. Overall increase in capacitance was about 0.2 $\mu F/cm^2$.

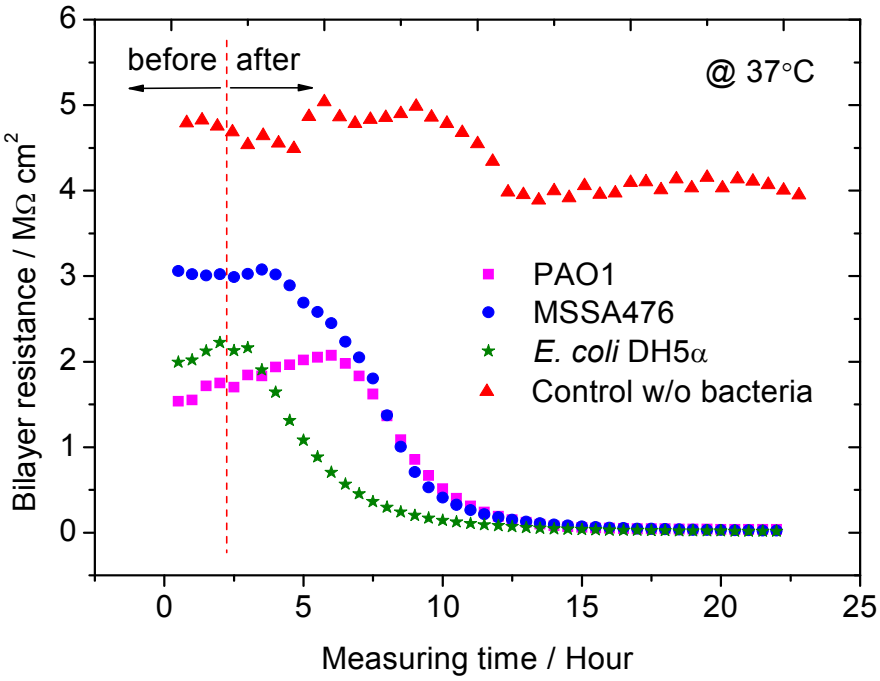

Figure 5.8 Bilayer resistance of a modified pTBLM at the presence of MSSA476, PAO1 and *E. coli* DH5α bacteria (all the bacteria induced change in resistance of lipid bilayer probably due to biofilm formation or lipid-utilization by bacteria – while the resistance of control pTBLM in LB medium without bacteria was relatively stable)

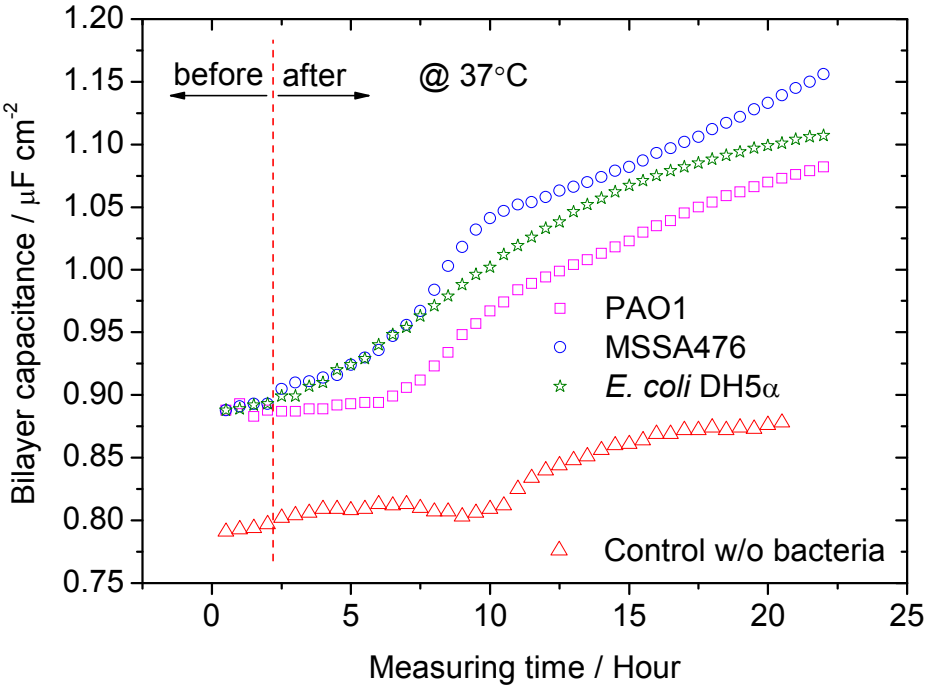

Figure 5.9 Bilayer apacitance of a modified pTBLM at the presence of MSSA476, PAO1 and *E. coli* DH5α bacteria (all the bacteria induced change in capacitance of lipid bilayer probably due to biofilm formation or lipid-utilization by bacteria – while the capacitance of control pTBLM in LB medium without bacteria was relatively stable)

This implied that there might have possible interaction between the lipids of modified pTBLM and the bacteria which could possibly affect the impedance destructively (figure 5.7). To have more comprehensive comparison, resistance and capacitance responses of all these tested bacteria with control was plotted for analysis as shown in figure 5.8 and 5.9 respectively. Control resistance was stable throughout the experiment although signal linearity was not very good. All bacteria induced changed in resistance but in different time frames upon interaction with lipid bilayer. Since OD of all bacteria at least doubled at the end of experiment, the growth of bacteria on the surface (on top of lipid bilayer probably) might be partly responsible for change in impedance.

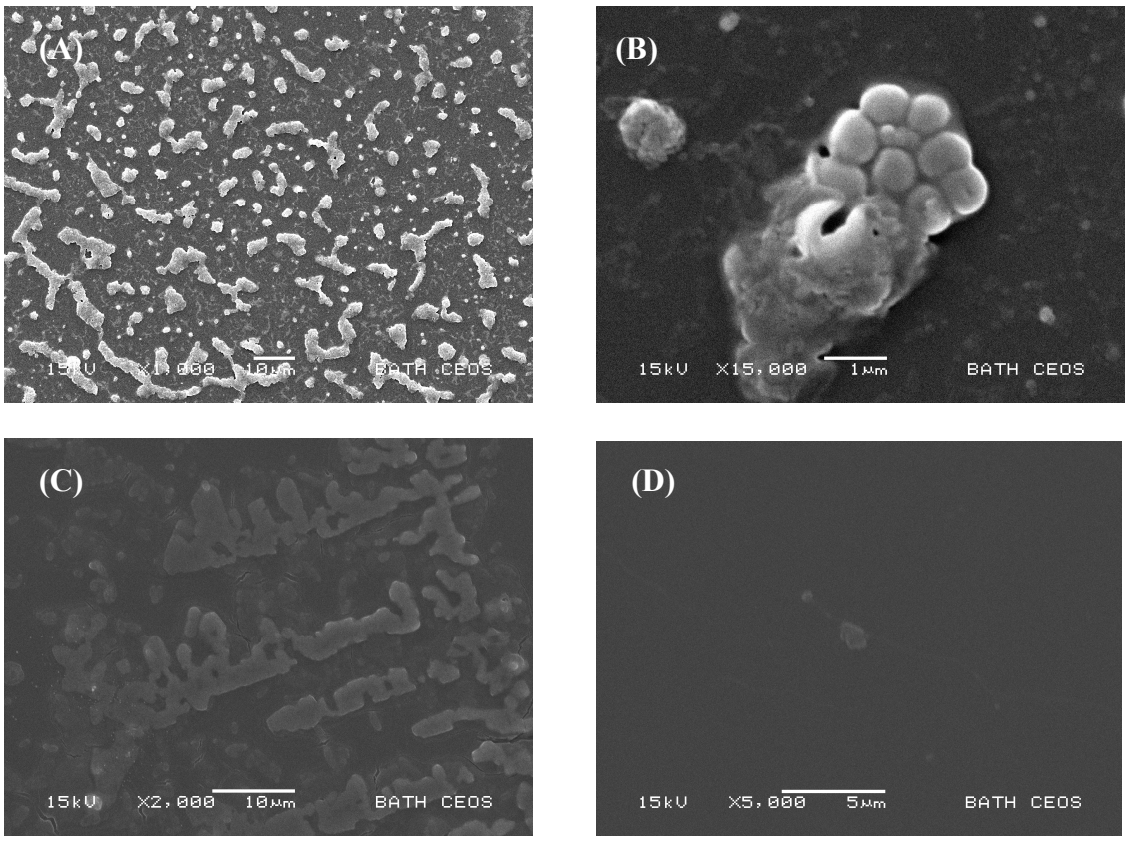

Figure 5.10 SEM images of TSG surface (with pTBLM) measured with bacteria: (A) MSSA476 initiated the pre-attachment onto surface, (B) a cluster of MSSA476, (C) the clusters of PAO1, and (D) *E. coli* DH5α – surface tested with *E. coli* DH5α was relatively clean and neither pre-attachment of bacteria nor the presence of bacteria was traced

In order to inspect the lipid bilayer-bacteria interaction, the measured surface areas of TSG at the end of experiment were examined under scanning electron microscope. The TSG chips were dismantled from the measurement cell and examined the surface without further cleaning before SEM. The images of surface spots measured with

MSSA476, PAO1 and *E. coli* DH5α were presented in figure 5.10. Evidence of initial attachment of bacteria onto TSG surface was observed in both MSSA476 (figure 5.10A) and PAO1 (figure 5.10C). Close up of a cluster of MSSA476 bacteria initiating the pre-attachment can be seen in figure 5.10B. It is widely known that all of *S. aureus*, *P. aeruginosa* and *E. coil* are prone to form biofilms on surfaces [89, 242]. There are many factors involved in the bacterial attachment and biofilm formation on surfaces [243]. On the other hand it took about 20 hours for an entire measurement in stationary condition which probably was long enough for the initial attachment of bacteria on the surface. In EIS measurement with bacteria, complication arose when the lipid bilayer was interacted with bacteria. Therefore apart from bacterial toxins, either possible bacterial attachment or lipids-utilization by bacteria was believed to be responsible for change in impedance. Additionally, it is necessary to include the additional circuit elements for data fitting and interpretation when the bacteria attach onto the surface [182]. To avoid the complication with the involvement of bacteria as well as to discriminate the effect of toxins from the presence of bacteria, more EIS experiments were conducted using the supernatant of bacterial growth LB medium and the results were discussed in the following sections.

5.3 Modified pTBLM with supernatant bacterial toxins

Basically effect of lipid damaging or pore-formation by purified toxins using artificial lipid bilayer membranes *in-vitro* experiments was relatively simple and the results were easy to analyze. Complication arose with the variety of toxins and enzymes produced by pathogens involved in experiments. Above all, involvement of pathogenic bacteria in experiments with artificial lipid bilayers *in-vitro* was even more complicated as the interaction of bacteria with lipid bilayer at the molecular level was mostly unknown. Probably for this reason, most of research works done by artificial lipid bilayer membranes used commercially available purified form of bacterial toxins including cholera, tetanus, pertussis and alpha toxins [114, 119, 199, 200, 210]. Regardless of exploring such interaction of individual toxins with lipid bilayer by different analytical techniques, the experimental results and findings did not represent the broad and combined effect of various toxins produced by pathogens *in-vivo*. Despite the fact that these purified toxins are only a fraction of toxins produced by different strains of clinically significant bacteria, the effect of other major toxins responsible for causing several diseases are still not well understood. The potentially synergistic, multiple

interactions of pathogenic bacterial toxins with lipid bilayer membrane *in-vitro* have only been little explored. In this experiment, to differentiate the effect of combined toxins form the presence of bacteria, EIS and SPR experiments with just the supernatant of bacterial toxins were conducted.

5.3.1 Supernatant bacterial toxins

The type and concentration of bacterial toxins depends on the bacterial genotype i.e. species and strains, and their growth conditions such as nutrient, temperature and pH of the medium. At the same time, optimum secretion of exotoxins is believed to be in association with bacterial growth [244, 245]. Therefore supernatant solution of cultured medium used in bacterial growth is enriched with various toxins associated with bacteria and it is suitable to test with the lipid bilayer membrane. Method and condition of culturing pathogens MSSA476, PAO1 and *E. coli* DH5α were described in section 5.2.2. Overnight bacterial cultured LB medium after recording the OD contained millions of bacteria which were first centrifuged in the small tubes at 12000 rpm for 3 minutes. Then the supernatant of LB medium was extracted and filtered through the porous filter with 220 nm pore diameter, to remove the bacteria from supernatant. This filtered supernatant was stored in protected tubes and subjected at 37 ºC prior to injection onto modified pTBLM in both EIS and SPR measurements.

All modified pTBLM employed in following experiments were made of 50 % DPhyTL and 50 % CholPEG in volume in monolayer and 67 % DPhyPC and 33 % cholesterol in mole in bilayer. In EIS experiment, modified pTBLM was first formed on TSG surface in an electrolyte of 100 mM NaCl. As the bilayer was formed, NaCl solution was replaced with filtered LB medium and the Teflon cell carrying the bilayer was subjected and maintained at 37 ºC in mini-incubator while EIS data was continuously recording. When the resistance and capacitance of lipid bilayer reached the steady values with time, LB medium in Teflon cell was replaced with supernatant LB of desired bacterium. EIS data was measured and recorded typically for overnight until the impedance change in time became insignificant.

In SPR experiment, same lipid bilayer was formed first in 100 mM NaCl electrolyte. SPR channel 1 was always used as control while channel 2 was used for the injection of toxins. When pTBLM was formed in both chambers, the electrolyte was replaced with filtered LB medium. As SPR angle minimum reached steady value in LB, both chambers were subjected and maintained at 37 ºC by external heating. Again it was

waited until SPR angle minimum in both channels reached to steady value before LB in channel 2 was replaced with the supernatant LB of desired bacterium while the medium in channel 1 remained unchanged as the control. SPR signals for both channels were continuously recorded with time throughout the experiment.

5.3.2 Results and discussion

5.3.2.1 EIS

All modified pTBLM prior to injection of supernatant toxins in LB comprised the resistance and the capacitance of around 4 MΩ cm^2 and 0.85 μF/cm^2 respectively (figure 5.11). An immediate decrease in resistance ca. 1 MΩ cm^2 was observed when LB supernatant of MSSA476 and PAO1 were replaced with normal LB. Since the medium temperature was maintained at 37 ºC, this change in resistance was mostly attributed to the presence of toxins in supernatant after overnight culture of MSSA476 and PAO1. Effect of toxins on modified pTBLM was time dependent and the resistances were kept decreasing indicating the time-dependent effect of toxins on lipid bilayer membrane. However the trend in which the resistance decreased with time explained the major species of toxins involved and their mode of action in general (figure 5.11).

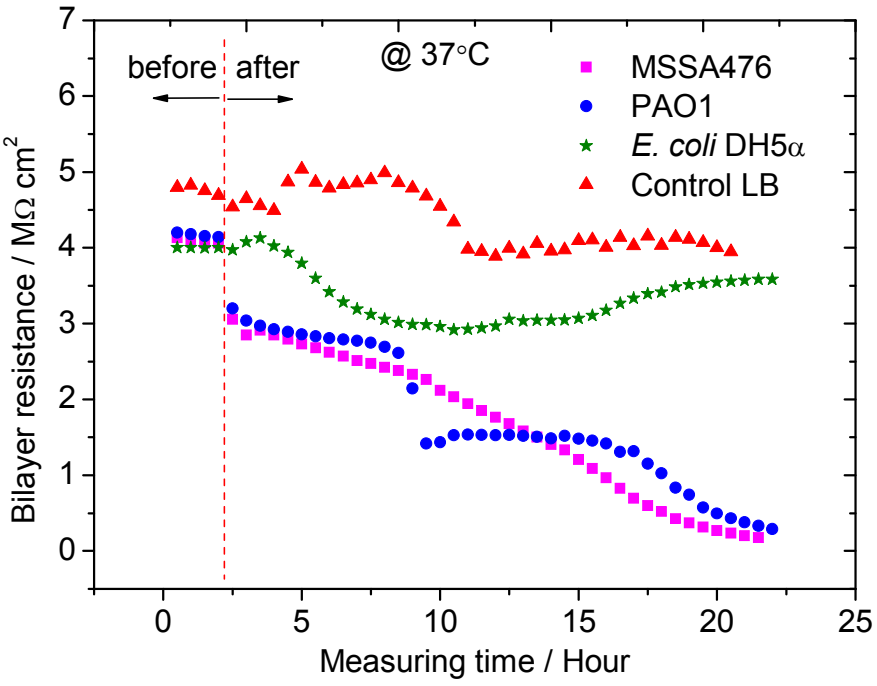

Figure 5.11 Bilayer resistance of a modified pTBLM at 37 ºC in response to LB supernatant with toxins secreted by MSSA476, PAO1 and *E. coli* DH5α (significant decrease in bilayer resistance with MSSA476 and PAO1 toxins is observed while there is no apparent change in resistance with *E. coli* DH5α as well as in control LB)

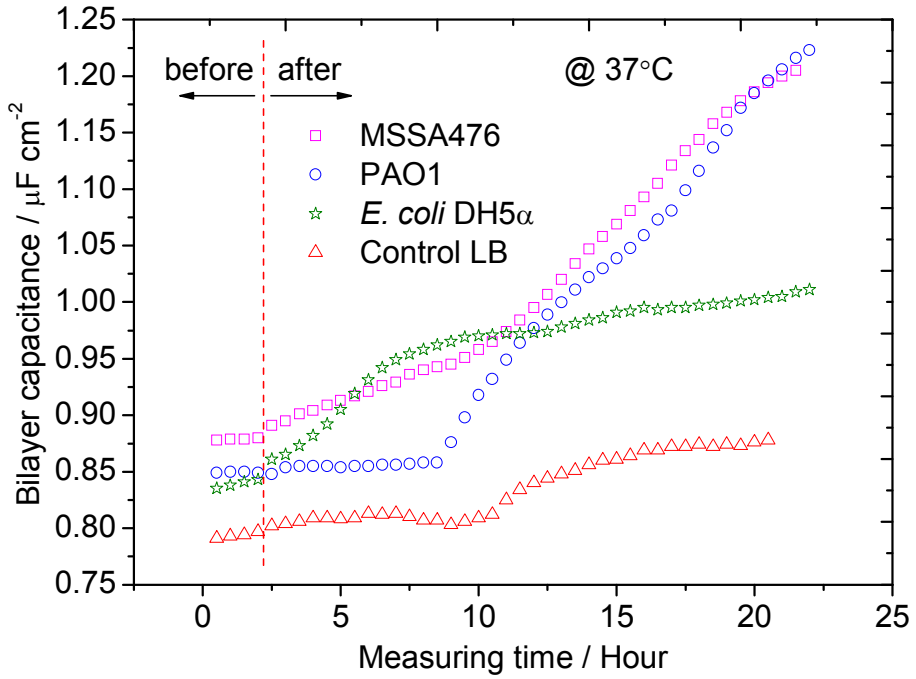

Figure 5.12 Bilayer capacitance of a modified pTBLM at 37 ºC in response to LB supernatant with toxins secreted by MSSA476, PAO1 and *E. coli* DH5α (significant overall increase in bilayer capacitance with MSSA476 and PAO1 toxins is observed while there is not much change in capacitance with *E. coli* DH5α as well as in control LB)

The supernatant toxins of MSSA476 induced steady but continuous decrease in resistance and increase in capacitance with time (figure 5.12). But in case of PAO1, after an initial decrease of about 1 MΩ cm^2, the resistance re-stabilized for a few hours before a rapid decrease in resistance (shaded circles in figure 5.11). This rapid decrease was accompanied by a sudden linear increase in capacitance with no significant change before (blank circles in figure 5.12). This observation could be explained by difference in two pathogenic strains of bacteria used in the experiment. The genome sequence of both *S. aureus* MSSA476 and *P. aeruginosa* PAO1 has been published [217, 218] and genome mining for putative virulence factors reveals genes encoding toxins and membrane-damaging agents. *S. aureus* MSSA476 genome carries several genes that encode mostly PFTs, haemolysin and leukocidin with a few lipases. It is possible that the lipid bilayer damaged by PFTs exhibits steady change in impedance with time because the toxin channels are stable in their heptameric state rather than in monomeric forms (figure 5.11 and 5.12). On the other hand, *P. aeruginosa* PAO1 genome carries genes for secretion of exotoxin A and haemolytic phospholipases. The only possible PFT might be the exotoxin A which mainly acts as an inhibitor of synthesis of intracellular proteins. Therefore the damage to lipid bilayer could be most likely due to

phospholipases and proteolytic enzymes of PAO1. Lipids in bilayer are in high mobility and their nature of self-healing to minimize the energy lost might be able to temporarily recover the lipid sites damaged by phospholipases. Such self-healing of lipids in bilayer might help maintain the bilayer to resist the uncontrolled flow of ions for a certain period, until the lipids falls apart and the sudden leaks of ions may attribute to an abrupt change in bilayer impedance (figure 5.11 and 5.12).

In contrast to the results above, there was no change in resistance of lipid bilayer immediately when the supernatant solution of *E. coli* DH5α was added (shaded stars in figure 5.11). This was probably due to DH5α strain of *E. coli* producing neither PFTs nor lipid damaging toxins. The impedance of lipid bilayer did not changed significantly upon addition of supernatant solution of *E. coli* although slight decrease in resistance and increase in capacitance were observed with time. These results correlate well with recent work looking at the lysis, and dye release from lipid vesicles exposed to the three species of bacteria discussed in this work [219]. In both figure 5.11 and 5.12, impedance of lipid bilayer without supernatant toxins was relatively stable with some fluctuations (represented by triangles in both figures).

5.3.2.2 SPR

SPR measurements with LB supernatant toxins were conducted as a complement to EIS data. Unlike EIS in which transport of ions across the modified pTBLM due to lipid damaging or pore-forming by toxins were electrochemically measured, SPR on the other hand reveals the binding (association) and unbinding (dissociation) of toxins onto the lipid bilayer in term of resonance angle minimum shifts optically. SPR in this work is capable of running two parallel measurements in which the effect of toxins binding is observed in parallel with the control. Detail about the modified pTBLM formation and measurements with SPR were discussed in section 5.2.1. Figure 5.13 below indicated the resonance angle minimum shift due to binding of MSSA476 supernatant toxins onto the lipid bilayer. Upon replacement of LB medium with MSSA476 supernatant, an initial upward shift of resonance angle about 25 mº was observed. This was followed by the gradual upward shift with time (figure 5.13). A total resonance angle upward shift of about 40 mº was observed in duration of 75 minutes while the resonance angle of control chamber almost remained unchanged throughout the measured duration.

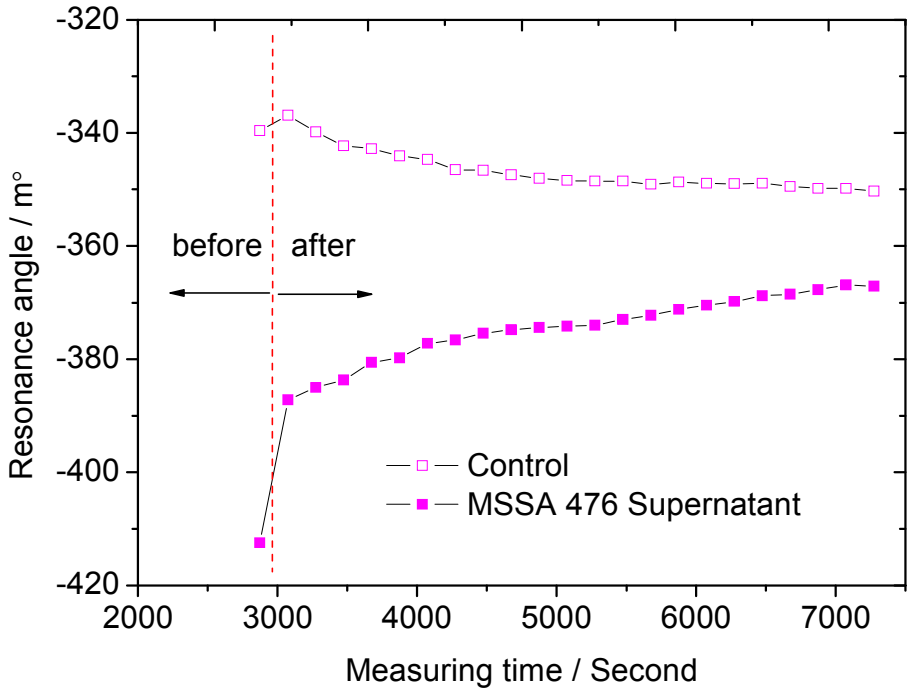

Figure 5.13 Resonance angle shift of a modified pTBLM at 37 ºC in response to LB supernatant containing toxins secreted by MSSA476 (upward resonance angle minimum shift is due to the possible bindings of PFTs onto the lipid bilayer)

This result, compared to the binding of purified α-HL onto modified pTBLM as indicated in figure 4.3 was insignificant in term of angle shift but the angle shift in upward direction was a good indication of association of toxins such as PFTs rather than lipid-damaging toxins enzymes. This result clearly pointed out that the majority of toxins involved with MSSA476 were neither lipases nor enzymes that could degrade the lipids but more on protein exotoxins such as PFTs. Therefore, there was *no lipid loss* from lipid bilayer upon interaction with the supernatant toxins of MSSA476. On the other hand, SPR signal was observed differently in case of interaction with supernatant toxins of PAO1 (figure 5.14). Resonance angle in this case was shifted downward with time while signal in control remained unchanged. A total of about 130 mº downward shift in reflective angle was observed in duration of about 5 hours. This downward angle shift was accompanied by the dissociation of lipids from modified pTBLM on the surface and a clear indication of lipid loss probably due to more lipid-damaging enzymatic endotoxins such as phospholipases (figure 5.14).

In both SPR experiments with MSSA476 and PAO1 supernatants, changes in measured signals i.e. resistance and capacitance in EIS and resonance angle shifts in SPR were not as much as those in experiments with purified α-HL and PLA2 (figure 4.3). As discussed previously, pathogenic bacteria secreted variety of toxins but not all of them,

in term of mode of action were relevant to function in artificial lipid bilayer membranes *in-vitro*. Only the fractions of toxins of bacteria were useful to function in lipid bilayers and this was the plausible reason for minimal SPR angle shift in experiments with supernatant toxins. Nevertheless, different SPR angle shifts in general represented possible type and mode of action of major toxins associated with MSSA476 and PAO1. These results were in agreement with and complement to the previous EIS results with supernatant toxins (figure 4.3).

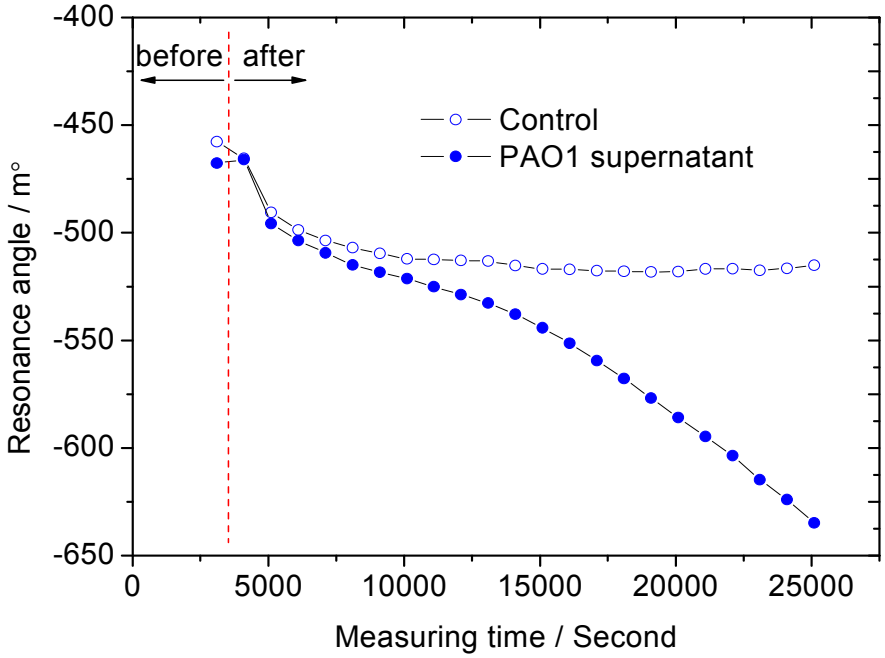

Figure 5.14 Resonance angle shift of a modified pTBLM at 37 ºC in response to LB supernatant with toxins secreted by PAO1 (downward angle shift is due to the possible loss of lipids from the upper half of lipid bilayer due to enzymatic lipid damaging endotoxins)

6 Nanopore suspended TBLM (Nano-psTBLM)

6.1 Substrate

The substrate used in membrane chip fabrication is a 4" diameter silicon wafer with double-side polished finishing. The crystal orientation is <100> and typical doping concentration lies between 1-10 Ω-cm with (p-type) Boron doping. A 100 nm thick Si_3N_4 film is grown on both sides of the silicon wafer by a low pressure chemical vapour deposition (LPCVD) process. LPCVD Si_3N_4 is preferable because of its high material (film) density and resistance to potassium hydroxide (KOH) in the subsequent anisotropic etching process. It is also used as a hard mask during KOH etching on one side of silicon wafer while it is formed a free standing Si_3N_4 membrane on the planar (opposite) side as depicted in figure 6.1.

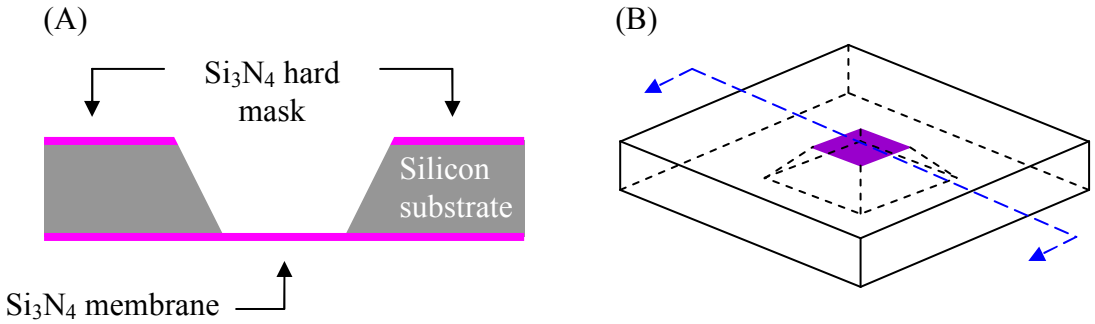

Figure 6.1 Schematic of Si_3N_4 membrane chip: (A) cross-section and (B) three dimensional drawing (drawings are not to scale)

6.1.1 Si_3N_4 membranes

6.1.1.1 Design

Photo mask was designed to produce membrane chips with 2.4 mm × 2.4 mm dimensions. It is required to do simple geometric calculation to define the size of the window opening based on known parameters such as the size of desired Si_3N_4 membrane, the thickness of the silicon wafer and the angle between <100> and <111> crystal planes as shown in figure 6.2. As every chip carries each fragile Si_3N_4 membranes, harsh separation methods such as wafer dicing and scribing with the diamond cutter to produce individual chips from the wafer after membrane fabrication cannot be used. These methods can also produce silicon particles which can contaminate the Si_3N_4 membrane. To avoid the use of harsh separation methods, breaking grooves are designed and integrated in the design of the photo mask in order to

produce the V-shape trenches perpendicular to primary and secondary flats of the silicon wafer, for easy separation of single membrane chips from the wafer (figure 6.3A). The photo mask is made of chrome plated soda lime glass with transparent windows (figure 6.3B).

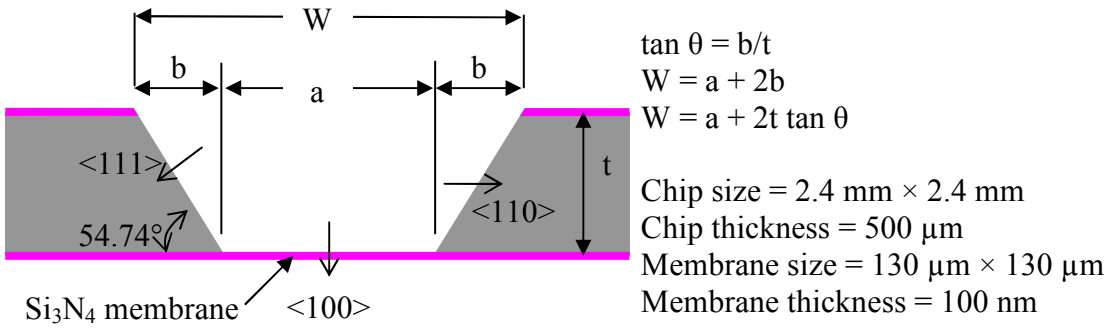

Figure 6.2 Geometric calculation of simple design of a membrane chip (drawing is not to scale)

6.1.1.2 Photolithography process

The entire fabrication process of Si_3N_4 membrane chips was done in a cleanroom environment. All process steps are explained in detail in the following sections:

I. Wafer Cleaning

Wafer cleaning is required to remove organic and inorganic contaminants from the wafer surface. Silicon wafers were chemically clean using the standard cleaning procedure as shown below:

(a) The wafers were placed in a Teflon process boat and the entire boat was immersed in a mixture of H_2SO_4: H_2O_2: H_2O (1: 1: 5) in a temperature of 60 °C for 15 minutes.

(b) The wafers were rinsed in continuous flow of Milli-Q water for 15 minutes.

(c) Then the wafers were blown dry with nitrogen and baked in an oven at 90 °C for about 10 minutes to remove the residual vapours.

II. Photoresist Coating

(a) Each wafer was placed on the vacuum chuck of a spin coater and aligned centrally.

(b) The photoresist, AZ5214E, was dispensed and covered on the entire wafer surface.

(c) Photoresist coating was done in two steps: firstly from 0 to 500 rpm by 100 rpm per second ramp for 5 seconds and secondly from 500 to 5000 rpm by 1000 rpm per second ramp and spin for 55 seconds.

(d) The wafer was then soft-baked in an oven at 90 °C for 30 minutes.

After soft-bake, about 25 % of resist thickness was reduced due to evaporation of solvent in resist film. It resulted the final resist film thickness of around 1 ~ 1.2 micron.

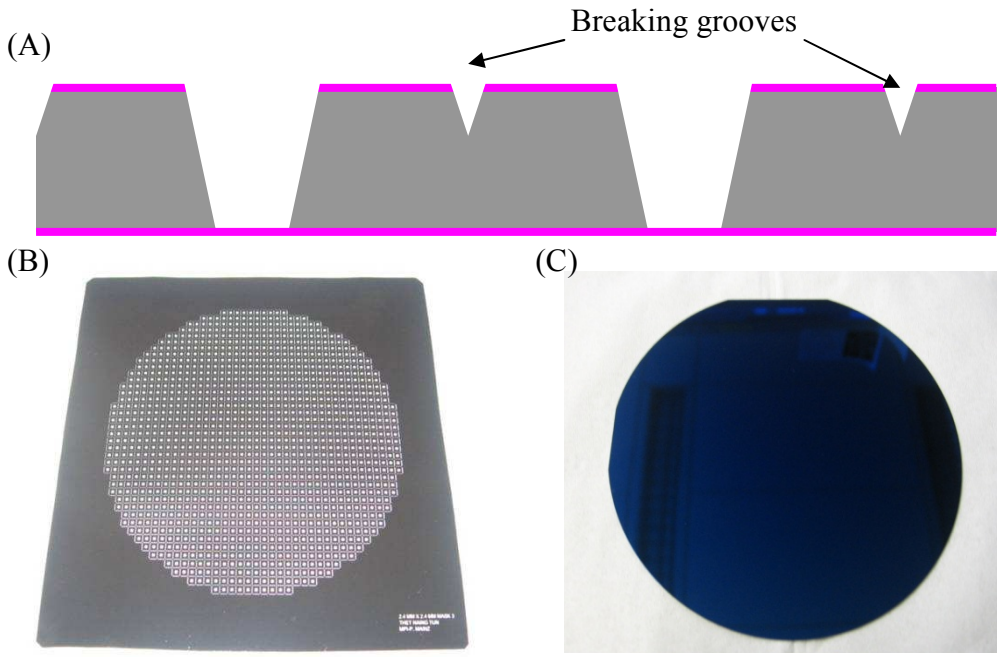

Figure 6.3 (A) Schematic cross section of silicon wafer showing breaking grooves between each membrane chips (drawing is not to scale); (B) photo mask and (C) 4" silicon wafer showing primary and secondary flats (top and left respectively)

III. Pattern Transfer Process (Mask Aligner)

(a) The wafer with photoresist film on top was positioned on the vacuum chuck of a mask aligner.

(b) The photo mask was placed in mask holder on top of the wafer and it was aligned onto wafer before the UV light exposure.

(c) Pattern transfer was taken placed by exposure of UV light through the photo mask onto the photoresist film on top of the wafer.

(d) Contact transfer mode was used and UV light with a constant power of 900 Watt in 365 nm wavelength was exposed onto resist film through the photomask for 25 seconds.

IV. Resist Pattern Development

(a) The wafer was placed in a mixture of resist developer (AZ Developer and DI water in a ratio of 1:4 in volume) for 25 seconds.
(b) The wafer was then thoroughly rinsed in flow of DI water and blown dry with nitrogen.
(c) The pattern features were examined under optical microscope.
(d) The wafer was then post-baked in oven at 120 °C for 30 minutes.
(e) Resist film thickness was measured using a surface profiler (KLA Tencor P-10)

Post-bake (or hard-bake) was required to make the resist film hardened to survive during the subsequent ion etching (dry etching) process.

V. Ion Etching

Ion etching was used to selectively remove the Si_3N_4 film from windows (open areas uncovered by photoresist film) for the subsequent KOH etching process.

(a) The wafer was mounted vertically on the chuck in the vacuum chamber.
(b) A mixture of CF_4, O_2 and Ar gases were used to etch Si_3N_4 film from the exposed area.
(c) After ion etching, the wafer was placed in acetone and undergone ultra-sonication for a few minutes until the photoresist was totally removed (figure 6.4A).
(d) The wafer was cleaned in running DI water and blown dry with nitrogen.
(e) The etch depth was measured by a micro profiler and it should be etched beyond the thickness of Si_3N_4 film.

6.1.1.3 Potassium Hydroxide (KOH) etching

KOH etching is selective anisotropic etching of Si material. Etching rates of silicon depend on the crystal orientation of the silicon wafer as well as on concentration and temperature of KOH solution during etching.

(a) KOH solution with 30% (in weight) concentration was prepared in the special beaker and heated to 70 °C on the hotplate with magnetic stirring facility (figure 6.4B).
(b) Each wafer was placed in the grip centrally located in the beaker and totally immersed in KOH solution.
(c) Measured etching rate along Si<100> direction in experiment was ~0.56 microns per minute.

(d) Once etching was completed, it could see through the etched cavities as the Si_3N_4 membranes formed at the end of cavities are optically transparent.

(e) The wafer was then rinsed in running DI water for about 15 minutes and blown dry by gentle flow of nitrogen.

(f) The wafer was stored in a desiccator under controlled humidity and temperature.

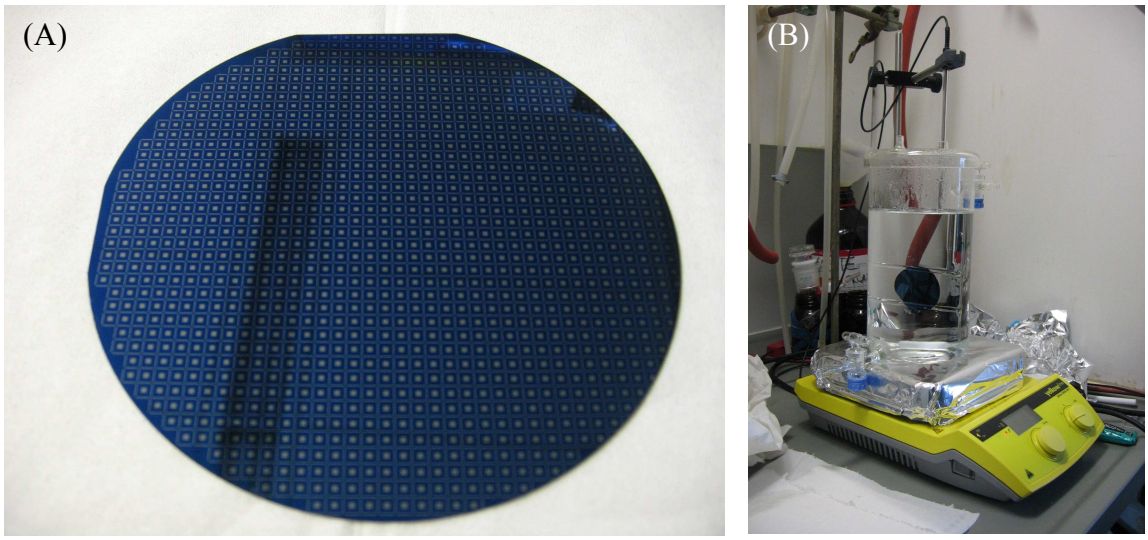

Figure 6.4 Silicon wafer (A) after ion etching of Si_3N_4 from window and breaking line areas and (B) undergoing the KOH etching with 30 % concentration and 70 °C temperature

6.1.1.4 Thermal oxidation of Si<111> side-walls

When studying ion transport of channel proteins, electrical current carried by metal ions (in electrolyte) through each protein channel is very small (in the order of 1×10^{-12} A). To be able to measure such tiny current accurately, stray currents should be minimized. In other words, ion current leaking through other ways rather than flowing through ion channels is undesirable because it creates additional noise in output signal and disturbs during electrical measurements. DC potential was applied across a bare Si_3N_4 membrane without nanopores and measured the electrical current using the PPC in order to examine the electrical behaviour of fabricated membrane chips. The plot of current response of the chip to +100 mV DC voltage is shown in figure 6.5.

There are two important things to be observed in figure 6.5. First the output current lies between 1000 pA to 1500 pA and this is believed to be due to a current leakage. Since the chips were unpassivated, the current could leak through unprotected side-walls of silicon substrate laterally to the edges of chip which were exposed to electrolyte

solution (schematic is shown in figure 6.6A). Secondly the nature of current against time is unstable with fluctuations and the noise of current measured is about 100 pA. If the current leaks into the silicon substrate, the current flux exposes to entire surface of the membrane chip, which is about 340 times larger in surface area than that of Si_3N_4 membrane at the centre. Since the parallel plate capacitance is directly propositional to surface area exposed to the current flux, this induces high capacitance creating high and unstable noise level in output current signal (figure 6.6B).

Figure 6.5 Leakage current of a membrane chip (without electrical passivation) against time at applied DC holding potential of +100 mV

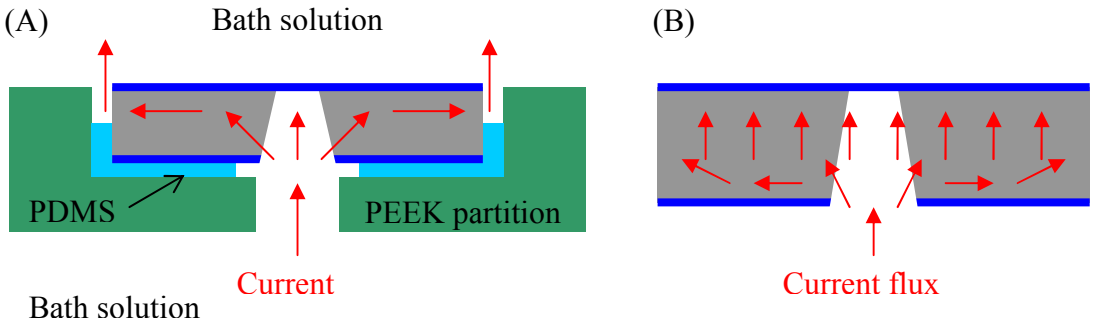

Figure 6.6 Schematics of (A) ionic current leakage through sides of the membrane chip and (B) ion current flux exposing the entire chip surface making high capacitive noise (drawings are not to scale)

These preliminary measurements indicated that a side-wall electrical passivation was required to stop the flow of current through the substrate. Electrical passivation can be done by two processes: growth of SiO_2 by thermal oxidation or deposition of passivation film (either Si_3N_4 or SiO_2) by plasma enhanced chemical vapour deposition (PECVD). Thermal oxide can be grown on a silicon surface either by wet or dry oxidation depending on the use of water vapour (steam) or molecular oxygen as the oxidant during high temperature process. The simple chemical reactions can be:

$Si\ (solid) + 2H_2O\ (vapour) \rightarrow SiO_2\ (solid) + 2H_2\ (vapour)$…….wet oxidation and

$Si\ (solid) + O_2\ (vapour) \rightarrow SiO_2\ (solid)$…….....dry oxidation.

Typically silicon wafers are stacked horizontally or vertically in high temperature furnace which is heated to high temperature (usually between 700 °C and 1300 °C). Depending on the type of oxidation, either water vapour or molecular oxygen is introduced with a controlled flow rate. Silicon has naturally good reaction to oxygen and high temperature process expedites the formation of thermal oxide. Growth rate of oxide is estimated using a Deal-Grove model. Since silicon itself is consumed during oxide growth, for every unit thickness of silicon consumed, 2.27 unit thickness of thermal oxide is generally formed. This is bidirectional formation and oxide film grows in both inward and outward directions from initial growth surface. Wet oxidation is preferred to dry method for growing thick oxide layers because of its higher growth rate but the oxide qualities such as film density and dielectric strength by wet method is not as good as the one grown by dry oxidation. On the other hand, dry oxidation has a slow growth rate and hence this is not preferable if thick oxide layers are required. Rate of oxidation also depends on the crystal orientation of the silicon wafer, for example growth rate on silicon <100> surfaces is slow compared to the one on <111> orientation. Other factors contributing to the growth rate are the doping level of wafer, the presence of halogen impurities in gas phase, plasma and photon flux during oxide growth [87].

Primary requirement of oxide layer in this work is to stop the flow of current by providing a high dielectric resistant. For this purpose, about 100 nm thick thermal oxide by wet oxidation was grown on silicon side-walls of membrane chips. Dielectric strength of amorphous silicon dioxide at 300 K is around 10^7 V/cm (i.e. 1V/nm) [88]. Applied voltage used during the electrical measurement across the lipid bilayer membrane is usually less than 1V. Therefore 100 nm is more than enough for required electrical passivation. It is important to have oxide film of full coverage on silicon side-walls if there are surface defects or steps on it. Wet oxidation was used at 950 °C for duration of 240 minutes to grow 100 nm thick oxide film on silicon <111> side-walls. For examination of growth oxide layer, one membrane chip is intentionally broken and the cross sectional side-wall is examined by scanning electron microscope (SEM) as shown in figure 6.7.

It is particularly required to create an effective electrical passivation at sharp profiles of the side-walls of membrane chip such as edges of KOH etched cavity and the junctions where silicon edge and Si_3N_4 membrane meet as shown in figure 6.7A. At these places, electrical leakage can occur most probably if the passivation is not good enough due to nature of profiles. It was observed that thermal oxide has formed and completely

covered the underlying silicon edges showing a complete passivation at the junctions (figure 6.7D). This is due to the nature of thermal oxidation which consumes silicon itself during the growth of oxide film and making sure that all the silicon surface exposed to water vapour during oxidation process are completely passivated. For the growth of oxide film on side-walls, figure 6.7C clearly reveals approximately 100 nm thick uniform oxide layer. Passivated membrane chips were electrically characterized by applying different DC voltage (from 0 to ±200 mV) in 100 mM NaCl buffer and measured the current using PPC measurement. There is no apparent current leaking across membrane chip between applied DC voltages of –200 and +200 mV. This proves that side-wall electrical passivation by thermal oxidation is sufficient and effective. Figure 6.8 shows the current response across a passivated membrane chip with applied +100 mV DC.

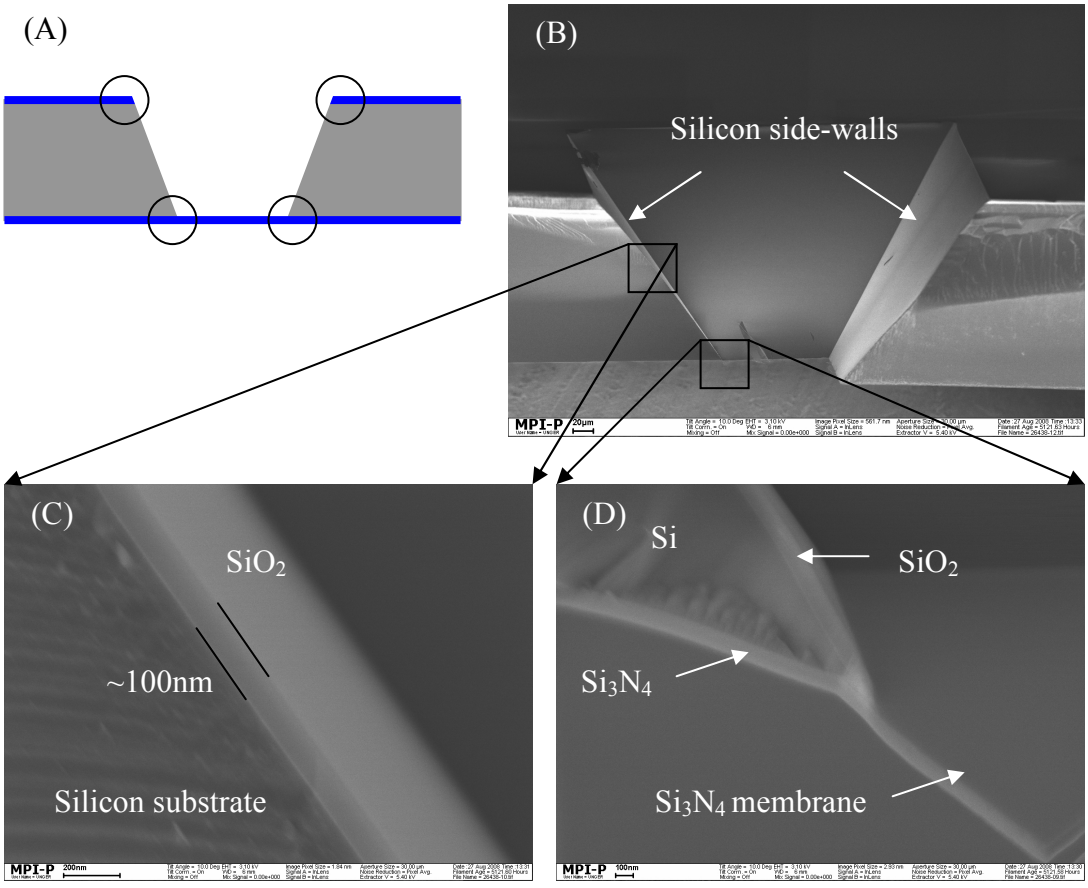

Figure 6.7 Schematic of (A) a membrane chip showing places of Si/Si_3N_4 junctions (indicated by circles) and SEM images of (B) a broken membrane chip showing side-walls, (C) ~100 nm thick thermal oxide grown on side-wall and (D) at the junction where the wedge of silicon substrate, SiO_2 and Si_3N_4 meets (showing effective passivation at the junction)

Figure 6.8 Leakage current measurement of a side-wall electrical passivated membrane chip at applied +100 mV DC

6.1.1.5 Evaporation of Au

A silicon wafer with membrane chips was clean in isopropanol (IPA) and ethanol (no ultrasonic-agitation) for about 5 minutes each, followed by rinsing thoroughly in Milli-Q water. The wafer was placed in an UV ozone cleaning chamber for 20 minutes and it was subsequently rinsed in Milli-Q water before blown dry with nitrogen. Au evaporation was done by a Balzers PLS 500 thermal evaporation system at the chamber pressure lower than 5×10^{-6} mbar. To promote the adhesion of Au onto Si_3N_4 membrane, 3 nm Cr was evaporated before 25 nm thick Au evaporation. Cr and Au were evaporated at room temperature with evaporation rates of 0.1 and 0.5 Å/second respectively. Surface roughness was previously measured on TSG and normally evaporated Au surface on Si_3N_4 film by static CA measurement (section 3.1.1.1 and figure 3.2). All Au surfaces are freshly prepared and performed the contact angle measurement before the contamination comes from the surrounding. Both TSG and normal Au surfaces showed hydrophilic nature but TSG was more hydrophilic than normal Au surface. This might probably be due to the surface roughness and grain sizes of Au which can be easily seen in figures 3.2.

6.1.1.6 Focus Ion Beam (FIB)

There are many advantages of using Si_3N_4 membranes when a lipid bilayer is spanned across the nanopore in it. Firstly the stability and the lifetime of the pore-spanning lipid bilayer can be enhanced if the pore size is smaller, from the micro to the nano scale. Secondly the amount of insertion of transmembrane proteins can be controlled, compared to suspended lipid bilayer on multi-porous substrates, and therefore the single channel measurement is possible. Thirdly the flow of ion current can be guided only through the nanopore making enhanced sensitivity of ion channels during the measurement. On the other hand, a nanopore should be well defined with a uniform

diameter. The outer rim of the polished side of the Si_3N_4 membrane should not affect the monolayer assembly with its surface profile or protrusion. In other words, surface topography of the polished Si_3N_4 membrane surface should not be affected by the existence of nanopore.

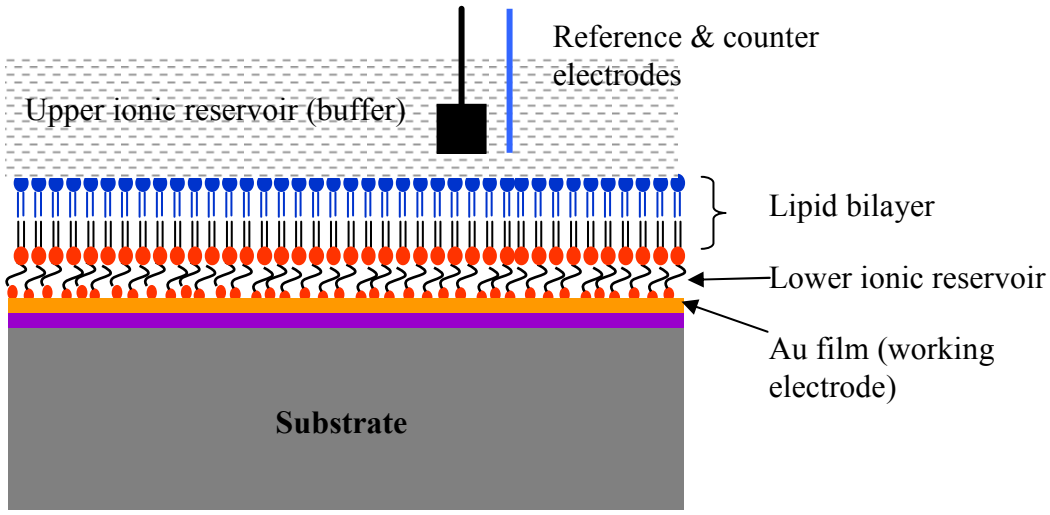

Figure 6.9 Schematic cross section of thiolipid based pTBLM system for EIS measurement

There are several ways to create nanopores on the semiconductor surfaces. One well known method of making nanopores, not only necessarily to nanopores but also to other nanostructures, is Electron Beam Lithography (EBL) with subsequent ion etching. However EBL requires using electron beam sensitive resist, such as polymethyl methacrylate (PMMA) by spin coating, which practically is difficult to work with a small chip carrying a thin Si_3N_4 membrane. Moreover, the surface of Si_3N_4 membrane can be contaminated with resist residues which affect the quality and formation of monolayer. Another alternative technique is Focus Ion Beam (FIB) which uses a high energy ion beam to bombard and directly cut the substrate materials to make nanostructures including nanopores. In this work, FIB was used to drill a single nanopore with sub 100 nm diameter in Si_3N_4 membrane of the chips. FIB used in this work is FEI Nova 600 Nanolab dual-beams system which is equipped with electron beam for SEM imaging and ion beam for drilling on surfaces. In order to leave the planar side of Si_3N_4 membrane clean and intact for self assembly of monolayer, nanopore was milled from backside (the side where KOH etching was carried out) of the membrane chip. SEM images of arrays of 1, 3 and 9 nanopores produced by FIB are shown in figure 6.10.

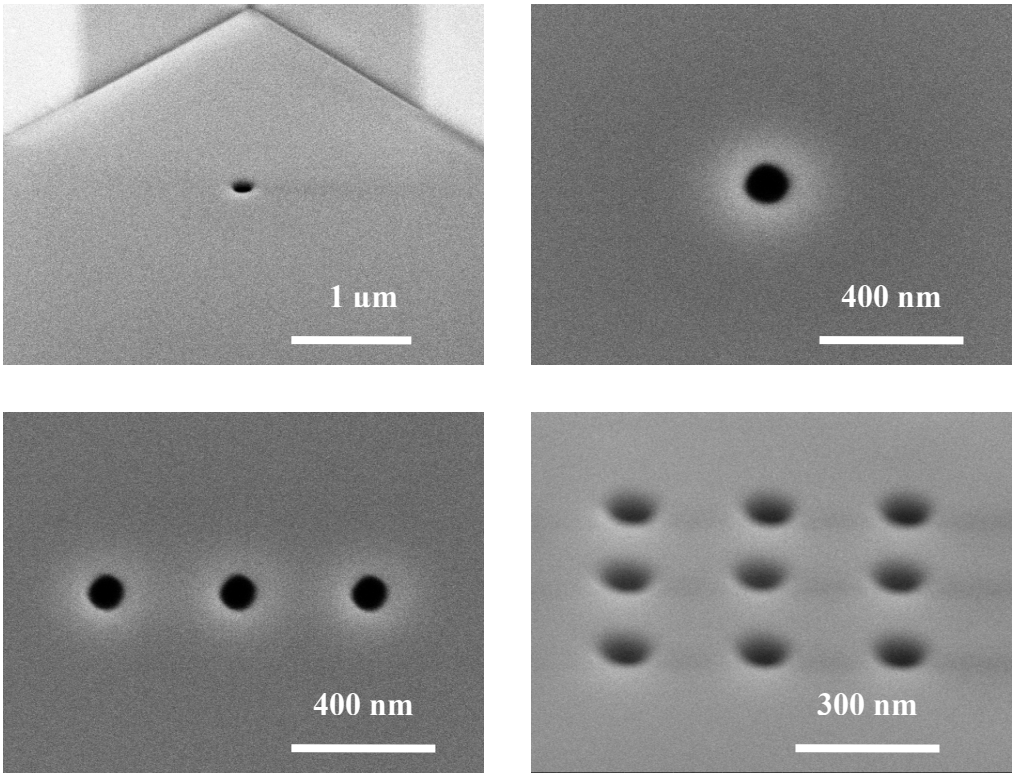

Figure 6.10 SEM image of an array of ~100 nm diameter (1, 3 and 9) nanopores milled through a 100 nm thick Si_3N_4 membrane by FIB

6.1.2 Characterization with planar patch clamping

6.1.2.1 Bare Si_3N_4 membrane

To understand the electrochemical response of fabricated membrane chips and to be able to interpret the measured results by PPC correctly, voltage clamping with a passivated Si_3N_4 membrane chip with neither nanopores nor monolayer (and subsequent Nano-psTBLM) on surface was carried out in the beginning. A Si_3N_4 membrane chip was fixed into the measurement cell (PEEK) (as discussed in section 2.3.2.1 and figure 2.21) and AC triangular potential of ±15 mV was applied. Output current response of the membrane chip is shown in figure 6.11. When a nanoporous chip is voltage-clamped, the output current is composed of two components; capacitive ($C\frac{dV}{dt}$) and conductive (GV) currents as shown in equation 6.1 below.

$$I = C\frac{dV}{dt} + GV \qquad 6.1$$

where, I is the overall current (pA)

C is the capacitance (nF)

dV is the change in applied potential (mV)

dt is the change in time (ms)

G is the conductance (nS)

V is the applied AC voltage (mV)

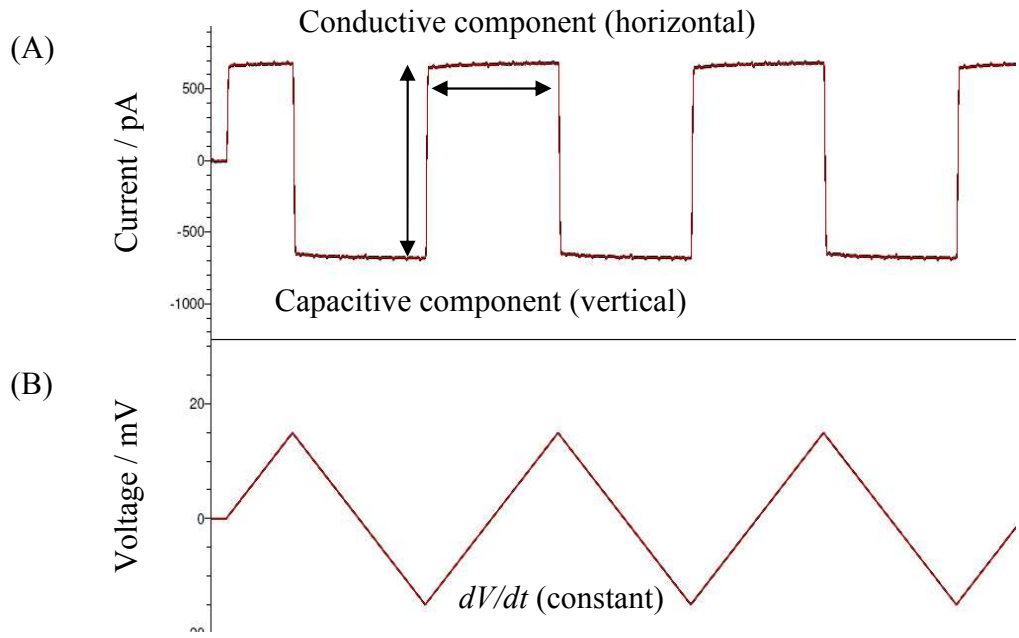

Figure 6.11 Current response of a bare Si_3N_4 membrane by ±15 mV AC triangular potential with (B) voltage vs. time and (A) current vs. time

The chip is fully passivated and there are no nanopores in the Si_3N_4 membrane. As a result there is no possibility for the electric current to flow across the membrane chip. Therefore, the conductive component of output current is zero. This can be seen in the output current curve where there is a flat plateau region with almost zero slopes (figure 6.11). However, there is a measured steady output current of around ±700 pA when the applied potential is increased or decreased with time. This is a capacitive current, according to the equation 6.1. At the peaks of each triangular voltage, instantaneous potential is constant at ±15 mV and there is no change in potential with time at these points. As a result, capacitive current stopped flowing. When the potential is reversed beyond the peak by either from positive to negative or vice versa, transient capacitive charging to Si_3N_4 membrane takes place in less than 1 millisecond and this can be seen in output current graph as a vertical abrupt switch between negative and positive currents (figure 6.11). After a short transient charging, then the rest of output current flow is due to capacitance of the Si_3N_4 membrane. Therefore, the capacitive component

dominates the overall output current in response to applied AC potential to a bare Si_3N_4 membrane.

Secondly a DC stepped potential from ±10 mV to ±35 mV with increments of ±5 mV was applied and the current and conductance response to the applied potential is shown in figure 6.12. At this time the output current and conductance are zero. The conductive component of the current is zero because there are no nanopores in the Si_3N_4 membrane. In applied DC potential, there is no change in voltage with time ($dV/dt = 0$) and hence capacitive component is also zero although there is a noticeable capacitive current during increase or decrease of 5 mV. This transient capacitive charging takes place in rather long duration of about 50 milliseconds. If there were a nanopore in Si_3N_4 membrane, then the output current would be the conductance of nanopore. Therefore, the conductance component dominates the overall output current in response to applied DC potential (figure 6.12).

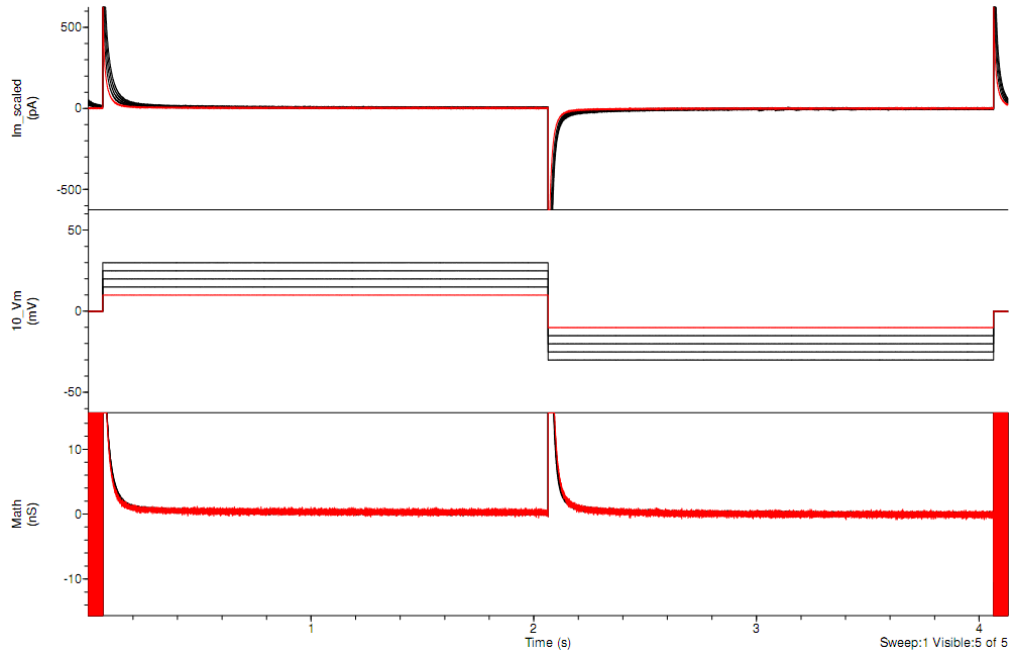

Figure 6.12 Current and conductance response of a bare Si_3N_4 membrane by step DC potential (±10 mV to ±35 mV with increment of ±5 mV) with current Vs time (top), applied DC potential Vs time (middle) and conductance Vs time (below)

6.1.2.2 Single nanoporous Si_3N_4 membrane

The output current through a ~100 nm diameter single nanopore in Si_3N_4 membrane to an applied AC triangular voltage is composed of both capacitive and conductive current components (figure 6.13). In response to input voltage, the output current response showed two distinct regions in response to voltage increments from -15 mV to +15 mV. First transient current sharply increased almost vertically in a very short period due to

capacitive effect of Si_3N_4 membrane. Then the current continued increasing with a positive slope until the applied potential reached +15 mV. This second portion of the current is effect of conductance due to flow of ions through the nanopore, and the slope gives the information on conductance i.e. the steeper the slope, the higher the conductance of the nanopore.

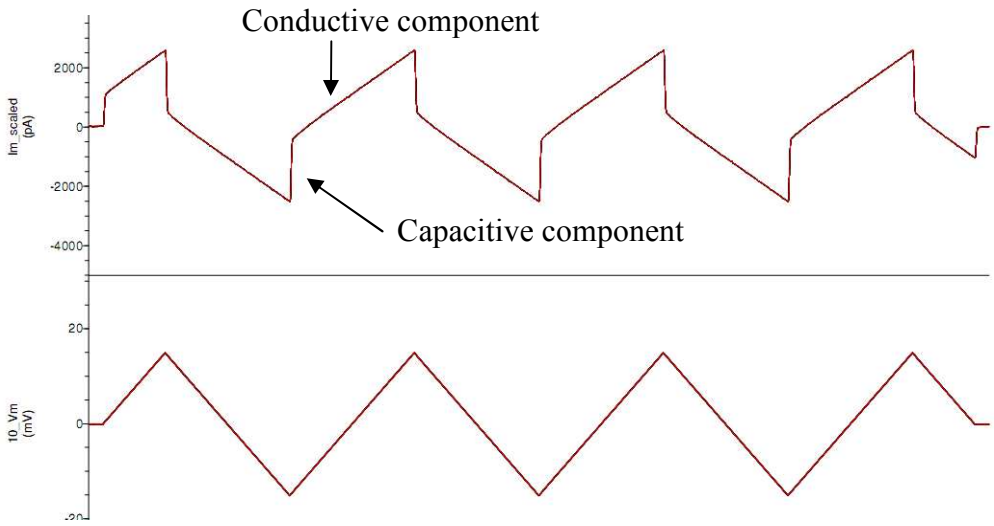

Figure 6.13 Current response of a Si_3N_4 membrane with ~100 nm diameter single nanopore by applied AC ±15 mV triangular potential (membrane capacitance and current is 0.98 nF and 998 pA respectively)

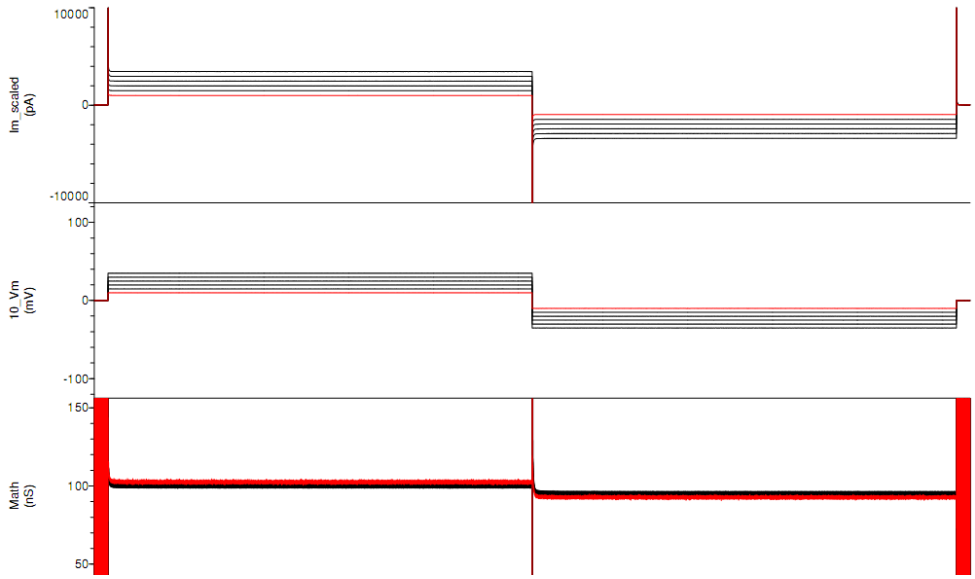

Figure 6.14 Current and conductance response of ~120 nm diameter single nanopore in Si_3N_4 membrane by applied step DC voltage (measured conductance here is approximately 102 nS)

In this experiment, the capacitance of the Si_3N_4 membrane is 0.98 nF and the output current is around 1 nA (figure 6.13). Conductance measurement was then carried out by

applying a stepped DC potential and the graph is shown in figure 6.14. The measured conductance is around 102 nS (equivalent to a resistance of about 10 MΩ). The plot of conductance against time to different stepped DC voltage (figure 6.14) is quite stable as it is only defined by the size of nanopore and type of ions transporting the ionic current in the buffer solution.

6.1.2.3 Number of nanopores vs. ionic conductance

The parameters of interest from electrochemical measurement using PPC through nanopores in Si_3N_4 membrane are ion conductance, current and capacitance in response to alternative and direct electrical potentials. Conductance across nanopores is measured in nano-siemens (nS) while current and capacitance are measured in pA and nano-farad (nF) respectively. When a nanoporous Si_3N_4 membrane is partitioned between two ionic reservoirs and an electrical potential is applied via Ag/AgCl electrodes, the ions in the buffer solution are driven to flow through the nanopores. Flow of electric charges is measured and converts to useful data of current, capacitance and conductance. While capacitance of nanopores remains mostly unchanged regardless of different potential, current and conductance vary directly with the number of nanopores and amount of applied potential. To understand this electrochemical relationship between voltage and current, different numbers of nanopores were milled by FIB in Si_3N_4 membrane for the purpose of conductance measurement in order to plot the conductance against the area of nanopores. This type of conductance calibration curve is useful to estimate the average conductance of each pore if the pore area is known, without requiring the immediate PPC measurement.

Bare and Au coated Si_3N_4 membranes with 1, 3 and 9 nanopores were fabricated while diameter of each pore was maintained approximately to 100 nm (figure 6.10). Pore diameters were measured on SEM image of nanopores (taken at the same magnification) and the total opening area were calculated for each membrane chip. Measurements were conducted in 100 mM NaCl electrolyte with stepped DC applied potential from ±10 mV to ±35 mV with increment of ±5 mV. The result of several measurements which is plotted in conductance against nanopore area is shown in figure 6.15. The conductance of ~100 nm single nanopore is about 50 nS and that of three ~100 nm pores lies between 150 and 220 nS. This rather broad variation in conductance of three nanopores could be due to some variation in nanoporous area especially when the number of pores is increased. On the other hand, conductances of single nanopores

have only small variations and the result is reasonably accurate. Throughout the measurement, capacitance for each Si_3N_4 membrane remained mostly unchanged.

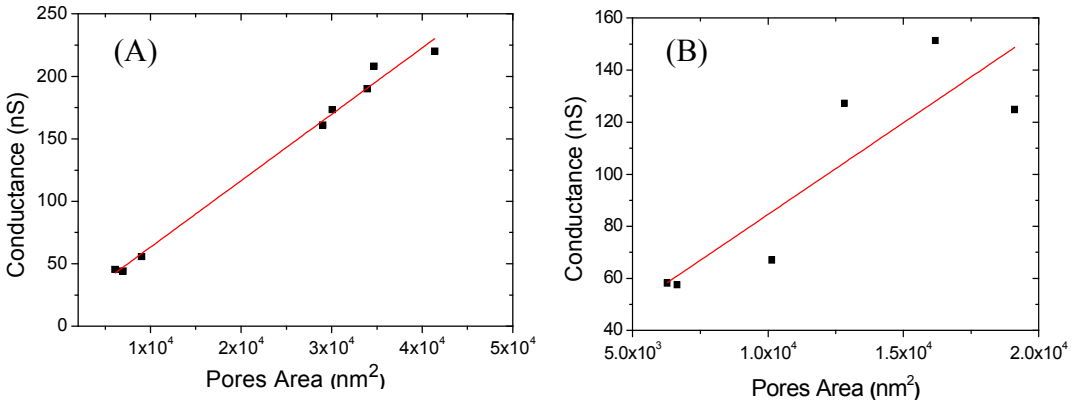

Figure 6.15 Calibration curves of pores area vs. conductance of (A) bare Si_3N_4 membrane and (B) Si_3N_4 membrane coated with 50 nm Au by thermal evaporation

6.1.2.4 Additional capacitive effect by Au surface

The Au surface on the substrate not only serves as a support for the assembly of thiolipid monolayer but it is also used as a working electrode during the electrochemical measurement with EIS (figure 6.9). With this configuration, the measured capacitance of a pTBLM is about 0.8 $\mu F/cm^2$ (figure 3.11). This is close to the capacitance of a typical cell membrane [2]. The capacitance of a lipid bilayer membrane depends on its thickness and the surface area exposed to an electrochemical environment (buffer solution surrounding the electrodes). However, EIS data cannot reveal the real time ion transport events of channel proteins in a pTBLM. Direct observation of ion channel events can only be monitored by ionic current measurement using PPC.

When a Nano-psTBLM is formed across a nanopore in Si_3N_4 membrane, the capacitive effects of underlying Si_3N_4 membrane have to be taken into account. DPhyTL have a high capacitance when assembled on Si_3N_4 membrane across a nanopore. This is due to an alternative arrangement of Si_3N_4, Au and pTBLM which are simply insulative, conductive and insulative in nature (figure 6.16A). When these only several nanometer thick alternating layers are exposed to large electrolyte solution on each side, this configuration becomes analogous to a parallel plate capacitor and the output current is associated with high capacitive noise. Basically this could interfere with the measured signal with relatively low signal to noise ratio, and high capacitance contributed to lipid bilayer from external sources is always required to be minimized or, if possible, eliminated. This effect of parallel plate capacitance can be reduced if the Au surface is removed and the underlying Si_3N_4 surface is employed for silane based monolayer

assembly (figure 6.16B). Therefore, another silane based molecule, triethoxysilane DPTTE, was exploited as an alternative of DPhyTL and this will be discussed in the following section.

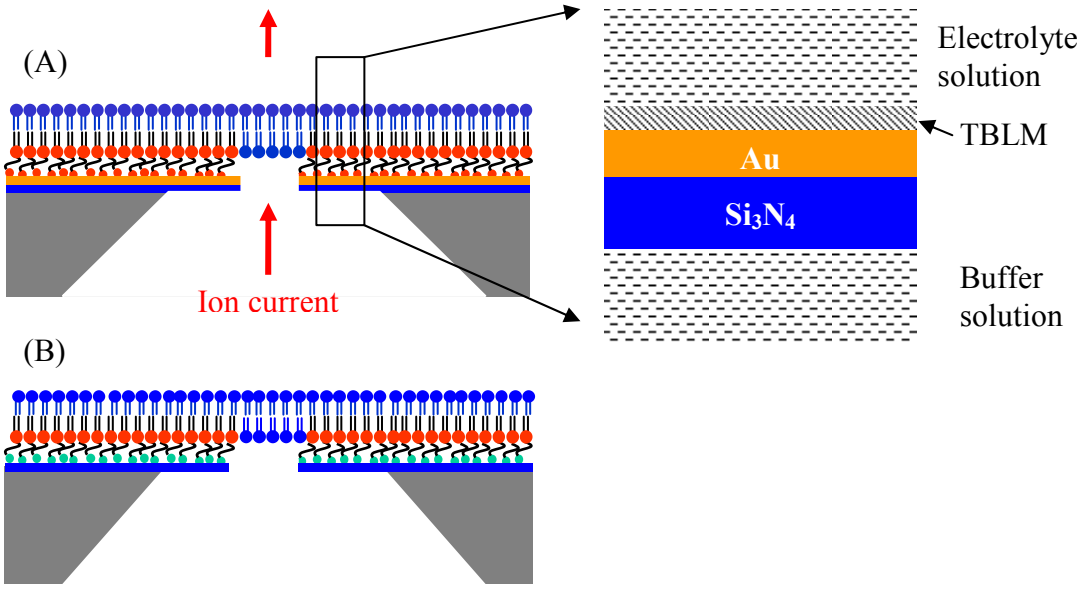

Figure 6.16 Schematics of (A) DPhyTL based Nano-psTBLM on Au coated Si_3N_4 membrane with inset showing alternate insulative/conductive/insulative arrangement of Si_3N_4, Au and pTBLM in bulk electrolyte solution, and (B) alternative to Au, by triethoxysilane monolayer based Nano-psTBLM on Si_3N_4 membrane with a nanopore (schematics are not to scale)

6.1.2.5 Si_3N_4 Surface for triethoxysilane monolayer

Polished silicon or Si_3N_4 with native thin oxide layer is an ideal surface for silane based monolayer assembly. The surface roughness of Si_3N_4 film examined by AFM shows an RMS value less than 0.3 nm (figure 3.2A). Clean planar Si_3N_4 surfaces with minimum surface roughness can promote the better electrical sealing of monolayer for subsequent formation of a pTBLM. A series of cleaning procedures and surface treatment can increase the surface coverage with OH-groups for the silanation reaction with ethoxysilane molecules [230, 233]. Surface cleaning procedure for bare Si_3N_4 membrane chips is same as that of the wafer for Au evaporation. Surface cleaning of Si_3N_4 membrane chips was carried out before FIB milling of nanopore.

6.2 Materials

6.2.1 DPhyTL for Au surfaces

Molecular structure DPhyTL lipid is already described in sections 3.1.1.2. In Nano-psTBLM formation on Au nanoporous membrane and experiments, only DPhyTL (without CholPEG) was used.

6.2.2 DPTTE for Si_3N_4 surfaces

Molecular structure of DPTTE ethoxysilane lipid is described in sections 3.1.1.3 previously.

6.2.3 DPhyPC

Detail about DPhyPC lipid is previously described in section 3.2.1.1. Here in Nano-psTBLM formation on Au and Si_3N_4 nanoporous membranes, pure DPhyPC without cholesterol is used to prepare large unilamellar vesicles (LUVs) for the fusion onto DPhyTL and DPTTE monolayer covered nanoporous Au and Si_3N_4 membranes respectively.

6.2.4 LUVs preparation

DPhyPC lipid solution preparations without cholesterol and vesicles extrusion were previously discussed in section 3.2.1.3. 2 mg/ml DPhyPC in Milli-Q water was extruded 21 times through 400 nm diameter polycarbonate porous membrane. LUVs were directly used for fusion after immediate extrusion. In order to observe the size distribution, LUVs were 10 times diluted in MilliQ water and characterized with dynamic light scattering (DLS) [238, 254]. DLS (also known as photon correlation spectroscopy) measures Brownian motion of the particles in a liquid medium and relates it to the size of the particles. Brownian motion is the movement of particles due to random collision with the molecules of the surrounding liquid medium. The particles are constantly (and randomly) moving all the time but their motion depends on the size of the particles; small particles move quickly while large particles move relatively slowly. The relationship between the size of a particle and its speed due to Brownian motion is defined by the Stokes-Einstein equation. The particles in the medium are illuminated by a laser and the intensity fluctuations in the scattered light by the particles

are detected and intensity signal is correlated with time by digital correlator. DLS deals with very small time scales and the length of time it takes for the intensity correlation to reduce to zero is in the order of one to tens of milliseconds. Then the rate of decay of intensity correlation function is related to particle size as the rate of decay is much faster for small particles than it is for large ones. Usually the DLS software uses algorithms to extract the decay rates for a number of size classes to produce the particular size distribution of particles. In this measurement, Zetasizer Nano system (Malvern Instruments Ltd, UK) (with fitted 633 nm laser light source and the detector optics to be able to capture the scattering light up to 90° scattering angle) was used to measure the size distribution of LUVs by intensity. The measured intensity distribution graph was shown in figure 6.17. The x-axis shows a distribution of diameter of vesicles while the y-axis shows the relative intensity of scattered light. According to the analysis, majority of vesicles fall within the range of 400-600 nm diameters in size.

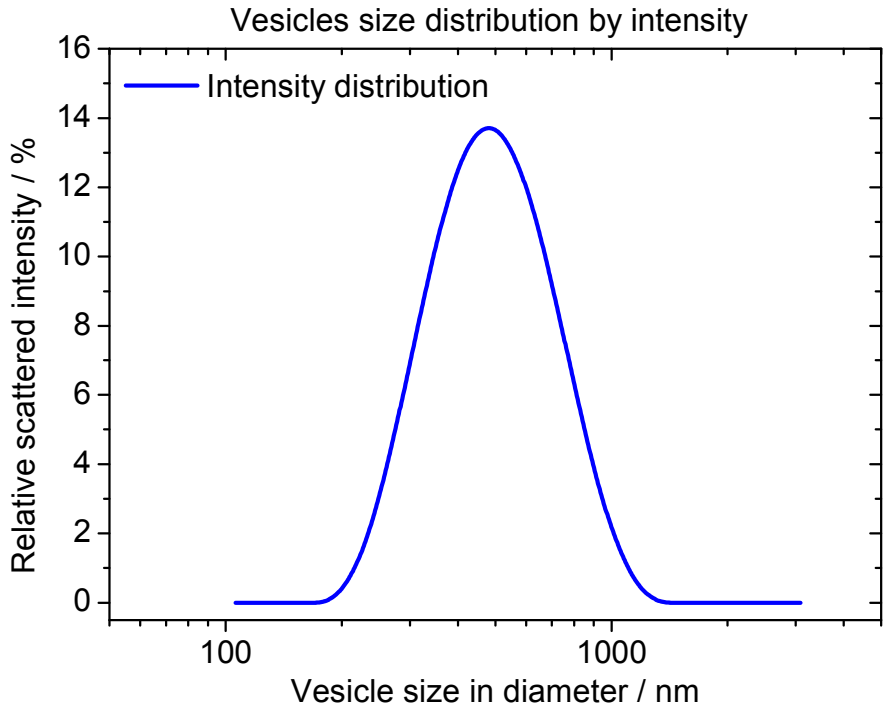

Figure 6.17 Size distribution of the extruded 400nm diameter LUVs measured by dynamic light scattering (DLS)

6.3 Monolayer

6.3.1 DPhyTL (Self-assembly vs. LB)

According to static contact angle measurements, self-assembled DPhyTL on Au surfaces provides relatively better monolayer packing density than that of DPhyTL on Au surfaces by LB transfer (figure 3.8). It is believed that the monolayer with high

surface hydrophobicity is required to support the fusion of lipid vesicles but very high hydrophobic surfaces are not really favourable for vesicles fusion. This is the case especially when the fusion of vesicles takes place on vertically positioned Si_3N_4 membrane with nanopores (figures 2.21 and 6.18). DPhyTL monolayer by self-assembly on normal Au surfaces gives CA about 105º which is higher than the normal monolayer quality for vesicles fusion. Same monolayer transfer onto normal Au by LB method yields CA of around 95º and hence DPhyTL by LB transfer was mainly used in Nano-psTBLM experiments.

6.3.2 DPTTE (Self-assembly vs. LB)

Triethoxysilane DPTTE on the other hand, provides better monolayer packing density when it was transferred by LB method. CA of DPTTE by LB transfer was around 90º (figure 3.8F) and it was the optimum surface hydrophobicity which supported the fusion of LUVs on DPTTE monolayer.

6.4 Bilayer over a single nanopore

6.4.1 DPhyPC LUVs fusion

Nano-psTBLM across a single nanopore is formed by fusion of LUVs. The use of LUVs ensures a full coverage of vesicles across the nanopore while fusion takes place. First, either a DPhyTL or DPTTE monolayer was assembled on a Si_3N_4 membrane chip with a single nanopore. The chip was then glued onto a 1 mm thick polyether ether ketone (PEEK) chip-holder plate with a 1 mm^2 opening at the centre, using PDMS and it was cured at 70°C for 15 minutes in induction oven (figure 2.21). In case of monolayer transferred by LB, gluing onto chip-holder was done first. The chip-holder was clamped in between two separate chambers (made of PEEK) with screws. This makes the chip-holder together with Si_3N_4 chip just partition between two compartments in measurement cell (figure 2.21 and 6.18). The monolayer was then hydrated with 4 ml of 1.0 M KCl + 20 mM $CaCl_2$ electrolyte, injected into each compartments of the cell. Using the PPC setup, conductance, capacitance and current across the nanopore were measured and recorded before the next step of vesicle fusion. Then 80 µl of LUVs solution was injected onto the planar side of Si_3N_4 membrane near the nanopore with hydrated monolayer. Since the chip-holder was vertically partitioned, a micro-pump was usually used to create the steady flow of vesicles containing buffer to

help induce the vesicles rupture and fusion on the monolayer. The flow speed was set at 0.5 µl/second and circulation was done for about 20 minutes. Schematic of Nano-psTBLM formation was depicted in figure 6.18.

When a Nano-psTBLM was formed across the nanopore, the conductance decreased from ~50 nS to below 10 nS. Then KCl + $CaCl_2$ electrolyte from both chambers was slowly exchanged by and electrolyte of 1.0 M KCl. Usually the conductance decreased with time as the TBLM on the bulk surface as well as across the nanopore was slowly undergone structural rearrangement and sealing the structural defects or voids by possible lipid fluidity. This Nano-psTBLM formation can be characterised by both PPC and EIS measurements. The results and observations are presented in next section.

6.4.2 Bilayer formation over a single nanopore

6.4.2.1 Characterization by PPC

The size of the nanopore in this experiment was ~200 nm in diameter and a DPTTE monolayer was transferred by LB as discussed in previous section. First, the current and capacitance of the chip with the monolayer was measured by an AC applied potential. The capacitance of the Si_3N_4 membrane was 1.32 nF and the overall output current was 1340 pA (figure 6.19A) while conductance of nanopore was about 230 nS (figure 6.19B). This conductance was equivalent to a membrane resistance of about 4.4 MΩ. Then 80 µl of 400 nm diameter DPhyPC LUVs was added onto the planar side of the Si_3N_4 membrane with the hydrated DPTTE monolayer on the surface. As stated in the previous section, the buffer solution together with the LUVs was circulated with a micro-pump with a flow of 0.5 µl/second. The flow was directed onto the Si_3N_4 membrane. After circulation for 20 minutes, the measurement cell was brought to the faraday cage and current, capacitance and conductance were measured (figure 6.20A).

The overall output current was reduced to 1280 pA. This decrease in ion current was due to partly formation of TBLM across or in the vicinity of the nanopore resulting in a decrease in conductance component of the output current. The capacitance also decreased to 1.26 nF while there was a huge decrease in conductance from 230 nS to 20 nS due to the possible preliminary formation of a Nano-psTBLM. This could also be seen as a huge increase in membrane resistance from 4.4 MΩ to 50 MΩ. In the current graph in figure 6.20A, there was also noticeable decrease in the slope of conductive component of the current which was an indication for the decrease in conductance.

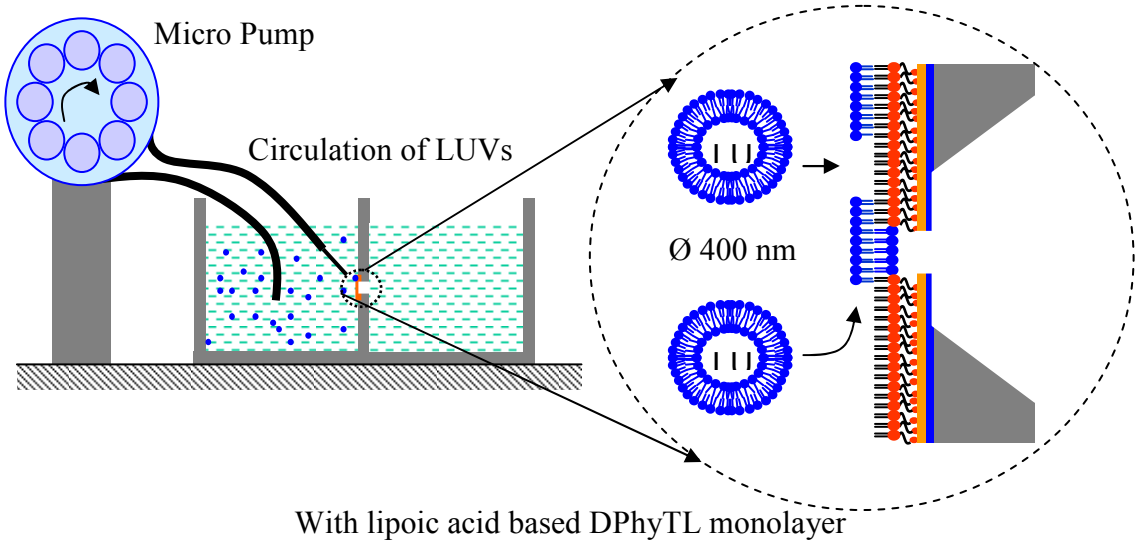

Figure 6.18 A schematic showing the PEEK measurement cell with a chip-holder (inset shows schmetically how LUVs could adsorb onto the monolayer and possibly fuse to form Nano-psTBLM across a nanopore for a better visualization)

To ensure the sufficient supply of vesicles flowing onto the monolayer surface, additional 80 µl of LUVs were added and the electrolyte was circulated for 90 minutes before the second measurement was conducted. After 90 minutes circulation, the electrolyte in both compartments of the measurement cell was thoroughly exchanged with a second electrolyte of 1.0 M KCl. Figure 6.20B shows the results of current, capacitance and conductance of the Nano-psTBLM. The conductance decreased further to 10 nS which is approximately equivalent to a bilayer resistance of about 100 MΩ (i.e. 0.1 GΩ) as an indication for a formation of a suspended TBLM across a nanopore. The bilayer capacitance decreased to 1.24 nF. It was not expected to decrease further once the bilayer was formed over the nanopore. The capacitance could be used to judge the bilayer formation because it decreases when the thickness of the capacitive layer increases as a bilayer is formed. At the same time, the ion current decreased slightly to 1260 pA. This ion current was the baseline current of the Nano-psTBLM, and if the seal between the bilayer and the surface was good then the baseline current should be lower.

6.4.2.2 Characterization by EIS

Electrochemical impedance spectroscopy was also used to monitor the formation, stability and lifetime of the Nano-psTBLM. Not like in pTBLM, Nano-psTBLM on nanoporous Si_3N_4 membrane with or without Au surface can be characterized by EIS. Here DPTTE monolayer was transferred by LB method onto a Si_3N_4 membrane with a

100 nm diameter nanopore. In this measurement, reference and counter electrode connections were joined and connected to an Ag/AgCl electrode and measured against working electrode (another Ag/AgCl) on the other side of membrane in the measurement cell. The impedance spectra of a single nanopore with DPTTE monolayer gave low membrane resistance and capacitance of around 1 nF.

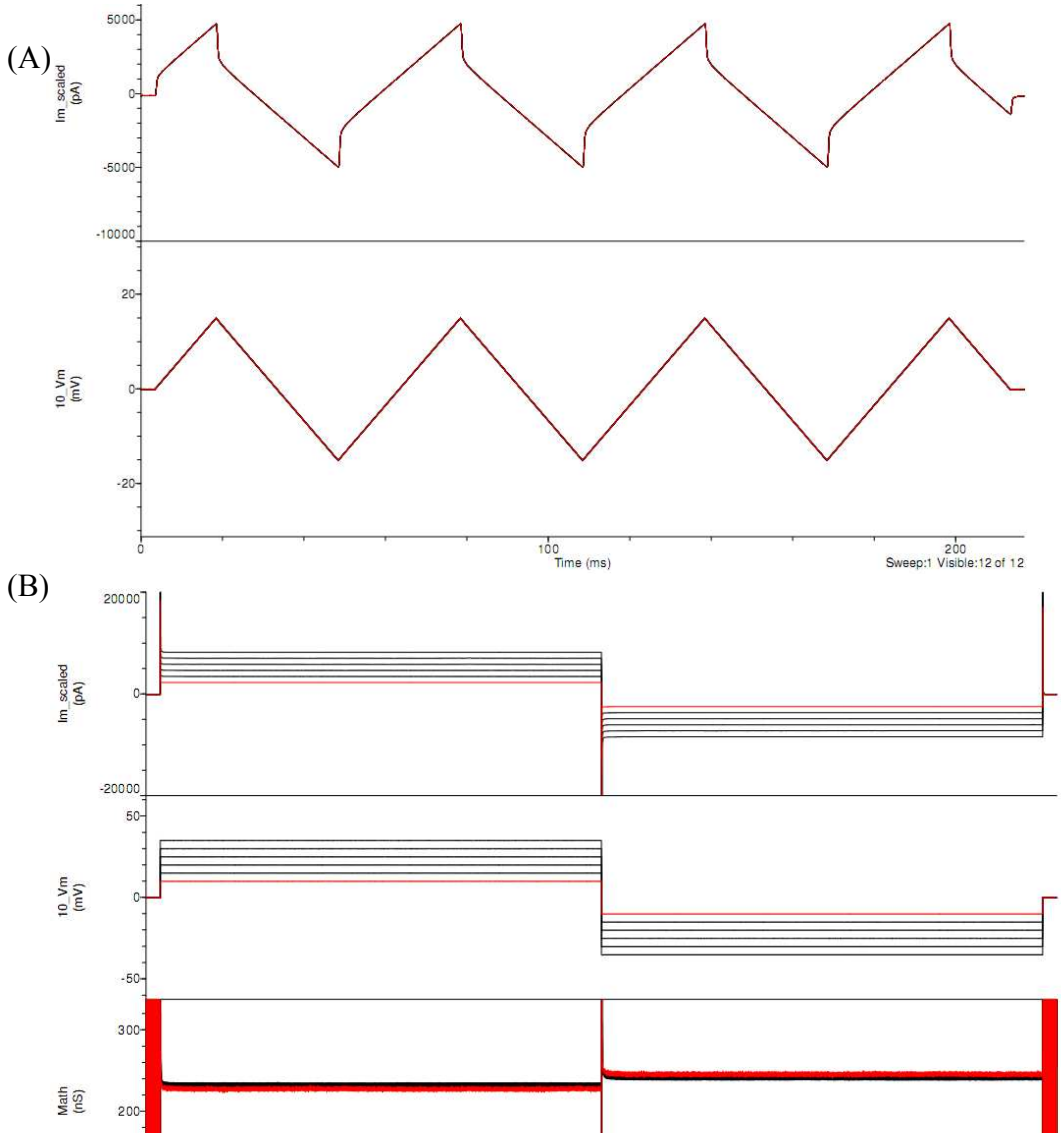

Figure 6.19 (A) Current (1340 pA) and capacitance (1.32 nF) and (B) conductance (230 nS) measurement of a Si_3N_4 membrane with a single ~200 nm diameter nanopore

All procedures for vesicles fusion, circulation of LUVs with the micro-pump and exchange of electrolyte after Nano-psTBLM formation were same as those described in previous section. After 80 µl LUVs vesicles injection and fusion, the impedance increased to 8.7 MΩ within 20 minutes of circulation. Fusion of LUVs took less than 2 hours but rearrangement of lipids and formation of good sealing take a few hours after initial formation of TBLM across a nanopore. After 21 hours after vesicles fusion, the

measurement was conducted again and the impedance went up to 1.8 GΩ, an indication for the formation of a TBLM across the nanopore. The first electrolyte was then exchanged with a second electrolyte of 1.0 M KCl and measurements were carried out everyday up to 5 days. Bode plot of the results are shown in figure 6.29.

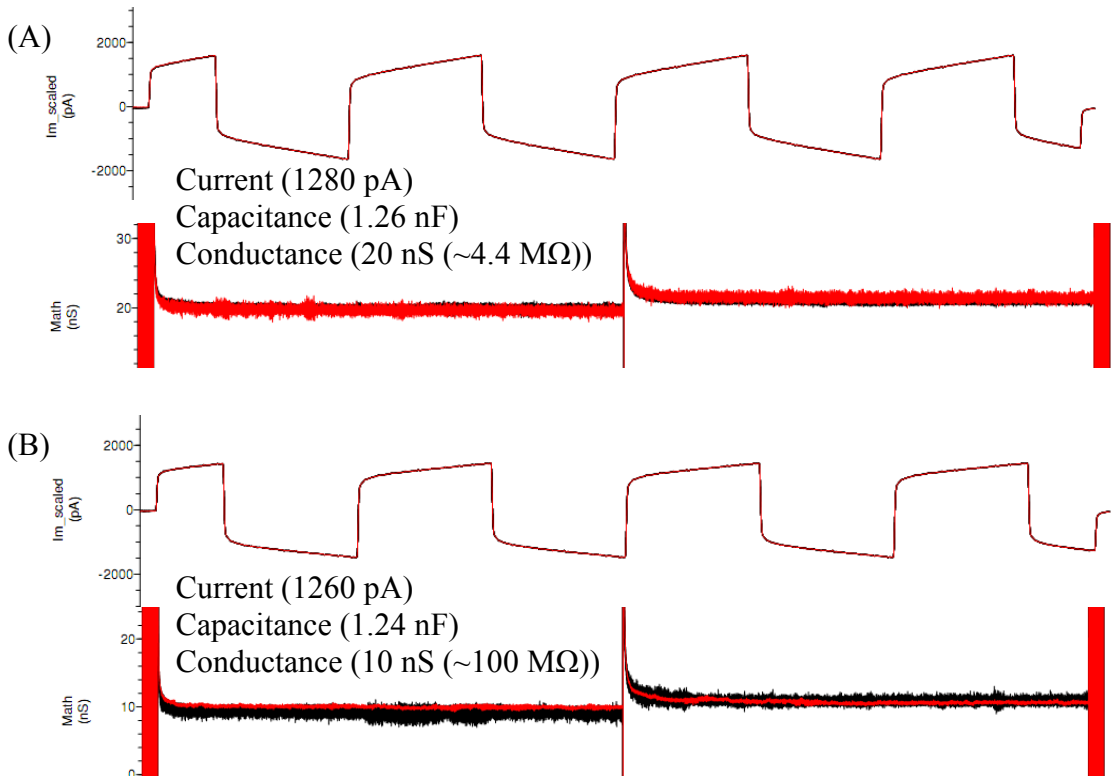

Figure 6.20 Output current and conductance plots of TBLM formation process measured by patch clamp amplifier setup (A) about 20 minutes after first injection of 80µl LUVs and circulation of electrolyte and (B) 90 minutes after second injection of 80 µl LUVs and circulation of electrolyte.

6.5 Single channel recording

6.5.1 Study with alpha hemolysin

Formation of DPTTE based Nano-psTBLM over a 200 nm single nanopore was verified by adding α-HL ion channels and single channel events were characterized by PPC. Current, capacitance and conductance of DPTTE monolayer and subsequent Nano-psTBLM are listed in table 6.1. The LUVs injection and fusion took place in 1.0 M KCl + 0.1 M $CaCl_2$ electrolyte (pH 6) which was then quickly exchanged with 1.0 M KCl after Nano-psTBLM formation. α-HL monomers were initially mixed with PBS into 0.5 mg/ml concentration comprising the toxin solution with 15 µM molar concentration. Then 5 µl of toxin solution was injected into 4 ml of electrolyte making final

concentration of α-HL to 18.75 nM. The solution was added from the backside (KOH etched cavity) to control the amount of α-HL monomer insertion (figure 6.21). The number of toxin monomers inserted would be uncountable if α-HL was added from planar side (front side) because the entired planar surface was covered by pTBLM. If there were defects in pTBLM sitting on the planar support, then the current would leak through the TBLM defects. Moreover, α-HL channels inserted far away from the nanopore may have less probability of participation in ions transport. The measured ion current might be due to the flow of ions through membrane defects as well as channels near (and some away from) the nanopore. This might be difficult to separate the measured current signal responsible only due to ion transport through the α-HL channels.

Table 6.1 Impedance data of DPTTE monolayer based Nano-psTBLM across a 200 nm diameter nanopore measured by PPC

	Conductance (nS)	**Resistance (GΩ)**	**Current (pA)**	**Capacitance (nF)**
DPTTE monolayer	230	0.004	1340	1.32
Nano-psTBLM (20 mins after LUV injection)	20	0.051	1280	1.26
Nano-psTBLM (90 mins after LUV injection)	10	0.103	1260	1.24

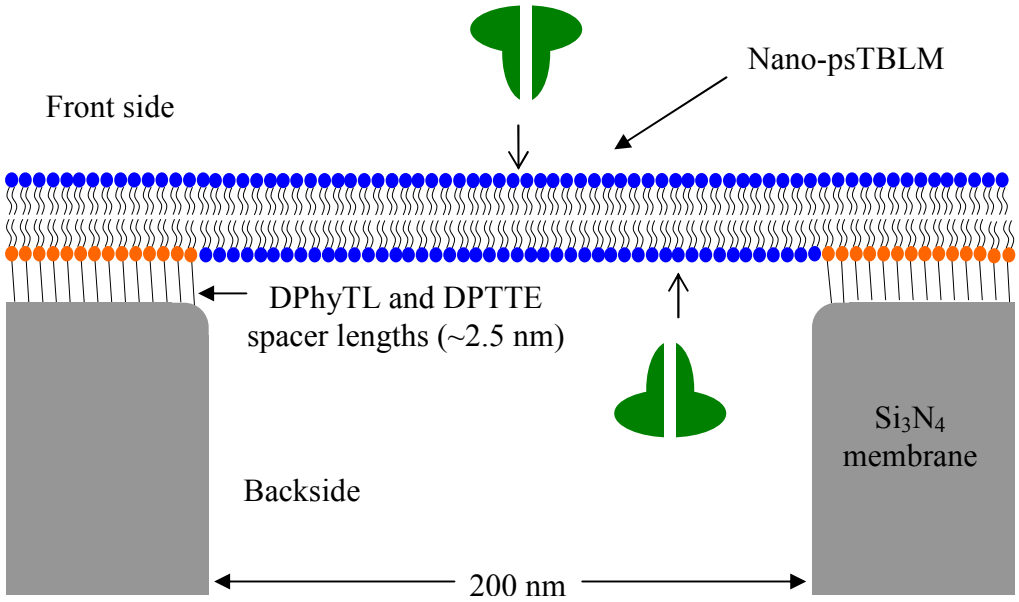

Figure 6.21 Schematic cross section of a Nano-psTBLM formed across a 200 nm diameter nanopore over a Si_3N_4 membrane showing how α-HL ion channels can be inserted from either front side or backside of the membrane

On the other hand, addition of toxins from the backside has control over the amount of α-HL channel insertion. The Nano-psTBLM could only take up a certain amount of channels due to the fact that the inserted channels in the suspended lipid bilayer could not laterally move over the Si_3N_4 surface (figure 6.21). This is simply due to the thickness of mushroom cap heptamer which is longer than the spacer length of the anchored monolayer DPTTE and DPhyTL (figure 6.21). Moreover, as the size of each α-HL channel is known (figure 4.1), another advantage of backside injection is to be able to predict the maximum number of α-HL channels to be inserted approximately because the size of nanopore is known and controllable.

The schematic of Nano-psTBLM with α-HL channels inserted from the backside can be seen in schematic of figure 6.21. Therefore α-HL monomers were added from the back side of membrane chip and then the electrical measurements were carried out by applied DC holding potentials in the range from 0 mV to ±200 mV. With the voltage clamping, it was possible to measure the ionic current from insertion/ ion transport events of α-HL channels as discrete up or down current jumps. Despite the fact that the ion channels response to different applied holding potentials [246, 247], only the results of ion channel events at –75 mV holding potential for 15 minutes measurement were discussed detail in this work because the response of channels to that potential was optimum and stable. The recorded current response with time for overall recording was shown in figure 6.22.

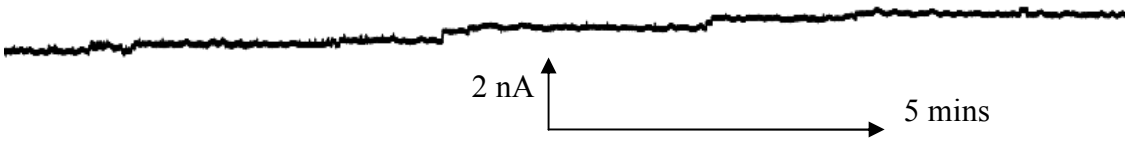

Figure 6.22 Overall ionic current recorded against time at –75 mV DC holding potential after 5 µl (18.75 nM) of α-HL in PBS solution was added from the backside of membrane chip (recording takes about 15 minutes and detail analysis of ion channel events in duration of five minutes each were done in the following figures 6.23, 6.24 and 6.25)

After addition of α-HL into the electrolyte from the backside of membrane chip, the recording was started by applying a holding potential of -75 mV DC and the details of ion current response in first five minutes was shown in figure 6.23. The points shown in figure 6.23 are only the events in which relative change in ionic current steps from the baseline current. Before the addition of α-HL, the baseline current was recorded around -1000 pA. To minimize the disturbance to the Nano-psTBLM, α-HL was injected first

before the measurement was resumed. It took about a minute between the injection and the recording of measurement. The baseline current was started around -1450 pA with current noise amplitude of around 40 pA. Ionic current across the lipid bilayer before and after injection of α-HL was –450 pA and this jump in baseline current was an indication of insertion of α-HL ion channels in the Nano-psTBLM. It was noticed, in figure 6.23 that the baseline current was not yet stable and the current signal was noisy in the beginning. This reflected that the seal formed by Nano-psTBLM was still not good enough to provide the stable baseline current for the measurement. Some very short channel flip-outs (less than the duration of 10 milliseconds) were observed in the beginning and the flip-out and re-insertion events were very occasional in the first few minutes (figure 6.23). However some relatively long channel events (around 100 milliseconds) were also observed after some time during the first period of recording.

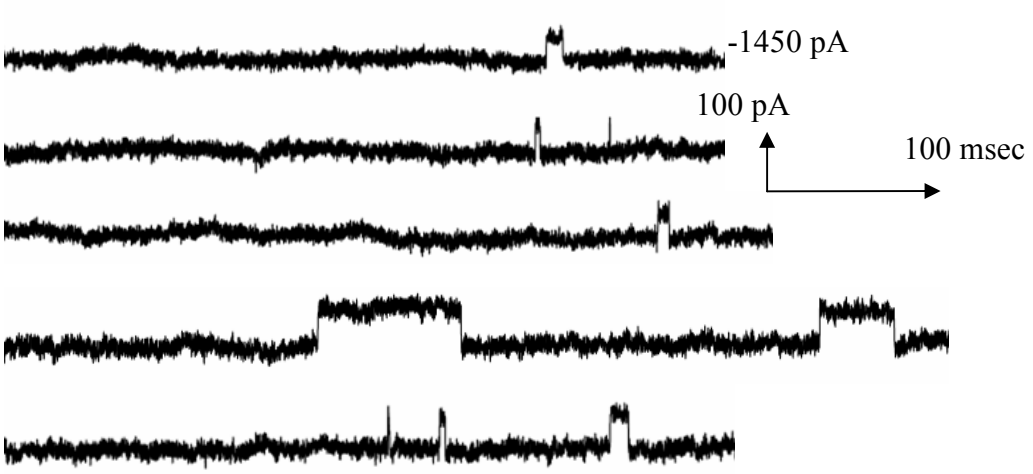

Figure 6.23 α-HL channel insertions and transport of ions as seen by instantaneous steps in current (closeup of activity points in the first 5 minutes of measurement at –75 mV holding potential, channel openings are downwards and closings (flip-outs) are upwards at negative potential)

During the second period of recording, the baseline current stabilized more and relatively longer ion channel events were observed (figure 6.24). Some short events were still noticed but they were much less than long events with more than a few seconds duration. Most importantly repeated channel flip-out events occurred (such as the third line in figure 6.24). This indicated that the new channels were flipping-out while previously left channels remained in buffer without re-insertions into the membrane. As a result of more flip-outs and less re-insertions of ion channels, the baseline current gradually shifted upward due to flowing of lesser ion currents through the channels. Ion channel flip-out or reinsertion steps could be differentiated from the

current fluctuations (for example due to external noise or instability of the membrane) by their instantaneous current pattern. When an ion channel inserted, there was a visible quantized insertion step with a jump of ionic current in less than 1 millisecond. The amount of current increase due to each insertion was quite uniform. Since α-HL is just an open channel, transport of ions instantaneously happens with insertion and this is considered as the channel opening. Similarly when the channel flip-outs or leaves the membrane, transport of ions by this specific channel stops and this is considered as the channel closing. The duration of channel to remain in either opening or closing states is quite random.

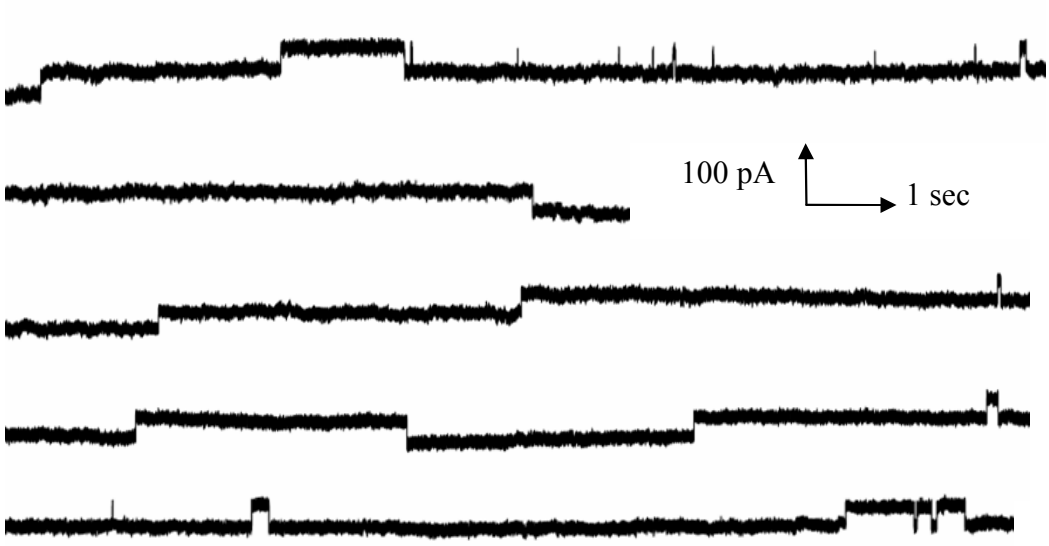

Figure 6.24 α-HL channel insertions and transport of ions as seen by steps in current (closeup of activity events in second 5 minutes of measurement at –75 mV holding potential)

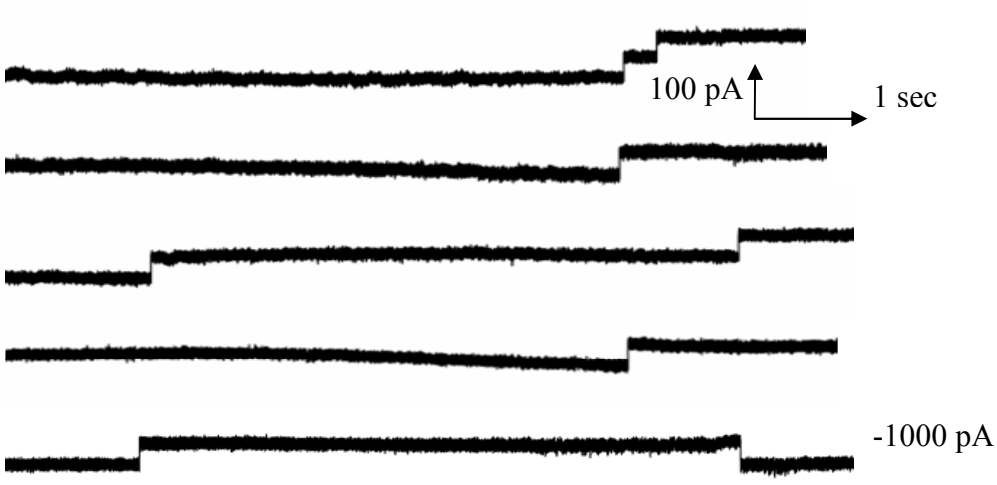

Figure 6.25 α-HL channel insertions and transport of ions as seen by steps in current (closeup of activity events in last 5 minutes of measurement at –75 mV holding potential)

In last five minutes, the baseline current was already stable enough as the seal of the membrane with Si_3N_4 surface over the nanopore improved (figure 6.25). Some re-insertion events of ion channels were observed but they were less compared to the flip-out events of the channels. The duration of ion channels in open or close states was also relatively longer for more than a few seconds (figure 6.25). Finally there were no more events of ion channels and the baseline current reached to about –1000 pA at the end of last five minutes measurement.

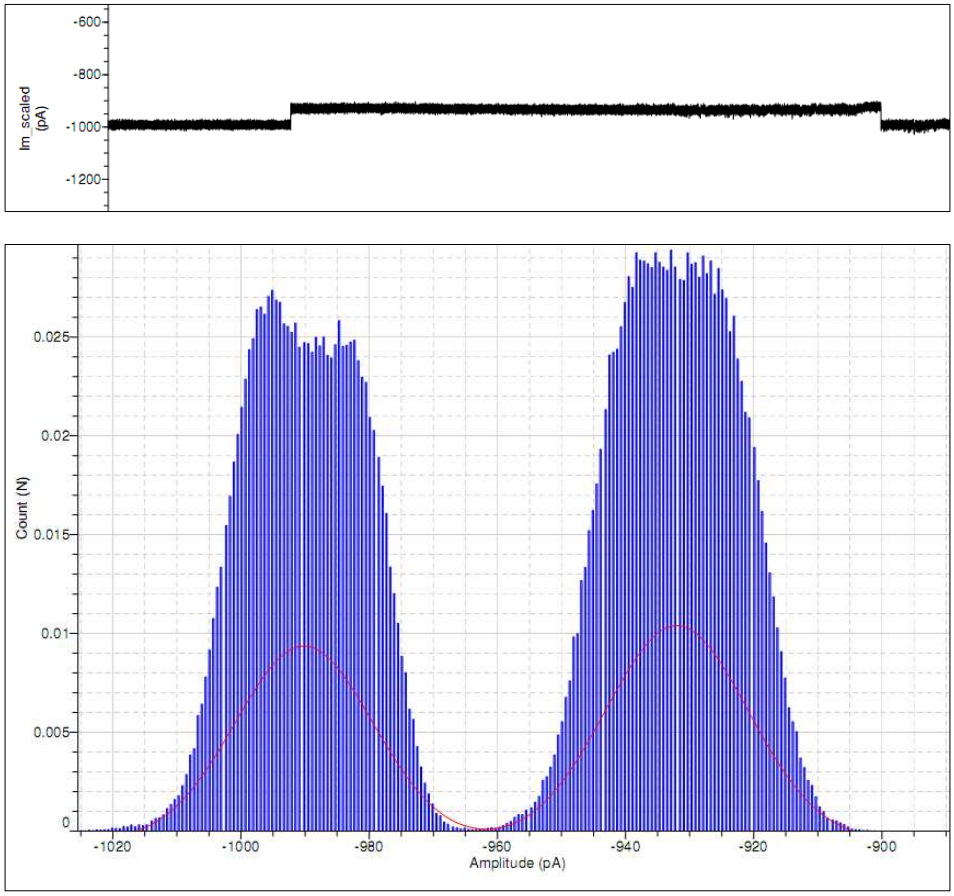

Figure 6.26 Single α-HL ion channel insertion event at the –75 mV holding potential (above) and the respective histogram of single channel event with a single 58 pA current step (below)

In principle, α-HL ion channels were stable and mostly remained in the lipid bilayer membrane once they were inserted [92]. However in our experiment, ion channels were flipped-out (or left) one after another, and this was due to the combining effect of mushroom-shaped head domain of α-HL channels and the backside injection (figure 6.21). Backside injection has an advantage of control over number of channel insertion into the Nano-psTBLM but the inserted channels might denature or unfold upon contact with the rim of nanopore in Si_3N_4 membrane. This might happen because the height of

cap domain of α-HL channel (~5 nm) as shown in figure 4.1A [90] is larger than the available space provided by the spacer length of tethered monolayer (~2.5 nm) [55]. It was possible to consider that the ion channels were denatured or unfolded because the number of ion channels leaving the membrane was more than those re-inserting back into the lipid bilayer after flipping-out of the membrane. This problem could be easily solved if α-HL ion channels were inserted from the front side instead or relatively small ion channels with no extra membranous domains such as Gramicidin D or Valinomycin were used to insert from the backside.

Nevertheless, we have observed the single α-HL ion channel events clearly in planar patch clamping experiment with Nano-psTBLM. There was a total decrease of approximately 450 pA ionic current during the overall measurement (figure 6.25). Throughout the experiment, events of ion channels leaving from and re-inserting into the membrane were counted and subsequent analysis revealed that only 9 channels were initially inserted upon addition of α-HL before the recording was started. This convinced that each channel transported an average ionic current of about 50 pA. The results here are in agreement with single channel recording of α-HL in 1 M KCl [249] and 1 M NaCl electrolytes [250]. On the other hand, a single channel event of α-HL channel was analysed with current histogram and the discrete step in current due to single channel insertion (opening) was around 58 pA (figure 6.26). This was closely agreed with the average ionic current carried by each α-HL channels by counting method. The ionic conductance of α-HL ion channels is directly proportional to molar concentration of electrolyte and typical single channel conductance of an α-HL ion channel is between 50 and 78 pS when it was measured in 100 mM KCl [92]. In our experiment, the single channel conductance is about 780 pS in 1 M KCl and this is closely agreed with the results in literature [92].

To evaluate the performance of Nano-psTBLM, the results were compared with that of previously formed conventional BLM with α-HL ion channels. The substrate for BLM was a Teflon sheet with an approximate 50 μm diameter single hole. A BLM was made of 1-palmitoyl-2-oleoyl-*sn*-glycero-3-phosphocholine (POPC) lipids with 2 mg/ml concentration in hexadecane using Muller-Montal method as depicted in figure 1.3. First the Teflon sheet was sandwiched between the two separate chambers with clamps for liquid seal. Both chambers were then filled with 1 M KCl electrolyte and POPC lipid solution was spread over buffer in one chamber. After allowing the evaporation of hexadecane for a few minutes, lipid monolayer was formed and hydrated on the water surface. Then by using the pipette to control the water level in the chamber, BLM was

formed over the hole. Then 5 µl of 15 µM α-HL was injected and measured the channel events with applied DC holding potential. The single ion channel measurement and respective current histogram of conventional BLM was shown in figure and the results of the two measurements were tabulated for comparison in table 6.2.

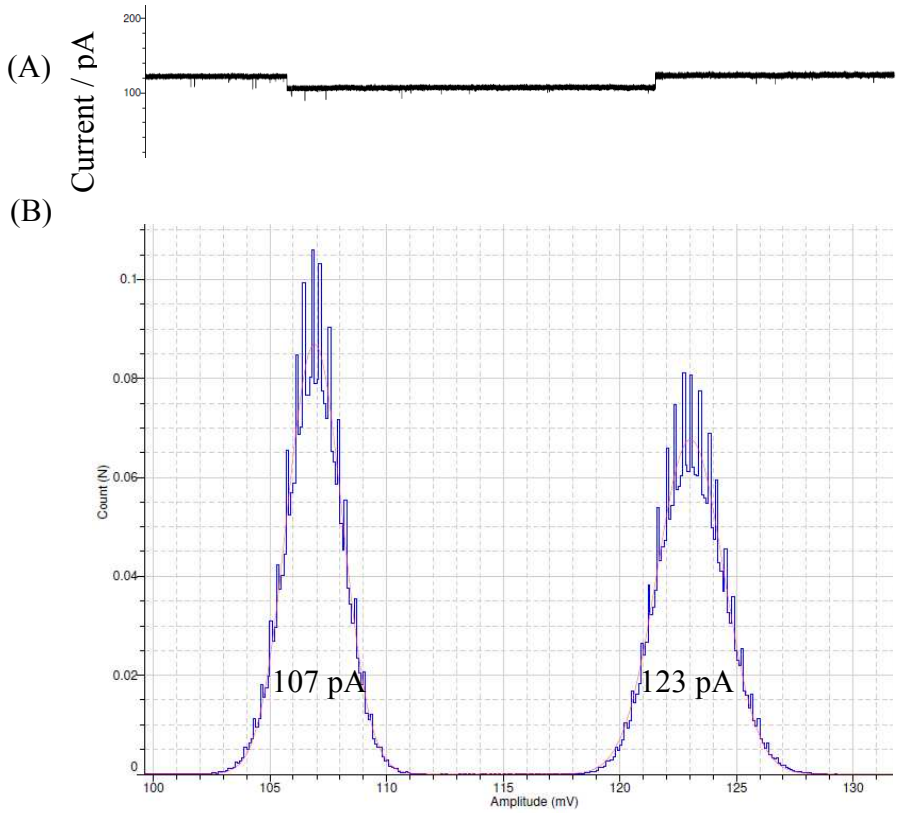

Figure 6.27 (A) An output current signal and (B) the respective current histogram of a single α-HL ion channel in 1 M KCl electrolyte at a DC holding potential of 150 mV displaying two current states (around 107 pA with close state and 123 pA with open state – the high of histogram (i.e., the count) indicates the duration of each state)

Table 6.2 Electrochemical measurement of Nano-psTBLM and conventional BLM by voltage clamp measurement by PPC for comparison

	Current amplitude (pA)	**Base line current (pA)**	**Single channel current drop (pA)**	**Applied DC holding potential (mV)**
BLM	~10	+120	16	+150
Nano-psTBLM	~40	-1000	58	-75

Current histogram reveals two informations; open or close states of current level and duration (figure 6.27). Under positive applied potential, increase in current level means the opening of ion channel. Figure 6.27 shows two current states. Around 107 pA is the baseline current where ion channel remained close or was not transporting the ions

through the channel. 123 pA is the channel in open state where transport of ions is allowed. Both current states have approximate same opening and closing time for the period of measurement. The difference between two current states gives the single ion channel current which is around 16 pA in this case (figure 6.27).

Although the applied holding DC potentials are different, these two systems can be compared in term of current amplitude, baseline current and single channel current drop as shown in table 6.2. Obviously even at the low applied holding DC potential; the amplitude of current of Nano-psTBLM is 4 times higher than that of BLM. The higher amplitude of ionic current is due to parallel leakage of ions elsewhere rather than flowing through ion channels. In Nano-psTBLM, leakage probably comes with insufficient seal of TBLM on the Si_3N_4 surface where it formed. In case of BLM, the seal of lipid bilayer across the hole is much better than that of a TBLM over a nanopore. When ionic current leaks through defects of lipid bilayer in parallel to ion channels, the noise in output current is magnified and higher. In terms of Nano-psTBLM configuration, ions can flow within the anchor region of the monolayer underneath the TBLM (figure 6.21). Noise and leakage current could be reduced if this flow of ion current through the spacer region of lipid bilayer on the surface is eliminated. Consequently due to possible leakage, the baseline current in case of Nano-psTBLM is higher than that of BLM. Therefore, higher amplitude of current noise and baseline is responsible for leakage of ions in TBLM suspended across a nanopore. In table 6.2, single channel current drop in BLM is almost 4 times less than that of Nano-psTBLM even at the higher holding potential of +150 mV. This could be due to relatively large membrane area (over 50 μm diameter compared to 200 nm diameter of Nano-psTBLM) available for the ion channels to be inserted in BLM, and as a result average ionic current carried by each channel is reduced. The nature of single channel events for both BLM and Nano-psTBLM can be seen in figure 6.28.

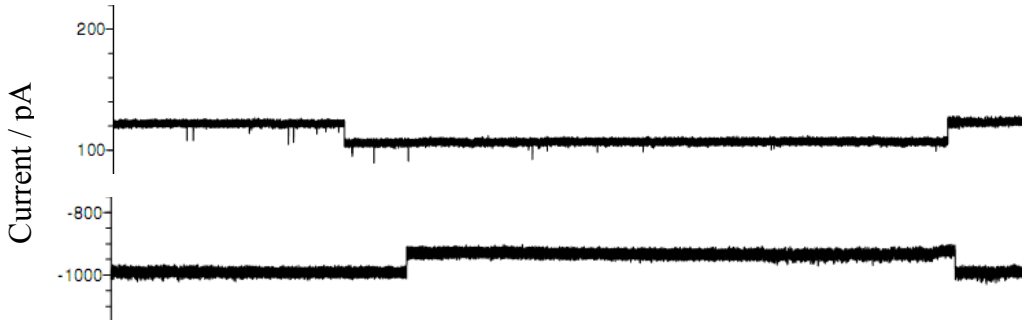

Figure 6.28 Comparison between BLM (above) and Nano-psTBLM (below) for α-HL single ion channel ion transport

6.6 Stability and life time

As it was discussed before, the drawbacks of mechanical fragility and short lifetime of conventional BLM have been improved by reducing the size of holes (from micro- to nanoscale) onto which the lipid bilayer is formed. As the size of holes reduced from micro- to nanoscale, considerable improvements in lipid bilayer stability and lifetime were achieved. In this work, pTBLM suspended over a nanopore is new and there were no previous works of this kind available for the comparison. Therefore, stability and lifetime between Nano-psTBLMs based on thiolipid DPhyTL and triethoxysilane lipid DPTTE were compared and analyzed.

6.6.1 DPhyTL based Nano-psTBLM

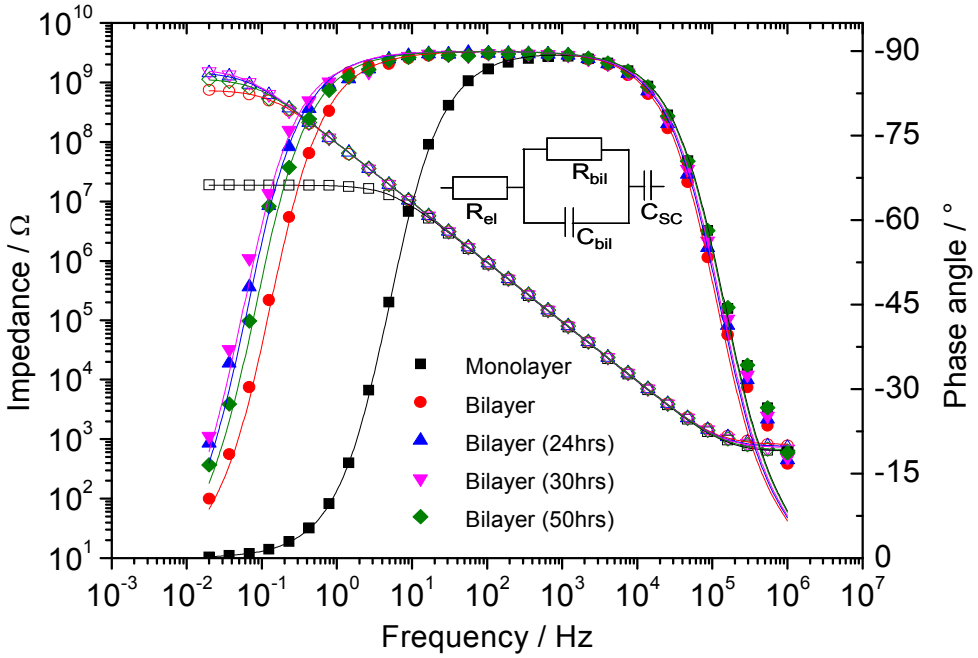

Figure 6.29 Bode plot showing the impedance of a DPhyTL monolayer based Nano-psTBLM formation over a 100 nm diameter nanopore as monitored by EIS measurement – showing stability and lifetime of the system in term of bilayer impedance over time (inset is an equivalent circuit used to fit the data to interpret impedance to resistance and capacitances)

LB transfer method was used to form a DPhyTL monolayer on a 25 nm thick Au (by normal thermal evaporation) coated Si_3N_4 surface with a 100 nm diameter single nanopore. EIS measurement was carried out in each step of Nano-psTBLM formation in 1 M KCl electrolyte and Bode plot of the results was shown in figure 6.29. All the procedures of Nano-psTBLM formation on DPhyTL based monolayer were same as

that of Nano-psTBLM formation DPTTE based monolayer as explained before in section 6.4.2. Resistance and capacitance of lipid bilayer over time was tabulated in table 6.3. The impedance data of both Nano-psTBLMs were fitted using the equivalent circuit model shown in inset of figure 6.29.

6.6.2 DPTTE based Nano-psTBLM

DPTTE based Nano-psTBLM formation was previously explained in section 6.4.2. Here in stability test, Nano-psTBLM was suspended over a 100 nm diameter single nanopore, and its stability and lifetime were measured up to 120 hours using EIS. The Bode plot of measurement was shown in figure 6.30 and the impedance results were tabulated in table 6.4.

Table 6.3 Resistance and capacitance of DPhyTL based Nano-psTBLM suspended across a 100 nm diameter nanopore (stability and lifetime up to 50 hours was measured)

	Resistance (GΩ)	**Capacitance (nF)**
DPhyTL (monolayer)	0.1865	1.711
Nano-psTBLM (bilayer)	0.7138	1.678
After 24 hours	1.373	1.712
After 30 hours	1.523	1.728
After 50 hours	1.086	1.707

Table 6.4 Resistance and capacitance of DPTTE based Nano-psTBLM suspended across a 100 nm diameter nanopore (stability and lifetime up to 120 hours was measured but only the selective measurements points were described in the table)

	Resistance (GΩ)	**Capacitance (nF)**
DPTTE (monolayer)	0.0052	1.313
Nano-psTBLM (20 minutes after injection of LUVs)	0.0087	1.254
After 21 hours	1.823	1.419
After 48 hours	4.556	1.402
After 120 hours	3.682	1.398

6.6.3 Discussion

The structural stability and lifetime of a DPTTE based Nano-psTBLM is shown in figure 6.30. The resistance of the lipid bilayer was above 3 GΩ for up to 120 hours without significant variations in the Giga Ohm range (figure 6.31). Measurements were recorded several times during 5 days and the fluctuations in membrane impedance were noticed. Fluctuations in impedance were probably due to external perturbations to

Nano-psTBLM such as shaking the measurement cell while it was being handled, vibrating buffer solution by placement of electrodes for measurement etc. Therefore it could be expected that the membrane impedance should be reasonably stable if external perturbations were kept away from the measurement cell. After 120 hours of lifetime, the quality of Nano-psTBLM was tested by adding α-HL toxins, and observed the insertions of ion channels and events of ion transport. Unfortunately maximum lifetime of the system was not tested due to time constraint and limited availability of the impedance equipment.

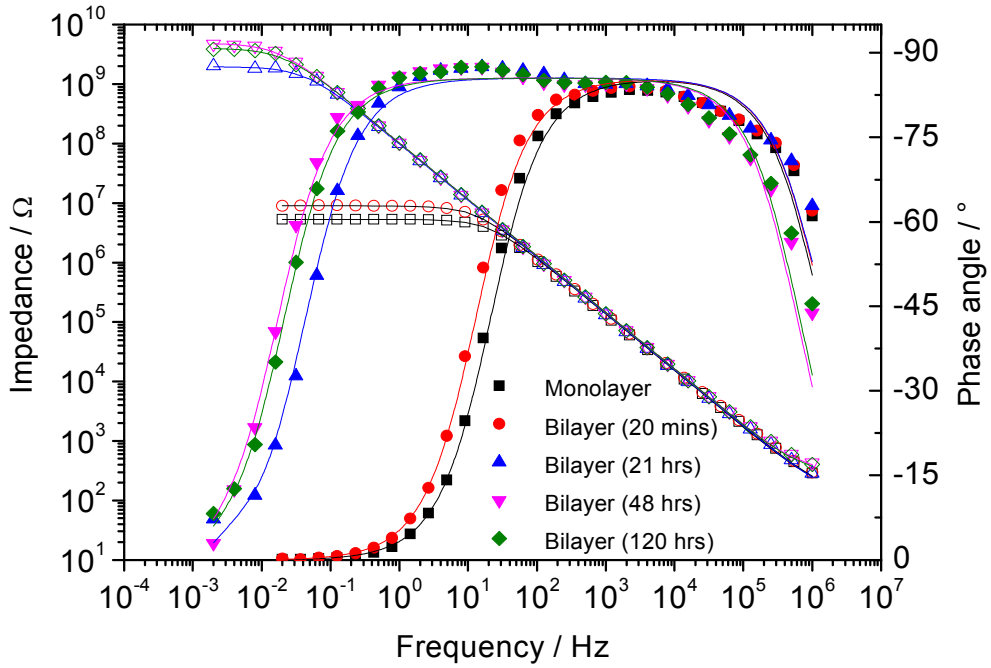

Figure 6.30 Bode plot showing the impedance of a DPTTE monolayer based Nano-psTBLM formation over a 100 nm diameter nanopore as monitored by EIS measurement – showing stability and lifetime of the system in term of bilayer impedance over time

On the other hand, the experimental data recorded throughout the experiment for DPhyTL based Nano-psTBLM was selectively listed in table 6.3. It was observed that the resistance of suspended bilayer was maintained well above 1 GΩ for up to 50 hours. When the data from table 6.3 and 6.4 were compared, the membrane capacitance in case of DPhyTL based Nano-psTBLM was slightly higher than that of DPTTE based one regardless of the same experimental procedure and parameters were used. Moreover, it was also noticed that the capacitances of the monolayer and subsequent Nano-psTBLMs were not much different, and in fact capacitance increased a little with time after Nano-psTBLM formation. This could explain the contribution of capacitance of tethered

monolayer to Nano-psTBLM in term of packing density. The surface density and assembly of the DPhyTL monolayer on Au surface was better than that of DPTTE on Si_3N_4 surface. Densely packed monolayers are more resistant to the flow of ions (current) within the tethered part making the capacitance of lipid bilayer slightly higher than that of the monolayer with relatively less packing density.

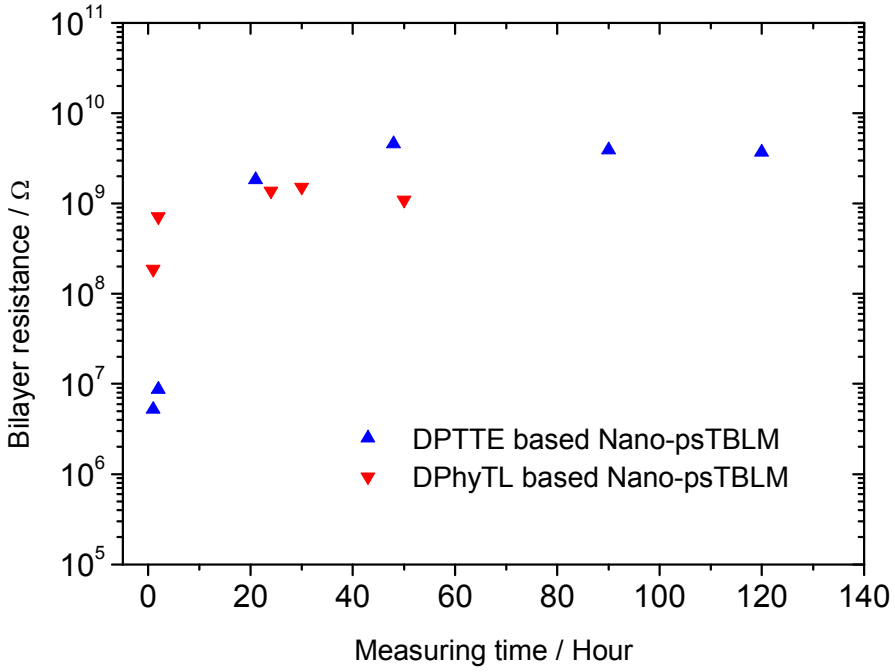

Figure 6.31 Lifetime of Nano-psTBLM based on lipoid acid based DPhyTL and tryethoxysilane based DPTTE monolayer (In both cases, initial resistance of Nano-psTBLM was low but it increases with time and maintained above 1 GΩ with stable membrane capacitances – importantly, resistances of Nano-psTBLMs were not deteriorated with time up to 120 hours in DPTTE-based and 50 hours in DPhyTL-based TBLMs)

To compare the stability and lifetime of Nano-psTBLMs in this work, the results were analyzed with those of similar Nano and Micro-BLMs studied before [77, 79 and 94]. Then the stability and lifetime in term of membrane resistance with time was compared (figure 6.31). Electrochemical seal resistance of DPTTE based (blue triangles) and DPhyTL based (red inverted-triangles) Nano-psTBLM were better than DPhPC based Nano-BLM [79] and DPPTE based Micro-psBLM [94] up to 120 hours. The seal was slowly decreased with time from a few GΩ to less than 1 MΩ in 5 days in case of DPhPC based Nano-BLM formed across the porous alumina substrate in their study [79]. Nanopore size was more or less comparable in both cases but only the difference was the type of lipid bilayer membrane. Again the seal resistance of Micro-psBLM [94]

formed over 1 ~ 2 μm diameter pores in silicon substrate went down to 1 GΩ (from initial resistance of 10 GΩ as of bilayer formation) within three days. On the other hand, lifetime and stability of another Nano-BLM studied by electrochemical impedance indicated that the electrochemical seal resistance of DPhPC based Nano-BLM formed over nanopores in Si_3N_4 membrane was deteriorated within 160 hours [77]. In all of previous works by individuals [77, 79, 94], the initial seal resistances of bilayers were very high up to 10 GΩ but they were quickly decreased to MΩ range within a few days. There are two major differences observed when the system in this work is compared with contemporary works [77, 79, 94]: (i) the number of nanopores and (ii) the way in which the lipid bilayer is attached and suspended on nanoporous substrate. In this work of Nano-psTBLMs, it was made only a single nanopore with well defined pore size in Si_3N_4 membrane in order to avoid the possible parallel leakage of ion current across the nanopores which were uncovered by the lipid bilayer if there were more than one pore in substrate (figure 6.10). The lipid bilayer is not fixed rigidly onto surface but it is anchored via long flexible tethered molecules which provide the stability as well as fluidity of the nanopore suspended lipid bilayer membrane (figures 3.1 and 3.3). Initially when the lipid bilayer was formed, the seal resistance of Nano-psTBLM was not so high but it was improved by time (figure 6.31). Most importantly the resistance was stable and remained relatively linear with time. This proves that the combined effect of single nanoporous surface with the tethered supports can enhance the stability and lifetime of Nano-psTBLM as it did in the case where TBLM was supported onto the template stripped gold (TSG) surface [58].

6.7 Comparison of pTBLM with Nano-psTBLM

Nano-psTBLM was tested for direct measurement of concentration of α-HL toxins in a given sample. Nano-psTBLM was based on DPhyTL monolayer and formed over a single 100 nm diameter nanopore. As it was discussed before, injection of α-HL was carried out from the backside of membrane chip and 7.5 nM of α-HL prepared in PBS solution was added. An impedance measurement, before and after injection of α-HL is shown in figure 6.32. It was observed that the decrease in impedance of Nano-psTBLM due to 7.5 nM α-HL was about 147 MΩ, 18 times more decrease in resistance for the approximately same α-HL concentration in experiment with pTBLM. Experiment with DPhyTL based pTBLM on TSG with 180 nM α-HL injection made impedance

decreased by 17.8 MΩ cm^2 (equivalent to about 64 MΩ). Therefore in term of sensitivity to α-HL toxin, Nano-psTBLM was better than pTBLM on TSG substrate.

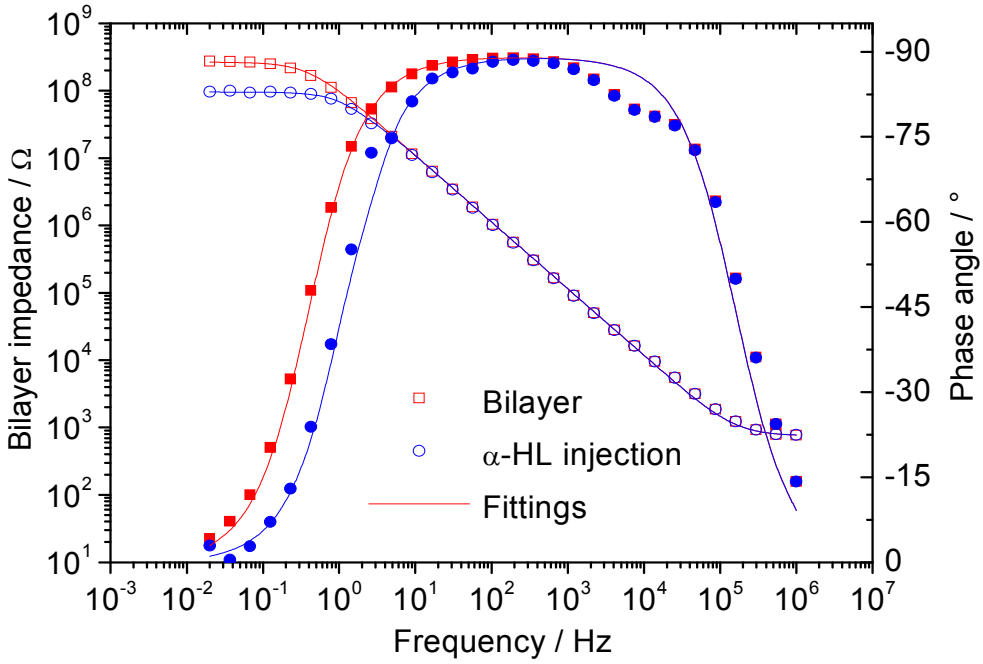

Figure 6.32 Impedance spectrums of DPhyTL based Nano-psTBLM over a 100 nm diameter single nanopore before and after addition of 7.5 nM α-HL prepared in PBS solution

7 Conclusion and outlook

In this work, planar tethered bilayer lipid membranes (pTBLM) were first investigated for the detection and possible identification of bacterial toxins, intending for use in future pathogen sensing applications. Sensing mechanism was based on common (but specific) modes of action of pathogenic bacterial toxins against the lipids in cell membrane. At the molecular level, lipid damaging (lipid loss) or pore-formation (no lipid loss) by particular toxins affects the ion permeability of lipid bilayer membranes differently, and thereby major types of toxins involved in sensing media are detected and identified. Ion permeability of pTBLM induced by bacterial toxins was measured by electrochemical impedance spectroscopy (EIS) while the interactions of pTBLM with bacterial toxins were alternatively detected by surface plasmon resonance spectroscopy (SPR). To provide the optimum sensing of bacterial toxins at human body temperature, ion permeability of pTBLM was tested with different composition of cholesterol at 37 °C. Cholesterol comprised in both leaflets of pTBLM but the percentage composition of cholesterol (CholPEG) in monolayer was explored. It was found out that the more CholPEG in monolayer, the better pTBLM was thermally stable at 37°C. However, incorporation of cholesterol relatively lowered the α-HL sensitivity of pTBLM to an extent. Based on experimental results on thermal stability, 50 % CholPEG incorporation to monolayer (while 33 % in mole cholesterol on upper half of pTBLM was maintained) was used throughout the work presented here as its ion permeability was not only stable at 37 °C but also its sensitivity to α-HL was optimal and relatively high.

Among all the virulence factors associated with many human pathogenic bacteria, pore-forming toxins (PFTs) and lipid damaging enzymes such as lipases were mostly common [110, 122, 123, 124, 128]. Both PFTs and selected phospholipases were secreted by clinically important human pathogens including *S. aureus*, *P. aeruginosa* and *E. coli* with different strains [217, 218, 117, 206, 207, 210]. On the other hand, their modes of action were known to work with artificial lipid bilayer membranes *in-vivo* and *in-vitro* [179, 144, 57, 93]. Therefore α-HL (from *S. aureus*) and PLA2 in their purified forms were first used in preliminary tests with modified pTBLM at 37 °C. It was observed that both α-HL and PLA2 induced ion permeability in term of decreased resistance and increased capacitance of modified pTBLM. Since both toxins enhanced the ion permeability by damaging the lipids, differentiation between their modes of action was rather difficult not much selective. However in case of experiment with SPR,

a clear indication of lipid damaging (lipid loss by PLA2) from modified pTBLM was observed by resonance angle downward shift. On the other hand, pore-formation (no lipid loss by binding of α-HL) in modified pTBLM was indicated by upward shift of the resonance angle. Hence the results measured with SPR revealed either lipid damaging by phospholipases or pore-formation by PFTs of human pathogens.

Impedance results of EIS experiments involving real bacterial pathogens (MSSA476, PAO1 and *E. coli* DH5α) were difficult to interpret. Ion permeation of modified pTBLM, in term of change in impedance, occurred but differently in all the tests with bacteria. Complications could possibly come from sedimentation of bacteria on lipid bilayer and initiation of biofilm formation on the surface during the experiment. Formation of biofilm is largely related to severe toxication of host cells and linked to several diseases [240]. This complication was avoided by eliminating the involvement of bacteria in subsequent experiments. In this sense, only the supernatant of bacterial growth LB medium with presence of bacterial toxins were used. EIS experiments with supernatant of bacteria with pathogenic strains (MSSA476 and PAO1) showed the impedance data different from that of non-pathogenic strains of *E. coli* DH5α. Supernatant of both MSSA476 and PAO1 induced decrease in resistance and increase in capacitance of pTBLM but in different ways. Analysis of impedance data indicated that most PFTs were associated with MSSA476 while more lipid damaging enzymes were accompanied by PAO1. This observation was supported by supernatant toxins of MSSA476 and PAO1 tested by SPR. MSSA476 supernatant caused the upward shift of resonance angle by possible binding of PFTs (no lipid loss) while PAO1 supernatant induced the downward shift of resonance angle by lipid damaging (lipid loss) with phospholipases. Comparatively, impedance data of pTBLM tested with supernatant of *E. coli* DH5α was relatively stable. These results indicated that the sensing of human pathogens is possible (and promising) by the specific toxins of bacteria with modes of action of lipid damaging and pore-formation. Moreover, by designing the lipid bilayer with a particular type of phospholipids, various human pathogens can be targeted and detected [128].

Additionally, pTBLM (without modification with cholesterol) was explored to enhance the sensitivity to toxins and expand the lifetime by transferring onto single nanoporous Si_3N_4 membrane. Si_3N_4 membrane was modified in such a way that both thiol and triethoxysilane based monolayers were able to assembled and subsequent nanopore suspended TBLM (Nano-psTBLM) was formed by LUVs fusion. In this way, Nano-psTBLM acquired the combining advantages of better stability and lifetime of pTBLM

and voltage clamping accessibility of conventional BLM. Si_3N_4 membrane chips were designed and fabricated in-house by photolithography process and single nanopore with 100 nm diameter was milled through 100 nm thick Si_3N_4 membrane in each chip. Silicon side <111> walls were then electrically passivated by the growth of 100 nm thick thermal oxide. Then the Nano-psTBLM formation and characterization were evaluated by both EIS and planar patch clamping (PPC). Both DPhyTL (lipoic acid) based and DPTTE (triethoxysilane) based Nano-psTBLMs were formed and characterized their electrical properties. Seal resistance above 1 GΩ was achieved in all Nano-psTBLMs and about 5 days of typical lifetime was demonstrated, without losing the seal resistance and membrane properties. For the same concentration of α-HL toxins, it was found out that the sensitivity of Nano-psTBLM was enhanced by about 18 times higher than that of pTBLM. By using DPTTE based Nano-psTBLM, single ion channel currents were measured through the incorporated α-HL ion channels and the system was evaluated by comparing the results with similar Micro- and Nano-BLMs on porous substrates. Single channel ionic current conducted through each α-HL ion channel was about 56 pA.

Both EIS and PPC measurements with Nano-psTBLM indicated that the improvements in sensitivity and lifetime of pTBLM were achieved when the system was transferred onto a single nanoporous surface. These improved sensitivity, stability and extended lifetime of Nano-psTBLM may pave the way for the realization of portable membrane chips for first and reliable analysis of ion channels in future applications.

References

1. N.J. Willumsen, M. Bech, S.P. Olesen, B.S. Jensen, M.P.G. Korsgaard and P. Christophersen, *High throughput electrophysiology: New perspectives for ion channel drug discovery*, Receptors and Channels, 9 (2003) 3-12
2. R.B. Gennis, *Biomembranes: Molecular Structure and Function*, Springer-Verlag (1989)
3. Cornell, B.A., Braach-Maksvytis, V.L.B., King, L.G., Osman, P.D. J., Raguse, B., Wieczorek, L., Pace, R.J., *A biosensor that uses ion-channel switches*. Nature 1997, 387, 580-583M
4. H.T. Tien and L.O. Angelica, *The lipid bilayer concept and its experimental realization: from soap bubbles, kitchen sink, to bilayer lipid membranes*. Journal of Membrane Science, 189 (2001) 83-117
5. P. Mueller, D.O. Rudin, H.T. Tien and W.C. Wescott, *Reconstitution of Cell Membrane Structure in vitro and its Transformation into an Excitable System*. Nature 1962, 194, 979-980
6. P. Mueller, D.O. Rudin, H.T. Tien and W.C. Wescott, *Methods for the formation of single bimolecular lipid membranes in aqueous solution*. Journal of Physical Chemistry, 67 (1963) 534-535
7. J.P. Dilger and S.G.A. McLaughlin, *The dielectric constant of phospholipids bilayers and the permeability of membranes to ions*, Science 206 (1979) 1196-1198
8. M. Montal and P. Mueller, *Formation of bimolecular membranes from lipid monolayers and a study of their electrical properties*, Proc. Nat. Acad. Sci. USA, 69 (1972) 3561-3566
9. V. Vodyanoy and R.B. Murphy, *Solvent-free lipid bimolecular membranes of large surface area*, Biochimica et Biophysica Acta, 687 (1982), 189-194
10. S.H. Wihte, *Formation of "solvent-free" black lipid bilayer membranes from glyceryl monooleate dispersed in squalene*, Biophysical Journal, 23 (1978), 337-347
11. L.V. Chernomordik, G.B. Melikyan, N.I. Dubrovina, I.G. Abidor and Yu. A. Chizmadzhev, *663-solvent-free bilayers from squalene solutions of phospholipids*, Bioelectrochemistry and Bioenergetics, 12 (1984), 155-166
12. W.D. Niles, R.A. Levis and F.S. Cohen, *Planar bilayer membranes made from phospholipids monolayers form by a thinning process*, Biophysical Journal, 53 (1988), 327-355
13. R. Benz, O. Fröhlich, P. Läuger and M. Montal, *Electrical capacity of black lipid films and of lipid bilayers made from monolayers*, Biochimica et Biophysica Acta, 394 (1975) 323-334
14. *The Axon CNS guide to electrophysiology and biophysics laboratory techniques*, Molecular Devices (2006)
15. D.P. Nikolelis and U.J. Krull, *Reliable and facile method for preparation of solventless bilayer lipid membranes for electroanalytical investigations*, Talanta, 39 (1992), 1045-1049
16. B. Sakmann and E. Nehr, *Single-channel recording*, (1983) Plenum Press, New York
17. O. Alvarez, E. Diaz and R. Latorre, *Voltage-dependent conductance induced by hemocyanin in black lipid films*, Biochimica et Biophysica Acta, 389 (1975), 444-448
18. J. Hall, *Toward a molecular understanding of excitability (Alamethicin in black lipid films)*, Biophysical Journal, 15 (1975), 934-939

19. W. Hanke and H. Breer, *Charactarization of the channel properties of a neuronal acetylcholine receptor reconstituted into planar lipid bilayers*, Journal of General Physiology, 90 (1987), 855-879
20. R.A. Brutyan, C. DeMaria and A.L. Harris, *Horizontal 'solvent-free' lipid bimolecular membranes with two-sided access can be formed and facilitate ion channel reconstitution*, Biochimica et Biophysica Acta, 1236 (1995), 339-344
21. S.B. Hladky and D.A. Haydon, *Discreteness of conductance change in bimolecular lipid membranes in the presence of certain antibiotics*, Nature, 225 (1970) 451-453
22. L. Bacri, A. Benkhaled, P. Guegan and L. Auvray, *Ionic channel behavior of modified cyclodextrins inserted in lipid membranes*, Langmuir, 21 (2005), 5842-5846
23. S.N. Alix and D.J. Woodbury, *Phospholipase A2 action on planar lipid bilayers generates a small, transitory current that is voltage independent*, Biophysical Journal, 72 (1997), 247-253
24. E.M. Nestorovich, C. Danelon, M. Winterhalter and S. M. Bezrukov, *Designed to penetrate: Time-resolved inter action of single antibiotic molecules with bacterial pores*, Proc. Nat. Acad. Sci. USA, 99 (2002), 9789-9794
25. S.H. White, *A study of lipid membrane stability using precise measurement of specific capacitance*, Biophysical Journal, 10 (1970) 1127-1148
26. S.H. White, *Analysis of the torus surrounding planar lipid bilayer membranes*, Biophysical Journal, 12 [1972] 432-445
27. B. Schuster, D. Pum, M. Sara, O. Braha, H. Bayley and U.B. Sleytr, *S-layer ultrafiltration membranes: A new support for stabilizing functionalized lipid membranes*, Langmuir, 17 (2001), 499-503
28. B. Schuster and U.B. Sleytr, *Single channel recordings of α-hemolysin reconstituted in S-layer-supported lipid bilayers*, Bioelectrochemistry, 55 (2002), 5-7
29. T.J. Jeon, N. Malmstadt and J.J. Schmidt, *Hydrogel-encapsulated lipid membranes*, Journal of American Chemical Society, 128 (2006), 42-43
30. T.J. Jeon, N. Malmstadt, J.L. Poulos and J. J. Schmidt, *Black lipid membranes stabilized through substrate conjugation to a hydrogel*, Biointerphases, 3 (2) 2008, FA96-FA100
31. R.F. Costello, I.R. Peterson, J. Heptinstall and D.J. Walton, *Improved gel-protected bilayers*, Biosensors and Bioelectronics, 14 (1999), 265-271
32. K.C. Weng, J.J.R. Stalgren, D.J. Duval, S.H. Risbud and C.W. Frank, *Fluid biomembranes supported on nanoporous aerogel/xerogel substrates*, Langmuir, 20 (2004), 7232-7239
33. E. Sackmann, *Supported membranes: Scientific and practical applications*, Science, 271/5245 (1996) 43-48
34. H. Schönherr, J.M. Johnson, P. Lenz, C.W. Frank and S.G. Boxer, *Vesicle adsorption and lipid bilayer formation on glass studied by Atomic Force Microscopy*, Langmuir, 20 (2004), 11600-11606
35. L. Zhang, M.L. Longo and P. Stroeve, *Mobile phospholipids bilayers supported on a polyion/alkylthiol layer pair*, Langmuir, 16 (2000), 5093-5099
36. E. Reimhult, M. Zäch, F. Höök and B. Kasemo, *A multitechnique study of liposome adsorption on Au and lipid bilayer formation on SiO2*, Langmuir, 22 (2006), 3313-3319
37. B.R. Dorvel, H.M. Keizer, D. Fine, J. Vuorinen, A. Dodabalapur and R.S. Duran, *Formation of tethered bilayer lipid membrane on gold surfaces: QCM-Z and AFM study*, Langmuir, 23 (2007), 7344-7355

38. C. Steinem, A. Janshoff, W.P. Ulrich, M. Sieber and H.J. Galla, *Impedance analysis of supported bilayer membranes: a scrutiny of different preparation techniques*, Biochimica et Biophysica. Acta, 1279 (1996), 169-180
39. P.S. Cremer and S.G. Boxer, *Formation and spreading of lipid bilayers on planar glass supports*, J. Phys. Chem. B., 103 (1999), 2554-2559
40. A.L. Plant, *Self-assembled phospholipids/alkanethiol biomimetic bilayers on gold*, Langmuir, 9 (1993), 2764-2767
41. P. Nollert, H. Kiefer and F. Jähnig, *Lipid vesicle adsorption versus formation of planar bilayers on solid surfaces*, Biophysical Journal, 69 (1995), 1447-1455
42. D. Kalt, S. Frey and L.K. Tamm, *Formation of supported planar bilayers by fusion of vesicles to supported phospholipids monolayers*, Biochimica et Biophysica Acta, 1103 (1992), 307-316
43. M. Seitz, E. Ter-Ovanesyan, M. Hausch, C.K. Park, J.A. Zasadzinski, R. Zentel and J.N. Israelachvili, *Formation of tethered supported bilayers by vesicle fusion onto lipopolymer monolayers promoted by osmotic stress*, Langmuir, 16 (2000), 6067-6070
44. M. Heim, G. Cevc, R. Guckenberger, H.F. Knapp and W. Wiegräbe, *Lateral electrical conductivity of Mica-supported lipid bilayer membranes measured by scanning tunneling microscopy*, Biophysical Journal, 69 (1995), 489-497
45. C.P. Michael, *Langmuir Boldgett films: An introduction*, Cambridge University Press (1996)
46. G. Wiegand, N. Arribas-Layton, H. Hillebrandt, E. Sackmann and P. Wanger, *Electrical properties of supported lipid bilayer membranes*, J. Phys. Chem. B., 106 (2002), 4245-4254
47. J. Spinke, J. Yang, H. Wolf, M. Liley, H. Ringsdorf and W. Knoll, *Polymer-supported bilayer on a solid substrate*, Biophysical Journal, 63 (1992), 1667-1671
48. M.L. Wagner and L.K. Tamm, *Tethered polymer-supported planar lipid bilayers for reconstitution of integral membrane proteins: Silane-polyethyleneglycol-lipid as a cushion and covalent linker*, Biophysical Journal, 79 (2000), 1400-1414
49. C.A. Naumann, O. Prucker, T. Lehmann, J. Rühe, W. Knoll and C.W. Frank, *The polymer-supported phospholipid bilayer: Tethering as a new approach to substrate-membrane stabilization*, Biomacromolecules, 3 (2002), 27-35
50. H. Lang, C. Duschl and H. Vogel, *A new class of thiolipids for the attachment of lipid bilayers on gold surfaces*, Langmuir, 10 (1994), 197-210
51. V. Atanasov, N. Knorr, R.S. Duran, S. Ingebrandt, A. Offenhäusser, W. Knoll and I. Köper, *Membrane on a chip: A functional tethered lipid bilayer membrane on silicon oxide surfaces*, Biophysical Journal, 89 (2005), 1780-1788
52. B. Raguse, V. Braach-Maksvytis, B.A. Cornell, L.G. King, P.D.J. Osman, R.J. Pace and L. Wieczorek, *Tethered lipid bilayer membranes: Formation and ionic reservoir characterization*, Langmuir, 14 (1998), 648-659
53. G. Krishna, J. Schulte, B.A. Cornell, R.J. Pace and P.D. Osman, *Tethered bilayer membranes containing ionic reservoirs: Selectivity and conductance*, Langmuir, 19 (2003), 2294-2305
54. S.M. Schiller, R. Naumann, K. Lovejoy, H. Kunz and W. Knoll, *Archaea analogue thiolipids for tethered bilayer lipid membranes on ultrasmooth gold surfaces*, Angew. Chem. Int. Ed., 42 (2003), 208-211
55. R. Naumann, S.M. Schiller, F. Giess, B. Grohe, K.B. Hartman, I. Kärcher, I. Köper, J. Lübben, K. Vasilev and W. Knoll, *Tethered lipid bilayers on ultraflat gold surfaces*, Langmuir, 19 (2003), 5435-5443
56. S. Terrettaz, M. Mayer and H. Vogel, *Highly electrically insulating tethered lipid bilayers for probing the function of ion channel proteins*, Langmuir, 19 (2003), 5567-5569

57. I.K. Vockenroth, D. Fine, A. Dodbalapur, A.T.A. Jenkins and I. Köper, *Tethered bilayer lipid membranes with giga-ohm resistances*, Electrochemistry Communications, 10 (2008), 323-328
58. I.K. Vockenroth, C. Ohm, J.W.F. Robertson, D.J. McGillivray, M. Lösche and I. Köper, *Stable insulating tethered bilayer lipid membranes*, Biointerphases, 3 (2) 2008, FA68-FA73
59. V. Atanasov, P.P. Atanasova, I.K. Vockenroth, N. Knorr and I. Köper, *A molecular toolkit for highly insulating tethered bilayer lipid membranes on various substrates*, Bioconjugate Chem. 17 (2006), 631-637
60. C.A. Hübner and T.J. Jentsch, *Ion channel diseases*, Human Molecular Genetics, 11 (20) 2002, 2435-2445
61. O.P. Hamill, A. Marty, E. Neher, B. Sackmann and F.J. Sigworth, *Improved Patch-Clamp techniques for high-resolution current recording from cells and cell-free membrane patches*, Pflügers Archieve, 391 (1981), 85-100
62. A. Stett, V. Bucher, C. Burkhardt, U. Weber and W. Nisch, *Patch-clamping of primary cardiac cells with micro-openings in polyimide films*, Medical and Biological Engineering and Computing, 41 (2003), 233-240
63. N. Fertig, R.H. Blick and J.C. Behrends, *Whole cell patch clamp recording performed on a planar glass chip*, Biophysical Journal, 82 (2002), 3056-3062
64. C. Schmidt, M. Mayer and H. Vogel, *A chip-based biosensor for the functional analysis of single ion channels*, Angew. Chem. Int. Ed., 39 (2000), 3137-3140
65. S.J. Wilk, L. Petrossian, M. Goryll, T.J. Thornton, S.M. Goodnick, J.M. Tang and R.S. Eisenberg, *Integrated platform for ion channel sensing*, IEEE, (2005), 1165-1168
66. S.D. Ogier, R.J. Bushby, Y. Cheng, S.D. Evans, S.W. Evans, A.T.A. Jenkins, P. F. Knowles and R.E. Miles, *Suspended planar phospholipids bilayers on micromachined supports*, Langmuir, 16 (2000), 5696-5701
67. T. Sordel, S. Garnier-Raveaud, F. Sauter, C. Pudda, F. Marcel, M.D. Waard, C. Arnoult, M. Vivaudou, F. Chatelain and N. Picollet-D'hahan, *Hourglass SiO_2 coating increases the performance of planar patch-clamp*, Journal of Biotechnology, 125 (2006), 142-154
68. Y. Cheng, R.J. Bushby, S.D. Evans, P.F. Knowles, R.E. Miles and S.D. Ogier, *Single ion channel sensitivity in suspended bilayers on micromachined supports*, Langmuir, 17 (2001), 1240-1242
69. R. Pantoja, D. Sigg, R. Blunck, F. Bezanilla and J.R. Heath, *Bilayer reconstitution of voltage-dependent ion channels using a microfabricated silicon chip*, Biophysical Journal, 81 (2001), 2389-2394
70. N. Fertig, Ch. Meyer, R.H. Blick, Ch. Trautmann and J.C. Behrends, *Microstructured glass ship for ion-channel electrophysiology*, Physical Review E, 64 (2001) 040901(Rapid Communications), 1-4
71. R.J. White, B. Zhang, S. Daniel, J.M. Tang, E.N. Ervin, P.S. Cremer and H. S. White, *Ionic conductivity of the aqueous layer separating a lipid bilayer membrane and a glass support*, Langmuir, 22 (2006), 10777-10783
72. D. Weiskopf, E.K. Schmitt, M.H. Klhr, S.K. Dertinger and C. Steinem, *Micro-BLMs on highly ordered porous silicon substrates: Rupture process and lateral mobility*, Langmuir, 23 (2007), 9134-9139
73. S.J. Wilk, L. Petrossian, M. Goryll, T.J. Thornton, S.M. Goodnick, J.M. Tang and R.S. Eisenberg, *Integrated electrodes on a silicon based ion channel measurement platform*, Biosensors and Bioelectronics, 23 (2007), 183-190
74. M.D. Mager, B. Almquist and N.A. Melosh, *Formation and characterization of fluid lipid bilayers on alumina*, Langmuir, 24 (2008), 12734-12737

75. N. Fertig, A. Tilke, R.H. Blick and J.P. Kotthaus, *Stable integration of isolated cell membrane patches in a nanomachined aperture*, Applied Physics Letters, 77(8) 2000, 1218-1220
76. C. Danelon, J.-B. Perez, C. Santschi, J. Brugger, and H. Vogel, *Cell membranes suspended across nanoaperture arrays*, Langmuir, 22 (2006), 22-25
77. X. Han, A. Studer, H. Sehr, I. Geissbühler, M.D. Berardino, F.K. Winkler and L.X. Tiefenauer, *Nanopore arrays for stable and functional free-standing lipid bilayers*, Advanced Materials, 19 (2007), 4466-4470
78. E.K. Schmitt, M. Vrouenraets and C. Steinem, *Channel activity of OmpF monitored in Nano-BLMs*, Biophysical Journal, 91 (2006), 2163-2171
79. W. Römer and C. Steinem, *Impedance analysis and single-channel recordings on Nano-black lipid membranes based on porous alumina*, Biophysical Journal, 86 (2004), 955-965
80. R.J. White, E.N. Ervin, T. Yang, X. Chen, S. Daniel, P.S. Cremer and H.S. White, *Single ion-channel recordings using glass nanopore membrane*s, Journal of American Chemical Society, 129 (2007), 11766-11775
81. M.S.M. Saifullah, K.R.V. Subramanian, E. Tapley, D.-J. Kang, M.E. Welland and M. Butler, *Sub-10 nm electron beam nanolithography using spin-coatable TiO2 resists*, Nano Letters, 3(11) 2003, 1587-1591
82. W. Chen and H. Ahmed, *Fabrication of 5-7 nm wide etched lines in silicon using 100 keV electron-beam lithography and polymethylmethacrylate resist*, Applied Physics Letters, 62(13) 1993, 1499-1501
83. E. Gouaux, *α-Hemolysin from Staphylococcus aureus: An archetype of ß-barrel, channel-forming toxins*, Journal of Structural Biology, 121 (1998), 110-122
84. V. Proux-Delrouyre, J.-M. Laval and C. Bourdillon, *Formation of Streptavidin-supported lipid bilayers on porous anodic alumina : Electrochemical monitoring of triggered vesicle fusion*, Journal of American Chemical Society, 123 (2001), 9176-9177
85. S.J. Wilk, S. Aboud, L. Petrossian, M. Goryll, J.M. Tang, R.S. Eisenberg, M. Saraniti, S.M. Goodnick and T.J. Thornton, *Ion channel conductance measurements on a silicon-based platform*, Journal of Physics: Conference Series, 38 (2006), 21-24
86. D.J. McGillivray, G. Valincius, F. Heinrich, J.W.F. Robertson, D.J. Vanderah, W. Febo-Ayala, I. Ignatjev, M. Lösche and J.J. Kasianowicz, *Structure of functional Staphylococcus aureus α-Hemolysin channels in tethered bilayer lipid membranes*, Biophysical Journal, 96 (2009) 1547-1553
87. R.C. Jaeger, *Introduction to Microelectronic Fabrication*, Second edition, Prentice Hall (2002)
88. N. Klein and H. Gafni, *The maximum dielectric strength of thin silicon oxide* films, IEEE transactions on Electron Devices, 13 (1966), 281-289
89. M.E. Olson, H. Ceri, D.W. Morck, A.G. Buret and R.R. Read, *Biofilm bacteria: formation and comparative susceptibility to antibiotics*, The Canadian Journal of Veterinary Research, 66 (2002), 86-92
90. L. Song, M.R. Hobaugh, C. Shustak, S. Cheley, H. Bayley and J.E. Gouaux, *Structure of Staphylococcal α-Hemolysin, a heptameric transmembrane pore*, Science, 274/5294 (1996), 1859-1866
91. A. Aksimentiev and K. Schulten, *Imaging α-Hemolysin with molecular dynamics: Ionic conductance, osmotic permeability and the electrostatic potential map*, Biophysical Journal, 88 (2005), 3745-3761
92. G. Menestrina, *Ionic channels formed by Staphylococcus aureus alpha-toxin: Voltage-dependent inhibition by divalent and trivalent cations*, J. Membrane Biology, 90 (1986), 177-190

93. H. Bayley, O. Braha and L.Q. Gu, *Stochastic sensing with protein pores*, Advanced Materials, 12/2 (2000), 139-142
94. W. Römer, Y.H. Lam, D. Fischer, A. Watts, W.B. Fischer, P. Göring, R.B. Wehrspohn, U. Gösele and C. Steinem, *Channel activity of a viral transmembrane peptide in Micro-BLMs: Vpu1-32 from HIV-1*, Journal of American Chemical Society, 126 (2004), 16267-16274
95. I. Mey, M. Stephan, E.K. Schmitt, M.M. Müller, M.B. Amar, C. Steinem and A. Janshoff, *Local membrane mechanics of pore-spanning bilayers*, Journal of American Chemical Society, 131 (2009), 7031-7039
96. J. Gorelik, Y. Gu, H.A. Spohr, A.I. Shevchuk, M.J. Lab, S.E. Harding, C.R.W. Edwards, M. Whitaker, G.W. J. Moss, D.C. H. Benton, D. Sánchez, A. Darszon, I. Vodyanoy, D. Klenerman and Y. E. Korchev, *Ion channels in small cells and subcellular structures can be studied with a smart patch-clamp system*, Biophysical Journal, 83 (2002), 3296-3303
97. A.P. Quist, A. Chand, S. Ramachandran, C. Daraio, S. Jin and R. Lal, *Atomic Force Microscopy imaging and electrical recording of lipid bilayers supported over microfabricated silicon chip nanopores : Lab-on-a-Chip system for lipid membranes and ion channels*, Langmuir, 23 (2007), 1375-1380
98. R.P. Rennie and J.P. Arbuthnott, *Partial characterization of Escherichia Coli haemolysin*, Journal of Medical Microbiology, 7 (1974), 179-188
99. E. Reimhult and K. Kumar, *Membrane biosensor platforms using nano- and microporous supports*, Trends in Biotechnology, 26 (2) 2007, 82-89
100. M.R. Nussio, G. Oncins, I. Ridelis, E. Szili, J.G. Shapter, F. Sanz and N.H. Voelcker, *Nanomechanical characterization of phospholipids bilayer islands on flat and porous substrates: A force spectroscopy study*, Journal of Physical Chemistry B, 113 (2009), 10339-10347
101. R.V. Goering, H.M. Dockrell, M. Zuckermann, D. Wakelin, I.M. Roitt, C. Mims and P.L. Chiodini, *Mim's medical microbiology*, 4th Edition, Mosby Elisever Press (2008)
102. W. Irving, T. Boswell and D. Ala'Aldeen, *Medical Microbiology*, Taylor & Francis Publication (2005)
103. V.V. Kingsley, *Basic Microbiology for the Health Sciences*, W.B. Saunders Company Press (1982)
104. H. Karch, P.I. Tarr and M. Bielaszewska, *Enterohaemorrhagic Escherichia coli in human medicine*, International Journal of Medical Microbiology, 295 (2005), 405-418
105. C.K. Schmitt, K.C. Meysick and A.D. O'Brien, *Bacterial toxins: friends or foes?*, Emerging Infectious Diseases, 5 (1999), 224-234
106. A. Nusrat, S.V. Sitaraman and A Neish, *Interaction of bacteria and bacterial toxins with intestinal epithelial cells*, Small Intestine, (2001), 392-398
107. J.E. Alouf, *Molecular features of the cytolytic pore-forming bacterial protein toxins*, Folia Microbiology, 48 (2003), 5-16
108. J.L. Arpigny and K.E. Jaeger, *Bacterial lipolytic enzymes: classification and properties*, Journal of Biochemistry, 343 (1999), 177-183
109. I. Steward, P.J. Schluter and G.R. Shaw, *Cyanobacterial lipopolysaccharides and human health – a review*, Environmental Health: A Global Access Science Source, 5 (2006), 1-23
110. R.H. Christian and C. Whitfield, *Lipopolysaccharide endotoxins*, Annual Review of Biochemistry, 71 (2002), 635-700
111. T. Proft and J.D. Fraser, *Bacterial superantigens*, Clinical and Experimental Immunology, 133 (2003), 299-306

112. M. Kotb, *Bacterial pyrogenic exotoxins as superantigens*, Clinical Microbiology Reviews, 8 (1995), 411-426
113. M. Llewelyn and J. Cohen, *Superantigens: microbial agents that corrupt immunity*, 2 (2002), 156-162
114. T.K. Sixma, S.E. Pronk, K.H. Kalk, E.S. Wartna, B.A.M. van Zanten, B. Witholt and W.G.J. Hol, *Crystal structure of a cholera toxin-related heat-labile enterotoxin from E. coli*, Nature, 351 (1991), 371-377
115. R.J. Collier, *Diphtheria toxin: mode of action and structure*, Bacteriological Reviews, 39 (1975), 54-85
116. S. Choe, M.J. Bennett, G. Fujii, P.M.G. Curmi, K.A. Kantardjieff, R.J. Collier and D. Eisenberg, *The crystal structure of diphtheria toxin*, Nature, 357 (1992), 216-222
117. P.V. Liu, *Extracellular toxins of Pseudomonas aeruginosa*, The Journal of Infectious Diseases, 130 (1974), S94-S99
118. W.A. Brodsky, J.C. Sadoff, J.H. Durham, G. Ehrenspeck, M. Schachner and B.H. Iglewski, *Effects of Pseudomonas toxin A, diphtheria toxin, and cholera toxin on electrical characteristics of turtle* bladder, Proceedings of the National Academy of Sciences USA, 76 (1979), 3562-3566
119. B.R. Singh, B. Li and D. Read, *Botulinum versus tetanus neurotoxins: why is botulinum neurotoxin but not tetanus neurotoxin a food poison*, Toxicon, 33 (1995), 1541-1547
120. M. Bukowski, B. Wladyka and G. Dubin, *Exfoliative toxins of Staphylococcus aureus*, Toxins, (2010), 1148-1165
121. M.W. Parker and S.C. Feil, *Pore-forming protein toxins: from structure to function*, Progress in Biophysics and Molecular Biology, 88 (2005), 91-142
122. R.J.C. Gilbert, *Pore-forming toxins*, CMLS Cellular and Molecular Life Sciences, 59 (2002), 832-844
123. M.R. Gonzalez, M. Bischofberger, L. Pernot, F.G. van der Goot and B. Frêche, *Bacterial pore-forming toxins: The (w)hole story?*, Cellular and Molecular Life Sciences, 65 (2008), 493-507
124. G. Belmonte, L. Cescatti, B. Ferrari, T. Nicolussi, M. Ropele and G. Menestrina, *Pore formation by Staphylococcus aureus alpha-toxin in lipid bilayers: Dependent upon temperature and toxin concentration*, European Biophysics Journal, 14 (1987), 349-358
125. P.F.F. Almeida, W.L.C. Vaz and T.E. Thompson, *Lipid diffusion, free area, and molecular dynamic simulations*, Biophysical Journal, 88 (2005) 4434-4438
126. H. Barth, K. Aktories, M.R. Popoff and B.G. Stiles, *Binary bacterial toxins: Biochemistry, biology, and applications of common Clostridium and Bacillus proteins*, Microbiology and Molecular Biology Reviews, 68 (2004) 373-402
127. A.B. Csoka, G.I. Frost and R. Stern, *The six hyaluronidase-like genes in the human and mouse genomes*, Matrix Biology, 20 (2001), 499-508
128. J.G. Songer, *Bacterial phospholipases and their role in virulence*, Trends in Microbiology, 5 (1997), 156-161
129. R. Gupta, N. Gupta and P. Rathi, *Bacterial lipases: an overview of production, purification and biochemical properties*, Applied Microbiology and Biotechnology, 64 (2004), 763-781
130. H.M. Alouf, C. Carnoy, M. Simonet and J.E. Alouf, *Superantigen bacterial toxins: state of the art*, Toxicon, 39 (2001), 1691-1701
131. R.G. Ulrich, S. Bavari and M.A. Olson, *Bacterial superantigens in human disease: structure, function and diversity*, Trends in Microbiology, 3 (1995), 463-468

132. H. Li, A. Llera, E.L. Malchiodi and R.A. Mariuzza, *The structural basis of T cell activation by superantigens*, Annual Reviews of Immunology, 17 (1999), 435-466
133. J.E. Alouf and H.M. Alouf, *Staphylococcal and Streptococcal superantigens: molecular, biological and clinical aspects*, International Journal of Medical Microbiology, 292 (2003), 429-440
134. Y. Choi, B. Kotzin, L. Herron, J. Callahan, P. Marrack and J. Kappler, *Interaction of Staphylococcus aureus toxin "superantigens" with human T cells*, Proceedings of the National Academy of Sciences USA, 86 (1989), 8941-8945
135. B. Geny and M. R. Popoff, *Bacterial protein toxins and lipids: pore formation or toxin entry into cells*, Biology of the Cell, 98 (2006), 667-678
136. E.A. Dennis, *Diversity of group types, regulation, and function of phospholipase A2*, The Journal of Biological Chemistry, 269 (1994), 13057-13060
137. R.W. Titball, *Bacterial phospholipases C*, Microbiological Reviews, 57 (1993), 347-366
138. S. Bhakdi and J. Tranum-Jensen, *Alpha-toxin of Staphylococcus aureus*, Microbiological Reviews, 55 (1991), 733-751
139. S.J. Tilley, E.V. Orlova, R.J.C. Gilbert, P.W. Andrew and H.R. Saibil, *Structural basis of pore-formation by the bacterial toxin pneumolysin*, Cell, 121 (2005), 247-256
140. G. Xiong, M. Struckmeier and F. Lutz, *Pore-forming Pseudomonas aeruginosa cytotoxin*, Toxicology, 87 (1994), 69-83
141. Y. Endo, K. Tsurugi, T. Yutsudo, Y. Takeda, T. Ogasawara and K. Igarashi, *Site of action of a Vero toxin (VT2) from Escherichia coli O157:H7 and of Shiga toxin on eukaryotic ribosomes*, European Journal of Biochemistry, 171 (1988), 45-50
142. C. Pezard, P. Berche and M. Mock, *Contribution of individual toxin components to virulence of Bacillus anthracis*, Infection and Immunity, 59 (1991), 3472-3477
143. K. Aktories, *Rho proteins: targets for bacterial toxins*, Trends in Microbiology, 5 (1997), 282-288
144. H.P. Vacklin, F. Tiberg, G. Fragneto and R.K. Thomas, *Phospholipase A2 hydrolysis of supported phospholipid bilayers: A neutron reflectivity and ellipsometry study*, Biochemistry, 44 (2005), 2811-2821
145. M. Murakami and I. Kudo, *Phospholipase A2*, Journal of Biochemistry, 131 (2002), 285-292
146. M. McDermott, M.J.O. Wakelam and A.J. Morris, *Phospholipase D*, Biochemistry and Cell Biology, 82 (2004), 225-253
147. R. Foronjy and J. D'Armiento, *The role of collagenase in emphysema*, Respiratory Research, 2 (2001), 348-352
148. D.R. Pokharel, R. Rai, P. Kumar, C. M. Chatuvedi and S. Rathaur, *Tissue localization of collagenase and leucine aminopeptidase in the bovine filarial parasite Setaria cervi*, Filaria Journal, 5 (2006), 1-8
149. V. Volfova, J. Hostomska, M. Cerny, J. Votypka and P. Volf, *Hyaluronidase of bloodsucking insects and its enhancing effect on Leishmania infection in mice*, PLoS Neglected Tropical Diseases, 2 (2008), e294, 1-8
150. T.T.A. Abdelghani, A. Kunamneni and P. Ellaiah, *Isolation and mutagenesis of streptokinase producing bacteria*, American Journal of Immunology, 1 (2005), 125-129
151. Y. Kuwabara, M. Maruyama, Y. Watanabe, S. Tanaka, M. Takakuwa and Y. Tamai, *Purification and some properties of membrane-bound phospholipase B from Torulaspora delbrueckii*, Journal of Biochemistry, 104 (1988), 236-241
152. R.K. Tweten, *Cholesterol-dependent cytolysins, a family of versatile pore-forming toxins*, Infection and Immunity, 73 (2005), 6199-6209

153. M.M. Monick and G.W. Hunninghake, *Activation of second messenger pathways in alveolar macrophages by endotoxin*, European Respiratory Journal, 20 (2002), 210-222
154. B. Ge and J. Meng, *Advanced technologies for pathogen and toxin detection in foods: current applications and future directions*, Journal of the Association for Laboratory Automation, 14 (2009), 235-241
155. S. Isaac and D. Jennings, *Microbial Culture*, BIOS Scientific Publishers Limited, 1995
156. D.M. Kemeny, *A Practical Guide to ELISA*, NY: Pergamon Press 1991
157. M.A. Kerr and R. Thorpe, *Chapter 9: Common immunological techniques: ELISA, Blotting, Immunohistochemistry and Immunocytochemistry, Immunochemistry*, BIOS Scientific Publishers Limited, 1994
158. B.K. Van Weemen and A.H.W. M. Schuurs, *Immunoassay using antigen-enzyme conjugates*, FEBS Letters, 15 (1971), 232-236
159. A. Burkovski, *Rapid detection of bacterial surface proteins using an enzyme-linked immunosorbent assay system*, Journal of Biochemical and Biophysical Methods, 34 (1997), 69-71
160. M.T. McCourt, D.A. Finlay, C. Laird, J.A. Smyth, C. Bell and H.J. Ball, *Sandwich ELISA detection of Clostridium perfringens cells and α-toxin from field cases of necrotic enteritis of poultry*, Veterinary Microbiology, 106 (2005), 259-264
161. M.L. Hale and B.G. Stiles, *Detection of Clostridium perfringens alpha toxin using a capture antibody ELISA*, Toxicon, 37 (1999), 471-484
162. V. Guglielmo-Viret, O. Attrée, V. Blanco-Gros and P. Thullier, *Comparison of electrochemiluminescence assay and ELISA for the detection of Clostridium botulinum type B neurotoxin*, Journal of Immunological Methods, 301 (2005), 164-172
163. P.A.W. Robertson, H.-S. Xu and B. Austin, *An enzyme-linked immunosorbent assay (ELISA) for the detection of Vibrio harveyi in penaeid shrimp and water*, Journal of Microbiological Methods, 34 (1998), 31-39
164. S.P. Yazdankhah, L. Sølverød, S. Simonsen and E. Olsen, *Development and evaluation of an immunomagnetic separation-ELISA for the detection of Staphylococcus aureus thermostable nuclease in composite milk*, Veterinary Microbiology, 67 (1999), 113-125
165. S.P. Yazdankhah, A.-L. Hellemann, K. Rønningen and E. Olsen, *Rapid and sensitive detection of Staphylococcus species in milk by ELISA based on monodisperse magnetic* particles, Veterinary Microbiology, 62 (1998), 17-26
166. T. Weissensteiner, H.G. Griffin and A. Griffin, *PCR Technology: Current Innovations*, Second edition, CRC press, 2004
167. N. Ramalingam, Z. Rui, H.-B. Liu, C.-C. Dai, R. Kaushik, B. Ratnaharika and H.-Q. Gong, *Real-time PCR-based microfluidic array chip for simultaneous detection of multiple waterborne pathogens*, Sensors and Actuators B: Chemical, 145 (2010), 543-552
168. L. Watterworth, E. Topp, H. Schraft and K.T. Leung, *Multiplex PCR-DNA probe assay for detection of pathogenic Escherichia coli*, Journal of Microbiological Methods, 60 (2005), 93-105
169. C. Palomares, M.J. Torres, A. Torres, J. Aznar and J.C. Palomares, *Rapid detection and identification of Staphylococcus aureus from blood culture specimens using real-time fluorescence PCR*, Diagnostic Microbiology and Infectious Disease, 45 (2003), 183-189
170. A.J. Gubala, *Multiplex real-time PCR detection of Vibrio cholerae*, Journal of Microbiological Methods, 65 (2006), 278-293

171. D.-Y. Lee, K. Shannon and L.A. Beaudette, *Detection of bacterial pathogens in municipal wastewater using an oligonucleotide microarray and real-time quantitative PCR*, Journal of Microbiological Methods, 65 (2006), 453-467
172. V. Atanassova, A. Meindl and C. Ring, *Prevalence of Staphylococcus aureus and staphylococcal enterotoxins in raw pork and uncooked smoked ham – a comparison of classical culturing detection and RFLP-PCR*, International Journal of Food Microbiology, 68 (2001), 105-113
173. M.C. Martín, M.A. González-Hevia and M.C. Mendoza, *Usefulness of a two-step PCR procedure for detection and identification of enterotoxigenic staphylococci of bacterial isolates and food samples*, Food Microbiology, 20 (2003), 605-610
174. M. Zschöck, D. Botzler, S. Blöcher, J. Sommerhäuser and H.P. Hamann, *Detection of genes for enterotoxins (ent) and toxic shock syndrome toxin-1 (tst) in mammary isolates of Staphylococcus aureus by polymerase-chain-reaction*, International Dairy Journal, 10 (2000), 569-574
175. P. Holochová, V. Růžičková, L. Dostálová, R. Pantůček, P. Petráš and J. Doškař, *Rapid detection and differentiation of the exfoliative toxin A-producing Staphylococcus aureus strains based on ϕETA prophage polymorphisms*, Diagnostic Microbiology and Infectious Disease, 66 (2010), 248-252
176. D.M. West, K.A. Sprigings, C. Cassar, P.R. Wakeley, J. Sawyer and R.H. Davies, *Rapid detection of Escherichia coli virulence factor genes using multiplex real-time TaqMan PCR® assays*, Veterinary Microbiology, 122 (2007) 323-331
177. M.A. Cooper, *Label-free screening of bio-molecular interactions*, Analytical and Bioanalytical Chemistry, 377 (2003), 834-842
178. M.M. Ngundi, C.R. Taitt, S.A. McMurry, D. Kahne and F.S. Ligler, *Detection of bacterial toxins with monosaccharide arrays*, Biosensors and Bioelectronics, 21 (2006), 1195-1201
179. G. Menestrina, C. Pederzolli, S. Forti and F. Gambale, *Lipid interaction of Pseudomonas aeruginosa exotoxin A*, Biophysical Journal, 60 (1991), 1388-1400
180. B.-K. Oh, W. Lee, B.S. Chun, Y.M. Bae, W.H. Lee and J.-W. Choi, *The fabrication of protein chip based on surface Plasmon resonance for detection of pathogens*, Biosensors and Bioelectronics, 20 (2005), 1847-1850
181. A.D. Taylor, Q. Yu, S. Chen, J. Homola and S. Jiang, *Comparison of E. coli O157:H7 preparation methods used for detection with surface Plasmon resonance sensor*, Sensors and Actuators B: Chemical, 107 (2005), 202-208
182. X. Muñoz-Berbel, C. García-Aljaro and F.J. Muñoz, *Impedimetric approach for monitoring the formation of biofilms on metallic surfaces and the subsequent application to the detection of bacteriophages*, Electrochimica Acta, 53 (2008), 5739-5744
183. X. Muñoz-Berbel, F.J. Muñoz, N. Vigués and J. Mas, *On-chip impedance measurements to monitor biofilm formation in the drinking water distribution network*, Sensors and Actuators B: Chemical, 118 (2006), 129-134
184. X. Muñoz-Berbel, N. Vigués, J. Mas, A.T.A. Jenkins and F.J. Muñoz, *Impedimetric characterization of the changes produced in the electrode-solution interface by bacterial attachment*, Electrochemistry Communications, 9 (2007), 2654-2660
185. X. Muñoz-Berbel, N. Vigués, A.T.A. Jenkins, J. Mas and F.J. Muñoz, *Impedimetric approach for quantifying low bacteria concentrations based on the changes produced in the electrode-solution interface during the pre-attachment stage*, Biosensors and Bioelectronics, 23 (2008), 1540-1546
186. V.M. Mirsky, M. Riepl and O.S. Wolfbeis, *Capacitive monitoring of protein immobilization and antigen-antibody reactions on monomolecular alkylthiol films on gold electrodes*, Biosensors and Bioelectronics, 12 (1997), 977-989

187. R. Naumann, D. Walz, S.M. Schiller and W. Knoll, *Kinetics of valinomycin-mediated K^+ ion transport through tethered bilayer lipid membranes*, Journal of Electroanalytical Chemistry, 550-551 (2003), 241-252
188. O. Purrucker, H. Hillebrandt, K. Adlkofer and M. Tanaka, *Deposition of highly resistive lipid bilayer on silicon-silicon oxide electrode and incorporation of gramicidin studied by ac impedance spectroscopy*, Electrochimica Acta, 47 (2001), 791-798
189. T.L. Williams and A.T.A. Jenkins, *Measurement of the binding of cholera toxin to GM1 gangliosides on solid supported lipid bilayer vesicles and inhibition by europium (III) chloride*, Journal of American Chemical Society, 130 (2008), 6438-6443
190. J.E. Wedekind, C.B. Trame, M. Dorywalska, P. Koehl, T.M. Raschke, M. McKee, D. FitzGerald, R.J. Collier and D.B. McKay, *Refined crystallographic structure of Pseudomonas aeruginosa exotoxin A and its implications for the molecular mechanism of toxicity*, Journal of Molecular Biology, 314 (2001), 823-837
191. R. Ratts and J.R. Murphy, *Diphtheria toxins, diphtheria-related fusion protein toxins, and the molecular mechanism of their action against eukaryotic cells*, Topics in Current Genetics, Vol. 11, Microbial Protein Toxins, (2004)
192. L. Rose and A.T.A. Jenkins, *The effect of the ionophore valinomycin on biomimetic solid supported lipid DPPTE/EPC membranes*, Bioelectrochemistry, 70 (2007), 387-393
193. M. Asmild, N. Oswald, K.M. Krzywkowski, S. Friis, R.B. Jacobsen, D. Reuter, R. Taboryski, J. Kutchinsky, R.K. Vestergaard, R.L. Schrøder, C.B. Sørensen, M. Bech, M.P. G. Korsgaard and N.J. Willumsen, *Upscaling and automation of electrophysiology: toward high throughput screening in ion channel drug discovery*, Receptors and Channels, 9 (2003), 49-58
194. N.J. Willumsen, *Ion channels in physiology, pathophysiology, and future drug discovery*, Ion Channels, (2003) 18-22
195. B.M. Burkhart, R.M. Gassman, D.A. Langs, W.A. Pangborn, W.L. Duax and V. Pletnev, *Gramicidin D conformation, dynamics and membrane ion transport*, Biopolymers (Peptide Science), 51 (1999), 129-144
196. J. Kutchinsky, S. Friis, M. Asmild, R. Taboryski, S. Pedersen, R.K. Vestergaard, R.B. Jacobsen, K. Krzywkowski, R.L. Schrøder, T. Ljungstrøm, N. Hélix, C.B. Sørensen, M. Bech and N.J. Willumsen, *Characterization of potassium channel modulators with QPatch™ Automated Patch-Clamp technology: system characteristics and performance*, ASSAY and Drug Development Technologies, 1 (2003), 685-693
197. Nanion Notes, *Bilayer recordings with the Port-a-Patch©,* Issue 5 (2006)
198. J.M. Moran-Mirabal, J.B. Edel, G.D. Meyer, D. Throckmorton, A.K. Singh and H.G. Craighead, *Micrometer-sized supported lipid bilayer arrays for bacterial toxin binding studies through total internal reflection fluorescence microscopy*, Biophysical Journal, 89 (2005), 296-305
199. A. Janshoff, C. Steinem, M. Siever, A.e. Bayâ, M.A. Schmidt and H.-J. Galla, *Quartz crystal microbalance investigation of the interaction of bacterial toxins with ganglioside containing solid supported membranes*, European Biophysical Journal, 26 (1997), 261-270
200. A.L. Slade, J.S. Schoeniger, D.Y. Sasaki and C.M. Yip, *In situ scanning probe microscopy studies of tetanus toxin-membrane interactions*, Biophysical Journal, 91 (2006), 4565-4574
201. K.S. Phillips and Q. Cheng, *Microfluidic immunoassay for bacterial toxins with supported phospholipid bilayer membranes on poly(dimethylsiloxane)*, Analytical Chemistry, 77 (2005), 327-334

202. D.R. Lide, *CRC handbook of chemistry and physics:* 89th ed., (2008-2009), CRC Press
203. M. Palmer, *Cholesterol and the activity of bacterial toxins*, FEMS Microbiology Letters, 283 (2004), 281-289
204. K. Yamauchi, K. Doi and M. Kinoshita, *Archaebacterial lipid models: stable from 1-alkyl-2-phytanyl-sn-glycero-3-phosphocholines*, Biochimica et Biophysica Acta, 1283 (1996), 163-169
205. M. Luckey, *Membrane Structural Biology (with biochemical and biophysical foundations)*, Cambridge University Press, 2008
206. M. Huseby, K. Shi, C.K. Brown, J. Digre, F. Mengistu, K.S. Seo, G.A. Bohach, P.M. Schlievert, D.H. Ohlendorf and C.A. Earhart, *Structure and biological activities of beta toxin from Staphylococcus aureus*, Journal of Bacteriology, 189 (2007), 8719-8726
207. I.-M. Nilsson, O. Hartford, T. Foster and A. Tarkowski, *Alpha-toxin and gamma-toxin jointly promote Staphylococcus aureus virulence in murine septic arthritis*, Infection and Immunity, 67 (1999), 1045-1049
208. J.E. Fitton, A. Dell and W.V. Shaw, *The amino acid sequence of the delta hemolysin of Staphylococcus aureus*, FEBS Letters, 115 (1980), 209-212
209. S. Kasimir, W. Schönfeld, J.E. Alouf and W. König, *Effect of Staphylococcus aureus delta-toxin on human granulocyte functions and platelet-activating-factor metabolism*, Infection and Immunity, 58 (1990), 1653-1659
210. A. Hildebrand, M. Pohl and S. Bhakdi, *Staphylococcus aureus α-toxin*, The Journal of Biological Chemistry, 266 (1991), 17195-17200
211. H.M. Nguyen, M.A. Rocha, K.R. Chintalacharuvu and D.O. Beenhouwer, *Detection and quantification of Panton-Valentine Leukocidin in Staphylococcus aureus cultures by ELISA and Western blotting: Diethylpyrocarbonate inhibits binding of protein A to IgG*, Journal of Immunological Methods, 356 (2010, 1-5
212. J. Schümann, S. Angermüller, R. Bang, M. Lohoff and G. Tiegs, *Acute hepatotoxicity of Pseudomonas aeruginosa exotoxin A in mice depends on T cells and TNF*, The Journal of Immunology, 161 (1998), 5745-5754
213. T. Zehavi-Willner, *Induction of murine cytolytic T lymphocytes by Pseudomonas aeruginosa exotoxin A*, Infection and Immunity, 56 (1988), 213-218
214. S.I. Blot, *Outcome and attributable mortality in critically ill patients with bacteremia involving methicillin-suspectible and methicillin-resistant Staphylococcus aureus*, Archives of International Medicine, 162 (2002), 2229-2235
215. A.P. Johnson, H.M. Aucken, S. Cavendish, M. Ganner, M.C.J. Wale, M. Warner, D.M. Livermore, B.D. Cookson and the UK EARSS participants, *Dominance of EMRSA-15 and -16 among MRSA causing nosocomial bacteraemia in the UK: analysis of isolates from the European Antimicrobial Resistance Surveillance System (EARSS)*, Journal of Antimicrobial Chemotherapy, 48 (2001), 141-156
216. M.P. Jevons, *Celbenin-resistant Staphylococci*, To-day's Drug Correspondence, (1961), 124-125
217. M.T.G Holden, E.J. Feil, J.A. Lindsay, S.J. Peacock, N.P.J. Day, M.C. Enright, T.J. Foster, C.E. Moore, L. Hurst, R. Atkin, A. Barron, N. Bason, S.D. Bentley, C. Chillingworth, T. Chillingworth, C. Churcher, L. Clark, C. Corton, A. Cronin, J. Doggett, L. Dowd, T. Feltwell, Z. Hance, B. Harris, H. Hauser, S. Holroyd, K. Jagels, K.D. James, N. Lennard, A. Line, R. Mayes, S. Moule, K. Mungall, D. Ormond, M.A. Quail, E. Rabbinowitsch, K. Rutherford, M. Sanders, S. Sharp, M. Simmonds, K. Stevens, S. Whitehead, B.G. Barrell, B.G. Spratt and J. Parkhill, *Complete genomes of two clinical Staphylococcus aureus strains: evidence for the*

rapid evolution of virulence and drug resistance, Proceedings of the National Academy of Sciences USA, 101 (2004), 9786-9791
218. G.L. Winsor, T.V. Rossum, R. Lo, B. Khaira, M.D. Whiteside, R.E.W. Hancock and F.S.L. Brinkman, *Pseudomonas benome database: facilitating user-friendly, comprehensive comparisons of microbial genomes*, Nucleic Acids Research, 37 (2009), D483-D488
219. J. Zhou, A.L. Loftus, G. Mulley and A.T.A. Jenkins, *A thin film detection/response system for pathogenic bacteria*, Journal of American Chemical Society, 132 (2010), 6566-6570
220. S. Gritsch, P. Nollert, F. Jähnig and E. Sackmann, *Impedance spectroscopy of porin and gramicidin pores reconstituted into supported lipid bilayers on indium-tin-oxide electrodes*, Langmuir, 14 (1998), 3118-3125
221. A.Y. Peleg and D.C. Hooper, *Hospital-acquired infections due to gram-negative bacteria*, The New England Journal of Medicine, 362 (2010), 1804-1813
222. G. Hutton and J. Bartram, *Global cost of the Millennium development goal for water supply and sanitation*, Bulletin of the World Health Organization, 86 (2008), 13-19
223. W.R. Mac Kenzie, N.J. Hoxie, M.E. Proctor, M.S. Gradus, K.A. Blair, D.E. Peterson, J.J. Kazmierczak, D.G. Addiss, K.R. Fox, J.B. Rose and J.P. Davis, *A massive outbreak in Milwaukee of Cryptosporidium infection transmitted through the public water supply*, The New England Journal of Medicine, 331 (1994), 161-167
224. R.R. Roberts, B. Hota, I. Ahmad, S.D. Scott, S.D. Foster, F. Abbasi, S. Schabowski, L.M. Kampe, G.G. Ciavarella, M. Supino, J. Naples, R. Cordell, S.B. Levy and R.A. Weinstein, *Hospital and social costs of antimicrobial-resistant infections in a Chicago teaching hospital: implications for antibiotic stewardship*, Clinical and Infectious Diseases, 49 (2009), 1185-1186
225. B. Cohen, E.L.Larson, W.P. Stone, M. Neidell and A.S. Glied, *Factors associated with variation in estimates of the cost of resistant infections*, Medical Care, 48 (2010), 767-775
226. P.W.Stone, E.C. Hedblom, D.M. Murphy and S B. Miller, *The economic impact of infection control: making the business case for increased infection control resources*, American Journal of Infection Control, 33 (2005), 542-547
227. L.-Q. Gu, O. Braha, S. Conlan, S. Cheley and H. Bayley, *Stochastic sensing of organic analytes by a pore-forming protein containing a molecular adaptor*, Nature, 398 (1999), 686-690
228. J. Mathé, A. Aksimentiev, D.R. Nelson, K. Schulten, and A. Meller, *Orientation discrimination of single-stranded DNA inside the α-hemolysin membrane channel*, Proceedings of the National Academy of Sciences USA, 102 (2005), 12377-12382
229. M. Hegner, P. Wagner and G. Semenza, *Ultralarge atomically flat template-stripped Au surfaces for scanning probe microscopy*, Surface Science, 291 (1993), 39-46
230. P. Silberzan, L. Léger, D. Ausserré and J.J. Benattar, *Silanation of silica surfaces. A new method of constructing pure or mixed monolayer*, Langmuir, 7 (1991), 1647-1651
231. C. Rossi and J. Chopineau, *Biomimetic tethered lipid membranes designed for membrane-protein interaction studies*, European Biophysical Journal, 36 (2007), 955-965
232. Y.-H.M. Chan and S.G. Boxer, *Model membrane systems and their applications*, Current Opinion in Chemical Biology, 11 (2007), 1-7
233. J.R. Vig, *UV / ozone cleaning of surfaces*, Journal of Vacuum Science and Technology A, 3 (1985), 1027-1034

234. S. Mabrey, P.L. Mateo, and J.M. Sturtevant, *High-sensitivity scanning calorimetric study of mixtures of cholesterol with dimyristoyl- and dipalmitoylphosphatidylcholines*, Biochemistry, 17 (1978), 2464-2468
235. S.W. Hui, C.M. Stewart, M.P. Carpenter and T.P. Stewart, *Effects of cholesterol on lipid organization in human erythrocyte membrane*, Journal of Cell Biology, 85 (1980), 283-291
236. C.R. Mateo, A.U. Acuña and J.-C. Brochon, *Liquid-crystalline phases of cholesterol/lipid bilayers as revealed by the fluorescence of trans-parinaric acid*, Biophysical Journal, 68 (1995), 978-987
237. C. Breffa, *New synthetic strategies to tethered bilayer lipid membrane*, PhD thesis, Johannes Gutenberg Universität Mainz, 2005
238. A.J. Jin, D. Huster, K. Gawrisch and R. Nossal, *Light scattering characterization of extruded lipid vesicles*, European Biophysical Journal, 28 (1999), 187-199
239. H.M. McConnell and A. Radhakrishnan, *Condensed complexes of cholesterol and phospholipids*, Biochimica et Biophysica Acta, 1610 (2003), 159-173
240. S.C. Davis, C. Ricotti, A. Cazzaniga, E. Welsh, W.H. Eaglstein and P.M. Mertz, *Microscopic and physiologic evidence for biofilm-associated wound colonization in-vivo*, Wound Repair and Regeneration, 16 (2008), 23-29
241. J.C. Love, L.A. Estroff, J.K. Kriebel, R.G. Nuzzo and G.M. Whitesides, *Self-assembled monolayers of thiolates on metals as a form of nanotechnology*, Chemical Reviews, 105 (2005), 1103-1169
242. C. Beloin, A. Roux and J.-M. Ghigo, *Escherichia coli biofilms*, Current Topics in Microbiology and Immunology, 322 (2008), 249-289
243. J. Palmer, S. Flint and J. Brooks, *Bacterial cell attachment, the beginning of a biofilm*, Journal of Industrial Microbiology and Biotechnology, 34 (2007), 577-588
244. P.H. Gilligan and D.C. Robertson, *Nutritional requirements of synthesis of heat-labile enterotoxin by enterotoxigenic strains of Escherichia coli*, Infection and Immunity, 23 (1979), 99-107
245. S.L. Kunkel and D.C. Robertson, *Factors affecting release of heat-labile enterotoxin by enterotoxigenic Escherichia coli*, Infection and Immunity, 23 (1979), 652-659
246. E.N. Ervin, R. Kawano, R.J. White and H.S. White, *Simultaneout alternating and direct current readout of protein ion channel blocking events using glass nanopore membranes*, Analytical Chemistry, 80 (2008), 2069-2076
247. Y.E. Korchev, G.M. Alder, A. Bakhramov, C.L. Bashford, B.S. Joomun, E.V. Sviderskaya, P.N.R. Usherwood and C.A. Pasternak, *Staphylococcus aureus alpha-toxin-induced pores: channel-like behavior in lipid bilayers and patch clamped cells*, Journal of Membrane Biology, 143 (1995), 143-151
248. M.R. Popoff and B. Poulain, *Bacterial toxins and the nervous system: neurotoxins and multipotential toxins interacting with neuronal cells*, Toxins, 2 (2010), 683-737
249. E.N. Ervin, R.J. White and H.S. White, *Sensitivity and signal complexity as a function of the number of ion channels in a stochastic sensor*, Analytical Chemistry, 81 (2009), 533-537
250. M. Misakian and J.J. Kasianowicz, *Electrostatic influence of ion transport through the αHL channel*, Journal of Membrane Biology, 195 (2003), 137-146
251. P.B. Bennett and H.R.E. Guthrie, *Trends in ion channel drug discovery: advances in screening technologies*, Trends in Biotechnology, 21 (2003), 563-569
252. V. Cabiaux, C. Wolff and J-,M. Ruysschaert, *Interaction with a lipid membrane: a key step in bacterial toxins virulence*, International Journal of Biological Macromolecules, 21 (1997), 285-298

253. S.L. Johnson and J.W. Woodbury, *Membrane resistance of human red cells*, The Journal of General Physiology, 47 (1964), 827-837
254. W. Brown, *Dynamic light scattering: the method and some applications*, (1993) Clarendon Press

Appendix

1. List of patents

- **Thet Naing Tun**, C. Joachim and N. Chandrasekhar, *Nano-Interconnects for Atomic and Molecular Scale Circuits*, PCT Patent Application No. PCT/SG2007/000247 (filed on 10 August 2007)

2. List of publications

- **Thet Naing Tun** and A. T. A. Jenkins, *An electrochemical impedance study of the effect of pathogenic bacterial toxins on tethered bilayer lipid membrane*, Electrochemistry Communications, July 2010 (accepted)
- Ma Han Thu Lwin, **Thet Naing Tun**, Hui Hui Kim, R. S. Kajen, N. Chandrasekhar and C. Joachim, *Silicon on insulator nanoscale backside interconnects for atomic and molecular scale circuits*, Journal of Vacuum Science and Technology B, 28 (2010), 978-984
- Ma Han Thu Lwin, **Thet Naing Tun** and N. Chandrasekhar, *Wetting behaviour of thin gold nanowires*, Encyclopaedia of Nanoscience and Nanotechnology, 2010 (in press)
- **Thet Naing Tun**, Ma Han Thu Lwin, Hui Hui Kim, N. Chandrasekhar and C. Joachim, *Wetting studies on Au nanowires deposited through nanostencil masks*, Nanotechnology, 18 (2007), 335301
- **Thet Naing Tun**, Toh Siew Lok, Tay Cho Jui, Ramam Akkipeddi and M. Rahmam, *Contact pressure measurement using silicon-based semiconductor pressure sensors*, Sensors and Actuators A**,** 118 (2005), 190-201